Design, synthesis, photophysical and electroluminescence studies of triphenylamine and carbazole derivatives

THESIS SUBMITTED TO **AcSIR** FOR THE AWARD OF THE DEGREE OF
DOCTOR OF PHILOSOPHY IN CHEMISTRY
UNDER THE FACULTY OF SCIENCE

By
Athira Krishna
Enrollment No: 10CC12A39013

Under the Supervision of
Dr. R. Luxmi Varma

ORGANIC CHEMISTRY SECTION
CHEMICAL SCIENCES AND TECHNOLOGY DIVISION
CSIR-NATIONAL INSTITUTE FOR INTERDISCIPLINARY
SCIENCE AND TECHNOLOGY (CSIR-NIIST)
THIRUVANANTHAPURAM - 695019, KERALA

December 2018

Dedicated to

Achan, Amma, Sreejithettan and Luxmi Madam

Declaration

I hereby declare that the matter embodied in this thesis entitled as "***Design, synthesis, photophysical and electroluminescence studies of triphenylamine and carbazole derivatives***" is the result of the investigations carried out by me at the Organic Chemistry Section of the Chemical Sciences and Technology Division, CSIR-National Institute for Interdisciplinary Science and Technology, Thiruvananthapuram, under the supervision of Dr. R. Luxmi Varma and the same has not been submitted elsewhere for any other degree.

In keeping with the general practice of reporting scientific observations, due acknowledgement has been made whenever the work described is based on the findings of other investigation.

Thiruvananthapuram   Athira Krishna

December 2018

CSIR-National Institute for Interdisciplinary Science and Technology

Council of Scientific & Industrial Research (CSIR)
Industrial Estate P.O., Trivandrum - 695 019
Kerala, INDIA

Dr. R. Luxmi Varma   **Tel: 91-471-2515 275**
Senior Principal Scientist & Head
Chemical Sciences and Technology Division   **E-mail: rluxmivarma@niist.res.in**

CERTIFICATE

This is to certify that the work incorporated in this Ph.D. thesis entitled "**Design, synthesis, photophysical and electroluminescence studies of triphenylamine and carbazole derivatives**" submitted by **Ms. Athira Krishna** to the Academy of Scientific and Innovative Research (AcSIR), in partial fulfilment of the requirements for the award of the **Degree of Doctor of Philosophy** in **Chemical Sciences**, embodies the original research work carried out under my supervision and guidance at the Chemical Science and Technology Division of the CSIR-National Institute for Interdisciplinary Science and Technology (CSIR-NIIST), Trivandrum. I further certify that this work has not been submitted to any other University or Institution in partor full for the award of any degree or diploma. Any text, illustration, table etc., used in the thesis from other sources, have been duly cited and acknowledged.

Athira Krishna   Dr. R Luxmi Varma

December 2018   (Thesis supervisor)

Acknowledgement

I am deeply thankful to my parents Shri. Krishnakumar V and Smt. Vijayakumari A for their support, care and blessings. I thank Shri. Sreekumaran Nair and Smt. Girija Kumari my in- laws, for their prayers. I thank Dr. S. Sreejith, my husband, for his constant source of encouragement and love. I thank my sister, Meera Krishna for her silly queries that ignited my research mind. I thank my brothers and sisters, Mr Praveen, Mr. Manoj, Ms. Sreeja and Ms. Sheeja for their love and support. My little daughter Ms. Avni Krishna S, the most adjustable kid needs a special mention, along with her brothers Manu Krishnan, Hari Krishnan, Jeevan Krishnan and Jaya Krishnan. I bow to Kumaranallor Amma for all blessings showered on me.

Thiruvanthapuram   Athira Krishna

December 2018

Contents

Preface

Developing, novel conjugated small organic donor-acceptor molecules for organic light emitting diodes (OLEDs) is an active area of research due to advantages like low cost, flexibility, lightweight, transparency, colour tenability etc. which make them suitable as modern light source. Among different organic molecules used for OLEDs, triphenylamines have gained considerable interest over the period mainly due to their inherent properties like low-oxidation potential, propeller-like geometry to mention a few. Due to the low oxidation potential triphenylamines are extensively used as hole transporting materials in OLEDs. Carbazoles are another class of donor molecules widely used for the organic light emitting applications. High-temperature stability, blue emission and the hole transporting properties of carbazoles make them attractive. Moreover, in the current research of OLEDs, a new generation of molecules was introduced which uses thermally activated delayed fluorescence (TADF) as their key process to achieve high electroluminescence efficiencies and 3, 6 substituted carbazoles were found to be having low ΔE_{ST} and a delayed fluorescence (DF). In this regard, the present thesis describes the design, synthesis, photophysical and electroluminescence properties of a few small organic molecules based on triphenylamines and carbazoles for organic light emitting diode applications. The thesis is divided into four chapters.

Chapter 1 gives a brief introduction to the conjugated, small organic molecules based on triphenylamines and carbazoles followed by a description about their applications in the area of organic light emitting diodes. The chapter also highlights recent developments in this field and major objectives of the present thesis.

The chapter 2 deals with the design, synthesis, photophysical and electroluminescence studies of three triphenylamine-thiophene donor-acceptor molecules (**TPT, TPT-Ben and TPT-Ac**) followed by the demonstration of their use as RGB emitters in the white light generation. The structures of all the molecules were characterized using mass and NMR techniques. **TPT** showed an emission in the blue region whereas upon substitution with donor unit, the resultant molecule (**TPT-Ben**) emitted in the green region and the acceptor appended **TPT-Ac** showed a shift towards the red region of the visible light spectrum. The

observation of primary colour generation prompted us to examine the emission spectra of a mixture of all the three compounds in the solution state (in DMSO) at micromolar (μM) concentrations as well as in the solid state using PMMA matrix and the results are discussed in detail. To have an insight into the structural, electronic and optical properties of the molecules, density functional theory (DFT) studies on the molecules were carried out and the results are discussed. Un-optimized solution processable devices with configurations, ITO/ MoO$_3$ (10 nm)/ **TPT-Ben** or **TPT-Ac** (30 nm)/ BCP (10 nm)/ Alq$_3$ (20 nm)/ LiF/Al were fabricated and the results are discussed.

Chapter 3 discusses the design, synthesis, photophysical and electroluminescence studies of a carbazole derivative (**Cz(PhCF$_3$)$_2$).** This molecule exhibited a blue emission in its solution state (QY 35%) and solid state (QY 13.9%). The ΔE_{ST} value for the molecule was found to be 0.6 eV. However the molecule showed no ICT character regardless of the presence of an active donor carbazole and an active acceptor trifluoromethyl group. DFT calculations on the molecule were carried out. An unoptimized solution processable device with the following configuration: (ITO/ NPB/ **Cz(PhCF$_3$)$_2$**/ BCP/ Alq$_3$/ LiF) (Device 1) was fabricated. It gave a broad electroluminescent emission with two peak maxima at 426 nm and 528 nm. The white light emission with CIE coordinates at (0.31, 0.44), from the device started from about 7 V and was stable up to 16 V. The chapter discusses in detail about the device characteristics.

The high triplet energy of **Cz(PhCF$_3$)$_2$**, comparable to many of the commercially available host materials, prompted us to examine the host properties of the molecule along with Rubrene (yellow) and DCJTB (red) as EL materials. As there is efficient energy transfer between the host and the luminescent materials, two devices were fabricated with the following configurations ITO/ PEDOT:PSS/ NPB/ **Cz(PhCF$_3$)$_2$** + Rubrene/ BCP/ Alq$_3$/ LiF/Al for the yellow device with rubrene and ITO/ PEDOT:PSS/ NPB/ **Cz(PhCF$_3$)$_2$** + Rubrene+ DCJTB/ BCP/ Alq$_3$/ LiF/Al for the red device. The devices showed device properties at very low turn-on voltages and gave emissions akin to the electroluminescent materials used, confirming the utility of our molecule, **Cz(PhCF$_3$)$_2$** as a host for yellow and red devices.

Chapter 4 discusses on the design, synthesis, photophysical and electroluminescent studies of another carbazole derivative **(Cz(PhBz)$_2$)**. **Cz(PhBz)$_2$**, exhibited a better EL (4-fold increase) compared to that of **Cz(PhCF$_3$)$_2$**. It showed a structure-less emission with an obvious solvatochromism in its emission profile. The Stokes shift value of **Cz(PhBz)$_2$** was calculated as 23,345.45 cm^{-1} in DMF. The relative quantum yield for the molecule was found to be 43%. The ΔE_{ST} value of **Cz(PhBz)$_2$** was found to be 0.20 eV . DFT calculations of the molecule was carried out and the results are discussed. To examine the electroluminescent properties **Cz(PhBz)$_2$**, we fabricated a device with the following stacking (structures unoptimized) by solution processing: ITO/ PEDOT: PSS/ NPB:/ **Cz(PhBz)$_2$**/ BCP/ Alq$_3$/ LiF / Al. This device also showed white electroluminescence with a colour coordinate of (0.29, 0.35) and a luminance value of 120 cd/m^2.

The relevance of our work lies in the fact that the current strategy of harvesting both singlet and triplet emissions in electroluminescence with appropriate molecule design, gives an easy and straightforward method for achieving single molecule solution processable white electroluminescent materials.

List of figures

versus luminance, and c) EL spectrum characteristics of the multilayer devices in a structure of ITO/ HATCN (5 nm)/ NPB (40 nm)/ TCTA (5 nm)/ EML (20 nm) / TPBI (40 nm)/ LiF (1 nm)/ Al. EML: NI-1-TPA, NI- 2-TPA, NI-1-PhTPA, or NI-2-PhTPA. Inset: The configuration and energy diagram of the multi-layer devices. **PPI-PPITP**

xviii

curve for the devices

List of charts

List of schemes

List of tables

Abbreviations

1.	^{13}C NMR	:	Carbon NMR
2.	^{1}H NMR	:	Proton NMR
3.	3D	:	Three dimensional
4.	Å	:	Angstrom
5.	ACN	:	Acetonitrile
6.	Ag	:	Silver
7.	AgCl	:	Silver chloride
8.	Alq$_3$	:	Tris-(8-Hydroxyquinoline)–Aluminium
9.	Ar	:	Argon
10.	B3LYP	:	Becke, 3-parameter, Lee-Yang-Parr
11.	BCP	:	Bathocuproine
12.	CBP	:	4,4′-Bis(*N*-carbazolyl)-1,1′-biphenyl
13.	cd/A	:	Candelas per ampere
14.	cd/m^2	:	Candela per meter square
15.	CDCl$_3$	:	Deuterated chloroform
16.	CIE	:	Commission Internationale de l'Elcairage
17.	CRI	:	Colour rendering index
18.	CV	:	Cyclic voltametry
19.	D	:	Debye
20.	D-A	:	Donor-Acceptor
21.	DF	:	Delayed fluorecence
22.	DFT	:	Density functional theory
23.	DMF	:	Dimethylformamide
24.	DMSO	:	Dimethyl sulfoxide
25.	DPAA	:	4,4'-bis[9-(10 pyrenylanthracene)]triphenylamine
26.	DSC	:	Differential scanning calorimetry
27.	E_{Fc}	:	Oxidation potential ferrocene
28.	EL	:	Electroluminascence
29.	EML	:	Emissive layer

30.	E_{ox}	:	Oxidation potential
31.	EPA	:	Diethyl ether, isopentane and ethanol
32.	EQE	:	External Quantum Efficiency
33.	ESI	:	Electron spray ionization
34.	ESIPT	:	Excited state Intramolecular proton transfer
35.	*et al.*	:	et alia
36.	ETL	:	Electron Transporting Layer
37.	eV	:	Electron volt
38.	F	:	Fluorescence
39.	FIrpic	:	iridium(III)[bis(4,6-difluorophenyl)-pyridinato-N,C2']picolinate complex
40.	FMO	:	Frontier molecular orbitals
41.	g	:	Gram
42.	h	:	Hour
43.	HCl	:	Hydrochloric acid
44.	HIL	:	Hole Injecting Layer
45.	HOMO	:	Highest occupied molecular orbital
46.	HRMS	:	High resolution mass spectrometry
47.	HTL	:	Hole transporting layer
48.	i.e.	:	That is
49.	ICT	:	Intramolecular charge transfer
50.	IP	:	Ionization potentials
51.	IQE	:	Internal quantum efficiency
52.	Ir	:	Iridium
53.	IrL3	:	(9,9-diethyl-7-pyridinylfluoren-2-yl)- diphenylamine
54.	ISC	:	Inter system crossing
55.	ITO	:	Indium tin oxide
56.	K	:	Kelvin
57.	k_{isc}	:	Rate of intersystem crossing
58.	k_{nr}	:	Rate of non-radiative radiations
59.	k_r	:	Rate of radiative radiations

60.	k_{RISC}	:	Rate of reverse intersystem crossing
61.	L M^{-1} cm^{-1}	:	litter mole per centimeter per
62.	LCDs	:	Liquid crystal displays
63.	LEDs	:	Light emitting diodes
64.	LiF	:	Lithium fluoride
65.	lm/W	:	Lumens per watt
66.	LUMO	:	Lowest unoccupied molecular orbital
67.	M	:	Molar
68.	m/z	:	Mass per charge
69.	Max	:	Maximun
70.	mCP	:	1,3-bis(9-carbazolyl)benzene
71.	MEH-PPV	:	poly[2-methoxy-5-(20- ethyl-hexyloxy)-1,4-phenylenevinylene]
72.	Mg	:	Magnesium
73.	mg	:	Milli-gram
74.	MHz	:	Mega hertz
75.	Min	:	Minute
76.	mL	:	Milli-liter
77.	MoO_3	:	Molybdenum trioxide
78.	mV	:	Milli-volt
79.	n	:	Refractive index
80.	N	:	Normal
81.	NBS	:	N-Bromosuccinimide
82.	nm	:	Nanometer
83.	NMR	:	Nuclear magnetic resonance
84.	NPB	:	4,4'-bis[N- (1-naphthyl)-N-phenylamino]biphenyl
85.	ns	:	Nanosecond
86.	^{o}	:	Degree
87.	O_2	:	Oxygen
88.	O_3	:	Ozone
89.	°C	:	Degree celsius

90.	OLED	:	Organic light emitting diode
91.	P	:	Phosphorescence
92.	$Pd(PPh_3)_4$	:	Tetrakis(triphenylphosphine)palladium(0)
93.	PFO	:	poly(9,9-dioctylfluorene)
94.	pH	:	Potant hydrogen
95.	$P\bar{\imath}$	:	Triclinic space group
96.	PL	:	Photoluminascence
97.	PMMA	:	Poly(methyl methacrylate)
98.	ppm	:	Parts per million
99.	Pt	:	Platinum
100.	RGB	:	Red, green, blue
101.	RISC	:	Reverse intersystem crossing
102.	RPM	:	Rotations per minute
103.	RTP	:	Room temperature phosphorescence
104.	s	:	Second
105.	S^0	:	Singlet Ground State
106.	S^1	:	Singlet excited state
107.	SCE	:	Standard calomel electrode
108.	SOC	:	Spin-orbit coupling
109.	STA	:	Singlet-triplet annihilation
110.	T^1	:	Triplet excited state
111.	TA	:	Transient absorption
112.	TADF	:	Thermally activated delayed fluorescence
113.	TCSPC	:	Time correlated single photon count
114.	T_d	:	Decomposition temperature
115.	TG	:	Thermogravimetry
116.	T_g	:	Glass transition temperature
117.	THF	:	Tetrahydrofuran
118.	TLC	:	Thin layer chromatography
119.	TMS	:	Tetramethylsilane
120.	TPA	:	Triple-polaron annihilation

121.	TPA	:	Triphenylamine
122.	TPBI	:	2,2',2''-(benzene- 1,3,5-triyl)-tris(1-phenyl-1H-benzimidazole)
123.	TTA	:	Triplet-triplet annihilation
124.	TV	:	Tele vision
125.	UV	:	Ultra violet
126.	V	:	Voltage
127.	vs	:	Versus
128.	WOLED	:	White organic light emitting diodes
129.	XRD	:	X-ray diffraction
130.	ΔE_{ST}	:	Singlet–triplet energy gap
131.	Δf	:	Polarizability factor
132.	Φ	:	Quantum yield
133.	Φ_R	:	Quantum yield for the reference
134.	ε	:	Di-electric constant
135.	λ_{exc}	:	Lamda excitation
136.	λ_{max}	:	Lamda maximum
137.	μM	:	Micro-molar
138.	@	:	at

Small organic molecules as emitters in organic light emitting diodes: An overview
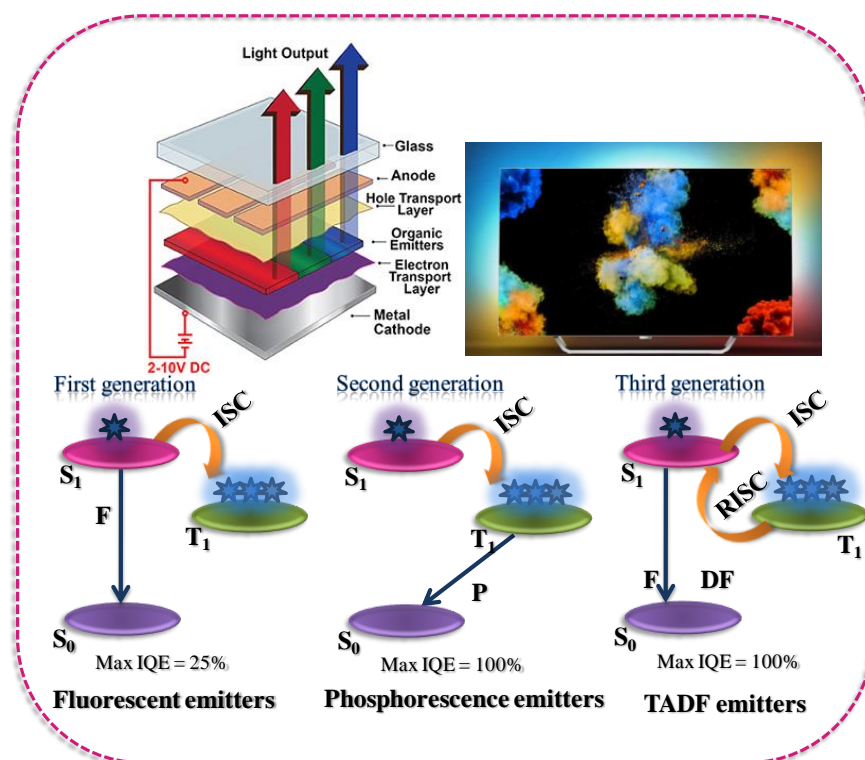
1.1 Introduction

Ever since the original work by Tang and VanSlyke[1] in 1987, organic light emitting diodes (OLEDs) attracted enormous attention due to their widespread applications. The attraction and fascination of this field is mainly due to its interdisciplinary nature, which includes synthetic and physical chemistry, physics and electrical engineering. The organic light emitting diode is basically converts electrical energy to light energy. It consists of different organic layers sandwiched between cathode and a transparent anode, generally indium tin oxide (ITO). The common structure for an organic light emitting diode (OLED) is as shown in Figure 1.1 which includes a cathode, conducting layers like hole transporting layer (HTL), hole injection layer (HIL), electron

transporting layer (ETL) etc, emissive layer (EML) and an anode (ITO). The working principle for OLEDs is ***electroluminescence (EL)***. In the initial stage, the anode will be kept as positive with respect to the cathode, forcing electrons to flow from cathode to anode. But these electrons will be blocked before reaching the anode, creating a flow of holes from the anode. These holes and electrons will combine with each other in the emissive layer, forming excitons. Formation of excitons will result in an emission of light depending upon the band gap of the material used as the emissive layer. So a variety of colours can be generated from OLEDs by modulating the band gap of the emissive layer. (Figure 1.1)
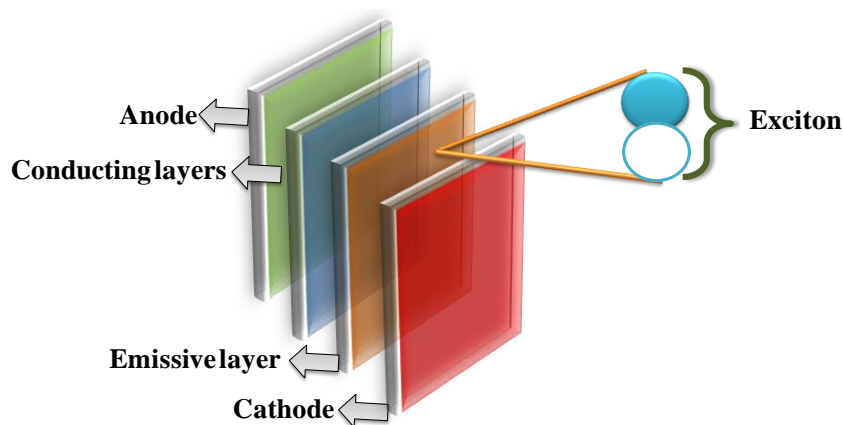
Figure 1.1. *General structure for an OLED*

The first OLED was developed at Kodak by Tang and VanSlyke.[1] They developed a device with Alq_3 as the emitter and this OLED gave a green electroluminescence. Since then this particular field of developing new OLEDs attained a huge progress. Now there are a large number of smart phones and TV displays using OLED technology. Properties like thin structure, flexibility and foldability, transparency, solution processability, low cost, versatility in the emitting colours etc. place OLEDs above conventional liquid crystal displays (LCDs) or inorganic LEDs. Due to the properties listed above, the OLEDs can be used for a wide varieties of applications like lighting, display, transparent windows etc. The solution processability of OLEDs makes them amenable for fabrication thereby reducing the cost of production. Also the properties can be tuned in the case of OLEDs since organic materials can be designed and functionalized effortlessly. Compared with existing liquid-crystal displays (LCDs), OLEDs provide improved image quality and contrast, have faster response times/refresh rates, are

viewable over wider viewing angles and are thinner and lighter. These devices can be fabricated on flexible substrates, where we can fold an OLED display like a poster.[2] This particular feature was beyond imagination in the case of older display technologies. OLEDs are also more energy efficient because they do not require a backlighting system. According to reports lighting alone constitute about 20% of the energy consumption, an OLED with very low energy requirement will reduce the total electricity usage (Chart 1.1).[3]
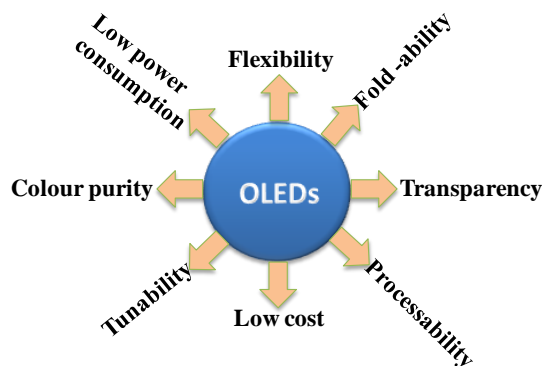
Chart 1.1 *Advantages of OLEDs*

Above all the advantages listed here, the organic light emitting diodes have some disadvantages also; which include the stability, lifetime etc. The phosphorescent OLEDs, widely used nowadays in the smart phones and TV displays, are easily affected by UV light, moisture and oxygen which reduce their lifespan. Also in the case of phosphorescent OLEDs, the incompatibility of organic host and inorganic metals (like iridium) is contributing directly towards its instability.

1.2 Generations of organic light emitting diodes
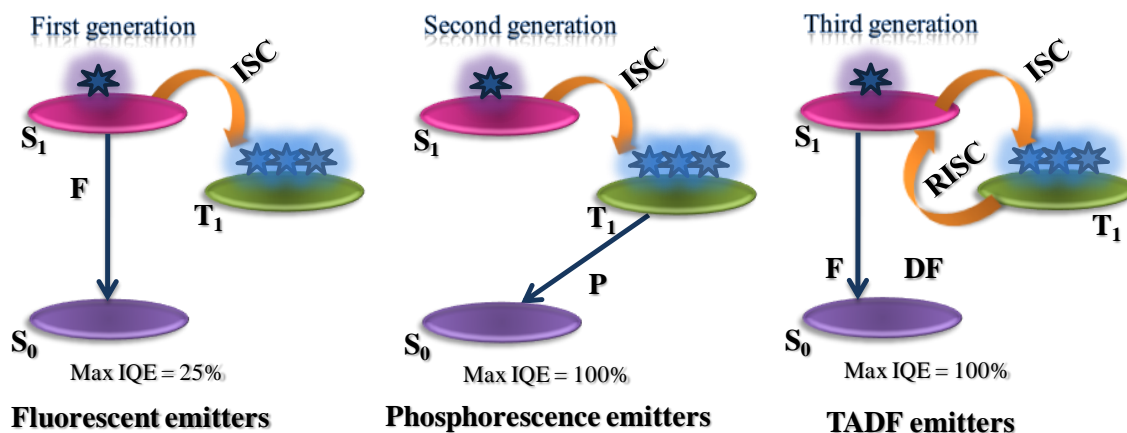
Figure 1.2. *Three generations of OLEDs*

The first report on electroluminescence can be traced back to 1963 when Pope et al. applied a direct current to an anthracene single crystal under a bias of 400 V using silver-paste electrodes.[4]Even though a light came from anthracene in a practical point of view, a driving voltage of 400 V was not feasible. The report of a double-layered device fabricated using tris-(8-hydroxyquinoline)aluminum (Alq_3) as the emitting and electron-transporting layer by Tang and VanSlyke in 1987 is considered as an important milestone in the development of OLEDs. The green-emitting device showed external quantum efficiency (EQE) of about 1% when driven at less than 10 V. Since this invention onwards a great attention was drawn to this particular group of materials both from industry and from academia.

The organic light emitting diodes can be classified into three generations based on the emissive layer used: 1) fluorescent emitters 2) phosphorescent emitters and 3) TADF emitters as shown in Figure 1.2. In small organic molecules based OLEDs, the electron excitation can produce 25% singlet and 75% triplet, according to spin statistics.[5]Due to the spin- forbidden nature of 75% triplet emission,the organic light emitting diodes can only harvest the 25% singlet excitons. The very long emission lifetime makes the triplet excitons vulnerable to non-radiative deactivation as heat loss to the surroundings. Assuming Lambertian emission and a light out coupling efficiency of 20%, the maximum external quantum efficiency (EQE) for an OLED with a fluorescent emitter is only 25% of 20% = 5%[6] (Figure 1.3).

To overcome this shortcoming in device efficiency, the usage of an organometallic platinum complex PtOEP was reported by Baldo *et al.* in 1998 and the electroluminance spectrum of PtOEP and the device configuration are reproduced in (Figure 1.4).[7] Through efficient energy transfer from the host to the emitter, both singlets and triplets were harvested for light emission with reported external and internal quantum efficiencies (IQE) of 4% and 23%, respectively. This report in 1998 resulted in the rise of a new era in OLED research, and a new generation of materials called "phosphorescent OLEDs" was evolved. The organometallic compounds improve the efficiency via intersystem crossing (ISC) from the singlet excited state through strong spin–orbit coupling (SOC) mediated by the heavy metal (e.g., Ir and Pt) present in the complexes.[7,8] Since 2001, devices based on organometallic complexes with nearly 100% IQE have been reported.[9] Commercial OLED devices for displays presently rely on green and red-emitting cyclo-metalated iridium complexes.[10-13] However, the scarcity of the heavy metal

which contributed to the increased cost of the device as well as the environmental pollution associated
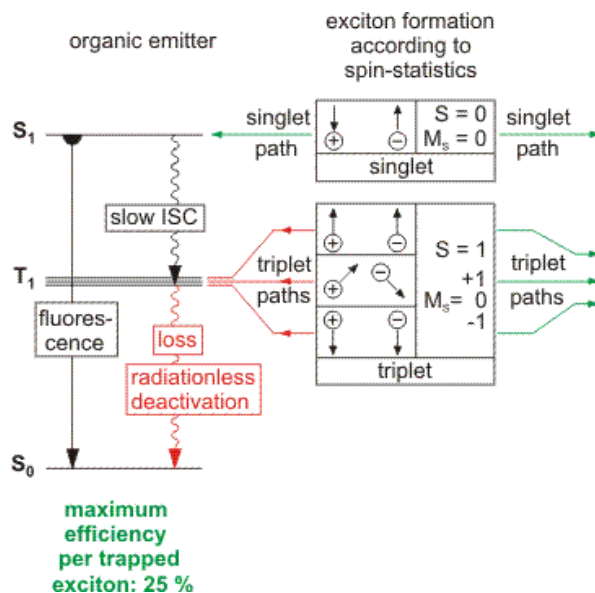
Figure 1.3. *Dynamics of exciton formation. It is assumed that at first the hole (+) is trapped on the doped emitter molecule. The exciton formation starts due to Coulomb interaction between the trapped hole and the electron (–) on a matrix molecule. In the beginning of the exciton formation the spins of hole and electron are already correlated to one singlet and three triplet sub-states. This corresponds in a statistical limit to a ratio of 25 % to 75 %. The S-path and T-paths populate the excited states of the emitter molecule. (Reproduced as such from reference)[6]*

with the use of heavy metals were of serious concern. Even though the performance of green and red phosphorescent emitters were sufficiently good, the blue counterpart was not satisfactory in terms of their combined stability, color purity and brightness during the device operation.[14]
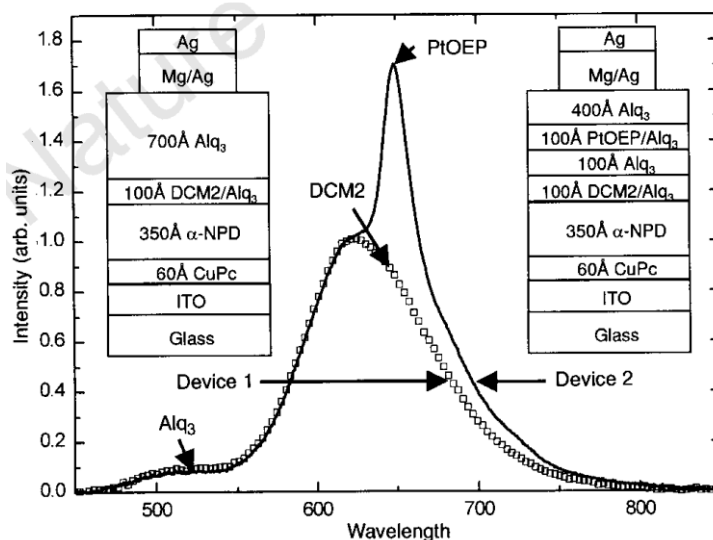
Figure 1.4. *Electroluminescence profile and device configuration[7]*

These difficulties in developing pure blue emitters with phosphorescent materials paved way for the development of new emitters. In 2011 Adachi *et al.*[63] introduced a new strategy for harvesting excitons in OLEDs termed thermally activated delayed fluorescence (TADF). He reported the first purely organic TADF material as emissive layer in an organic LED and achieved an EQE of about 5.3%, reaching the theoretical limit for a fluorescent emitter.[64] Since then, tremendous attention were given to develop TADF materials as effective replacement for phosphorescent materials.[15] Similar to phosphorescent organometallic emitters, purely organic TADF emitters can harvest both singlet and triplet excitions for light emission and hence achieve 100% IQE.[16] One important advantage of TADF emitters is that they are purely organic, thus circumventing most of the problems associated with the use of heavy-metal-based organometallic complexes.[17] TADF relies on a small singlet–triplet energy gap, ΔE_{ST}, defined as the gap between the lowest energy triplet state (T^1) and the lowest energy singlet state (S^1). When ΔE_{ST} is sufficiently small, (<0.1 eV), thermal up-conversion from the triplet state to the singlet state by reverse intersystem-crossing (RISC) becomes possible.[18]

1.3 White organic light emitting diodes

In most of the houses we can still see the usage of incandescent bulbs invented by Thomas Alva Edison. According to reports, the incandescent bulb can only convert 5% of its input energy into light output and 95% of their output energy is emitted in the form of heat.[19] The power efficiency of incandescent lamp is only15 lm/W. Fluorescent tubes took the position as the next generation lights. Even though they showed comparatively good power efficiency of 100 lm/W, they also have some serious drawbacks. The quoted efficiency is for a bare lamp at room temperature. When the lamp is assembled into a finished product such as a luminaire, the efficiencies are greatly reduced to 30–40 lm/W range. Additionally, the lifetimes quoted by suppliers assume the light is operated continuously in an ideal environment (usually stated at 25 ºC, whilst most lights operate far above this temperature). Switching the light on and off, as in a typical residential setting, has been shown to vastly reduce lifetimes of the lights. Another drawback is that the colour-rendering index (CRI) of the fluorescent tubes are very poor leading to visual problems. It is the measure of purity a particular colour with respect to a reference, normally a black body source. Also these fluorescent tubes contain very small amount of mercury that can create some environmental hazards. In the present day scenario

lighting contributes to about 20% of energy consumption with worldwide demand for lighting rapidly increasing, so we need new efficient means for lighting.[19]Organic light emitting diodes were introduced as a meaningful solution to this particular problem. Traditionally, the efficiency of OLEDs is reported as either their external quantum efficiency (EQE) or in candelas per ampere (cd/A). However, lighting sources are usually quoted in terms of power efficiency (or efficacy), i.e., the efficiency taking into account the response of the human eye, which is sensitive to light only in the visible spectrum (ca. 400–700 nm) with a maximum sensitivity to green light (555 nm). Power efficiency is reported in lumens per watt which for the most ideal monochromatic green light source has a maximum value of 683 lm/W. For white light with a CRI of 90 the maximum value is 408 lm/W and for a CRI of 100 it is 240 lm/W. Whilst the white point, or equal energy point, on the CIE chart is defined as (0.33, 0.33) the desired coordinates for lighting fall along the black body curve.

White light emission from an organic light emitting diode can be achieved by 1) combining the emission of RGB emitters, 2) combining monomer excimer emission, 3) ESIPT emitters, 4) combining non-aggregate emission with aggregate emission and 5) incorporating different emitters into one single molecule (Chart 1.2). In literature there are many tutorial reviews on white organic light emitting diodes,[20-23] which will give more vivid figure for the scenario. A detailed discussion in that area is out of the scope of this thesis, so we are presenting only a few examples from selected categories are just mentioned below.
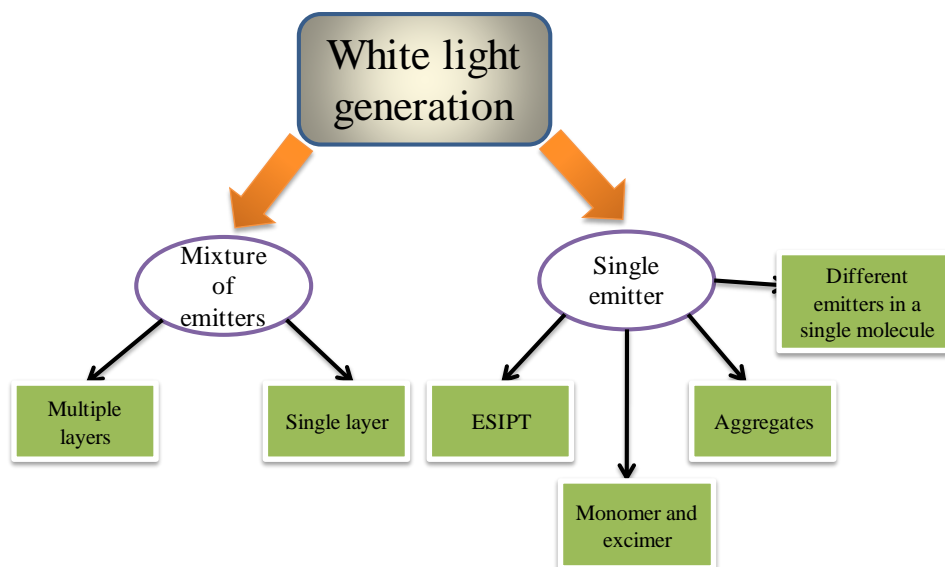
***Chart 1.2.** Different modes for generating white light in organic molecules*

1.3.1 WOLEDs based on multiple layers emitting different colours

In this case, light from three primary colours (red, green, blue) or from two complimentary colours is obtained from different layers of a multilayer device. Each emissive layer is composed of a host material doped with a fluorescent or phosphorescent emitter. Individual emitting layers are physically separated, using in some cases barrier films, in order to prevent interlayer mixing, undesired exciton migration and energy transfer phenomena. White light is harvested from the synchronized emission of stacked layers, provided that the thickness of each individual film and the dopant concentrations are properly adjusted on the basis of the luminescence spectra and efficiency of the single emitters.[24] Chemical and morphological stability of each layer is critical for the device lifetime.

Complexity of the device fabrication, high operating voltages due to large overall thickness and difficulty in controlling the charge transfer process are some major drawbacks of this approach.[22] This approach was used to generate white light from two stacked layers (Figure 1.5) emitting complementary colours composed of the blue iridium(III)[bis(4,6-difluorophenyl)-pyridinato-N,C20] picolinate complex (**FIrpic**) and the orange complex of iridium with the ligand (9,9-diethyl-7-pyridinylfluoren-2-yl)- diphenylamine (IrL3, Figure 1.5b) doped in proper concentration into 1,3-bis(9-carbazolyl)benzene (mCP) and 4,40-N,N0-dicarbazolebiphenyl (CBP) hosts, respectively.[25] The device showed a turn-on voltage of 10 V with CIE coordinates (0.31, 0.41) and a maximum efficiency exceeding 17 cd/A
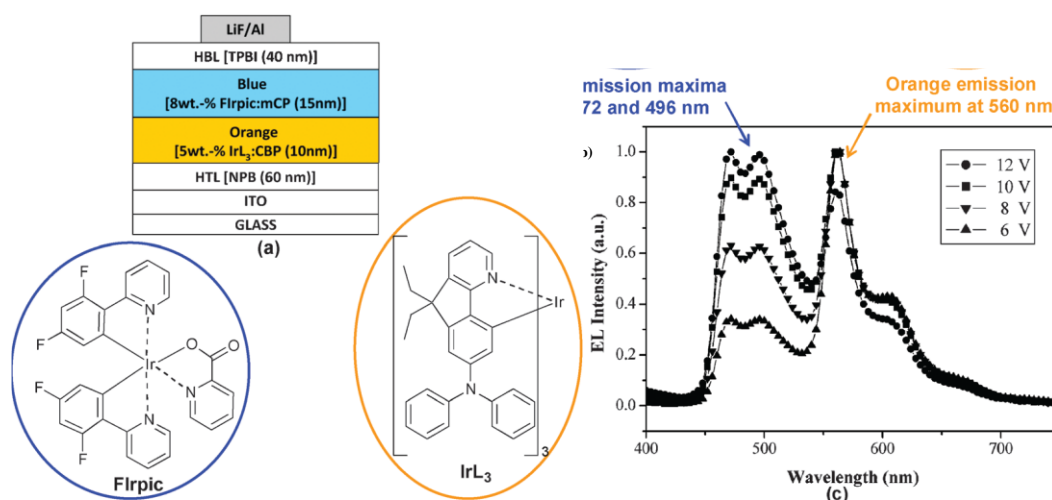
Figure 1.5. *(a) WOLED scheme [TPBI: 2,20,200-(benzene-1,3,5-triyl)-tris-(1-phenyl-1H-benzimidazole); NPB: 4,40-bis[N-(1-naphthyl)-N-phenylamino]biphenyl]. (b) Chemical structures of FIrpic and IrL₃. (c) Electroluminescence spectra at different operating voltages. (Reproduced as such from reference)[25]*

1.3.2. WOLEDs based on multiple emitters mixed in a single layer

WOLEDs based on multiple emitters can be fabricated using two different ways 1) blending polymers with two complementary or three fundamental colours; 2) doping small percentages of one or more molecular emitters in a wide energy gap host that acts as the charge transporting material and, in some cases, as the blue emitting component. This method is in fact very attractive towards low cost WOLED fabrication since it enables the easy processing during fabrication. Proper control over the ratio between different layers and the morphology of emitting layer play critical roles in energy transfer process, thus helping in the optimization of device properties. The main issue here is represented by the possible differential aging of emitters as well as the changes in morphology of the emitting layer (e.g. mixing/de-mixing, aggregation influencing energy transfer processes) that may affect white colour stability.

An example for this approach is WOLED based on a binary blend of two common electroluminescent conjugated polymers: the blue emitting poly(9,9-dioctylfluorene) (**PFO**) and the orange-red emitting poly[2-methoxy-5-(20- ethyl-hexyloxy)-1,4-phenylenevinylene] (**MEH-PPV**) (Figure 1.6).[26] Simultaneous emission from both polymers is ensured by partial inhibition of energy transfer from the blue PFO to the orange-red **MEH-PPV**. This occurs in blends with **MEH-PPV: PFO** composition in the 5–28 wt% range, whose morphology is characterized by phase segregated nano crystalline PFO and amorphous **MEH-PPV** domains, thus limiting the energy transfer processes to the interfaces. At higher **MEH-PPV** concentration the blend is completely amorphous and effective energy transfer from PFO to **MEH-PPV** leads to orange-red electroluminescence only from the **MEH-PPV** polymer. For a given blend composition in the phase segregation range, the emission colour is dependent on the applied voltage: broad white electroluminescence spectrum with luminous efficiency of 3.7 cd/A is achieved for 5 wt% MEH-PPV at 14 V.

1.3.3. WOLEDs based on single molecular emitters forming excimers or electromers

A convenient method to attain white light emission from a single compound is based on chemical species that simultaneously emit blue light from molecular excited states and red-orange light from excited aggregates (excimers or electromers) formed in the solid state or from keto-enol isomers one emitting in the blue region and the other in the orange-red region.
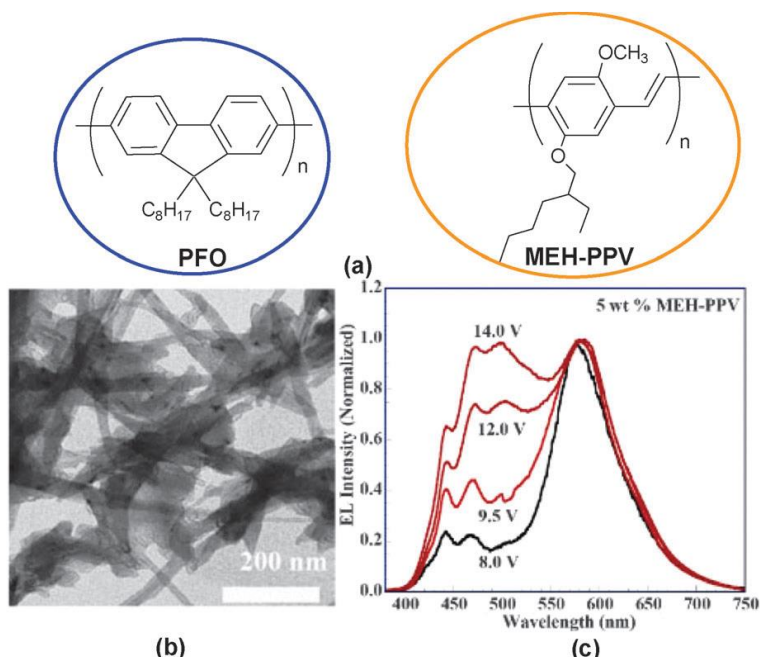
Figure 1.6 *a) PFO and MEH-PPV chemical structures. b) TEM image of 14 wt% MEH-PPV:PFO blend thin film showing phase segregation. c) Electroluminescence of 5 wt% blend device at different bias voltages. (Reproduced as such from the reference)[26]*

White electroluminescence resulting from simultaneous emission of monomers and electromers is observed with the 1,3,5-tris[2-(9-ethylcarbazolyl-3)ethylene]benzene (**TECEB**) emitter in WOLED with structure ITO/**TECEB**(50 nm)/ BCP(10 nm)/Alq$_3$(50 nm)/Mg:Ag.[27] In this case, the formation of electromers is contributed to the white light emission in EL, which was not observed in the case of PL spectra of **TECEB** film. The blue emission peaked at 450 nm, which is similar in both PL and EL spectra and can be attributed to singlet excitons of individual **TECEB** molecules, while the green and red emissions, which are present only in the EL spectra, are likely due to electromers produced in the device by electrical excitation. The luminous efficiency was found to be of 1.1 cd/A.

An example where excimers are used to produce white light is the fused terthiophene compound (3,5-dimethyl-2,6-bis(dimesitylboryl)- dithieno[3,2-b:20,30-d]thiophene) reported in Figure 1.7a, bearing two methyl and two dimesitylboryl substituents, which emits white light when used as the sole electroluminescent material in a simple device architecture (ITO/PEDOT:PSS/light emitting layer/LiF/Al).[28]

10
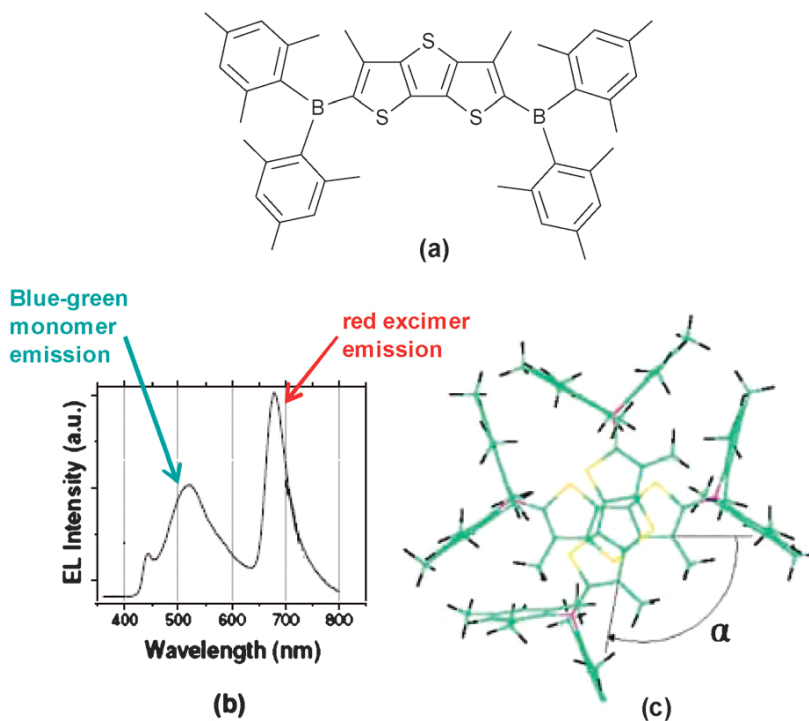
Figure 1.7. *a) Structure of the emitter. b) Electroluminescence spectrum. c) Arrangement of the excimer aggregate involving two molecules in a cross-like disposition[28]*

1.4 Triphenyl amines in organic light emitting diodes

Triphenylamine and its derivatives have received considerable interest in the field of organic light emitting diodes (OLED) as they are excellent hole transport material which constitute one of the essential layer of OLED. Remarkable performance of triphenylamine derivatives as hole transporting materials is attributed to relatively high hole mobility and low ionization potentials. The electro- active site of triphenylamine is the nitrogen centre, which is linked to three phenyl group in a propeller like geometry.

The choice of a donor and acceptor with suitable optical and self-assembly properties is the most important aspect in the design of light emitting diodes. Triphenylamine group is well known for its good hole transporting ability due to the presence of the radical cation species with high stability. It can improve the bulk volume and thermal stability. Its oligomers have been widely investigated for almost two decades because these compounds have shown excellent solubility, thermal and electrochemical stability, electron donating ability and optoelectronic properties. Due to their amorphous film forming ability and their carrier mobility they have been widely used in electroluminescent devices. Organic molecules with

donor acceptor architectures have recently attracted considerable academic and research attention because they generally provide large π electron delocalization over the molecules, which could lead to desirable semiconducting properties for electrical and optoelectronic applications such as in OLEDs.

Ma *et al*[29] developed two novel star shaped compounds (Figure 1.8) in order to obtain highly efficient and stable blue electroluminescence. These compounds are composed of two functional groups, central triphenylamine and peripheral anthracene or phenanthrene which segregate electronic density distribution characteristics between the highest occupied molecular orbital and the unoccupied molecular orbital. In addition to the highly efficient deep blue electroluminescence, they have good stability in OLEDs as a light emitting layer. This triphenylamine based device can reach a quantum efficiency of 7.23% and the lifetime of this device is also improved. The peak maximum of the EL spectra of the **TPA-AN** and **TPA-PA** devices are 468 nm with CIE coordinates at (0.15, 0.07) respectively. In particular, the CIE coordinates of the **TPA-PA** device are close to the blue standard (0.14, 0.08) of the national television standard committee.
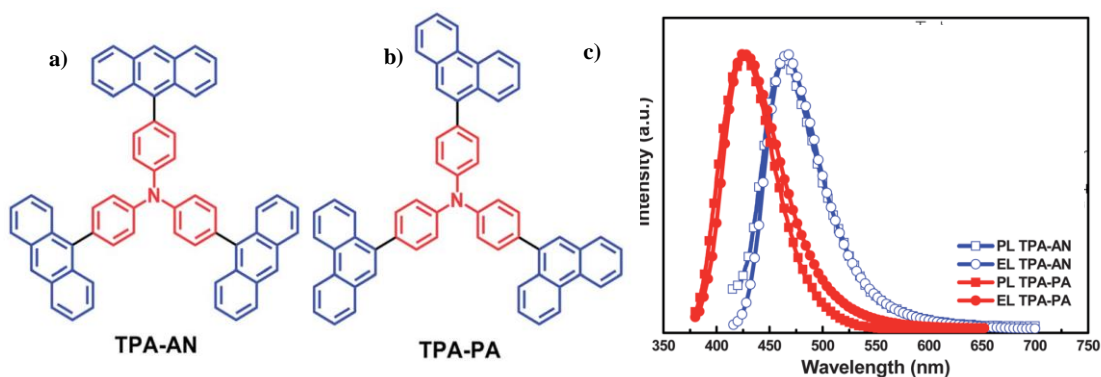
Figure 1.8. *a) The molecular structure for **TPA-AN** and **TPA-PA** b) The normalized PL spectra in films and EL spectra of **TPA-AN** (blue line) and **TPA-PA** (red line)[29]*

Promarak *et al*[30] reported a red EL triphenylamine derivative namely **CAPTB** with benzothiozole and carbazole groups (Figure 1.9a). They fabricated a simple double layer device with device configuration, ITO/PEDOT:PSS/**CAPTB** (spin-coating)/ BCP (40 nm)/ LiF (0.5 nm)/ Al (150 nm). The **CAPTB** spin coating double-layer device exhibited a high λ_{max} of 12,325 cd/m^2 at 15.2 V, a η_{max} of 3.97 cd/A, and a low turn on voltage of 2.2 V, which

is considered to be one of the lowest turn-on voltages for solution processed red and orange-red OLEDs reported.
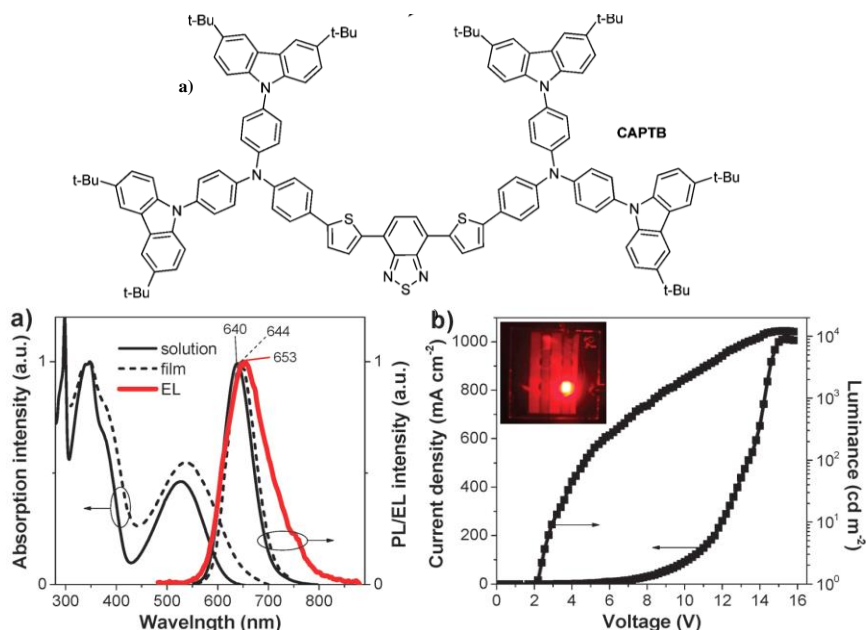
Figure 1.9. *a) Molecular structure for **CAPTB** b) (a) UV-Vis absorption and PL spectra measured in CH_2Cl_2 and as the thin film, and EL spectrum of the OLED. (b) J–V–L characteristics of the OLED device[30]*

Jing Zhang and Yang[31] reported red emission OLEDs based on solution processible organic molecule with TPA as a core and benzothiadiazole – 4 (hexyl)thiophene (**BT-4HT**) as arms. Bi-armed molecule (**TPA-BT-4HT**) and star shaped tri- armed molecule (**TPT-BT-4HT**) both show pure red emission peaked at 646 and 657 nm respectively. The red emission OLED with (**TPA-BT-4HT**) as the emitting layer displayed a higher maximum luminescence of ~ 7794 cd/m^2 and a maximum EL efficiency of 0.91 cd/A. (Figure 1.10)

1.5. Carbazoles in organic light emitting diode

Carbazole is one of the extensively explored molecules in the field of organic light emitting diodes. Generally, they are used as hole transporters and emitters, in the form of oligomers, dendrimers and polymers.[32-34] The ascendancy of carbazole derivatives can be attributed to a number of factors like, 1) in-expensive starting material, (2) the presence of nitrogen atom which can be easily derivatized, (3) possibility of further functionalization(4) aromatic properties that confer stability under a wide range of conditions.[35]The foremost report on

carbazole dates back to 1878.[36]Carbazole was earlier extracted from the anthracene fraction of coal tar.

Carbazoles in the ground state show hydrogen bonds in protic solvents and the dipole moment of carbazole changes from 2 D in ground state to 3.1 D in the excited state.[37] The absorption spectrum of carbazole in methanol is characterized by three weak absorption bands at 335 nm, 323 nm and 294 nm with extinction coefficients around 10^3 L M^{-1} cm^{-1} and three absorption bands at 252 nm, 244 nm and 233 nm with a 10 fold higher extinction coefficient of 10^4 L M^{-1} cm^{-1}.[38]The absorption spectrum in a single-crystal matrix of fluorene at very low temperature (15 K) yields absorption bands at 330 nm, 290 nm, 255 nm, and 230 nm. Carbazole shows a mirror image relationship between absorption and fluorescence with a quantum yield of 0.38. The fluorescence lifetime of carbazole is 15 ns at 77 K in polar EPA (diethyl ether, isopentane and ethanol (5:5:2) solvent.[39] The high triplet energy (3.02 eV) of carbazole makes it a good host material.[40]A phosphorescence lifetime of 7.7 s was determined at 77 K in polar EPA.[41]The phosphorescence is influenced by the direct spin-orbit coupling mechanism to 1B2 ground state.[41] The electrochemical behavior of carbazole was thoroughly reviewed by Karonand Lapkowski.[42] Nascent carbazole exhibits one-electron oxidation with a potential of 1.2 eV vs SCE. The oxidation leads to dicarbazyls and is sensitive to pH. The cation is unstable unless the nitrogen as well as positions 3 and 6 of the ring system are blocked.[43] The importance of carbazoles in organic light emitting diodes is very evident from the large number of publications. A detailed discussion about the different carbazole derivatives used in OLEDs can be obtained from the tutorial review of Kafarani *et al.*[34]

 In the current scenario of research, the carbazole derivatives are attaining great interest mainly because of 1) small $\Delta E_{ST,}$ 2) intrinsic spin orbit coupling and 3) the susceptibility to show delayed fluorescence. Uoyama *et al.*[44] realized a series of TADF materials (Figure 1.10) based on carbazole (donor) and dicyanobenzenes (acceptor) where the HOMO and LUMO of the molecules are localized on each part separately with an observed small ΔE_{ST}.

Increasing the power efficiency of a device is achieved by decreasing the drive voltage. Seino *et al.* were able to utilize **4CzIPN** to create a device designed with carrier- and exciton confinement combined with energy transfer from an exciplex which resulted in a green OLED

with high power efficiency of over 100 lm/W. This performance is comparable to PHOLEDs containing iridium-based emitting species.[45]
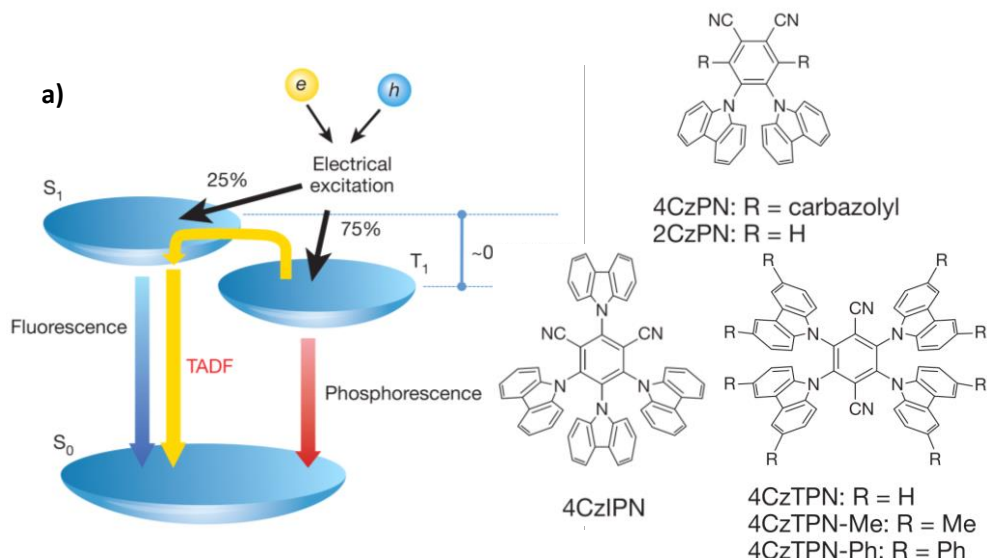
Figure 1.10. *Energy diagram and molecular structures of **CDCBs**. a, Energy diagram of a conventional organic molecule. b, Molecular structures of CDCBs. Me, methyl; Ph, phenyl. (Reproduced from the original report)*[44]

Wang *et al.*[46] reported **4CzIPN** (Figure 1.11) and utilized this material to provide evidence that the mechanism of electroluminescence of devices based on **4CzIPN** is based on the recombination of injected carriers in the (near) absence of energy transfer processes. On the other hand, Kim *et al.*[47] utilized **4CzIPN**, which has a deep lying HOMO level, to create a solution-based simplified OLED device. The integration of a deep HOMO level buffered material hole injection layer, which due to its self-assembly process has an increasing work function as well as an engineered emission layer which avoids exciton quenching. (Figure 1.11)
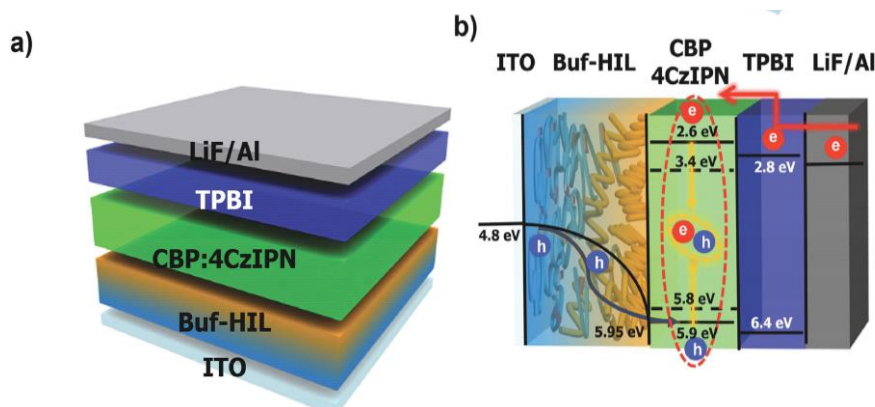
Figure 1.11. *a) Solution-processed **4CzIPN**-based OLED structure using Buf-HIL and b) energy level diagram of 4CzIPN-based OLEDs. (Reproduced as such from the reference)*[46]

Kretzschmar *et al*[48] synthesized mono and dihalogenated derivatives of TADF fluorophors **4CzIPN-Me** and **4CzTPN** and derived materials of low singlet triplet gap of ~0.04 eV (experimentally determined), fluorescence lifetimes combined with improved ISC due to heavy-atom effects of the halogens.[94] Reduced operational stability observed in TADF devices may be due to the long-lived triplet energy species leading to unwanted chemical reactions. Reduced operational stability observed in TADF devices may be due to the long-lived triplet energy species leading to unwanted chemical reactions. Devices that include an assistant dopant exhibited increased operational lifetime (time at which luminance drops to 0.5 of initial luminance). Furukawa *et al*[49] incorporated an assistant dopant (**4CzIPN-Me)** with large k_{isc}~10 along with an emitting species TBRb (Figure 1.12). This mixture showed an operational time of 1,472 hours, thus proving that, the device stability could be achieved with the help of assistant fluorophores with even shorter triplet lifetimes.
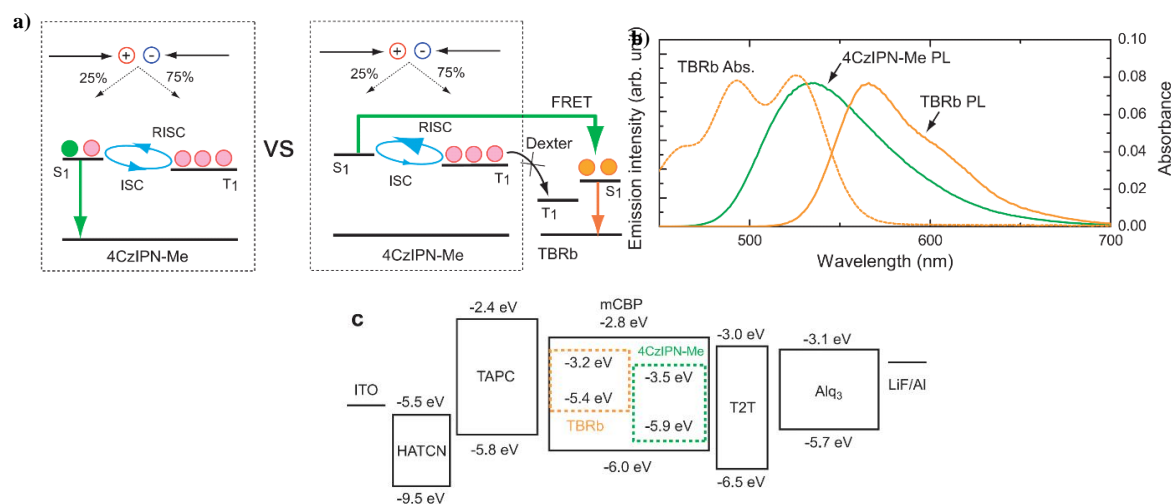
Figure 1.12. *(a) Schematic illustration of the conceived energy transfer mechanism for the 4CzIPN-Me (assistant dopant):TBRb (fluorescent emitter) system under electrical excitation (right). The left figure shows a conventional energy diagram for 4CzIPN-Me as emitter. (b) PL spectra of a 11 mol%-4CzIPN-Me:mCBP co-deposited film and TBRb solution (CH$_2$Cl$_2$, 1025 mol L21). The dashed line indicates the absorption spectrum of the TBRb solution. The Fö̈rster radius was obtained from the overlap of the PL spectrum of the exciton donor and the absorption spectrum of the exciton acceptor based on the assumptions of random molecular orientation and a refractive index of 1.8 for the mCBP medium. (c) Energy diagram of the OLEDs used in this work. (Adapted from reference)[49]*

Cho *et al.*[50] prepared materials for solution-processable TADF approaches by inclusion of methyl groups and *t*-butyl groups in positions 3,6 on each of the four carbazole substituents of the **4CzIPN** emitter leading to new materials **m4CzIPN** and **t4CzIPN**. The *t*-butyl groups led

to increased solubility and stabilized film morphologies. Devices were prepared via both the solution and the vacuum processing techniques. (Figure 1.13)
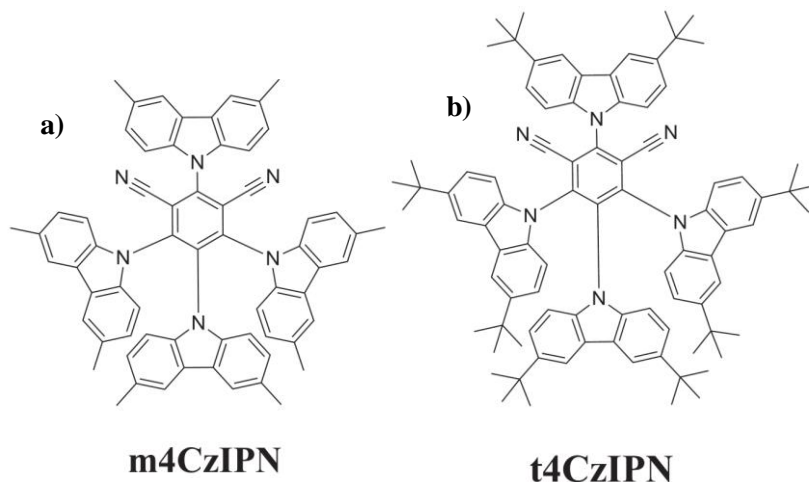
Figure 1.13. *Molecular structures of **m4CzIPN** and **t4CzIP** [50]*

Carbazole-based TADF materials have been utilized for WOLED applications.[51-55] hybrid white organic light-emitting diode (WOLED) with an external quantum efficiency above 20% was developed using a blue thermally activated delayed fluorescent material, 4,6-di(9H-carbazol-9-yl)isophthalonitrile (**DCzIPN**). **DCzIPN** showed high quantum efficiency of 16.4% as a blue emitter and 24.9% as a host for a yellow phosphorescent emitter. The hybrid WOLEDs exhibited high external quantum efficiency of 22.9% with a warm white color coordinate of (0.39, 0.43).[56]
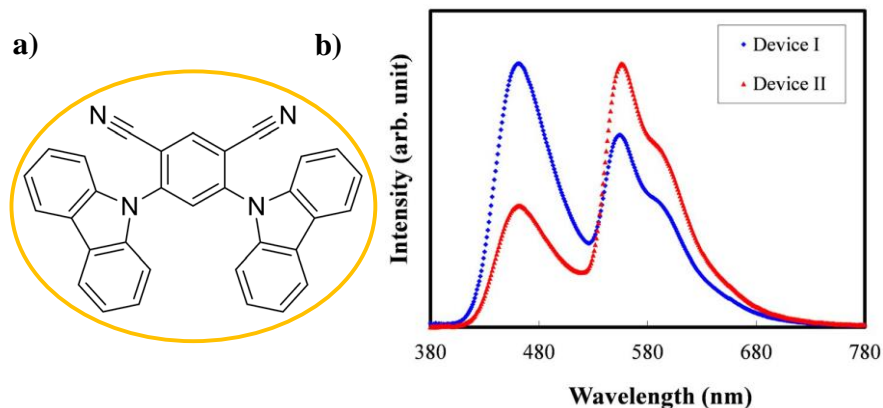
Figure 1.14. *a) Molecular structure for **DCzIPN** b) EL spectrum for the hybrid WOLED[56]*

Lee *et al.*[57] introduced two carbazole derivatives by incorporating benzothiophene (**BTCz-2CN**) and benzofuran (**BFCz-2CN).** This material showed an efficiency of 12% at a doping concentration of 1%. (Figure 1.15)
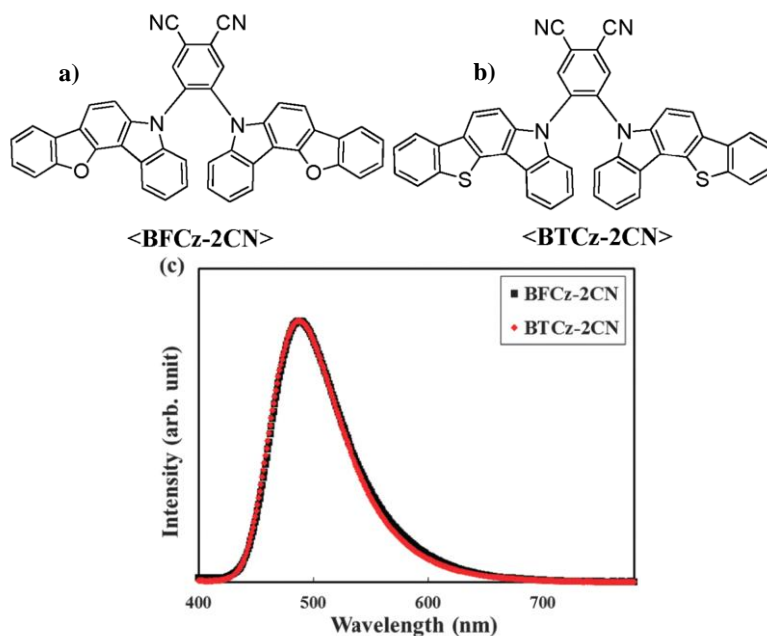
Figure 1.15. *a) Molecular structure for **BFCz-2CN** b) Molecular structure for **BTCz-2CN***

Zang *et al* reported blue emitters with thermally activated delayed fluorescence (TADF) which is having the potential to achieve 100% internal quantum efficiency. But, unluckly, strategies to design and develop stable blue TADF emitters remains unexplored. Here, the high efficiency and improved stability are achieved simultaneously for blue or sky blue TADF emitters through a wise design of molecular structures using tert-butyl units. The tertbutyl substituents acts like a shield surrounding the luminance core, not only promoting the photoluminance efficiency, but also improving the stability of the compounds. Consequently, device with the sterically shielded emitter achieves a maximum external quantum efficiency as high as 21.2% and a record long T50 (time to 50% of initial luminance) of 770 h at an initial luminance of 500 cd/m^2 , corresponding to a half lifetime of 12,873 h at 100 cd/m^2 .[58] (Figure 1.16)

Cho *et al*[59] initiated a blue-emitting TADF material **5CzCN** for both vacuum and solution processing. In this molecule benzonitrile was acted as the acceptor unit with five carbazole donor units. The device showed a maximum external quantum efficiency of 19.7% and 18.7% in vacuum deposited and solution processed TADF devices, respectively. (Figure 1.17)
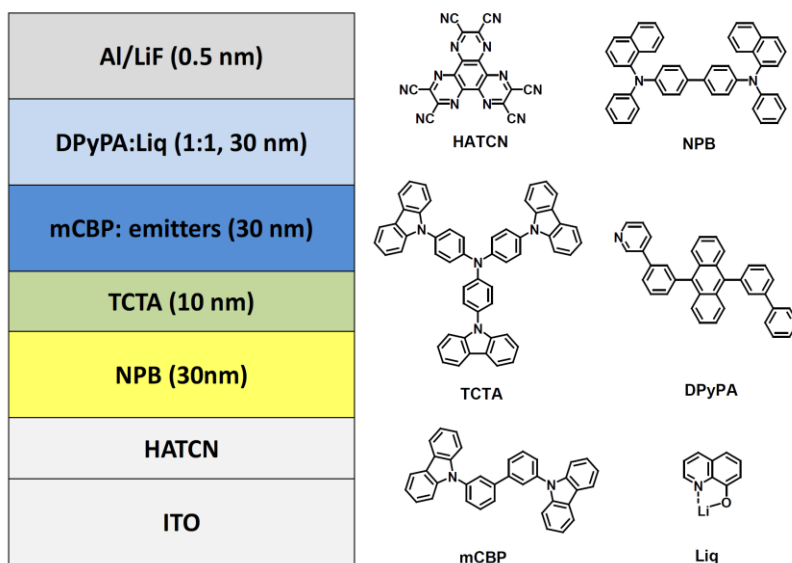
Figure 1.16. *Device configuration and molecular structure for the materials used[58]*
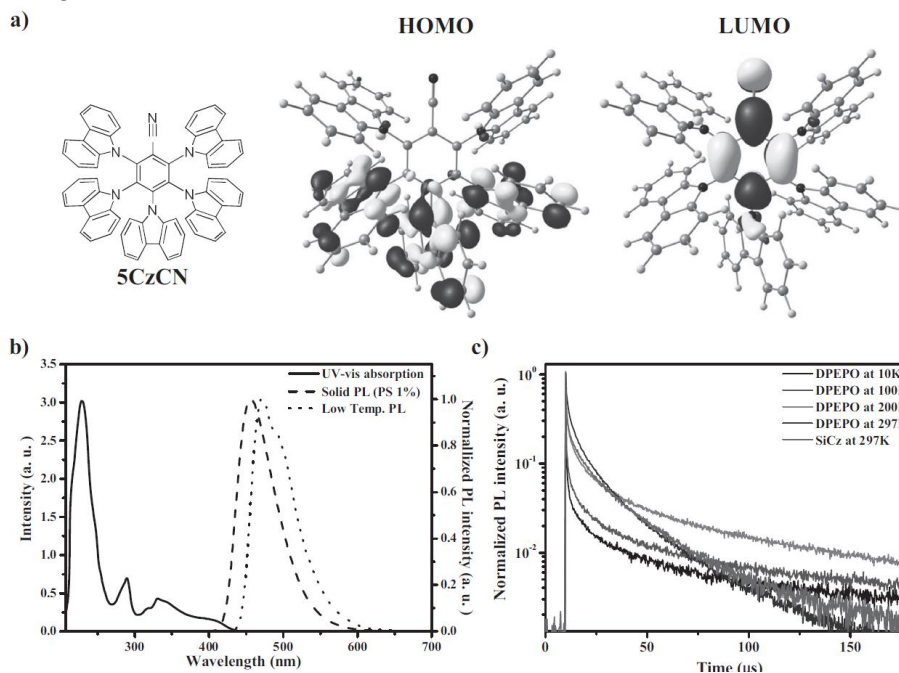
Figure 1.17. *a) Chemical structure and Gaussian simulation images. b) UV–vis absorption and PL emission spectra of **5CzCN**. c) Transient PL spectra of 5CzCN doped DPEPO and SiCz films according to temperatures[59]*

Rajamalli utilized benzoylpyidine (BP) building block with carbazole units.[60,61] Specifically, **mDCBP** exhibited mechano- and piezochromism.[61] Four devices were prepared with 10-30 wt% **mDCBP** in DPEPO. The blue emitter reached an external quantum efficiency of 18.4% as reported. In addition, Rajamalli *et al.* included two nascent or two *t*-butylcarbazole donor units on the meta- and *ortho* carbons of the benzoylpyridines acceptor, i.e. *para* to each other, to create **DCBPy** and **DTCBPy** (Figure 1.18). Herein, the group applied the concept of intra-

molecular space interactions between the donor and acceptor units to create molecules with small ΔE_{ST} of 0.03 and 0.04 eV and EQE of above 24%.[60]
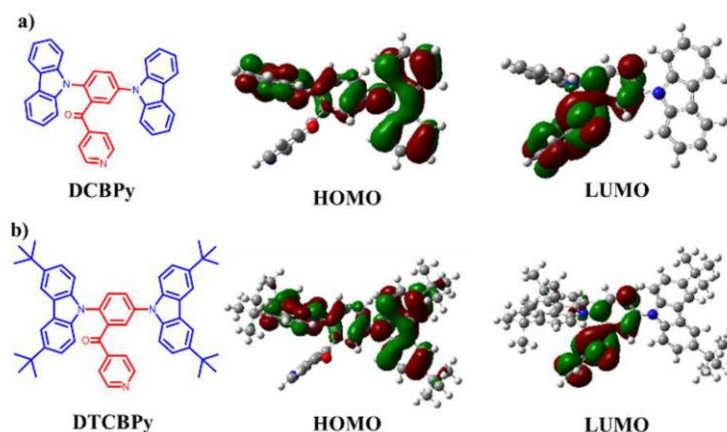
Figure 1.18. *The structures and molecular orbitals of a) **DCBP** and b) **DTCBPy**[60]*

Lee *et al.*[62] prepared a tetramethylated carbazole-unit linked to xanthon entitled **MCz-XT** along with a series of xanthon-based TADF materials to address the Dexter energy transfer that is the predominating factor for concentration quenching in TADF materials. In Dexter energy transfer, triplet excitons interact via electron-exchange interactions of triplet excitons, whereby a minimal modulation of the molecular geometry in the emitter allows to suppress quenching.
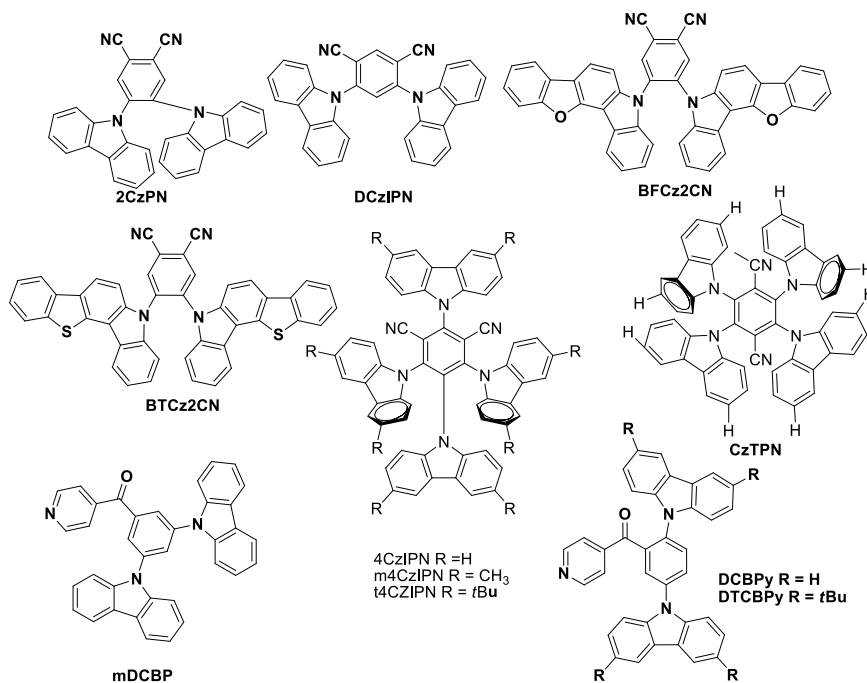
1.6 Definition of the problem

Design and synthesis of novel small organic molecules for OLED have been the subject matter of intense research from the pioneering work by Tang and VanSlyke. The organic small molecules place themselves above to the conventional phosphorescent emitters or polymeric substances with their 1) easy procassibility 2) low cost 3) tunable energy and 4) easy functionalization. High efficient organic light emitting diodes can be achieved by proper molecular design and also by choosing appropriate molecular cores. Molecules like triphenylamines, carbazoles, etc have been extensively studied for developing new efficient donor-acceptor systems for new generation OLED, which is one of the prime concerns of present-day energy conservation research. Hence, the objective of the present thesis is to design, synthesize and investigate on the photophysical, thermal, electrochemical and electroluminescent properties of some novel donor-acceptor molecules as future emitters in OLEDs. We have chosen triethylamine and carbazole as the core molecules for designing donor-acceptor systems based on their advantageous properties for OLED applications. Their synthesis, characterization, photophysical and electroluminescence studies are the subject matter of this thesis. The device properties of the molecules synthesized as emitters or as host molecules are also discussed.

1.7 Reference

1. Tang, C. W.; Vanslyke, S. A. Organic Electroluminescent Diodes. *Appl. Phys. Lett.* **1987**, *51* (12), 913–915.

2. Chen, H.; Lee, J.; Lin, B.; Chen, S.; Wu, S. Liquid Crystal Display and Organic Light-Emitting Diode Display : Present Status and Future Perspectives. *Nat. Publ. Gr.* **2018**, *7* (3), 17113–17168.

3. Fu, H.; Cheng, Y.; Chou, P.; Chi, Y. Feeling Blue ? Blue Phosphors for OLEDs. *Mater. Today* **2014**, *14* (10), 472–479.

4. Pope, M.; Kallmann, H. P.; Magnante, P. Electroluminescence in Organic Crystals. *J.Chem.Phys*.**1963**, 38(8), 2042-2043.

5. Huang, T.; Jiang, W.; Duan, L. Recent Progress in Solution Processable TADF Materials for Organic Light-Emitting Diodes. *Journal of Materials Chemistry C*. **2018**, 6(21), 5577-5596

6. Yersin, H. Triplet Emitters for OLED Applications . Mechanisms of Exciton Trapping and Control of Emission Properties. *Top Curr. Chem.* **2004**, *241* (2), 1–26.

7. Baldo, M. A.; Forrest, S. R. Highly Efficient Phosphorescent Emission from Organic Electroluminescent Devices. *Nature* **1998**, *395* (September), 151–154.

8. Impurity, A. J.; Baldo, M. A.; Thompson, M. E.; Forrest, S. R. High-Efficiency Fluorescent Organic Light-Emitting Devices Using a Phosphorescent Sensitizer. *Nature* **2000**, *403* (February), 1998–2001.

9. Adachi, C.; Baldo, M. A.; Thompson, M. E.; Forrest, S. R.; Adachi, C.; Baldo, M. A.; Thompson, M. E.; Forrest, S. R. Nearly 100 % Internal Phosphorescence Efficiency in an Organic Light Emitting Device. *J. Appl. Phys.* **2001**, 90 (10), 5048.

10. Xiao, L.; Chen, Z.; Qu, B.; Luo, J.; Kong, S.; Gong, Q. Recent Progresses on Materials for Electrophosphorescent Organic Light-Emitting Devices. *Adv. Mater.* **2011**, 23 (8), 926–952.

11. V. A.; Ho, C.; Wong, W. Small-Molecular Blue Phosphorescent Dyes for Organic Light-Emitting Devices. *New J.Chem*. **2013**, 37(6), 1665–1683.

12. Sasabe, H.; Kido, J. Recent Progress in Phosphorescent Organic Light-Emitting Devices. *Eur. J. Org. Chem.* **2013**, 36(34), 7653–7663.

13. Yook, K. S.; Lee, J. Y. Organic Materials for Deep Blue Phosphorescent Organic Light-Emitting Diodes. *Adv. Mater*. **2012**, 24(24), 3169–3190.

14. Lee, J.; Chen, H.; Batagoda, T.; Coburn, C.; Djurovich, P. I.; Thompson, M. E.; Forrest, S. R. Deep Blue Phosphorescent Organic Light-Emitting Diodes with Very High Brightness and Efficiency. *Nat. Mater.* **2016**, *15* (January), 92–99.

15. Liu, Y.; Li, C.; Ren, Z.; Yan, S.; Bryce, M. R. All-Organic Thermally Activated Delayed Fluorescence Materials for Organic Light-Emitting Diodes. *Nature review materials*, **2018,** 18020 (2018), 1-20.

16. Im, Y.; Kim, M.; Cho, Y. J.; Seo, J.; Yook, K. S.; Lee, J. Y. Molecular Design Strategy of Organic Thermally Activated Delayed Fluorescence Emitters. *Chem.Mater.***2017,** 29(5), 1946-1963.

17. Wong, M. Y.; Zysman-colman, E. Purely Organic Thermally Activated Delayed Fluorescence Materials for Organic Light-Emitting Diodes. Adv. Mater.**2017**, 29(22), *1605444 (1-54)*.

18. Dias, F. B.; Penfold, T. J.; Monkman, A. P. Photophysics of Thermally Activated Delayed Fluorescence Molecules. *Methods Appl. Fluoresc*.**2017**, 23(280), 1-19.

19. Tyan, Y. Organic Light-Emitting-Diode Lighting Overview. *J.Photonics for energy*, **2018,** 1(1), 011009 (1-15).

20. Thomschke, M.; Lüssem, B.; Leo, K.; Reineke, S.; Leo, K.; Thomschke, M. White Organic Light-Emitting Diodes : Status and Perspective. *Rev. Mod. phsics* **2014**, *85* (4), 1245–1293.

21. Chang, Y.; Lu, Z. White Organic Light-Emitting Diodes for Solid-State Lighting. *J. Disp. Technol.* **2013**, *9* (6), 459–468.

22. Andrade, B. B. W. D.; Forrest, S. R. White Organic Light-Emitting Devices for Solid-State Lighting. *Adv. Mater.* **2004**, *16* (18), 1585–1595..

23. Farinola, G. M.; Ragni, R. Electroluminescent Materials for White Organic Light Emitting Diodes. *Chemical Society Reviews*. 2011, pp 3467–3482.

24. Andrade, B. B. W. D.; Thompson, M. E. Controlling Exciton Diffusion in Multilayer White Phosphorescent Organic Liht Emitting Devices. *Adv. Mater.* **2002**, *14* (2), 147–151.

25. Yu, X.; Kwok, H.; Wong, W.; Zhou, G.; May, R. V; Re, V.; Recei, M.; August, V. High-Efficiency White Organic Light-Emitting Devices Based on a Highly Amorphous Iridium (III) Orange Phosphor. *Chem.Mater.* **2006**, 18(21), 5097–5103.

26. Zhen, H.; Xu, W.; Yang, W.; Chen, Q.; Xu, Y.; Jiang, J.; Peng, J.; Cao, Y. White-Light Emission from a Single Polymer with Singlet and Triplet Chromophores on the Backbone. *Macromol. Rapid Commun.* **2006**, 27(24), 2095–2100.

27. Jiu, B.; Li, Y.; Liu, D.; Ma, C.; Lengyel, O.; Lee, C.; Tung, C.; Lee, S. White-Light Emission from a Single-Emitting-Component Organic Electroluminescent Device. *Adv. Mater.* **2004**, *16* (17), 15–18.

28. Mazzeo, B. M.; Vitale, V.; Sala, F. Della; Anni, M.; Barbarella, G.; Favaretto, L.; Sotgiu, G.; Cingolani, R. Bright White Organic Light-Emitting Devices from a Single Active Molecular Material. **2005**, 17(1), 34–39.

29. Shi Tang, Weijun Li, Fangzhong Shen, Dandan Liu, Bing Yang and Yuguang Ma. Highly Efficient Deep-Blue Electroluminescence Based on the Triphenylamine- Cored and Peripheral Blue Emitters with Segregative HOMO – LUMO. *J. Mater. Chem.* **2012**, *22* (3), 4401–4408.

30. Online, V. A.; Khanasa, T.; Prachumrak, N.; Rattanawan, R.; Jungsuttiwong, S.; Keawin, T.; Sudyoadsuk, T.; Tuntulani, T.; Promarak, V. An Efficient Solution Processed Non-Doped Red Emitter Based on Carbazole–triphenylamine End-Capped Di(thiophen-2-Yl)benzothiadiazole for Pure Red Organic Light-Emitting Diodes. *Chem.Comm.* **2013**, 49(33), 66–68.

31. Jing, Z.; Yi, Y.; Chang, H. E.; Yongfang, L. I. Red-Emission Organic Light-Emitting Diodes Based on Solution-Processable Molecules with Triphenylamine Core and Benzothiadiazole-Thiophene Arms. *Science China*, **2011**, *54* (4), 695–696.

32. Jiang, H.; Sun, J.; Zhang, J. A Review on Synthesis of Carbazole-Based Chromophores as Organic Light-Emitting Materials. *Current organic chemistry*, **2012**, 16(17), 2014–2025.

33. Derivatives, T.; Lozano-hern, L.; Maldonado, J.; Garcias-morales, C. Efficient OLEDs Fabricated by Solution Process Based. *Molecules,* 2018, 23(2), 280 (1–19).

34. Wex, B; Kaafarani, B.R. A. Perspective on Carbazole- Based Organic Compounds as Emitters and Hosts in TADF Applications. *J. Mater. Chem. C.* **2017**, 5(34), 8622-8653 .

35. Blouin, N.; Leclerc, M. Poly(2,7-Carbazole)s: Structure - Property Relationships. **2008**, *41* (9), 1–10.

36. Yunker, M. B.; Macdonald, R. W. Composition and Origins of Polycyclic Aromatic Hydrocarbons in the Mackenzie River and on the Beaufort Sea Shelf. *Arctic* **1995**, *48* (2), 118 –129.

37. Kadiri, B. B. A. Etude Du Complexe Par Liaison Hydrogtine Du Carbazole G Mat Fondamental Par Spectroscopic UV. **1992**, *48* (5), 733–741.

38. Branch, E. K. The Absorption Spectra of Some N-Substituted P-Aminotriphenylmethyl Ions. *J. Am. Chem. Soc.* **1951**, *73* (1), 3341–3348.

39. Johnson, E.; Johnson, E. A Spectroscopic Study of Carbazole by Photoselectionl. J.Phys.Chem. **1974,** 78(15), 1512-1521.

40. Tsai, B. M.; Lin, H.; Su, H.; Ke, T.; Wu, C.; Fang, F.; Liao, Y.; Wong, K.; Wu, C. Highly Efficient Organic Blue Electrophosphorescent Devices Based on 3 , 6-Bis (Triphenylsilyl) Carbazole as the Host Material. Adv.Mater. **2006**, 18(9), 1216–1220.

41. Huber, B. J. R.; Adams, J. E. Effect of Molecular Geometry on the Electronic Structure of Aromatic Amines : *Berichte der Dtsch. Chem. Gesellschaft* **1974**, *2* (4), 217–308.

42. Karon, K.; Lapkowski, M. Carbazole Electrochemistry : A Short Review. *J. Solid state electrochem.* **2015**, 19(9),2601–2610.

43. Carbazole, I.; Derivatives, N.; Ambrose, J. F.; Nelson, R. F. Anodic Oxidation Pathways of Carbazoles. *J. electrochem. Soc.* 1968, 7–12.

44. Uoyama, H.; Goushi, K.; Shizu, K.; Nomura, H.; Adachi, C. Highly Efficient Organic Light-Emitting Diodes from Delayed Fluorescence. *Nature* **2012**, *492* (7428), 234–238.

45. Seino, Y.; Inomata, S.; Sasabe, H.; Pu, Y.; Kido, J. High-Performance Green OLEDs Using Thermally Activated Delayed Fluorescence with a Power Efficiency of over 100 Lm W − 1. **2016**, 2638–2643.

46. Wang, P.; Zhao, S.; Xu, Z.; Qiao, B.; Long, Z. The Electroluminescence Mechanism of Solution-Processed TADF Emitter 4CzIPN Doped OLEDs Investigated by Transient Measurements. *Molecules* **2016**, *1365* (21), 1–6.

47. Liu, Q.; Luedtke, N. W.; Tor, Y. A Simple Conversion of Amines into Monosubstituted Ureas in Organic and Aqueous Solvents. *Tetrahedron Lett.* **2001**, *42* (8), 1445–1447.

48. Kretzschmar, A.; Patze, C.; Schwaebel, S. T.; Bunz, U. H. F. Development of Thermally Activated Delayed Fluorescence Materials With Shortened Emissive Lifetimes Development of Thermally Activated Delayed Fluorescence Materials With Shortened Emissive Lifetimes. *J.Org.Chem.* **2015,** 80(18), 9126-9131.

49. Furukawa, T.; Nakanotani, H.; Inoue, M.; Adachi, C. Dual Enhancement of Electroluminescence Efficiency and Operational Stabilit B Rapid Upconversion of Triplet Excitons in OLEDs. *Sci. Rep.* **2015**, *5* (8429), 1–8.

50. Cho, Y. J.; Yook, K. S.; Lee, J. Y. High Efficiency in a Solution-Processed Thermally Activated Delayed-Fluorescence Device Using a Delayed- Fluorescence Emitting Material with Improved Solubility. *Adv. Mater.* **2014**, *26* (38), 6642–6646. https://doi.org/10.1002/adma.201402188.

51. Korea, S.; Korea, S.; Korea, S.; Korea, S. Energy Transfer Process in White Organic Light-Emitting Devices Based on Material. **2018**, *8* (7), 1833–1840.

52. Liu, W.; Zheng, C.; Wang, K.; Zhang, M.; Chen, D.; Tao, S.; Li, F.; Dong, Y.; Lee, C.; Ou, X.; et al. High Performance All Fluorescence White Organic Light Emitting Devices with a Highly Simpli Fi Ed Structure Based on Thermally Activated Delayed Fluorescence Dopants and Host. *ACS.Appl.Mater.Interfaces*, **2016**, 8(48), 32984-32991.

53. Zhang, D.; Cai, M.; Zhang, Y.; Zhang, D.; Duan, L.; Accepted, J. Highly Efficient Simplified Single-Emitting-Layer Hybrid WOLEDs with Low Roll-off and Good Color Stability Transfer through Enhanced Förster Energy. *ACS.Appl.Mater.Interfaces,***2015, 7**(51), 28693-28700.

54. Lee, H.; Lee, J.; Yi, Y.; Cho, S. W.; Kim, J. W.; Lee, H.; Lee, J.; Yi, Y.; Cho, W.; Kim, J. W. Anomalous Hole Injection Deterioration of Organic Light-Emitting Diodes with a Manganese Phthalocyanine Layer Anomalous Hole Injection Deterioration of Organic Light-Emitting Diodes with a Manganese Phthalocyanine Layer. *J.Appl.Phys.* **2015**, 117(3), *035503*(8–13).

55. Zhang, D.; Duan, L.; Li, Y.; Zhang, D.; Qiu, Y. Highly Efficient and Colour Stable Hbrid Warm White Organic Light-Emitting Diodes Using a Blue Material with Thermally Activated Delayed Fluorescence. *J. Mater. Chem. C Mater. Opt. Electron. devices* **2014**, 2(38), 8191–8197.

56. Cho, Y. J.; Yook, K. S.; Lee, J. Y. Cool and Warm Hybrid White Organic Light-Emitting Diode with Blue Delayed Fluorescent Emitter Both as Blue Emitter and Triplet Host. *Sci. Rep.***2015***, 5(7859), 1-7

57. Ito, J.; Takaya, Y.; Oshima, Y.; Niwa, M. New Oligostilbenes Having a Benzofuran from Vitis Vinifera "Kyohou."*Tetrahedron* **1999**, *55* (9), 2529–2544.

58. Dongdong Zhang, Minghan Cai, Yunge Zhang, D. Z. and L. D. Sterically Shielded Blue Thermally Activated Delayed Fluorescence Emitters with Improved Efficiency and Stability. *Mater. Horizons* **2016**, *3* (2), 145–151.

59. Cho, Y. J.; Jeon, S. K.; Lee, J. Y. Molecular Engineering of High Effi Ciency and Long Lifetime Blue Thermally Activated Delayed Fluorescent Emitters for Vacuum and Solution Processed Organic Light-Emitting Diodes. *Adv. Opt. Mater.* **2016**, *10* (4), 688–693.

60. Rajamalli, P.; Senthilkumar, N.; Gandeepan, P.; Huang, P.; Huang, M.; Yang, C.; Chiu, M.; Chu, L.; Lin, H.; Cheng, C.; et al. A New Molecular Design Based on Thermally Activated Delayed Fluorescence for Highly Efficient Organic Light Emitting Diodes A New Molecular Design Based on Thermally Activated Delayed Fluorescence for Highly Efficient Organic Light Emitting Diodes. *J.Am.Chem.Soc.***2016,** 130(2) 628-634.

61. Pachaiyappan Rajamalli, Natarajan Senthilkumar, Parthasarathy Gandeepan, Chen-Zheng Ren-Wu, H.-W. L. and C.-H. C. A Thermally Activated Delayed Blue Fluorescent Emitter with Reversible Externally Tunable Emission. *J. Mater. Chem. C* **2016**, *4* (5), 900–904.

62. Lee, J.; Aizawa, N.; Numata, M.; Adachi, C.; Yasuda, T. Versatile Molecular Functionalization for Inhibiting Concentration Quenching of Thermally Activated Delayed Fluorescence. *Adv. Mater.* **2016**, *16* (8), 1–6.

Design, synthesis and photophysical investigation of triphenylamine derivatives as RGB emitters for white light applications and their electroluminescence studies
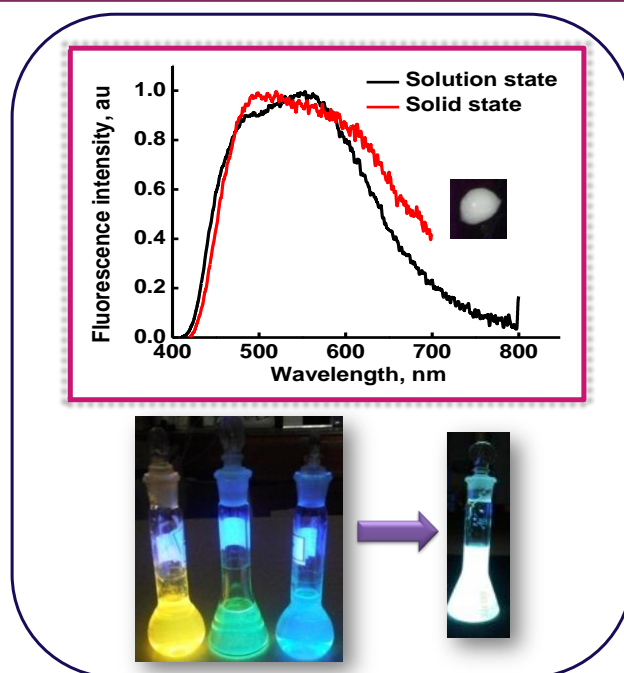
2.1 Abstract

*A set of three triphenylamine-bithiophene based Donor-Acceptor (D-A) molecules viz. **TPT**, **TPT-Ben** and **TPT-Ac** were designed, synthesized and studied for their photophysical properties. Systematic density functional theory (DFT) calculations have been performed on the synthesized molecules to gain insights into the structural, electronic and optical properties. The nanosecond transient absorption spectra of the molecules showed broad absorptions due to the presence of triphenylamine radical cation, with an average time constant of 3.5 µs. The **TPT, TPT**-**Ben** and **TPT-Ac** were found to emit in the blue, green and orange-red regions*

*respectively of the visible spectrum due to the differences in their Stokes shift values. Upon excitation at λ_{max} 400 nm, a 3:2:1 mixture by weight of **TPT**, **TPT-Ben** and **TPT-Ac** emitted at the white light region even at μM level concentration the solution state (DMSO) and in the solid state with colour coordinates (0.32,0.36) and (0.33,0.37) respectively. Both **TPT-Ben** and **TPT-Ac** showed device properties and the OLED fabricated with **TPT-Ben** showed green electroluminescence, while the one with **TPT-Ac** showed a pale yellowish white colour.*

2.2 Introduction

Design and development of functional materials for strategic materials, energy generation, storage conservation and for a host of applications to deal with contemporary problems are hot areas of research worldwide. Among different molecules very often used for developing functional materials, triphenylamine (TPA) derivatives enjoy an upper hand as modern electro-active functional materials showing semiconducting properties and as two-photon absorption probe. Many reviews and reports discussing the importance of TPA derivatives for different applications are available in the literature.[1-13] High demand for the TPA derivatives originates from its characteristics like semi-conducting properties,[14] propeller like structure, high hole-mobility,[15] easy crystallization,[16] thermal stability, photo and electroluminescent.

TPA derivatives, due to its two-photon absorption ability find applications in 3D microfabrication.[17,18] Since its inception less than a decade ago, the field of multi-photon fabrication has progressed rapidly, and multi-photon techniques are now being used to create functional micro-devices. Another prominent areas where TPA derivatives find application due to the two photon absorption property is the two-photon bio-imaging[19-21] and optical data storage.[22,23] Excellent semi-conducting properties, high hole mobility and thermal stability enabled them to become the best candidates for organic photovoltaics applications[24-26] and hole transporting materials in OLEDs.[27-33] The importance of D-A systems where TPA acts as a donor moiety can be well understood from the extent of scientific studies and reports available in the areas of organic photovoltaics, OLED and other applications.[34-46]

2.2.1 Triphenylamines in OLED

Triphenylamines belong to a class of molecules that are used extensively for diode applications. The low ionization potential of triphenylamines made them good candidates as hole-transporting materials in OLED fabrication. Development of a high performance OLED depends to a great extent on the design of a stable hole transport layer having high hole injection capability as well as adequate hole mobility.[28] Besides this property, the triphenylamines have high thermal stability and the propeller like nature of the three phenyl rings around the nitrogen atom reduces the possibility of aggregation. Donor-acceptor molecules based on triphenylamines thus invoked the interests of OLED researchers tremendously. Ma *et al.* reported a twisted D–A molecule -triphenylamine-phenanthro[9,10-d]imidazole (**TPA-PPI**) with a hybridized local and charge-transfer (HLCT) excited state.[47] In such an excited state, the lowest triplet cannot be up-converted to the emissive singlet state while the higher triplet can be up-converted to other higher singlet state. The higher singlet state then decays to the emissive lowest singlet state and realize triplet exciton harvest. **TPA-PPI** as a non-doped blue emitter achieved a maximum current efficiency (CE_{max}) of 5.66 cd A^{-1} and a maximum external quantum efficiency (EQE_{max}) of 5.02% with CIE coordinates at (0.15, 0.11), which are much higher values than for most of the traditional fluorescent emitters [48,49] with local excited states. (Figure 2.1)
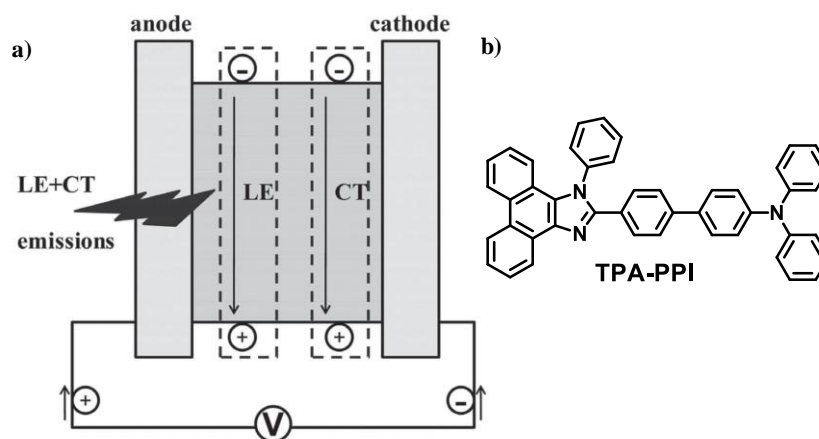
Figure 2.1. *a) Simple schematic representation of recombination of electrons and holes in the device with **TPA-PPI** as the emitter, which has the inter-crossed LE and CT state. b) Structure of **TPA-PPI**. (Reproduced as such from the reference)* [47]

Similar to this work, Liu *et al.*[50] reported a 'V' shape molecule **TPA-2PPI** with a HLCT emissive state, which is modified from the linear D–A type **TPA-PPI**. The non-doped device

based on the **TPA-2PPI** emitter still exhibits deep-blue emission peaking at 452 nm with CIE coordinates at (0.15, 0.10) and an EQE_{max} of 4.91%. Through comparing the emission color of different emitters with the same donor such as TPA but different acceptor, it can be inferred that imidazole unit could be the most mild acceptor ever reported and very promising building block to prepare highly efficient conventional deep blue emitters. (Figure 2.2)
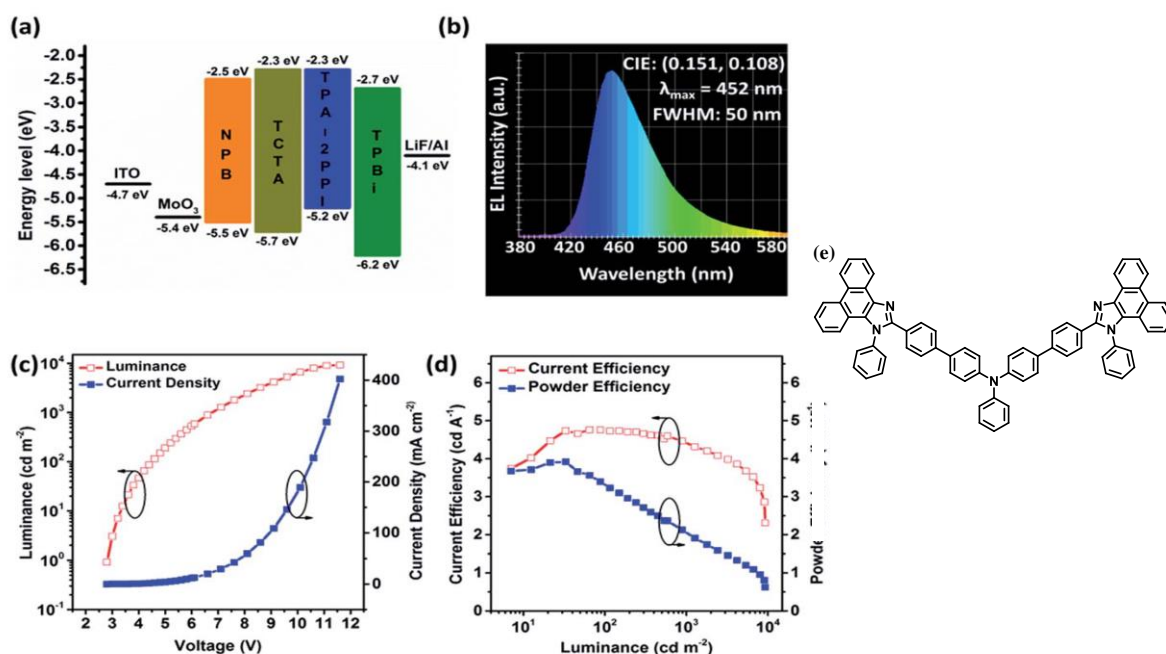
Figure 2.2. *a) Schematic energy level diagram of **TPA–2PPI** device. b) EL spectrum of **TPA–2PPI** device. c) Luminance–voltage–current density curves. d) Current efficiency–luminance–powder efficiency curves. (Reproduced as such from the corresponding reference)* [50]

Su' group developed four novel naphtho[1,2- d]imidazole derivatives **NI-1-TPA, NI-2-TPA, NI-1-PhTPA, and NI-2-PhTPA**.[51] Under common multilayered device structures, devices based on **NI-1-PhTPA**, and **NI-2-PhTPA** delivered an EQE_{max} of 6.08% and 5.95% with CIE coordinates at (0.14, 0.11) and (0.14, 0.10) respectively. The structures of the molecules and the EL results obtained for them are given in Figure 2.3
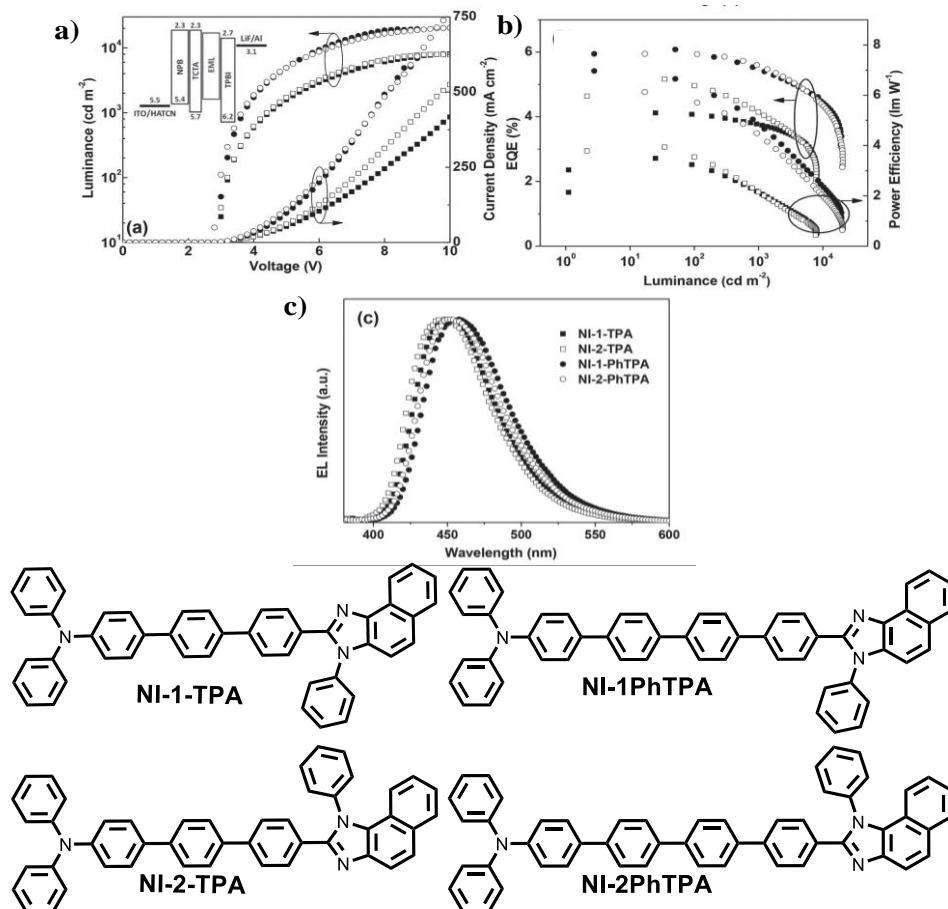
Figure 2.3 *a) Luminance and current density versus voltage, b) EQE and PE versus luminance, and c) EL spectrum characteristics of the multilayer devices in a structure of ITO/ HATCN (5 nm)/ NPB (40 nm)/ TCTA (5 nm)/ EML (20 nm) / TPBI (40 nm)/ LiF (1 nm)/ Al. EML: **NI-1-TPA**, **NI- 2-TPA**, **NI-1-PhTPA**, or **NI-2-PhTPA**. Inset: The configuration and energy diagram of the multi-layer devices. PPI-PPITP (reproduced as such from the corresponding reference)* [51]

2.2.2 Oligothiophenes and bithiophenes
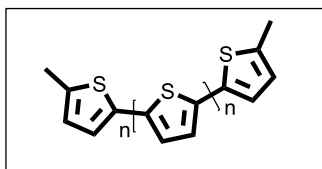
Figure 2.4. *An oligothiophene molecule where the n = 2 - 100*

Oligothiophenes are another class of molecules that are extensively being used for device applications due to their superior photophysical properties.[48-52] Oligothiophenes consist of two - 100 repeating thiophene units (Figure 2.4). The high chemical stability, full colour tenability, high processibility are other beneficial properties of oligothiophenes. The synthesis and

applications of the oligothiophenes can be obtained from the review by Mishra *et.al.*[53] Though conjugated thiophenes are attractive for a wide range of applications including conductive layers in materialistic applications,[54] photoactive layers in photovoltaics,[55] and in anti-static packaging, [56] their insolubility in organic solvents limits their potential usage.[57]

2.3 Definition of the problem

From the literature reports, it is evident that the Donor-Acceptor systems with TPA as donor conjugated with other acceptor moieties like imidazole can be promising building blocks to prepare highly efficient conventional deep blue emitters. Oligothiophenes have beneficial properties which make them suitable candidates for device applications. In order to circumvent the low solubility problem of oligothiophenes in organic solvents, without compromising on the electronic properties, the use of a bithiophene moiety may be beneficial. Hence in this study, it is proposed to synthesis D-A systems incorporating TPA (as donor moiety) and a bithiophene (as acceptor moiety). It is also decided to further modify the TPA-bithiophene conjugate (**TPT**) by incorporating dibenzothiophenyl (-Ben) /acetophenyl (-Ac) groups at the 3' position of **TPT**. The 3' position of **TPT** was particularly chosen as it might result in molecules that are chemically and photochemically inert.[58] In the set of three systems synthesized, in the case of **TPT**, triphenylamine acted as a donor and bithiophene part served as an acceptor. In **TPT-Ben,** the dibenzothiophene moiety would served the role of a donor, whereas in **TPT-Ac** acetophenone moiety, as an acceptor (Figure 2.5). The details of the synthesis, photophysical and electroluminescence properties of **TPT, TPT-Ben** and **TPT-Ac** (Figure 2.5) are the subject matter of this chapter.

2.4 Results and discussions

2.4.1 Synthesis and characterization

TPT was synthesized by reacting 4-bromotriphenylamine (1) with 2,2'-bithiophen-5-ylboronic acid (2) in THF/water system at 65-70 °C for a period of 12 h. It was then subjected to a controlled NBS bromination to get **TPT-Br** . It was further reacted with 4-dibenzothienyl
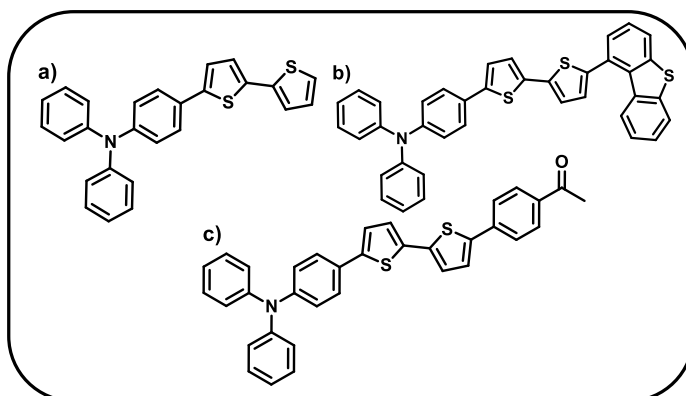
Figure 2.5. *Triphenylamine-bithiophene derivatives a)* ***TPT*** *b)* ***TPT-Ben*** *c)* ***TPT-Ac***

boronic acid/4-acetylphenylboronic acid under the same reaction conditions employed for the synthesis of **TPT**, to fetch **TPT-Ben** or **TPT-Ac** respectively (Scheme 2.1). The structures of all the three compounds were characterized by IR, ^{1}H and ^{13}C NMR spectroscopy and further confirmed by mass spectrometric analyses.

TPT was obtained in 64% yield as lemon yellow crystals. The IR spectrum showed two bands at 2924 and 2896 cm^{-1} corresponding to the C-H aromatic stretching. ^{1}H NMR spectrum of **TPT** showed aromatic protons corresponding to 19 hydrogen, ranging from 7.46 to 7.00 ppm. The ^{13}C NMR spectrum for **TPT** also showed aromatic peaks only, ranging from 147 to 122. The spectral values of **TPT** are in well agreement with the reported values.[62] In the mass spectrum **TPT** gave an (M+H)$^+$ peak as base peak and molecular peak at m/z 410.1024. The NMR and mass spectra for the molecule was presented at Figure 2.6.
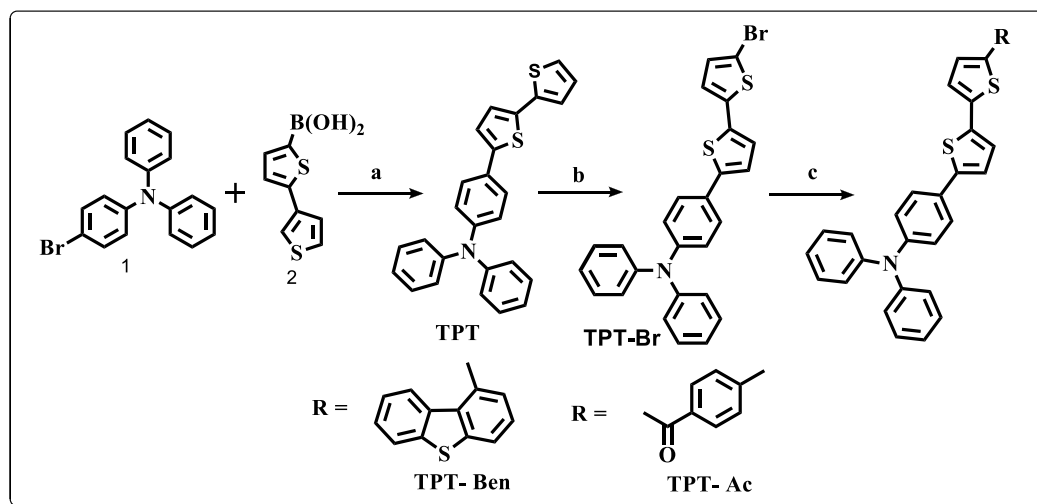
Scheme 2.1. *The synthetic route for the preparation of triphenylamine derivatives,* ***TPT****,* ***TPT-Ben****, and* ***TPT-Ac****. a) Pd(PPh$_3$)$_4$, Na$_2$CO$_3$, THF-Water, 65-70 ºC, 12 h, b) N- bromosuccinimide (re-crystallized), ⁰C, DMF, dark, c) Pd(PPh$_3$)$_4$, Na$_2$CO$_3$, THF-Water, 65-70 ºC, 12 h.*

a)

7.463
7.445
7.283
7.268
7.253
7.205
7.195
7.180
7.173
7.128
7.123
7.113
7.071
7.054
7.040
7.025
7.017
7.008

−0.000

2.00
4.74
0.99
0.93
5.91
5.09

b)

147.44
147.37
143.07
137.60
135.82
129.33
128.07
127.83
126.40
124.61
124.56
124.15
123.61
123.40
123.16
122.79
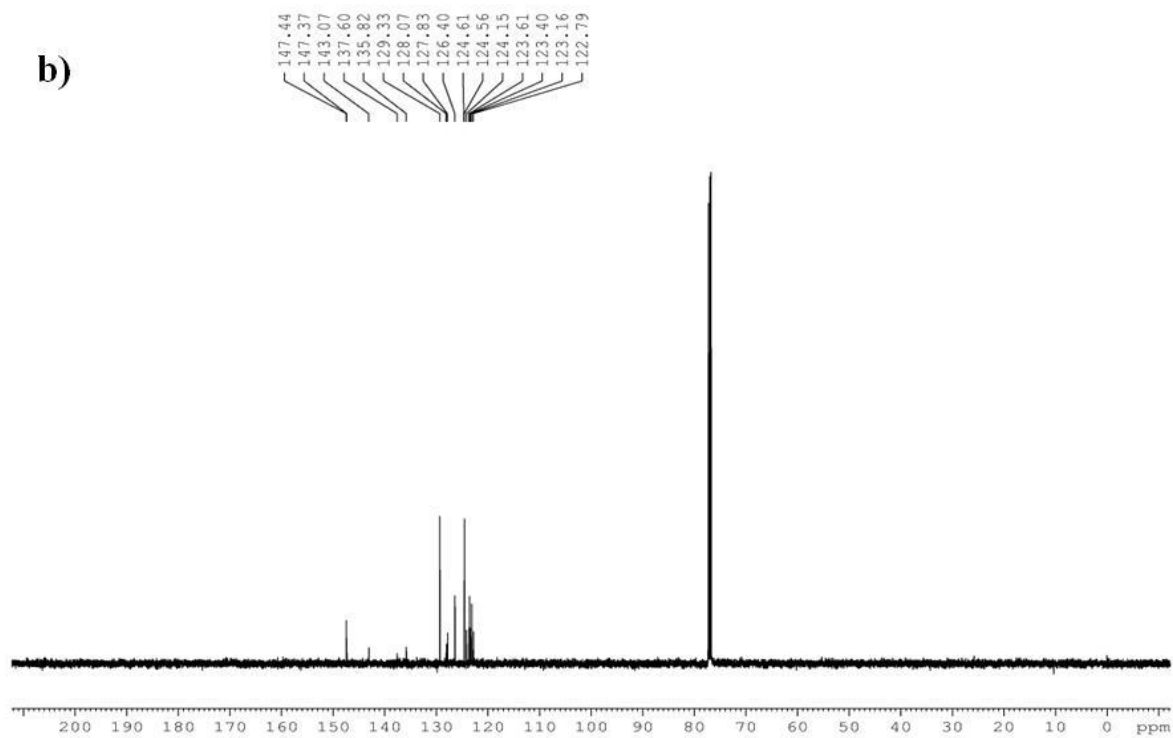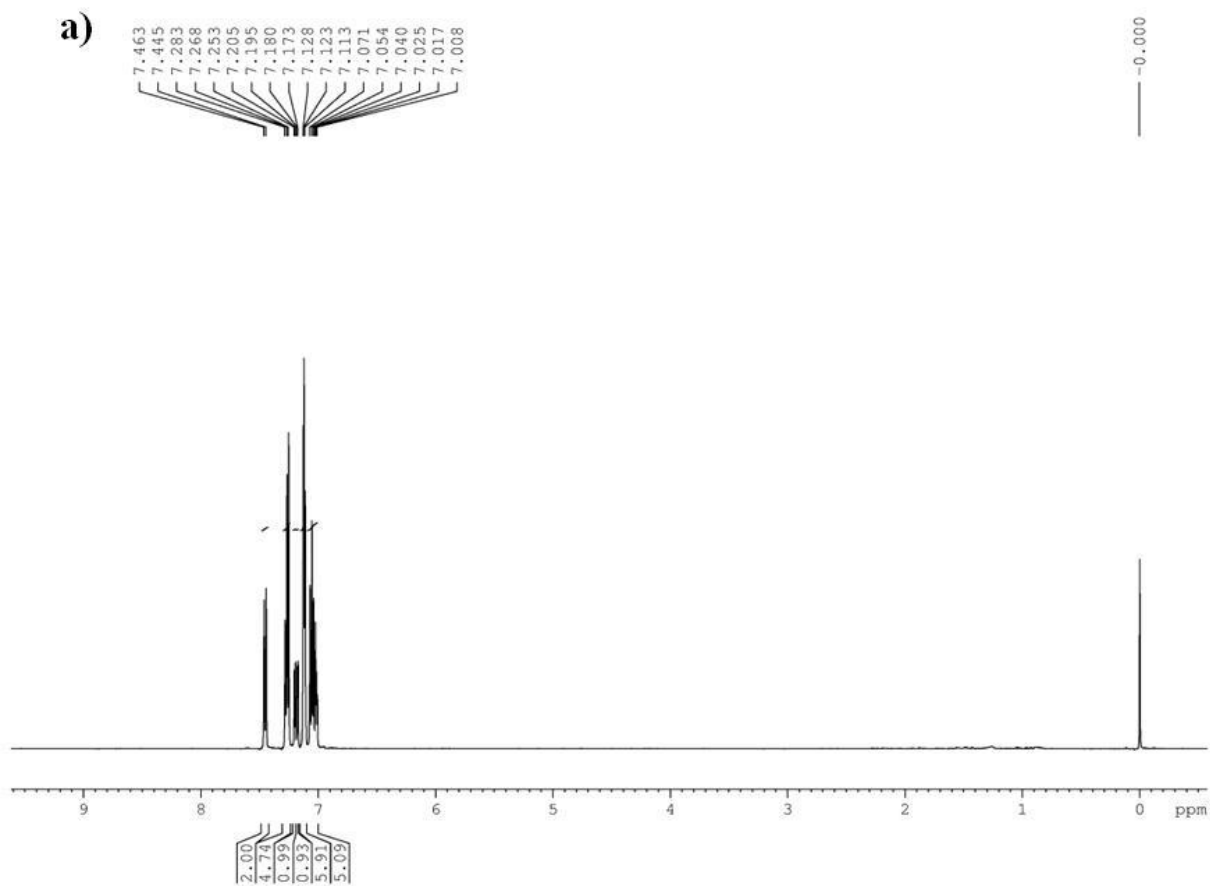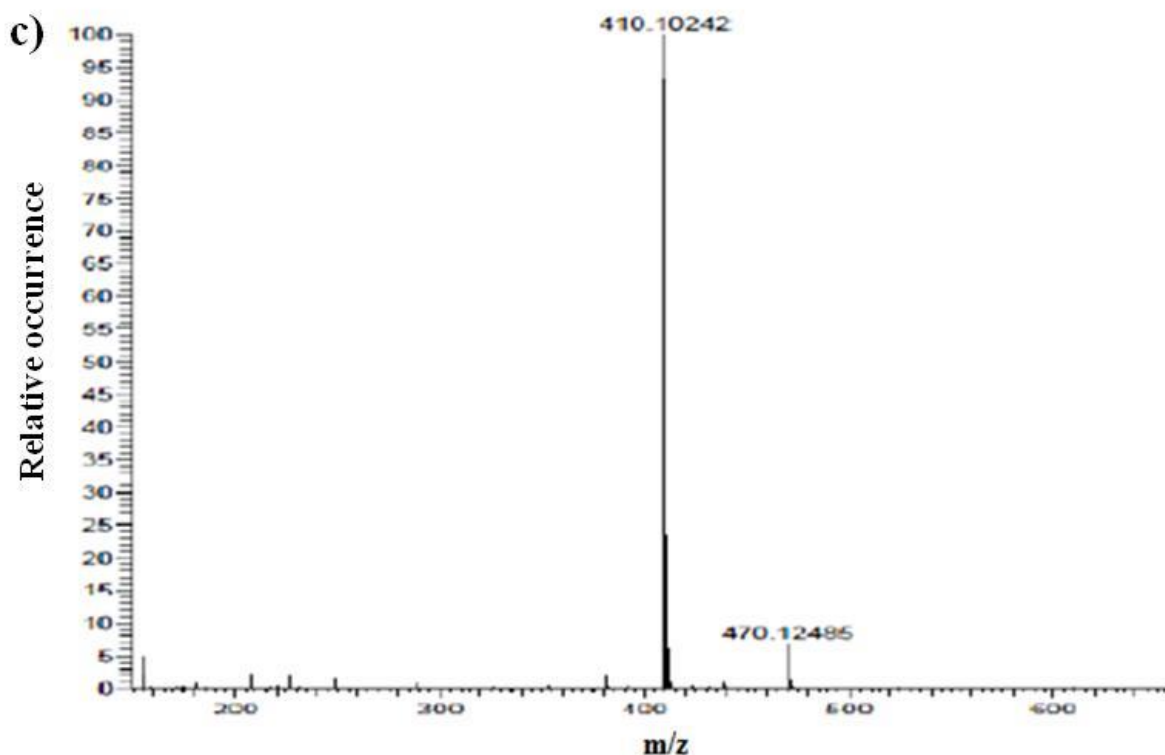
Figure 2.6. *a) ^{1}H NMR spectrum of **TPT** b) ^{13}C NMR spectrum of **TPT** c) Mass spectrum of **TPT***

Crystals of **TPT** were obtained by the slow evaporation of the solvent (DCM) and were analyzed by X-ray diffraction technique to elucidate the molecular structure and bulk- packing characteristics. (Figure 2.7) From the bulk packing we could deduce that, the triphenylamine rings are arranged alternatively to avoid steric hindrance in the molecule. The molecule is crystallized in triclinic space group *P$\bar{1}$,* with a = 10.276 Å, b = 10.405 Å, c = 21.563 Å, α = 94.824°, β = 95.581°, γ = 114.175°. From the data, it was interpreted that the molecule has mainly two interactions *viz*. CH- π interaction and parallel dispaced interaction. Parallel dispaced interaction is a kind of secondary interaction between the ends of two π systems. The results of single crystal XRD is summarized in experimental session. The sulphur atoms of two adjacent molecules are 6.534 Å apart and nitrogen atoms are 4.986 Å apart. Two thiophene rings are perfectly in plane. Three phenyl substituents of the triphenylamine (TPA) being symmetrically twisted from the plane of the central N-C-C-C moiety (propeller like geometry), consistent with the previous reports.[59,60] The phenyl rings resemble to the propeller blade. According to literature, the important geometrical parameter of TPA is the angle between the

central N-C-C planar moiety and the phenyl rings. Theoretically it is found to be 41.6° which is in agreement with our crystal results.
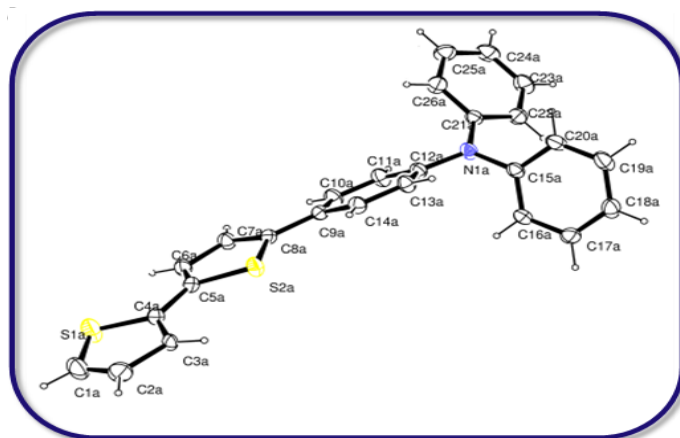
*Figure 2.7. ORTEP diagram for **TPT***

TPT-Ben was obtained in 73% yield as green powder. The IR spectrum consists of many vibrations corresponding to aromatic groups with most prominent bands at 3012 and 2924 cm^{-1} corresponding to aromatic C-H stretching. The proton NMR spectrum showed all aromatic proton peaks ranging from δ 8.21- 7.00 ppm. In the mass spectrum **TPT-Ben** showed a molecular ion peak at 592.122 (M+H$^+$). The NMR and mass spectra of **TPT-Ben** is presented in Figure 2.8.

b)

c)
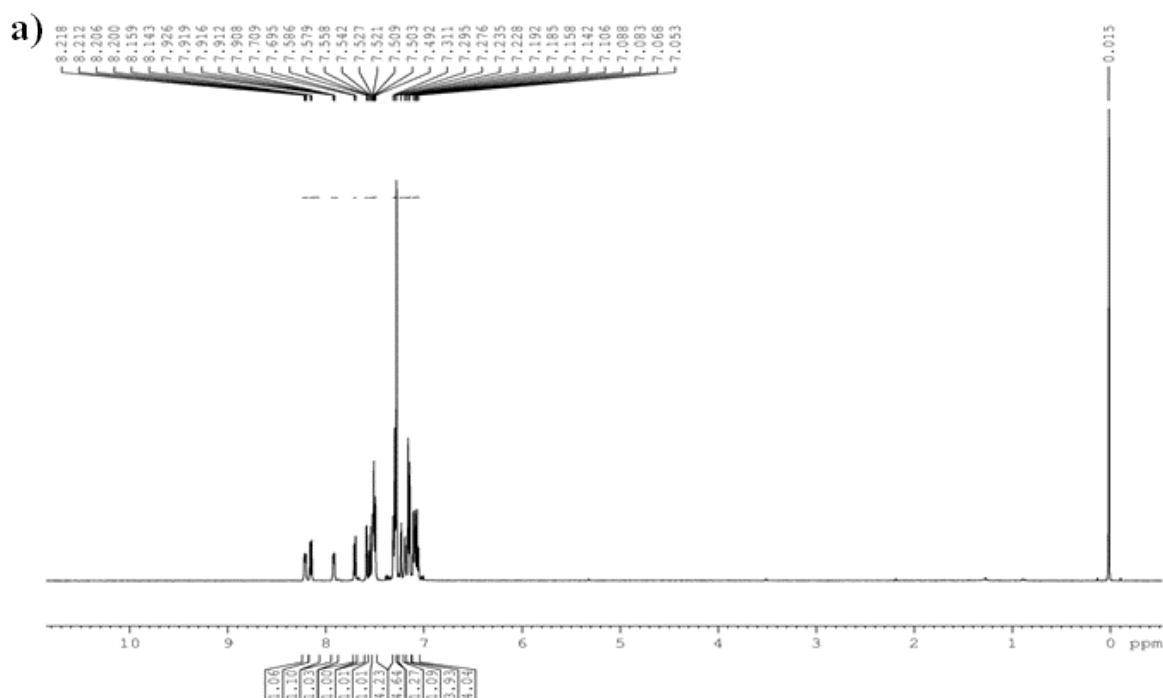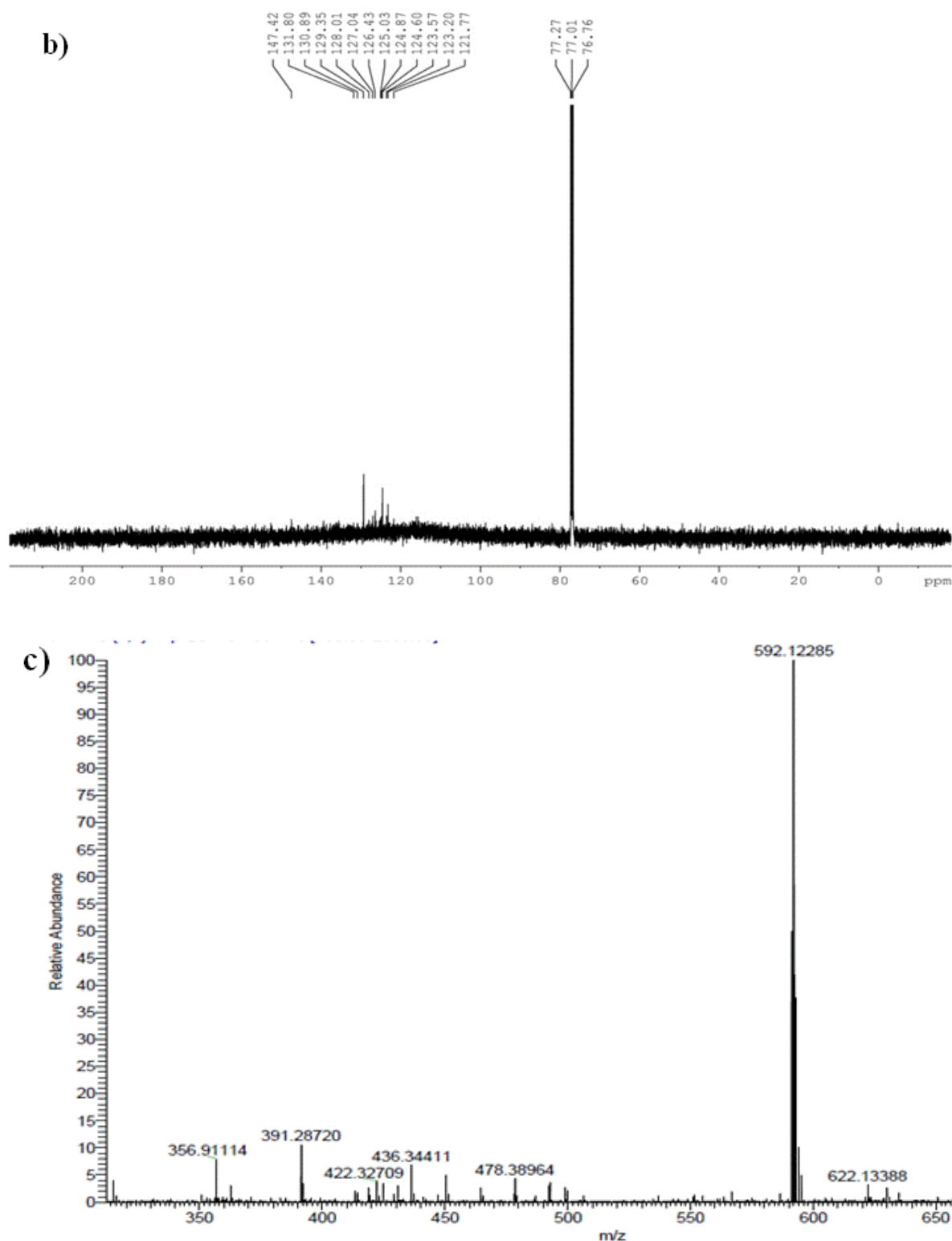
*Figure 2.8 a) ¹H NMR spectrum of **TPT-Ben** b) ¹³C NMR spectrum of **TPT-Ben** c) Mass spectrum of **TPT-Ben***

TPT-Ac was obtained in 70% yield as an orange powder. The IR spectrum showed C-H stretching as well as ketone group frequencies at 2918 and 2850 cm^{-1} and 1672 cm^{-1}

respectively as prominent peaks. In the ^{1}H NMR spectrum all the aromatic protons resonated between δ 7.90 to 7.00 ppm and the acetyl protons appeared at δ 2.63 ppm as a singlet corresponding to three hydrogens. In the ^{13}C spectrum the carbonyl carbon resonated at δ 192 ppm. The mass spectrum of the molecule gave (M+) peak at m/z 527.137. (Figure 2.9)
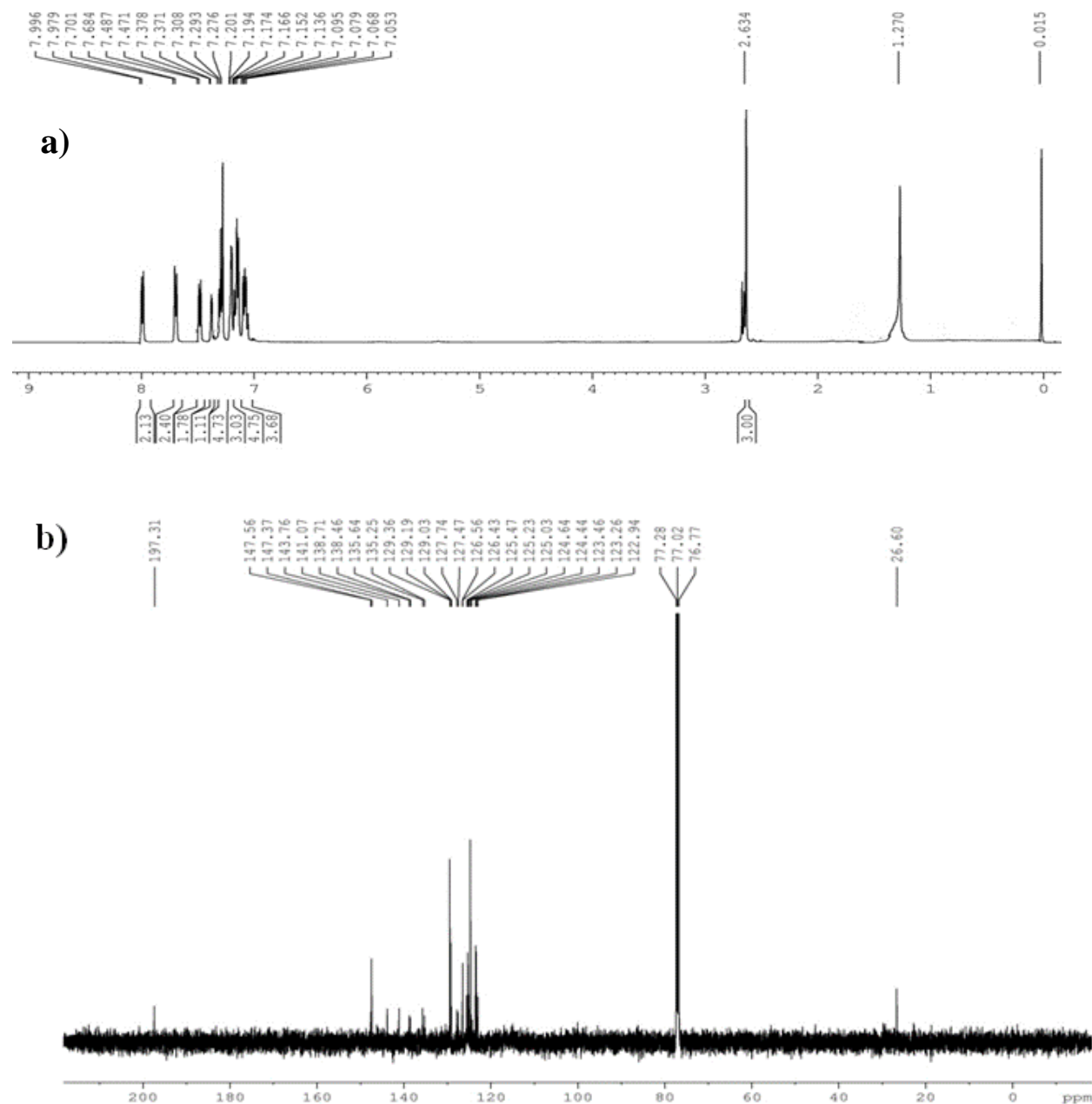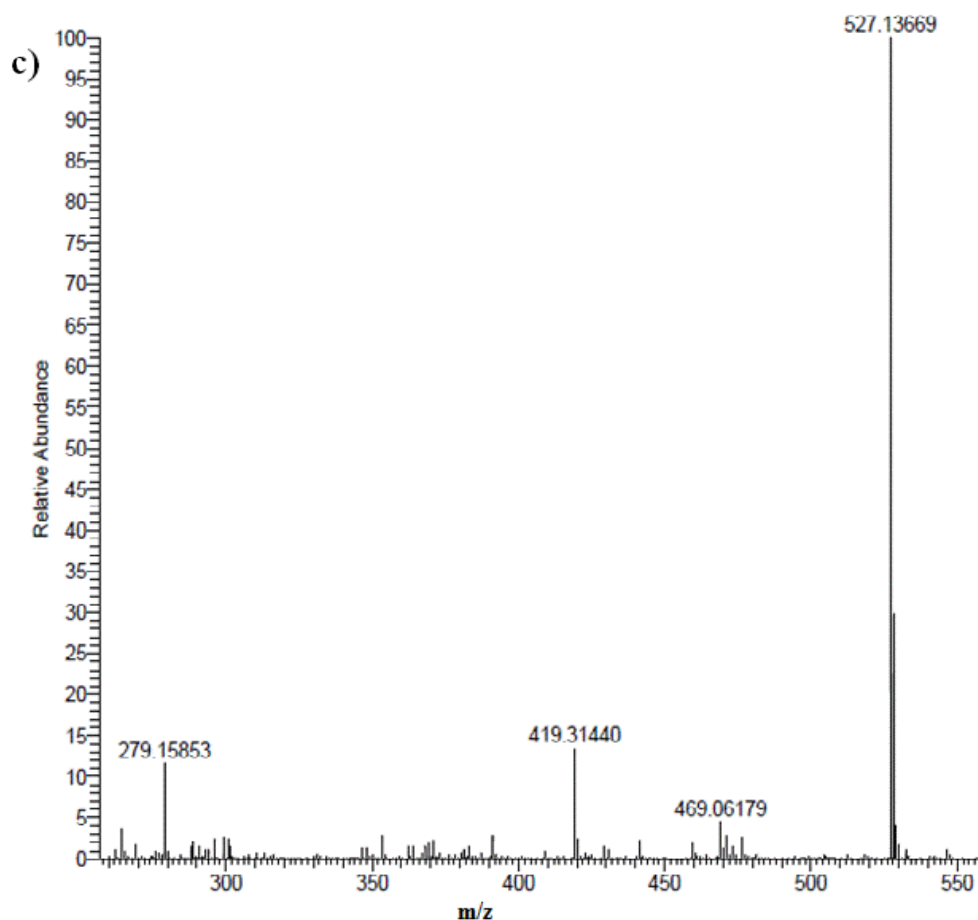
Figure 2.9. *a) ^{1}H NMR spectrum of **TPT-Ac** b) ^{13}C NMR spectrum of **TPT-Ac** c) Mass spectrum of **TPT-Ac***

2.4.2 Photophysical studies

2.4.2.1 Steady state absorption and emission studies in solution state
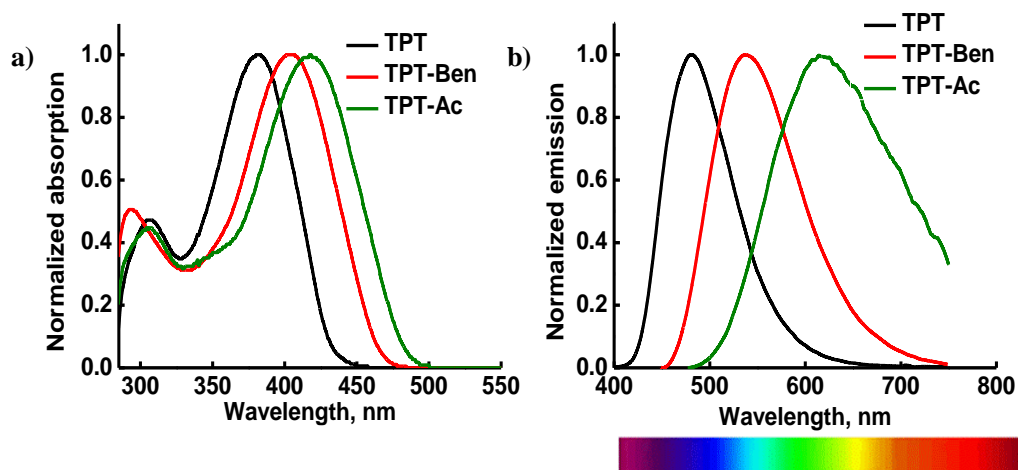
Figure 2.10. *a) Absorption and b) Emission spectra of **TPT** (black), **TPT-Ben** (red), and **TPT-Ac** (green) in DMSO at room temperature. λ_{exc} **TPT** = 380 nm, **TPT-Ben** = 410 nm **TPT-Ac** = 420 nm.*

The steady state absorption spectra of **TPT, TPT-Ben** and **TPT-Ac** were recorded in DMSO. (Figure 2.10a) **TPT** showed an absorption maximum at 383 nm while **TPT-Ben** and **TPT-Ac** exhibited theirs at 411 nm and 425 nm respectively. The high energy absorption band near 300 nm can be attributed to the n-π^* transition of the triphenylamine core[61] and the broad structureless absorption can be assigned to the π-π^* transition of thiophene and the CT transition.[62] Studies indicated that, the absorption spectra of the molecules are independent of the polarity of solvents (toluene, THF, ethylacetate, dioxane, methanol, acetonitrile and DMSO), used for the experiments (Figure 2.11). The molar extinction coefficients (ε) of the low energy bands were calculated as 38,000 M^{-1} cm^{-1}, 48,000 M^{-1} cm^{-1}, 20,000 M^{-1} cm^{-1} for **TPT**, **TPT-Ben** and **TPT-Ac** respectively (Figure 2.12).
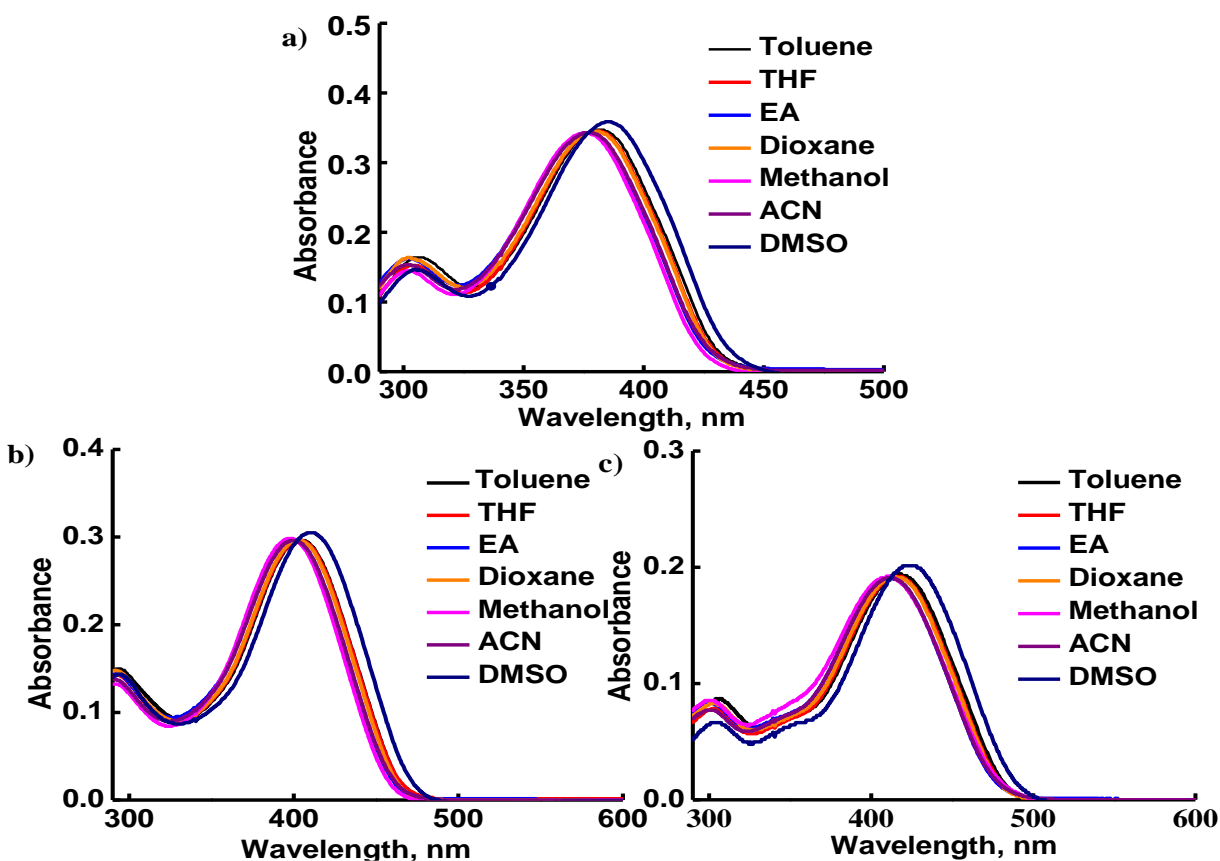
Figure 2.11. *Absorption profile of molecules in different solvents a) **TPT** b) **TPT-Ben** c) **TPT-Ac***
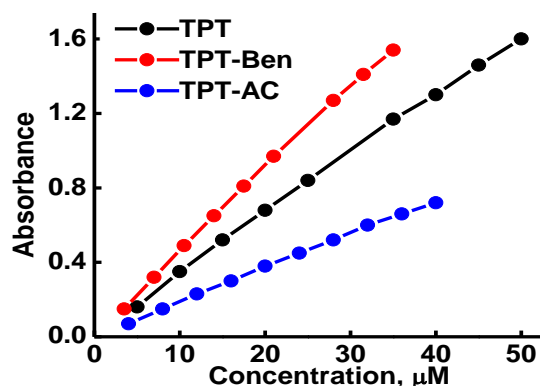
***Figure* 2.12.** *Absorbance Vs concentration of molecules in THF*

The molecules **TPT, TPT-Ben** and **TPT-Ac** exhibited their emission maxima at 481 nm (blue), 541 nm (green) and at 617 nm (orange-red) respectively in DMSO. Unlike solvent independent absorption profile (Figure 2.10b), their respective emission maxima were found to be greatly influenced by the polarity of the solvents in which their emission spectra were recorded (Figure 2.13). In the case of **TPT-Ac** and **TPT-Ben** the respective spectra got broadened as the polarity of the solvent increased (Figure 2.13). This observation shows that the geometry of these molecules changes from ground to excited state and this assumption was further confirmed by DFT calculations. In DMSO, the Stokes shift values for **TPT, TPT-Ben** and **TPT-Ac** were calculated as 5319.64cm^{-1}, 5846.61 cm^{-1} and 7321.96 cm^{-1} respectively.
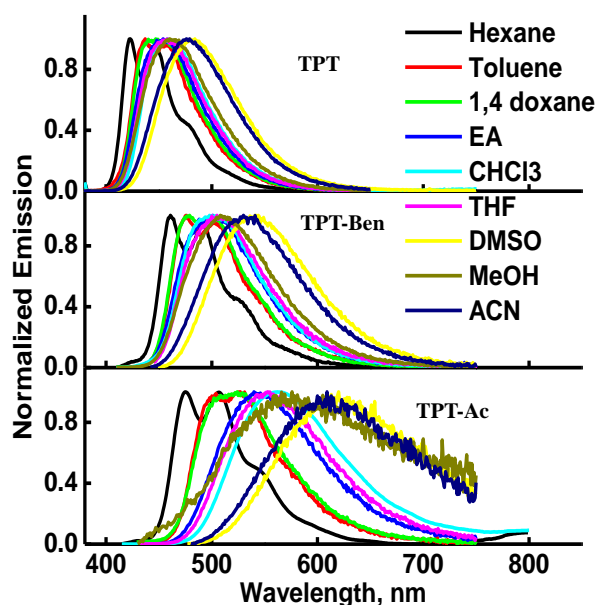
Figure 2.13. *The change in the emission spectra of **TPT, TPT- Ben** and **TPT- Ac** with respect to different solvents and their polarity. λ_{exc}**TPT** = 380 nm, **TPT-Ben** = 410 nm **TPT-Ac** = 420 nm.*

In Figure 2.14 the Stokes shifts (in wave-number) are plotted against solvent orientation polarizability factor (Δf), where $f = (\varepsilon-1)/(2\varepsilon + 1) - (n^2-1)/(2n^2 + 1)$, in which ε is the di-electric constant and n is the refractive index).[63-65] The graphs for **TPT, TPT-Ben** and **TPT-Ac** showed a nonlinear relationship indicating the presence of an intramolecular charge transfer state in the molecules.[66] Quantum yields (Φ) of **TPT, TPT-Ben** and **TPT-Ac** were measured in different solvents and were found to increase with an increase in the solvent polarity. All the three derivatives showed highest quantum yield in DMSO. The result are presented in Table 2.2.
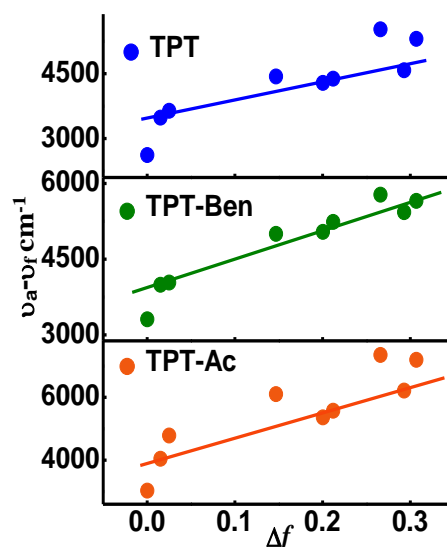
Figure 2.14. Relationship between solvent orientation polarizability (Δf) and Stokes shift (in wavenumber).

2.4.2.2 TCSPC measurements (Lifetime calculation)

The excited state decay dynamics of the molecules were measured in different solvents using time correlated single photon counting spectrometer by exciting at 375 nm using a LED source. All the molecules exhibited monoexponential decay profile with very short lifetime. The results are depicted in Table 2.1 and Figure 2.15.The radiative and (k_r) non-radiative (k_{nr}) rate constants were also calculated using fluorescence lifetime and quantum yield according to the equation 1 and the results are included in Table 2.2.

$$k_r = \frac{\Phi}{\langle\tau\rangle} = \frac{1}{\langle\tau\rangle} - k_{nr}$$　　——————————————————— (1)

where the k_r and k_{nr} are the radiative and non-radiative rate constants respectively, Φ is the quantum yield and $\langle\tau\rangle$ is the fluorescence mean lifetime.

Table 2.1. Lifetime values for the molecules in different solvents

Sl.No	Solvent	Lifetime TPT	Lifetime TPT- Ben	Lifetime TPT-Ac
1	Toluene	0.3 ns	0.4 ns	0.33 ns
2	THF	0.5 ns	0.47 ns	.38 ns
3	EA	0.4 ns	0.4 ns	0.9 ns
4	1,4-Dioxane	0.3 ns	0.4 ns	0.60 ns
5	Methanol	0.6 ns	0.55 ns	1.4ns
6	ACN	2 ns	1.04 ns	2 ns
7	DMSO	1.4 ns	1.4 ns	2.4 ns
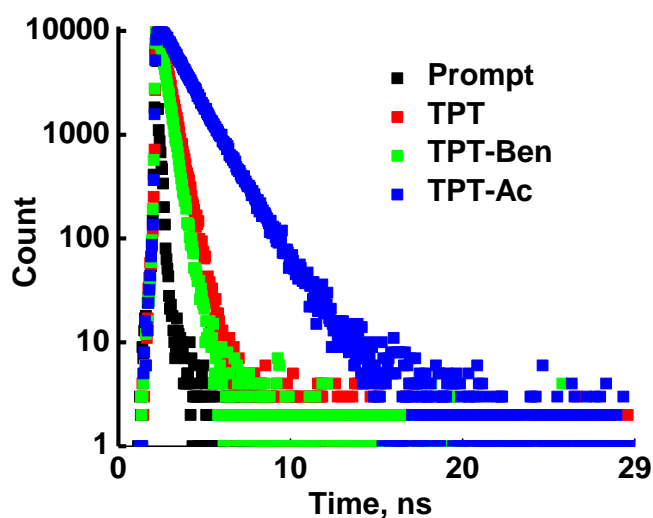
Figure 2.15 .Decay profiles for the molecules in DMSO

2.4.2.3 Aggregation studies

The aggregation studies of **TPT, TPT-Ben** and **TPT-Ac** were carried out in THF/water mixture. The corresponding absorption and emission spectra were presented in Figures 2.16 and 2.17 respectively. In the case of **TPT**, an increase in the fluorescence intensity was found with respect to the increase of water concentration upto 80%. But further increase in the concentration of water decreased the emission intensity tremendously and similar observations were found in the case of **TPT-Ben** also. This decrease in intensity may be due to the lack of solubility of the respective molecules in high concentrations of water. But in the case of **TPT-Ac**, the emission intensity showed a periodical decrease with respect to the water concentration showing the presence of conventional aggregation induced quenching in the case of **TPT-Ac** .
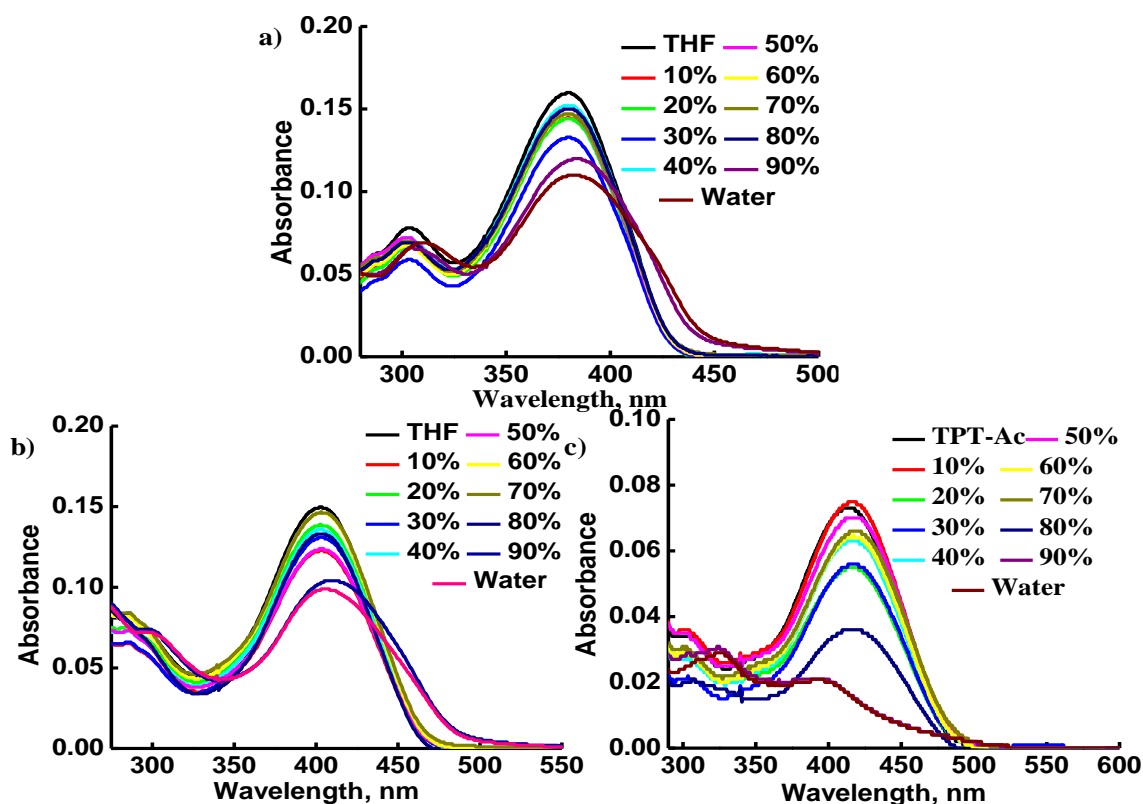
Figure 2.16. *Change in the absorption of the molecules with respect to the concentration of water a) **TPT** b) **TPT-Ben** c) **TPT-Ac***
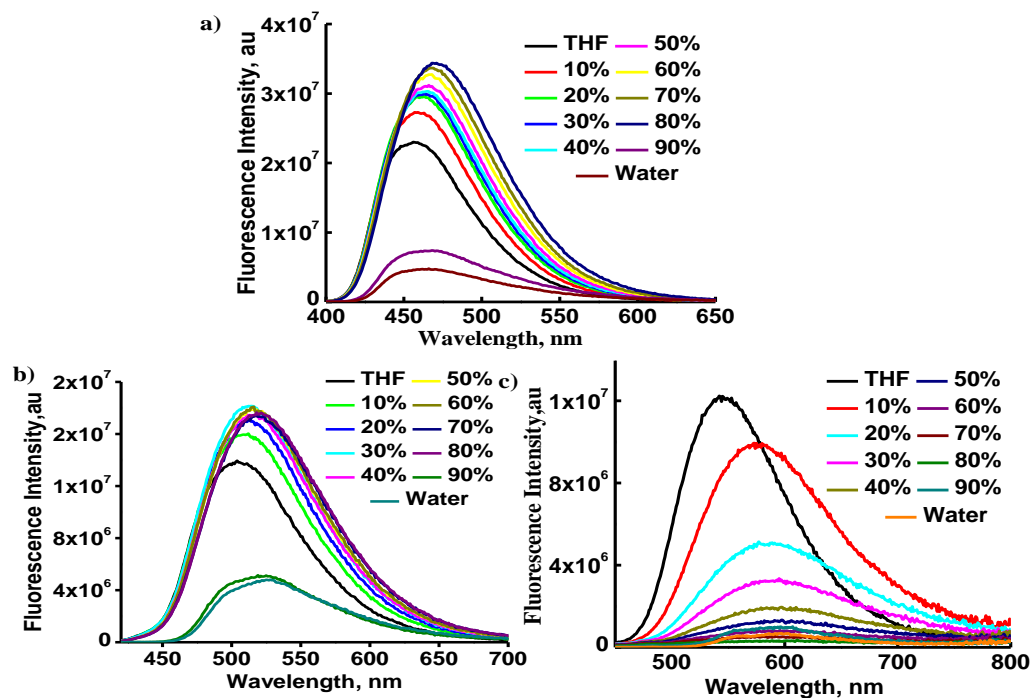
Figure 2.17. *Change in the emission of the molecules as the water content increases a)* **TPT** *b)* **TPT-Ben** *c)* **TPT-Ac**

Table 2.2: Summary of photophysical characterization of the molecules in different solvents

Compound	Solvent	Dielectric Constant ε	λ max (Abs) (nm)	λ max (Emis) (nm)	Stokes Shift (cm^{-1})	Φ	τ (ns)	k_r	k_{nr}
TPT	Toluene	2.25	380	440	3588.52	0.14	0.3	0.47	2.9
	Dioxane	2.38	380	437	3432.49	0.14	0.3	0.47	2.9
	THF	7.58	383	455	4131.64	0.18	0.5	0.36	1.64
	DMSO	46.7	383	481	5319.64	0.44	0.9	0.52	0.65
TPT-Ben	Dioxane	2.25	400	476,500	4508.20	0.15	0.6	0.25	1.4
	Toluene	2.38	400	475,503	4508.20	0.15	0.4	0.38	2.13

	THF	7.58	402	506	5112.78	0.16	0.5	0.32	1.7
	DMSO	46.7	411	541	5846.61	0.29	0.5	0.58	1.4
TPT-Ac	Dioxane	2.25	417	519	4712.99	0.16	0.6	0.27	1.4
	Toluene	2.38	418	501,525	4430.27	0.13	0.45	0.29	1.9
	THF	7.58	420	552	5693.58	0.36	0.9	0.40	0.71
	DMSO	46.7	425	617	7321.96	0.48	1.5	0.32	0.34

2.4.2.4 Steady state PL studies in solid state

To get good performing OLEDs, the molecules screened for the same must have superior solid state properties. In that context we also under took solid state studies of the TPT derivatives. They showed good solid state properties and have very good film forming ability, showing their potential towards OLED applications. Figure 2.18 depicts the solid state absorption and emission of the molecules. The molecules showed very broad absorption in the solid state. The solid state emissions were slightly red shifted on comparing with the respective emissions taken in the solution state. Lifetime measurements were also carried out and the results are summarized in table 2.3 (Figure 2.19).
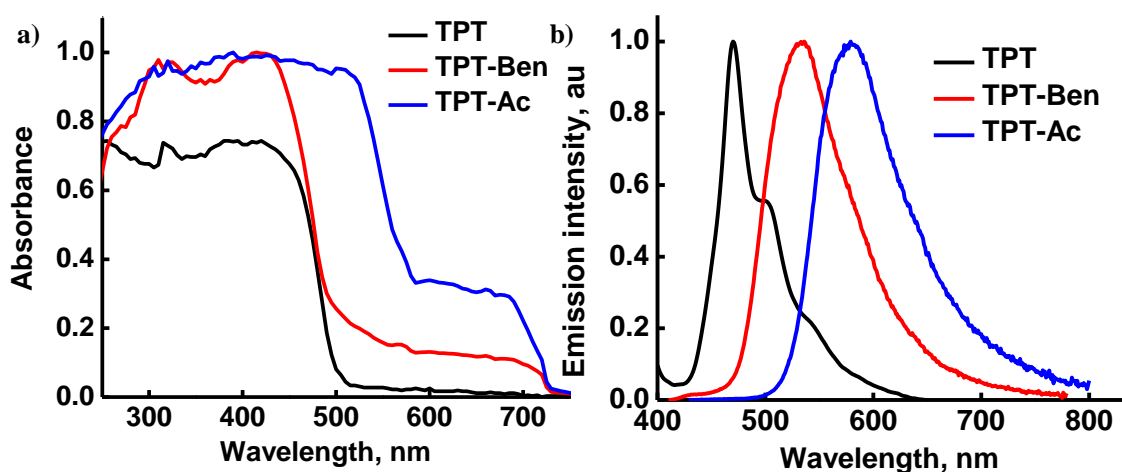
Figure 2.18. a) solid state absorption of **TPT** (Black), **TPT-Ben** (Red), **TPT-Ac** (Blue) b) Solid state emission of **TPT** (Black), **TPT-Ben** (Red), **TPT-Ac** (Blue)
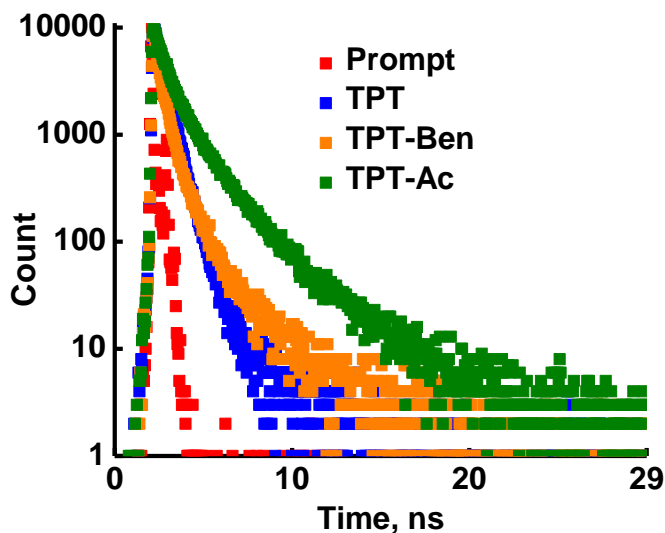
Figure 2.19. *Solid state lifetime for the molecules*

Table 2.3. Lifetime for the molecules in solid state

Compound	Lifetime (τ)
TPT	0.66 ns
TPT-Ben	0.51 ns
TPT-Ac	0.73 ns

2.4.2.5 Nanosecond laser flash Photolysis

To get an insight about the excited state properties of the molecules nanosecond transient absorption studies were carried out. Figure 2.19 shows the nanosecond transient absorption spectra of triphenylamine derivatives, **TPT, TPT- Ben and TPT- Ac,** in Ar saturated THF obtained by exciting at 355 nm using nanosecond laser flash photolysis. It shows abroad transient absorption maximum around 600 nm. The first negative signal near 400 nm in the transient absorption spectra of the derivatives corresponds to the ground state bleach. In the presence of oxygen there is no significant change in the spectral dynamics. The time constant of the transient maxima around 600 nm for **TPT**, **TPT-Ben** and **TPT-Ac** was estimated be around 3.5, 4.88 and 2.9 µs respectively. Based on the literature [67-69] and on the fact that there is no significant change in the time constant in the oxygen medium, the transient maxima are attributed to formation of the radical cation of the triphenylamine core. The decay profiles for

the molecules are also given in Figure 2.20. Figure 2.21 to Figure 2.23 show the transient absorption as well as decay profiles of the molecules in both Ar saturated and O_2 saturated conditions.
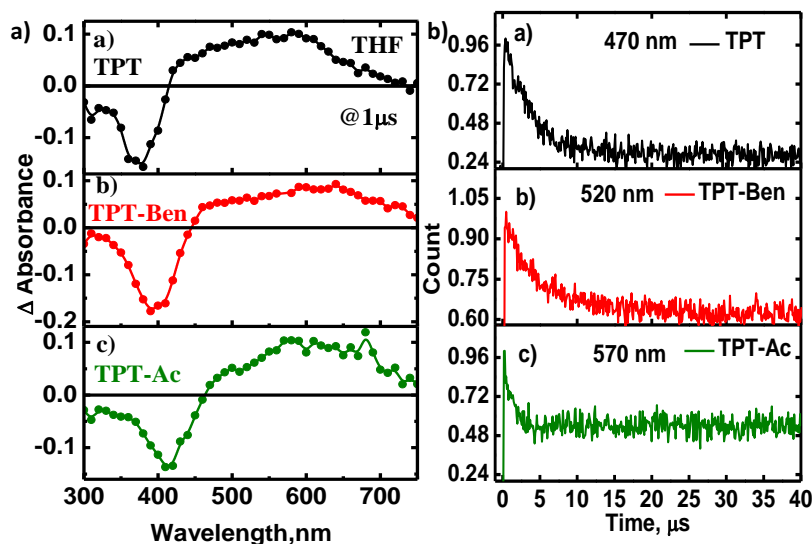
Figure 2.20. *a) Nanosecond transient absorption spectra of **TPT** derivatives obtained by laser flash photolysis at 355 nm excitation in Ar saturated THF b) Corresponding decay kinetics*
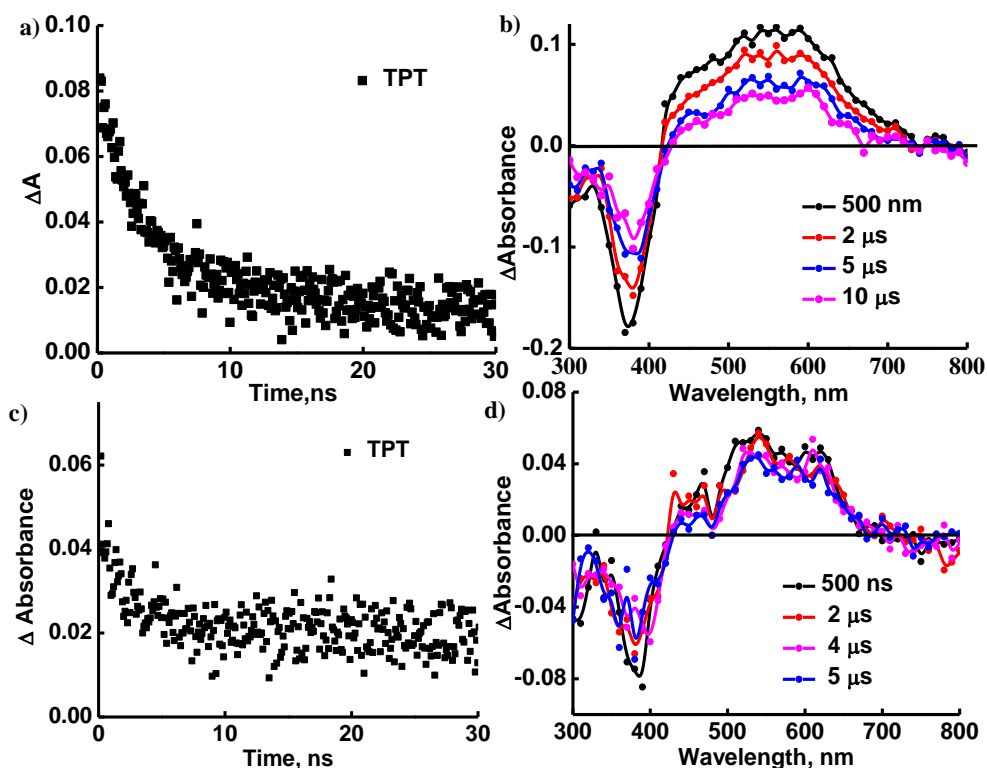
Figure 2.21. *a) Transient decay profile for **TPT** in Ar atmosphere b) transient absorption profile for **TPT** in Ar atmosphere c) Transient decay profile for **TPT** in O_2 atmosphere b) transient absorption profile for **TPT** in O_2 atmosphere*
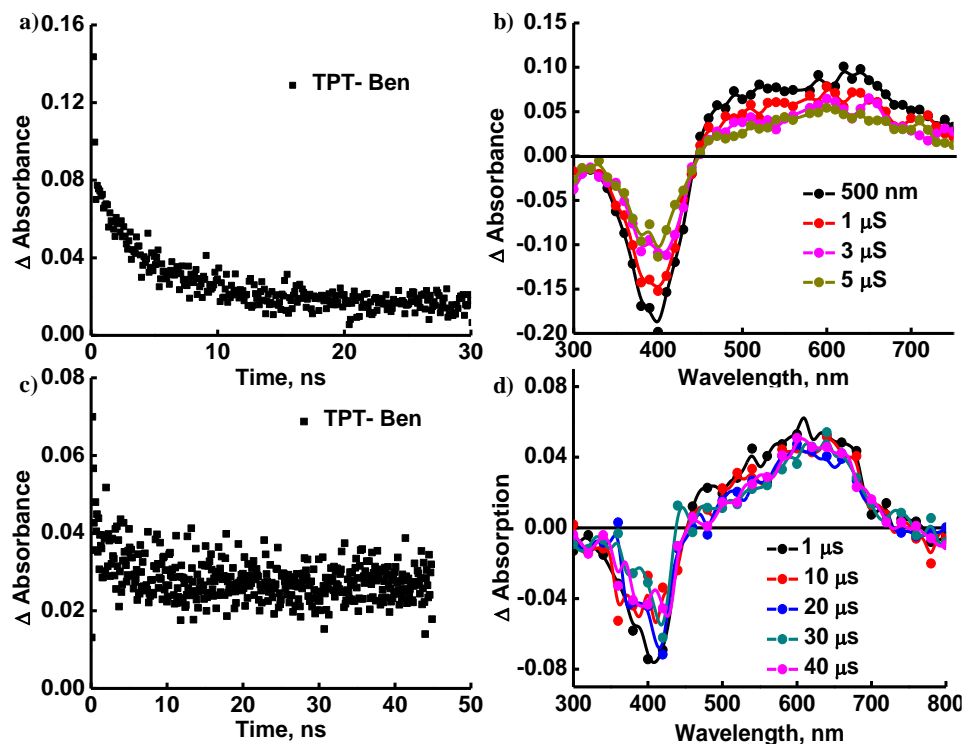
Figure 2.22. *a) Transient decay profile for **TPT-Ben** in Ar atmosphere b) transient absorption profile for **TPT-Ben** in Ar atmosphere c) Transient decay profile for **TPT-Ben** in O₂ atmosphere b) transient absorption profile for **TPT-Ben** in O₂ atmosphere*
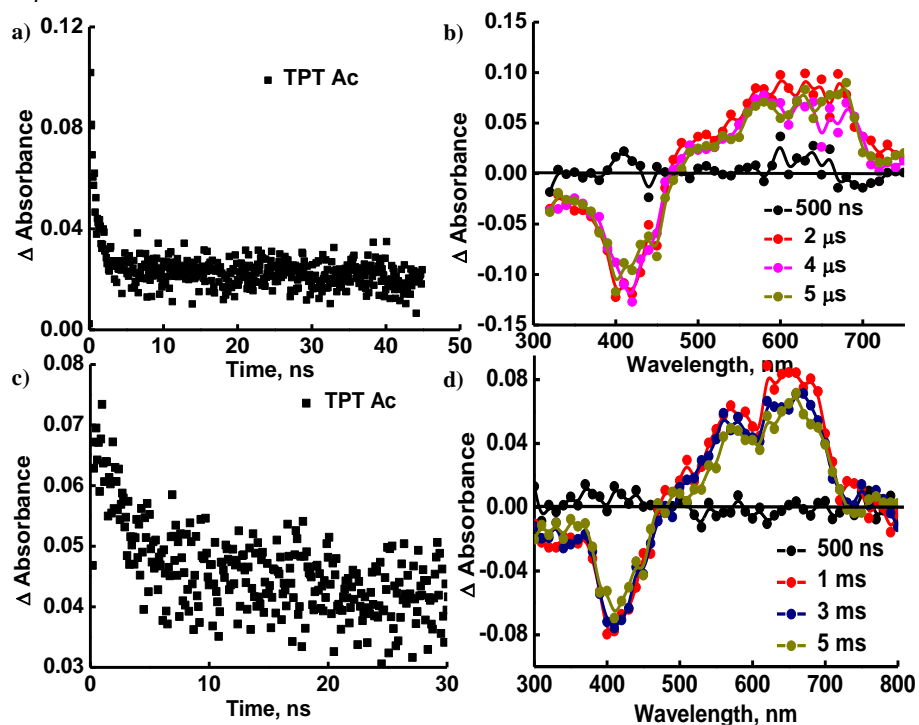
Figure 2.23. *a) Transient decay profile for **TPT-Ac** in Ar atmosphere b) transient absorption profile for **TPT-Ac** in Ar atmosphere c) Transient decay profile for **TPT-Ac** in O₂ atmosphere b) transient absorption profile for **TPT-Ac** in O₂ atmosphere*

2.4.4 Cyclic voltametric analysis and HOMO/LUMO calculations

To get the electrochemical properties of the molecules and also to calculate the HOM-LUMO values CV experiments were carried out (Figure 2.24). The measurements were taken in accetonitrile solutions, taking ferrocene as the internal standard. The CV curve of all the three molecules showed two oxidation potentials that can be assigned to the triphenyalamine radicals.[70] The HOMO values for the molecules were calculated from the oxidation potentials and was found to be -5.26 eV, -5.29 eV and -5.14 eV respectively for **TPT**, **TPT-Ben** and **TPT-Ac**. The LUMO value for the molecules were derived from the HOMO and the optical band gap obtained from solid state absorption profile. LUMO value for **TPT** was calculated as -2.51 eV, for **TPT-Ben** as -2.76 eV and for **TPT-Ac -**3.01 eV (Figure 2.25). The compiled results for electrochemical studies are presented in table 2.4.
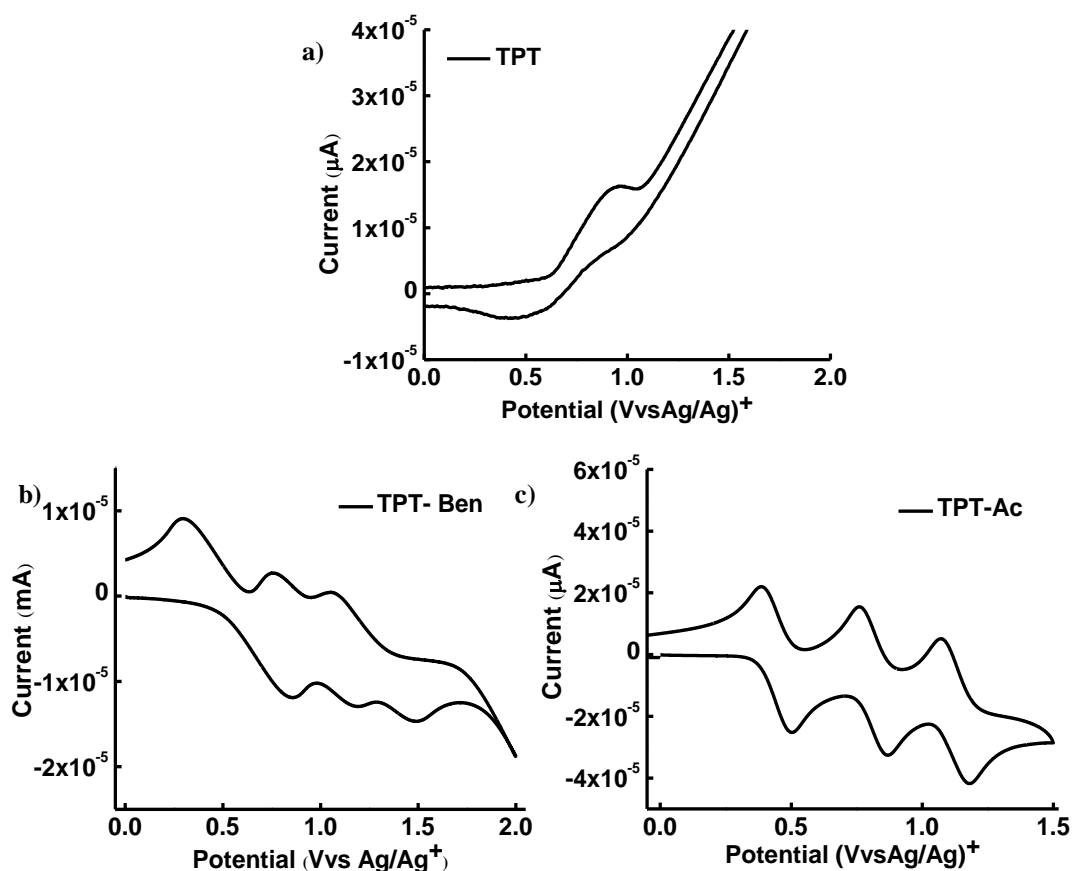
Figure 2.24. CV diagram for the TPT derivatives
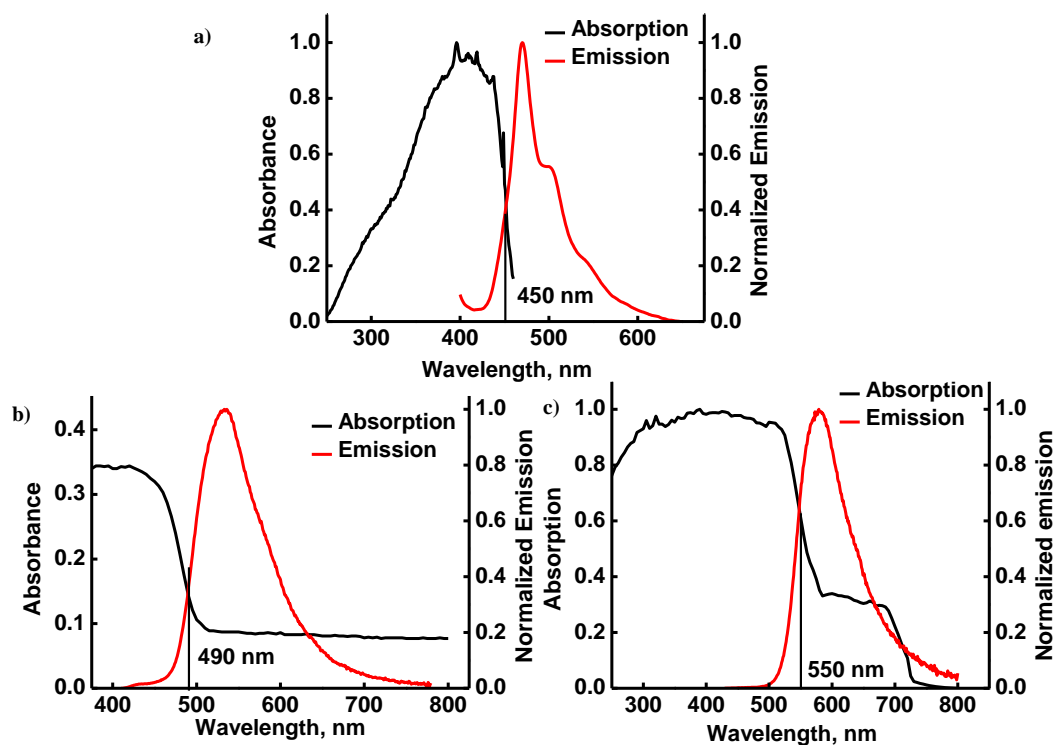
Figure 2.25. *Band gap calculation for the molecules from the solid state absorption and emission*

Calculation of HOMO/LUMO values

TPT

E_{Fc} (Vs Ag/AgCl)	=	0.41V E_{ox} (Vs Ag/AgCl)	=0.87V
E_{ox} (Vs Fc)	=	0.87-0.41	= 0.46V
	=	{-E_{ox} (Vs Fc) - 4.8 eV}	= {-0.46-4.8eV}
		HOMO	= **-5.26eV**
		LUMO	= 5.26- 2.75
			= -**2.51 eV**

TPT-Ben

E_{Fc} (Vs Ag/AgCl)	=	0.41V E_{ox} (Vs Ag/AgCl)	=0.9V
E_{ox} (Vs Fc)	=	0.9-0.41	= 0.49V
	=	{-E_{ox} (Vs Fc) - 4.8 eV}	= {-0.49-4.8eV}
		HOMO	= **-5.29 eV**
		LUMO	= 5.29- 2.53

$$= \text{-}2.76 \text{ eV}$$

TPT-Ac

E_{Fc} (Vs Ag/AgCl)	=	0.41V	E_{ox} (Vs Ag/AgCl)	=0.75V
E_{ox} (Vs Fc)	=	0.75-0.41		= 0.34V
	=	{-E_{ox} (Vs Fc) - 4.8 eV}		= {-0.34-4.8 eV}
		HOMO		= **-5.14eV**
		LUMO		= 5.26- 2.25
				= **-3.01 eV**

Table 2.4. HOMO/LUMO values for the molecules

Compound	HOMO (eV)	LUMO (eV)
TPT	-5.26	-2.52
TPT-Ben	-5.29	-2.62
TPT-Ac	-5.14	-2.61

2.4.5. Thermal analysis
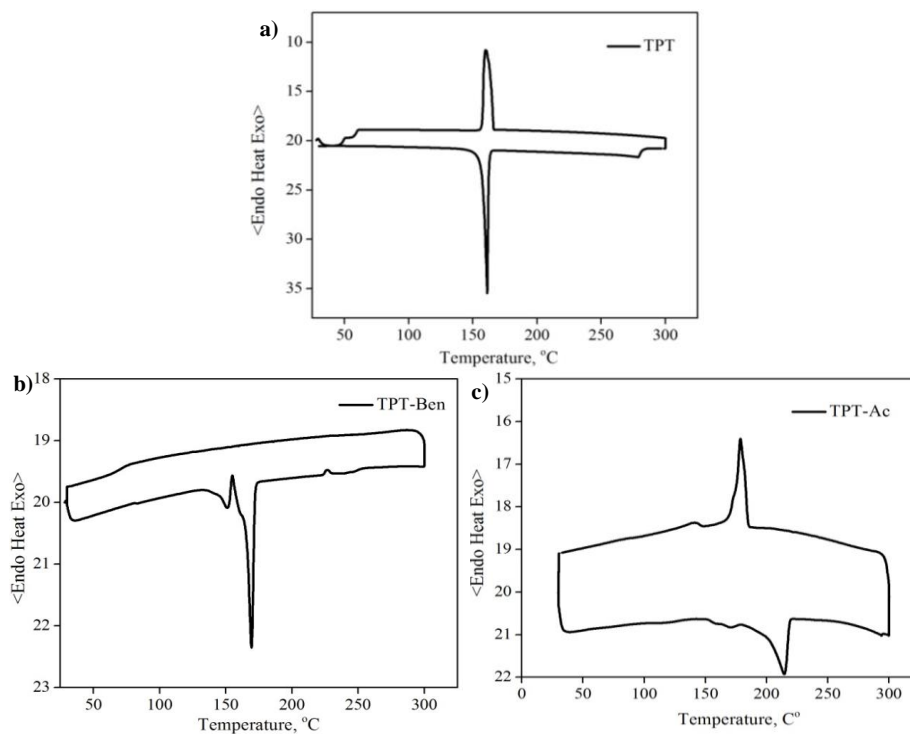
Figure 2.26. DSC curves for a) **TPT** b) **TPT-Ben** c) **TPT-Ac**
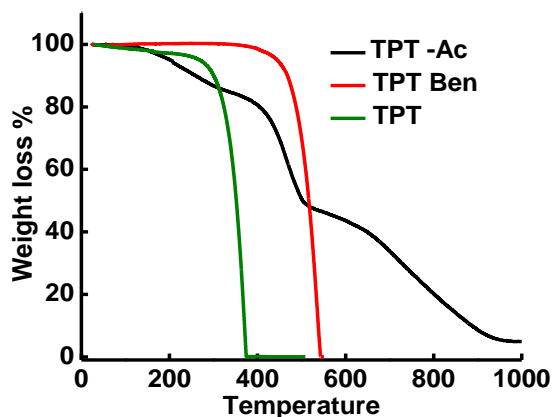
Figure 2.27. *TGA diagram for a) **TPT** b) **TPT-Ben** c) **TPT-Ac***

For using molecules in diode applications, it should have fairly good thermal properties. The thermal stability of the synthesized molecules were examined by DSC and TG analysis (Figure 2.26 and Figure 2.27). The **TPT** derivatives were found to be thermally stable. **TPT** decomposed at 268 °C, **TPT-Ben** at 400 °C while **TPT-Ac** showed a decomposition at 200 °C. From thermal analysis we could conclude that the molecules can be considered as good candidates for emissive layers in OLEDs.

Table 2.5. Decomposition temperatures for different molecules

Sl. No	Name of the compound	T_d
1	**TPT**	268 ºC
2	**TPT- Ben**	444 ºC
3	**TPT- Ac**	200ºC

2.4.6 Density functional theory (DFT) studies

Density functional theory (DFT) at the B3LYP/6-31G* level was carried out to gain a better insight on the nature of the electronic transition and frontier molecular orbital (FMO) distributions.[71,72] The calculated FMO distributions of model systems are presented in Figure 2.28. It is evident from the figure that, in all the model systems studied, the HOMO is delocalized on the TPA (triphenyalmine) and thiophene moieties. On the other hand the LUMO is delocalized over thiophene and acceptor units. This feature confirms that, there is an intramolecular charge transfer (ICT) transition between the TPA and end acceptor groups. It is evident from Figure 2.28 that substituting -Ac moiety on the 5-postion of bithiophene in **TPT**

core leads to a clear charge separated state when compared to substitution by the -Ben unit at the same position. Hence the molecule **TPT-Ac** exhibited red shift in the absorption spectrum when compared to **TPT-Ben**. Comparing the molecules **TPT** and **TPT-Ben**, the degree of charge transfer is almost the same which indicates that charge transfer state of these molecules is primarily determined by the **TPT** and the bithiophene moieties. Moreover, there is no significant effect of the secondary donor (-Ben moiety) unit on the charge transfer state.

TD-DFT calculations were also performed to find out the orbitals involved in the dominant excited state electronic transitions and their corresponding energies and oscillator strength. It was found that for all the molecules, the ICT peaks arised from the HOMO to LUMO transition. The excited and ground state geometries were also computed using B3LYP/6-31G* level. It was found that **TPT-Ben** and **TPT-Ac** showed a twist on excitation from ground to excited state. They tend to be more planar in their S^1 state. Figure 2.29 shows the ground and excited state geometries of the molecules. The emission spectrum of **TPT-Ac** was getting broad in polar solvents, this observation may be addressed with this conformation change from ground to excited state. In the case of **TPT-Ac** twist angle between the thiophene and phenylacetlene is 21.1°,which become 0° in the exited state. **TPT-Ben** was nearly perpendicular in the ground sate with a twist angle of 87.6°. In the exited state the calculated angle between thiophene and dibenzothiophene was 37.7°.
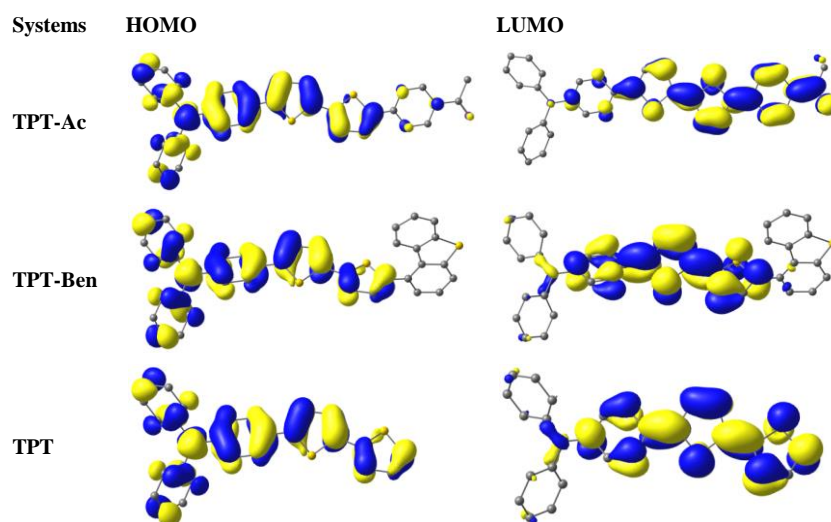
Figure 2.28. *Contour plots (isosurface value= 0.025 au) of the HOMO and LUMO levels of the derivatives at B3LYP/6-31G* level. The hydrogen atoms are omitted for clarity.*
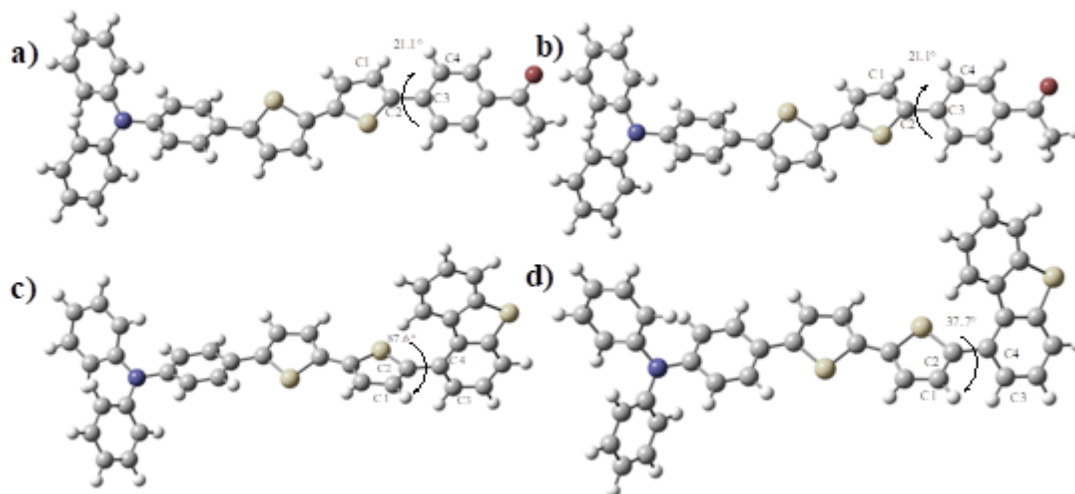
Figure 2.29. *Optimized molecular structures in ground and excited singlet states at B3LYP/6-31G* level of theory. a) Singlet ground state of* **TPT-Ac** *b) Singlet excited state of* **TPT-Ac** *c) Singlet ground state of* **TPT-Ben** *d) Singlet excited state of* **TPT-Ben**

2.5 White light generation using TPT-derivatives
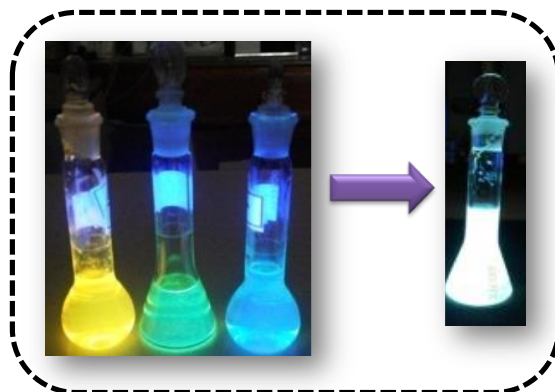
Figure 2.30. *Pictorial representation of the generation of white light using a 3: 2: 1 combination of the synthesized triphenylamine derivatives* **TPT, TPT- Ben and TPT- Ac.**

Generating white light is always fascinating due to its applications in solid state lighting and displays. An interesting observation made after the photoluminascent studies of **TPT, TPT-Ben** and **TPT- Ac** was that, the molecules emitted in blue, green and orange regions and also the Stokes shift values for the derivatives increased from the blue emitter to the orange-red emitter. As a result the molecules can be excited using same excitation wavelength. Based on this observation we examined the emission of a mixture of the three derivatives in solution state (DMSO) (Figure 2.30) as well as in the solid state. In both the cases, the mixture showed white light emission with a colour coordinate of (0.32, 0.36) and (0.33, 0.37) respectively. The

mixture of **TPT**, **TPT-Ben**, and **TPT-Ac** was excited at a 400 nm and they emitted white light for different permutations of concentrations *i.e*. the white light generation is independent of the slight variations in concentration. The best colour coordinate of the white light emission in solution state was obtained at 400 nm excitation with a ratio of 3:2:1 by weight for **TPT**, **TPT-Ben** and **TPT–Ac** (Figure 2.31). The colour coordinates obtained for different permutation combinations of concentration are given in table 2.6. The emission of the mixture of three molecules in solid state was also checked on a PMMA matrix. The ratio between the three was kept the same as that used for the solution state studies.
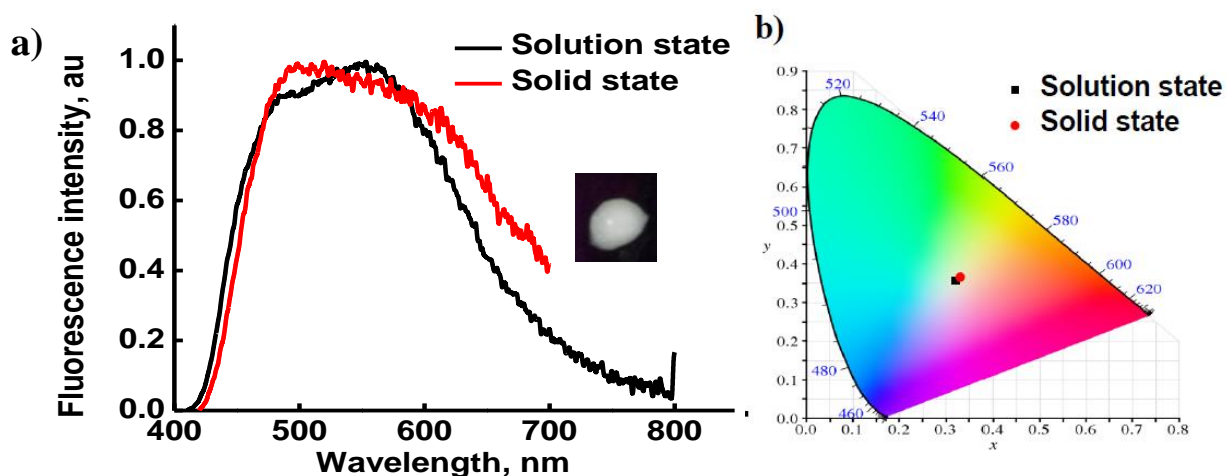
Figure 2.31. a) Fluorescence emission profile for the mixture of **TPT**, **TPT-Ben** and **TPT-Ac**in solution state and in film state at micromolar concentration (λ_{exc}= 400 nm). Inset shows the photograph of solid state emission for the mixture at the μM concentration and at 3:2:1 ratio of triphenylamine derivatives under 365 nm excitation) b) The CIE colour coordinate for the white light emission in solid state and in solution state.

Table 2.6. Solution state white light colour coordinate for different ratio by weight of the molecules at different excitation

Composition			Excitation	Coordinates
TPT	TPT-Ben	TPT-Ac		
3	2	1	380	(0.29, 0.34)
3	2	1	390	(0.31, 0.35)
3	2	1	400	(0.32, 0.36)
3	2	1	410	(0.35, 0.40)
3	2	2	380	(0.29, 0.35)

3	2	2	390	(0.31,0.36)
3	2	2	400	(0.33, 0.39)
3	2	2	410	(0.33, 0.40)

Table 2.7. Solid state white light colour coordinate for different ratio by weight of the molecules at different excitation wavelength

Composition			Excitation	Coordinates
TPT	TPT-Ben	TPT-Ac		
2	1	4	380	(0.41,0.40)
2	1	4	390	(0.37, 0.42)
2	1	4	400	(0.36, 0.42)
1	1	1	380	(0.38, 0.39)
1	1	1	400	(0.31, 0.40)
1	1	1	410	(0.35, 0.38)
1	1	1	395	(0.30, 0.38)
1	1	1	405	(0.33, 0.37)
1	1	2	400	(0.32, 0.40)
1	1	2	405	(0.33, 0.43)
1	1	2	395	(0.32, 0.41)
1	1	2	410	(0.35, 0.41)
1	2	3	390	(0.34, 0.40)
1	2	3	395	(0.33, 0.40)
1	2	3	400	(0.33, 0.39)
1	2	3	410	(0.38, 0.40)

1	2	3	390	(0.36, 0.42)
1	2	4	395	(0.34, 0.43)
1	2	4	400	(0.34, 0.43)
1	2	4	405	(0.35, 0.44)
1	2	4	410	(0.35, 0.44)

2.6 Electroluminescence studies

Among the three devices fabricated only two, the ones with **TPT-Ben** and **TPT-Ac** showed electroluminescence. The device with **TPT** did not have any electroluminescence. Figure 2.32 shows the device configurations as well as the images of the devices with **TPT-Ben** and **TPT-Ac.** Figure 2.33 presents the device characterization of **TPT-Ben** and Figure 2.34 gives the same for **TPT-Ac**. Table 2.8 summarizes the values for device performance of **TPT-Ben** and **TPT-Ac**
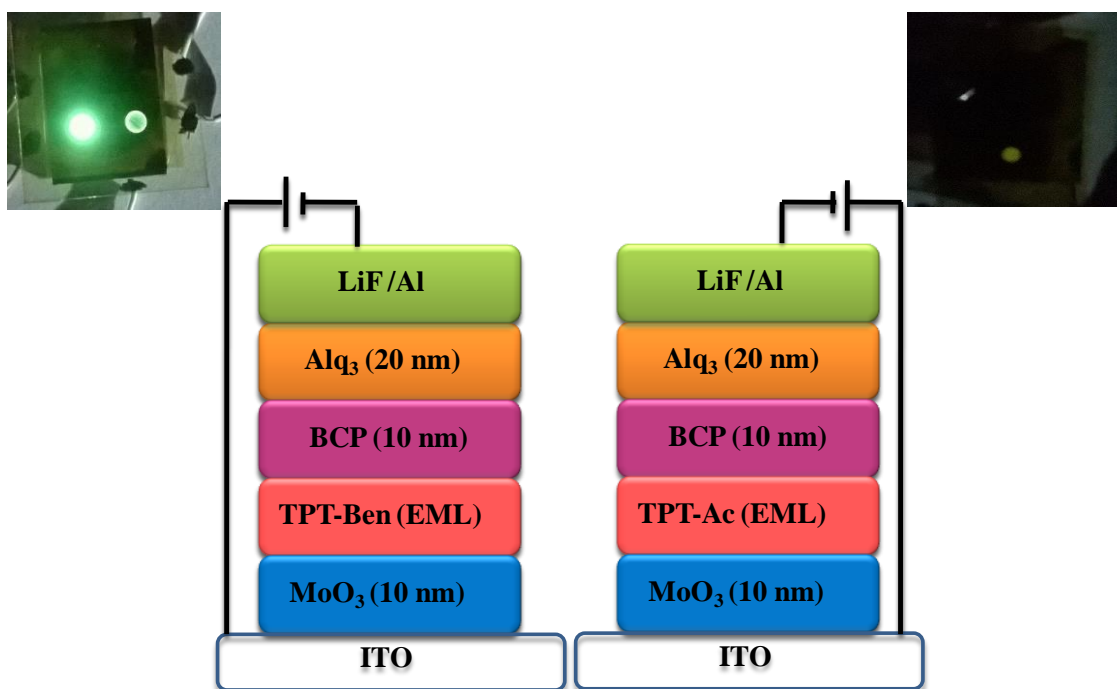
Figure 2.32. *Device configuration and picture of the fabricated devices*

ITO|MoO$_3$ (10nm)|TPT-Ben|BCP(10nm)|Alq$_3$(20nm)|LiF(1nm)|Al(150nm)
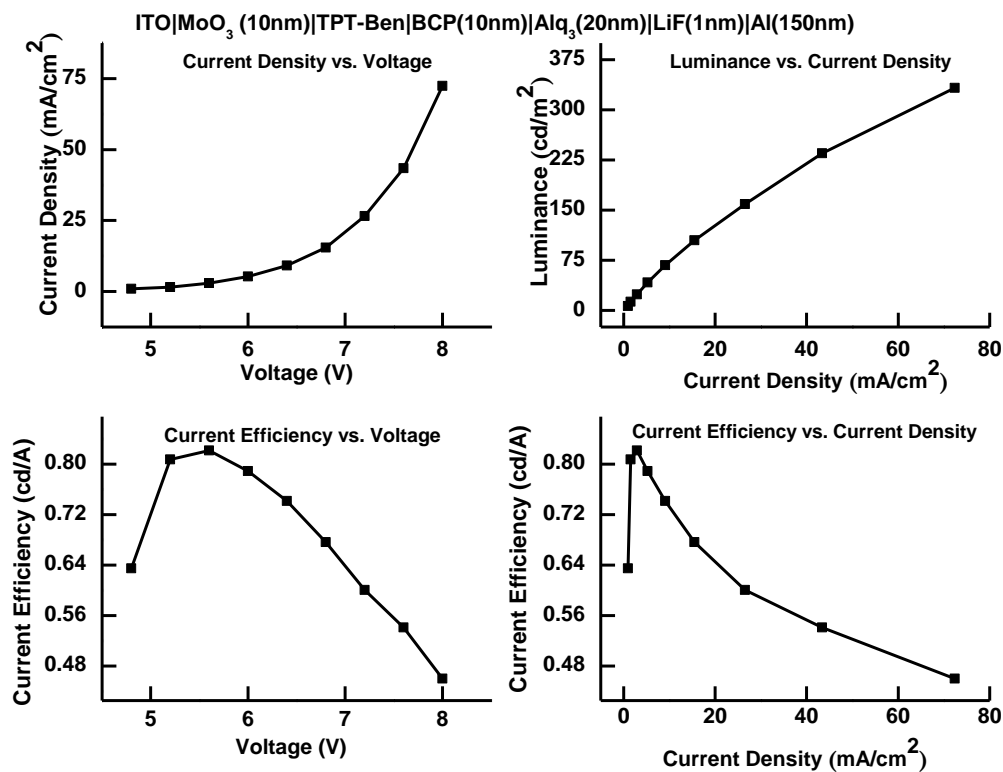
Figure 2.33. Device characterization of TPT-Ben

ITO|MoO$_3$ (10nm)|TPT-Ac|BCP(10nm)|Alq$_3$(20nm)|LiF(1nm)|Al(150nm)
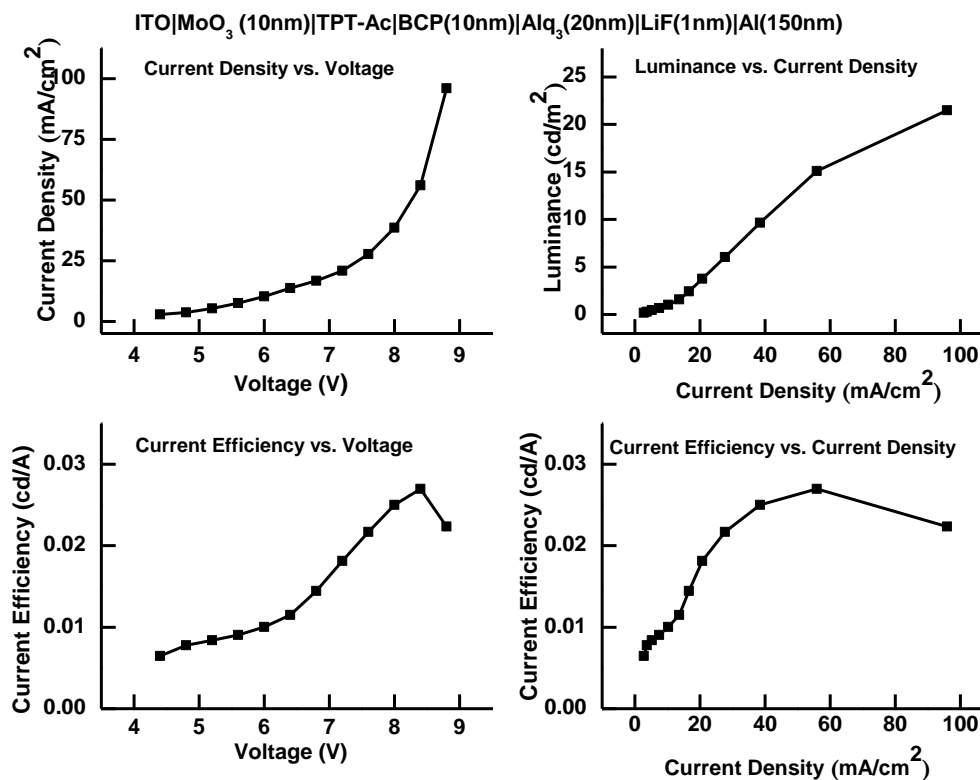
Figure 2.34. Device characterization of **TPT-Ac**

61

Table 2.8. The summary of EL studies

Name of the compound	Voltage (V)	Current (A)	Luminance (Lv)	Colour coordinates	Current Density (mA/cm^2)	Current efficiency (cd/A)	Power Efficiency (Im/W)
TPT Ben	8	9.00	332.7	(0.32,0.58)	72.37	0.50	0.18
TPT Ac	9	12.10	21.46	(0.41,0.51)	95.94	0.02	0.01

2.7 Conclusion

In summary, we demonstrated the synthesis and characterization of a set of three triphenylamine-bithiophene based donor-acceptor molecules **TPT**, **TPT- Ben**, and **TPT- Ac**. The emission from these molecules was successfully tuned from blue to orange-red. A 3: 2: 1 mixture by weight of the molecules produced white light emission in both solid and solution state employing the near lying absorption maxima. We strongly believe that these triphenylamine based donor-acceptor systems can find applications in the field of white light emitting diodes. With the molecules two devices were fabricated. Among the three molecules synthesized, two molecules showed good device properties namely **TPT-Ben** and **TPT-Ac**. **TPT-Ben** gave a green colour emission while **TPT-Ac** showed a pale yellowish white emission.

2.8. Experimental Section

2.8.1. General Information and Materials

The solvents purchased from Merck Millipore. Boronic acids and 4-bromotriphenylamine were purchased from Sigma Aldrich and used without further purification. NBS was purchased from Spectrohem and used after re-crystallizing from water. Na_2CO_3, Na_2SO_3 and activated aluminium oxide for column chromatography were also purchased from Spectrochem. The

catalyst Pd(PPh$_3$)$_4$ and silica gel for column chromatography were purchased from Alfa Aesar. Reactions were carried out under an inert atmosphere of argon in oven-dried glassware. The progress of the reaction was monitored using commercial Silica Gel TLC plates (Merck-Millipore, 60 F254) and UV detection (254 nm and 365 nm). Column chromatography was done using activated aluminium oxide and silica gel. The ^{1}H and ^{13}C NMR spectra were recorded using Bruker NMR spectrometer (AV500) with working frequency of 500 MHz for ^{1}H NMR and 125 MHz for ^{13}C NMR. The chemical shifts are reported in δ (ppm) relative to TMS as an internal standard. The signal splitting is abbreviated as follows: s = singlet; d = doublet; t = triplet; q = quartet; and m = multiplet. All coupling constants (*J*) given are in Hertz (Hz) Mass spectra were recorded using ESI/ HRMS at 60000 resolutions (Thermo Scientific Exactive)

2.8.1.1 General Procedure for the Suzuki-Miyaura Coupling[73]

The boronic acid (1 equivalent.) and bromo compound (1 equivalent) were taken in a reaction vessel along with Pd(PPh$_3$)$_4$. To this, THF was added with 2 N Na$_2$CO$_3$ dissolved in water in the ratio 2:1. The reaction mixture was degassed and filled with argon and allowed to stir at 65-70 °C for 12 h.

2.8.1.2 Synthesis of 4-(2,2'-bithiophene-5-yl)-N,N diphenylaniline (TPT)[62]

4-bromotriphenylamine (500 mg, 0.002 mol) and 2,2'-bithiophene-5-ylboronic acid (0.3718 mL, 0.002 mol) were added to the Schlenk tube along with the Pd(PPh$_3$)$_4$ as the catalyst. THF and 2N Na$_2$CO$_3$ in 2:1 ratio was added to the Schlenk tube. The reaction mixture was degassed and filled with argon and allowed to stir at 65-70 °C for 12 h. The extent of the reaction was monitored by the TLC and on completion, the residue was obtained by evaporation was subjected to column chromatography on activated aluminium oxide using hexane as eluent to afford the final product in good yield.

Spectral characterization of TPT
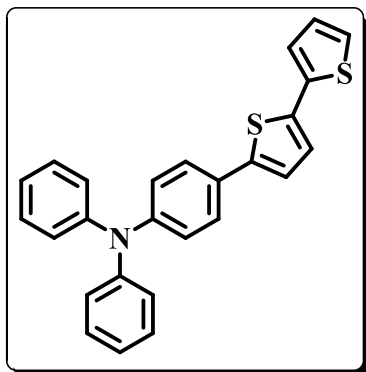
Yield:63% as a yellow crystal.

¹H NMR (500 MHz, CDCl₃): δ 7.45 (d, 2H, J = 9 Hz), 7.29 (t, J = 7.5 Hz, 4H), (d, J = 7.8 Hz, 1H), 7.17 (d, J = 3.5 Hz, 1H), 7.12 (t, J = 5 Hz, 6H), 7.07-7.01 (m, 5H).ppm

¹³C NMR (125 MHz, CDCl₃): δ 147.4, 147.3, 143.1, 137.6, 135.8, 129.3, 128.1, 127.8, 126.4, 124.6, 124.5, 124.2, 123.6, 123.4, 123.2, 122.8. ppm

HRMS (ESI) m/z calculated for $C_{26}H_{19}NS_2$, $(M+H)^+$: 410.1037, Found: 410.1024

2.8.1.3 Synthesis of 4-(5'-bromo-2,2'-bithiophen-5-yl)-N,N-diphenylaniline (TPT-Br)[62]

In the absence of light, a solution of NBS (220 mg, 0.00122 mol) in DMF (4 mL) was added dropwise to a solution of TPT (500 mg, 0.00122 mol) in DMF (10 mL). The mixture was cooled to 0 °C and kept stirring for 2 h at this temperature. The reaction was allowed to complete, by keeping it at room temperature for 1 h. On completion, 1 M aqueous solution of HCl (30 mL) was added to quench the reaction. The product was extracted using dichloromethane (100 mL) and the resulting organic layer was washed with water (4 x 300 mL), dried over Na_2SO_3 and concentrated to dryness. The product was purified by column chromatography on activated aluminium oxide (Hexane).

Spectral characterization of TPT-Br
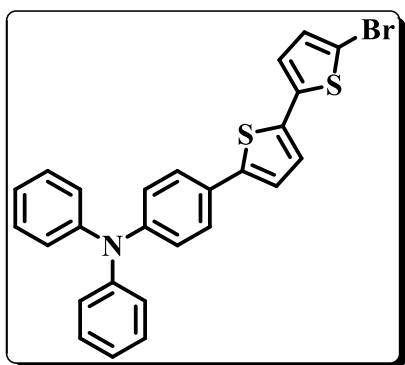
Yield: 54% as a yellow solid.

¹H NMR (500 MHz, CDCl₃): δ 7.45 (d, J = 8.7 Hz, 2H,); 7.32-7.24 (m, 4H), 7.16-7.02 (m, 10H),6.97 (d, 1H, J = 3.9Hz), 6.91 (d, J = 3.9 Hz, 1H,).ppm

¹³C NMR (125 MHz, CDCl₃): δ 147.6, 147.5, 143.7, 139.2, 134.8, 130.8, 129.5, 127.8, 126.5, 125.0, 124.7, 123.6, 123.5, 123.4, 122.9, 110.7.ppm

HRMS (ESI) for $C_{26}H_{18}BrNS_2$, Calcd 489.0026, Found: 489.0043 (M+).

Crystallographic data for TPT

Parameter	TPT

Crystal system	Triclinic	
Space group	*P*ī	
a	10.276Å	
b	10.405Å	
c	21.563Å	
α	94.824°	
β	95.581°	
γ	114.175°	
Volume	2073.8 (15) Å$_3$	**2.8.1.4**
Z	2	
Density	1.312 mg/m^3	
Absorption coefficient	0.269 mm^{-1}	
F(000)	856	

Synthesis of 4-(5'-(dibenzo[b,d]thiophen-2-yl)-2,2'-bithiophen-5-yl)-N diphenylaniline (TPT-Ben)

 4-(5,-bromo-2,2,-bithiophene-5-yl)-N, N-diphenylaniline, (500 mg, 0.000844 mol) and 4-dibenzothienyl boronic acid (211 mg, 0.0009 mol) were taken in a three-necked round bottom flask along with the Pd(PPh$_3$)$_4$ as the catalyst. THF and 2 N Na$_2$CO$_3$ solution in 2:1 ratio were added to the flask. The reaction mixture was degassed and filled with argon and allowed to stir at 65-70 °C for 12 h. The extent of the reaction was monitored by TLC and on completion, the residue was obtained by evaporation was subjected to column chromatography on silica gel using ethyl acetate/hexane (1:4) mixture as eluent to afford the product in good yield.

 Spectral Characters of TPT-Ben
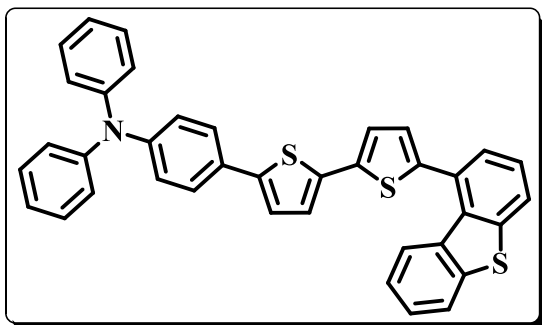
Yield: 73% as green solid.

¹H NMR [500 MHz, CDCl₃]: δ 8-8.2 (m, 1H), 8.15 (d, *J* = 8 Hz, 1 H), 7.92-7.90 (m, 1H), 7.70 (d, *J* = 7 Hz, 1 H), 7.58 (d, *J* = 3.5 Hz, 1 H), 7.55 (d, *J* = 8 Hz, 1 H), 7.527-7.492 (m, 4H), 7.30 (d, *J* = 8 Hz, 4H), 7.18 (d, *J* = 3.5 Hz, 1H), 7.15 (d, *J* = 8 Hz, 4H), 7.10- 7.05 (m, 4 H). ppm

¹³C NMR [125 MHz, CDCl₃]: δ 147.5, 131.8, 130.9, 129.4, 128.0, 127.0, 126.4, 125.0, 124.9, 124.6, 123.6, 123.2, 121.8. ppm

HRMS (ESI) m/z calculated for $C_{38}H_{25}NS_3$, (M+H)⁺: 592.1285, Found: 592.1227

2.8.1.5 Synthesis of the compound 1-(4-(5'-(4-(diphenylamino)phenyl)-2,2'-bithiophen-5-yl)phenyl)ethanone (TPT-Ac)

4-(5'-bromo-2,2',-bithiophen-5-yl)-N,N-diphenylaniline (500 mg, 0.000948 mol) and 4-acetylphenylboronic acid (169 mg, 0.010 mol)were taken in a three-necked round bottom flask along with the Pd(PPh₃)₄ as the catalyst. The mixture is degassed. THF and 2N Na₂CO₃ in 2:1 ratio was added to the flask. The reaction mixture was degassed and filled with argon and allowed to stir at 65-70 ᵒC for 12 h. The extent of the reaction monitored by the TLC and on completion, the residue was obtained by evaporation, which was subjected to column chromatography on silica gel using ethyl acetate/hexane (1:5) mixture as eluent to afford the product in good yield.

Spectral characterization of TPT-Ac

2.8.2 Instrumentation

2.8.2.1 X-ray Crystallographic Analysis

The diffraction data of the single crystal were collected on a Rigaku Saturn 724+ diffractometer using graphite monochromated Mo-Kα radiation. The data were processed using the Rigaku Crystal Clear software.[74] The structure solution was carried out by direct methods, and the refinements were performed by full-matrix least-squares on F2 using the SHELXTL suite of
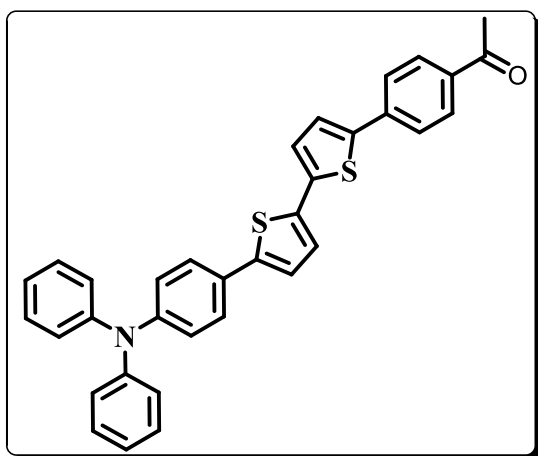
Yield: 70% as orange solid.

^{1}H NMR (500 MHz, CDCl$_3$): δ 7.98 (d, J = 8.5 Hz, 2H), 7.69 (d, J = 8.5 Hz, 2H), 7.47 (d, J = 5 Hz, 2H),7.37 (d, J = 3.5 Hz, 1H), 7.30 (d, J = 7.5 Hz, 4H), 7.19 (d, J = 3.5 Hz, 3H), 7.20-7.13 (m, 5H), 7.09-7.05 (m, 4H). 2.63 (s, 3H) ppm

^{13}C NMR (125 MHz, CDCl$_3$): δ 197.3, 147.6, 147.4, 143.8, 141.1, 138.7, 138.5, 135.6, 135.2,129.4, 129.2, 129.0, 127.7, 127.5, 126.6, 126.4,125.5, 125.2, 125.0,124.6, 124.4, 123.5, 123.3,122.9, 26.6. ppm

HRMS (ESI) m/z calculated for C$_{34}$H$_{25}$NOS$_2$, (M+): 527.1377 Found: 527.136.

programs.[75]All of the hydrogen atoms were placed in geometrically ideal positions (using the corresponding HFIX) and refined in the riding mode. Final refinements included the atomic positions of all the atoms, anisotropic thermal parameters for all of the non-hydrogen atoms, and isotropic thermal parameters for all of the hydrogen atoms.

2.8.2.2 Thermal Analysis

Thermo-gravimetric analyses were performed on an EXSTAR TG-DTA 6200 instrument (SII Nanotechnology Inc.) heated from 30 to 1000 °C in flowing nitrogen at the heating rate of 10 °C min^{-1}. The temperature at which a 5% weight loss occurred has been considered as the decomposition temperature (Td). Differential scanning calorimetry was performed using a TA Q20 general-purpose DSC instrument in sealed aluminum pans under nitrogen flow at a heating/cooling rate of 5 °C min^{-1}.

2.8.2.3 Photophysical studies

Absorption spectra were recorded using a Shimadzu UV-2600 UV-Visible spectrophotometer. The optical diffuse reflectance spectra were measured for solid samples using the aforementioned spectrometer equipped with an integrating sphere. BaSO$_4$ was used as the

reference material, and the solid samples were ground well before the measurement. The absorption (α/S) data were calculated from the reflectance spectra using the Kubelka–Munk function: α/S= (1 - R)2/2R, in which R is the reflectance at a given wavelength, α is the absorption coefficient, and S is the scattering coefficient (practically wavelength independent when the particle size is larger than 5 mm). Steady-state fluorescence experiments were performed using FluoroLog-322 (Horiba) which was equipped with a 450 W Xe arc lamp by using optically dilute solutions. The fluorescence quantum yields in various solvents were determined by the relative method employing an optically matched solution of quinine sulphate in 0.1Nsulphuric acid as the reference (Φ_R = 0.54). The following equation (1) was used for calculating the quantum yield,[76]

$$\Phi_S = \frac{Abs_R}{Abs_s} \times \frac{Area_S}{Area_R} \times \frac{nS^2}{nR^2} \times \Phi_R \tag{1}$$

where the subscript R and S refer to the reference and samples respectively. Abs, Area, and n are the absorbance at the excitation wavelength, the area under the fluorescence spectrum and refractive index of the solvent respectively. Solid state photoluminescence spectra were also recorded using the front face mode with the same Fluorolog spectrofluorimeter. Time-resolved fluorescence spectra and lifetime experiments were performed by using an IBH picosecond single photon counting system employing the 375 nm nano LED as excitation sources and a Hamamatsu C4878-02 microchannel plate (MCP) detector. Decay in the fluorescence intensity (I) with time (t) was fitted either by a double/triple-exponential function:

$$I = A_1 e^{-t/\tau_1} + A_2 e^{-t/\tau_2} \tag{2}$$

$$I = A_1 e^{-t/\tau_1} + A_2 e^{-t/\tau_2} + A_3 e^{-t/\tau_3} \tag{3}$$

where τ_1, τ_2, and τ_3 are the lifetimes of different species, and A_1, A_2, and A_3 are their respective amplitudes. The weighted mean lifetime ($\langle\tau\rangle$) was calculated according to equation (4):

$$\langle\tau\rangle = \Sigma\tau_i A_i \tag{4}$$

The quality of the fits was checked by examining the residual distribution and the χ^2 value. The solid state samples were recorded with the front face mode. All the experiments were conducted at room temperature.

2.8.2.4 Cyclic voltammetry

Cyclic voltammetry experiments were carried out using a BAS 50 W voltammetric analyzer using three electrode cell assemblies. Platinum wires were used as counter electrodes, a silver wire was used as an Ag/Ag+ quasi-reference electrode, and a platinum electrode was used as a working electrode. Measurements were carried out in acetonitrile solution with tetrabutylammoniumhexafluorophosphate as the supporting electrolyte at a scan rate of 100 mV s^{-1}. Concentrations of the molecules and the supporting electrolyte were 5×10^{-3} and 0.1 M, respectively. The ferrocenium/ferrocene couple (FeCp2^{+}/FeCp2^{0}) was used as an internal reference. The energy level of FeCp2^{+}/FeCp2^{0} was assumed at -4.8 eV to vacuum.[77]All solutions for the electrochemical studies were deaerated with pre-purified argon gas before the measurements.

2.8.2.5 Computational methods

The ground (S^{0}) geometries of model systems **TPT-Ac**, **TPT-Ben** and **TPT** were optimized by using density functional theory (DFT) based method with Becke's three-parameter functional and the Lee-Yang-Parr functional (B3LYP) with 6-31G* basis set. Based on the gas phase optimized geometry of **TPT-Ac**, **TPT-Ben** and **TPT** spectral properties in chloroform were calculated by time dependent density functional theory (TD-DFT) method with Polarizable Continuum Model (PCM) at PBE0/6-31G* level. All the calculations were carried out using Gaussian 09 program package.

2.8.2.6 Device fabrications

OLEDs were fabricated on an indium-tin oxide (ITO) coated glass substrates (sheet resistance of 20 ohm sq^{-1}) by first cleaning them using trichloroethylene, acetone, and isopropyl alcohol and deionized water sequentially for 20 m using an ultrasonic bath and dried under flowing nitrogen. Before film deposition, the ITO substrates were treated with UV-ozone for 5 m. Organic molecules and cathode were subsequently added using the spin coating. The emissive layers were spin coated using a solution of 5 mg of the respective molecules dissolved in 1 mL

toluene to get a uniform film of about 40 nm thickness. The device configurations used for the electroluminescence studies was (ITO/ MoO_3/ **TPT** or **TPT-Ben** or **TPT-Ac** (40nm)/ BCP (10 nm)/ Alq_3 (20 nm)/ LiF (1 nm)/ Al (150 nm)). In the given stacking MoO_3 is used as a hole injection layer followed by the emissive layer. BCP is used as a hole blocking layer and Alq_3 as electron transporter. EL spectra were measured using an Ocean Optics high-resolution spectrometer (HR-2000CG UVNIR). The J–V–L characteristics were measured with a luminance meter (LMT l-1009) and a Keithley 2400 programmable voltage-current digital source meter. All the measurements were carried out at room temperature under ambient conditions.

Steps followed for the device fabrication by solution processing is listed below

1. Patterning
2. Pixellization
3. RCA cleaning
   - RCA solution
   - 20 min boiling at 75 °C
4. Ozonization
   - 10 min pretreatment
   - 10 min Ozon treatment
   - 10 min O_3 flow
5. MoO_3 coating
   - Spin Solution of Liquor Amonia (5ml)+ 5mg MoO_3. After stirring it for 24 hours,
   - 12 hour stirring
   - coated that @ 4000 RPM for 1 minute.
   - Drying was done @ 200 ºC for 10 minutes over hot plate.
6. triphenylamine derivatives coating
   - Tuluene as the solvent (5mg/mL)
   - 12 hour stirring
   - 2000 RPM for 1 min

7. BCP coating 10 nm
8. Alq$_3$ coating 20 nm
9. LiF coating 1 nm
10. Al coating 150 nm
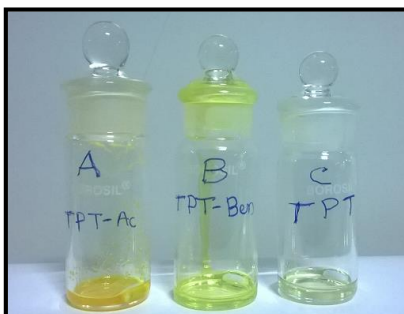
Figure 2.35. *Solutions of the triphenylamine derivatives in toluene used for the device fabrication*

2.9 Reference

1. Shirota, Y. Organic Materials for Electronic and Optoelectronic Devices. **2000**, No. 10, 1–25.

2. Shirota, Y. Photo- and Electroactive Amorphous Molecular Materials - Molecular Design, Syntheses, Reactions, Properties, and Applications. *J. Mater. Chem.* **2005**, *15* (1), 75–93.

3. Thelakkat, M. Star-Shaped, Dendrimeric and Polymeric Triarylamines as Photoconductors and Hole Transport Materials for Electro-Optical Applications. *Macromol. Mater. Eng.* **2002**, *287* (7), 442–461.

4. Manifar, T.; Rohani, S. Synthesis and Analysis of Triphenylamine: A Review. *Can. J. Chem. Eng.* **2004**, *82* (2), 323–334.

5. Shirota, Y.; Kageyama, H. Charge Carrier Transporting Molecular Materials and Their Applications in Devices. *Chem. Rev.* **2007**, *107* (4), 953–1010.

6. Ning, Z.; Tian, H. Triarylamine: A Promising Core Unit for Efficient Photovoltaic Materials. *Chem. Commun.* **2009**, 37(2), 5483–5495.

7. Mishra, A.; Fischer, M. K. R.; Bäuerle, P. Metal-Free Organic Dyes for Dye-Sensitized Solar Cells: From Structure: Property Relationships to Design Rules. *Angew. Chemie Int. Ed.* **2009**, *48* (14), 2474–2499.

8. Wu, H.; Ying, L.; Yang, W.; Cao, Y. Progress and Perspective of Polymer White Light-Emitting Devices and Materials. *Chem. Soc. Rev.* **2009**, *38* (12), 3391–3400.

9. Clifford, J. N.; Martínez-Ferrero, E.; Viterisi, A.; Palomares, E. Sensitizer Molecular Structure-Device Efficiency Relationship in Dye Sensitized Solar Cells. *Chem. Soc. Rev.* **2011**, *40* (3), 1635–1646.

10. Iwan, A.; Sek, D. Polymers with Triphenylamine Units: Photonic and Electroactive Materials. *Prog. Polym. Sci.* **2011**, *36* (10), 1277–1325.

11. Yen, H. J.; Liou, G. S. Solution-Processable Triarylamine-Based Electroactive High Performance Polymers for Anodically Electrochromic Applications. *Polym. Chem.* **2012**, *3* (2), 255–264.

12. Liang, M.; Chen, J. Arylamine Organic Dyes for Dye-Sensitized Solar Cells; *Chem Soc Rev.* **2013**, 42 (42), 3453–3488.

13. Mahmood, A. Triphenylamine Based Dyes for Dye Sensitized Solar Cells: A Review. *Sol. Energy* **2016**, *123* (April), 127–144.

14. Pron, A.; Gawrys, P.; Zagorska, M.; Djurado, D.; Demadrille, R. Electroactive Materials for Organic Electronics: Preparation Strategies, Structural Aspects and Characterization Techniques. *Chem. Soc. Rev.* **2010**, *39* (7), 2577–2632.

15. Bujak, P.; Kulszewicz-Bajer, I.; Zagorska, M.; Maurel, V.; Wielgus, I.; Pron, A. Polymers for Electronics and Spintronics. *Chem. Soc. Rev.* **2013**, *42* (23), 8895–8999.

16. Song, Y.; Di, C. A.; Xu, W.; Liu, Y.; Zhang, D.; Zhu, D. New Semiconductors Based on Triphenylamine with Macrocyclic Architecture: Synthesis, Properties and Applications in OFETs. *J. Mater. Chem.* **2007**, *17* (42), 4483–4491.

17. Wenhui, Z.; Stephen, M. K.; Kevin, L. B.; Tianyue, Y.; Kevin, C. J.; Christopher, K. O.; Joseph, W. P.; Seth, R. M. An Efficient Two-Photon-Generated Photoacid Applied to Positive-Ton 3D Microfabrication. *Science.* **2002**, *296* (MAY), 1106–1109.

18. Lafratta, C. N.; Fourkas, J. T.; Baldacchini, T.; Farrer, R. A. Multiphoton Fabrication. *Angew. Chemie - Int. Ed.* **2007**, *46*, 6238–6258.

19. Gan, X.; Wang, Y.; Ge, X.; Li, W.; Zhang, X.; Zhu, W.; Zhou, H.; Wu, J.; Tian, Y. *Triphenylamine Isophorone Derivatives with Two Photon Absorption: Photo-Physical Property, DFT Study and Bio-Imaging*; Elsevier Ltd, 2015; Vol. 120.

20. Allain, C.; Schmidt, F.; Lartia, R.; Bordeau, G.; Fiorini-Debuisschert, C.; Charra, F.; Tauc, P.; Teulade-Fichou, M. P. Vinyl-Pyridinium Triphenylamines : Novel Far- Red Emitters with High Photostability and Two- Photon Absorption Properties for Staining DNA. *ChemBioChem* **2007**, *8*, 424–433.

21. Chennoufi, R.; Bougherara, H.; Gagey-Eilstein, N.; Dumat, B.; Henry, E.; Subra, F.; Bury-Moné, S.; Mahuteau-Betzer, F.; Tauc, P.; Teulade-Fichou, M. P.; Deprez, E. Mitochondria-Targeted Triphenylamine Derivatives Activatable by Two-Photon Excitation for Triggering and Imaging Cell Apoptosis. *Sci. Rep.* **2016**, *6* (21458), 1– 12.

22. Jiang, Y.; Wang, Y.; Yang, J.; Hua, J.; Wang, B.; Qian, S.; Tian, H. Synthesis, Two-Photon Absorption, and Optical Power Limiting of New Linear and Hyperbranched Conjugated Polyynes Based on Bithiazole and Triphenylamine. *J. Polym. Sci. Part A Polym. Chem.* **2011**, *49* (8), 1830–1839.

23. Anémian, R.; Morel, Y.; Baldeck, P. L.; Paci, B.; Kretsch, K.; Nunzi, J. M.; Andraud, C. Optical Limiting in the Visible Range: Molecular Engineering around N4,N4′-bis(4-Methoxyphenyl)-N4,N4′-Diphenyl-4,4′-Diaminobiphenyl. *J. Mater. Chem.* **2003**, *13* (9), 2157–2163.

24. Echeverry, C. A.; Cotta, R.; Insuasty, A.; Ortíz, A.; Martín, N.; Echegoyen, L.; Insuasty, B. Synthesis of Novel Light Harvesters Based on Perylene Imides Linked to Triphenylamines for Dyes Sensitized Solar Cells. *Dye. Pigment.* **2018**, *153 (8)*, 182– 188.

25. Surya, P. S.; M, S. R.; Thomas, K. R. J.; Balaiah, S.; Bhanuprakash, K.; Sharma, G. D. New Triphenylamine-Based Organic Dyes with Different Numbers of Anchoring Groups for Dye-Sensitized Solar Cells. *J. Phys. Chem. C* **2012**, *116 (5)*, 5941–5960.

26. Xu, W.; Peng, B.; Chen, J.; Liang, M.; Cai, F. New Triphenylamine-Based Dyes for Dye-Sensitized Solar Cells. *J. Phys. Chem. C* **2008**, *112* (3), 874–880.

27. Kawasumi, K.; Wu, T.; Zhu, T.; Chae, H. S.; Van Voorhis, T.; Baldo, M. A.; Swager, T. M. Thermally Activated Delayed Fluorescence Materials Based on Homoconjugation Effect of Donor-Acceptor Triptycenes. *J. Am. Chem. Soc.* **2015**, *137* (37), 11908–11911.

28. Hontz, E.; Chang, W.; Congreve, D. N.; Bulović, V.; Baldo, M. A.; Van Voorhis, T. The Role of Electron-Hole Separation in Thermally Activated Delayed Fluorescence in Donor-Acceptor Blends. *J. Phys. Chem. C* **2015**, *119* (45), 25591–25597.

29. Zhou, C.; Zhang, T.; Zhang, S.; Liu, H.; Gao, Y.; Su, Q.; Wu, Q.; Li, W.; Chen, J.; Yang, B. Isomerization Effect of Triphenylamine-Acridine Derivatives on Excited-State Modification, Photophysical Property and Electroluminescence Performance. *Dye. Pigment.* **2017**, *146*, 558–566.

30. Rybakiewicz, R.; Zagorska, M.; Pron, A. Triphenylamine-Based Electroactive Compounds: Synthesis, Properties and Application to Organic Electronics. *Chem. Pap.* **2017**, *71* (2), 243–268.

31. Agarwala, P.; Kabra, D. A Review on Triphenylamine (TPA) Based Organic Hole Transport Materials (HTMs) for Dye Sensitized Solar Cells (DSSCs) and Perovskite Solar Cells (PSCs): Evolution and Molecular Engineering. *J. Mater. Chem. A* **2017**, *5* (4), 1348–1373.

32. Tao, Y.; Yang, C.; Qin, J. Organic Host Materials for Phosphorescent Organic Light-Emitting Diodes. *Chem. Soc. Rev.* **2011**, *40* (5), 2943–2970.

33. Li, Z.; Wu, Z.; Fu, W.; Liu, P.; Jiao, B.; Wang, D.; Zhou, G.; Hou, X. Versatile Fluorinated Derivatives of Triphenylamine as Hole-Transporters and Blue-Violet Emitters in Organic Light-Emitting Devices. *J. Phys. Chem. C* **2012**, *116* (38), 20504–20512.

34. Sandberg, M. O.; Nagao, O.; Wu, Z.; Matsushita, M. M.; Sugawara, T. Generation of a Triplet Diradical from a Donor-Acceptor Cross Conjugate upon Acid-Induced Electron Transfer. *Chem. Commun.* **2008**, 32 (5), 3738–3740.

35. Tambara, K.; Pantoş, G. D. Supramolecular Chemistry of Donor-Acceptor Interactions. *Annu. Reports Prog. Chem. - Sect. B* **2012**, *108* (0), 186–201.

36. Guo, Z.; Lei, T.; Jin, Z.; Wang, J.; Pei, J. T-shaped donor– acceptor molecules for low-loss red-emission optical waveguide. *Org Lett*. **2013**, 15(14), 3530-3533.

37. Luponosov, Y. N.; Solodukhin, A. N.; Ponomarenko, S. A. Branched Triphenylamine-Based Oligomers for Organic Electronics. *Polymer Science Series C.* **2014**, 56(1),104–134

38. Diac, A.; Demeter, D.; Jungsuttiwong, S.; Grosu, I.; Roncali, J. ADDA and ADADA Systems Based on Triphenylamine as Molecular Donors for Organic Photovoltaics. *Tetrahedron Lett.* **2015**, *56* (31), 4607–4612.

39. Wu, F.; Zhao, S.; Lee, L. T. L.; Wang, M.; Chen, T.; Zhu, L. Novel D-π-A Organic Sensitizers Containing Diarylmethylene-Bridged Triphenylamine and Different Spacers for Solar Cell Application. *Tetrahedron Lett.* **2015**, *56* (10), 1233–1238.

40. Liao, J.; Wang, Y.; Xu, Y.; Zhao, H.; Xiao, X.; Yang, X. Synthesis, Optical and Electrochemical Properties of Novel Meso-Triphenylamine-BODIPY Dyes with Aromatic Moieties at 3,5-Positions. *Tetrahedron* **2015**, *71* (31), 5078–5084.

41. Zhang, Q.; Zhang, J.; Zuo, H.; Wang, C.; Shen, Y. A Novel Colorimetric and Fluorescent Sensor for Cyanide Anions Detection Based on Triphenylamine and Benzothiadiazole. *Tetrahedron* **2016**, *72* (9), 1244–1248.

42. Pluczyk, S.; Zassowski, P.; Quinton, C.; Audebert, P.; Alain-Rizzo, V.; Lapkowski, M. Unusual Electrochemical Properties of the Electropolymerized Thin Layer Based on a S-Tetrazine-Triphenylamine Monomer. *J. Phys. Chem. C* **2016**, *120* (8), 4382–4391.

43. Jiang, Y.; Wang, Y.; Yang, J.; Hua, J.; Wang, B.; Qian, S.; Tian, H. Synthesis, Two-Photon Absorption, and Optical Power Limiting of New Linear and Hyperbranched Conjugated Polyynes Based on Bithiazole and Triphenylamine. *J. Polym. Sci. Part A Polym. Chem.* **2011**, *49* (8), 1830–1839.

44. Khanasa, T.; Prachumrak, N.; Rattanawan, R.; Jungsuttiwong, S.; Keawin, T.; Sudyoadsuk, T.; Tuntulani, T.; Promarak, V. Bis(carbazol-9-Ylphenyl)aniline End-Capped Oligoarylenes as Solution-Processed Nondoped Emitters for Full-Emission Color Tuning Organic Light-Emitting Diodes. *J. Org. Chem.* **2013**, *78* (13), 6702–6713.

45. Neumann K, Schwarz C, Köhler A, Thelakkat M, Influence of the Excited-State Charge-Transfer Character on the Exciton Dissociation in Donor–Acceptor Copolymers, *J. Phys. Chem. C*, **2014**, 118 (1), 27–36.

46. Yasuda, T.; Shinohara, Y.; Kusagaki, Y.; Matsuda, T.; Han, L.; Ishi-I, T. Synthesis and Photovoltaic Properties of Naphthobisthiadiazole-Triphenylamine-Based Donor-Acceptor π-Conjugated Polymer. *Polym. (United Kingdom)* **2015**, *58*, 139–145.

47. Li, W.; Liu, D.; Shen, F.; Ma, D.; Wang, Z.; Feng, T.; Xu, Y.; Yang, B.; Ma, Y. A Twisting Donor-Acceptor Molecule with an Intercrossed Excited State for Highly Efficient, Deep-Blue Electroluminescence. *Adv. Funct. Mater.* **2012**, *22* (13), 2797–2803.

48. Zhu, X.-H.; Peng, J.; Cao, Y.; Roncali, J. Solution-Processable Single-Material Molecular Emitters for Organic Light-Emitting Devices. *Chem. Soc. Rev.* **2011**, *40* (7), 3509–3524.

49. Li, Y.; Liu, J. Y.; Zhao, Y. Di; Cao, Y. C. Recent Advancements of High Efficient Donor–acceptor Type Blue Small Molecule Applied for OLEDs. *Mater. Today,* **2017**, *20* (5), 258–266.

50. Liu, H.; Bai, Q.; Li, W.; Guo, Y.; Yao, L.; Gao, Y.; Li, J.; Lu, P.; Yang, B.; Ma, Y. Efficient Deep-Blue Non-Doped Organic Light-Emitting Diode with Improved Roll-off of Efficiency Based on Hybrid Local and Charge-Transfer Excited State. *RSC Adv.* **2016**, *6* (74), 70085–70090.

51. Liu, M.; Li, X. L.; Chen, D. C.; Xie, Z.; Cai, X.; Xie, G.; Liu, K.; Tang, J.; Su, S. J.; Cao, Y. Study of Configuration Differentia and Highly Efficient, Deep-Blue, Organic Light-Emitting Diodes Based on Novel Naphtho[1,2-D]imidazole Derivatives. *Adv. Funct. Mater.* **2015**, *25* (32), 5190–5198.

52. Mazzeo, M.; Pisignano, D.; Favaretto, L.; Barbarella, G.; Cingolani, R.; Gigli, G. Bright Oligothiophene-Based Light Emitting Diodes. In *Synthetic Metals*; **2003**; 139, 671–673.

53. Mishra, A.; Ma, C. Q.; Bäuerle, P. Functional Oligothiophenes: Molecular Design for Multidimensional Nanoarchitectures and Their Applications. *Chem. Rev.* **2009**, *109* (3), 1141–1176.

54. Junwu, C. A.; Yong, C. Development of Novel Conjugated Donor Polymers for High-Efficiency Bulk-Heterojunction Photovoltaic Devices. *Acc. Chem. Res.* **2009**, *42* (11), 1709–1718.

55. Song, M. S.; Nguyen, Q. P. B.; Song, C. H.; Lee, D.; Chai, K. Y. Synthesis of Some Green Dopants for OLEDs Based on Arylamine 2,3-Disubstituted Bithiophene Derivatives. *Molecules* **2013**, *18* (11), 14033–14041.

56. Persaud, K. C. Polymers for Chemical Sensing. *Mater. Today* **2005**, *8* (4), 38–44.

57. Bolduc, A.; Dong, Y.; Guérin, A.; Skene, W. G. Solvatochromic Investigation of Highly Fluorescent 2-Aminobithiophene Derivatives. *Phys. Chem. Chem. Phys.* **2012**, *14* (19), 6946.

58. Reva, I.; Lapinski, L.; Chattopadhyay, N.; Fausto, R. Vibrational Spectrum and Molecular Structure of Triphenylamine Monomer: A Combined Matrix-Isolation FTIR and Theoretical Study. *Phys. Chem. Chem. Phys.* **2003**, *5* (18), 3844–3850.

59. Barchiesi, E.; Bradamante, S. ^{15}N NMR of Nitranions: Opposite Shift Effects of σ and π Charge. *J. Phys. Org. Chem.* **1990**, *3* (3), 139–142.

60. Yang, X.; Huang, H.; Pan, B.; Aldred, M. P.; Zhuang, S.; Wang, L.; Chen, J.; Ma, D. Modified 4,4′,4″-Tri(N-Carbazolyl)triphenylamine as a Versatile Bipolar Host.pdf. *J. Phys. Chem. C* **2012**, *116*, 15041–15047.

61. Park, J. H.; Chung, D. S.; Lee, D. H.; Kong, H.; Jung, I. H.; Park, M. J.; Cho, N. S.; Park, C. E.; Shim, H. K. New Anthracene-Thiophene-Based Copolymers That Absorb across the Entire UV-Vis Spectrum for Application in Organic Solar Cells. *Chem. Commun.* **2010**, *46* (11), 1863–1865.

62. Leliège, A.; Blanchard, P.; Rousseau, T.; Roncali, J. Triphenylamine/Tetracyanobutadiene-Based D-A-D π-Conjugated Systems as Molecular Donors for Organic Solar Cells. *Org. Lett.* **2011**, *13* (12), 3098–3101.

63. Mataga, N.; Kaifu, Y.; Koizumi, M. The Solvent Effect on Fluorescence Spectrum, Change of Solute-Solvent Interaction during the Lifetime of Excited Solute Molecule. *Bull. Chem. Soc. Jpn.* **1955**, *28* (9), 690–691.

64. Mataga, N.; Kaifu, Y.; Koizumi, M. Solvent Effects upon Fluorescence Spectra and the Dipolemoments of Excited Molecules. *Bull. Chem. Soc. Jpn.* **1956**, *29* (4), 465–470.

65. Li, Y.; Li, Z.; Ablekim, T.; Ren, T.; Dong, W. J. Rational Design of Tetraphenylethylene-Based Luminescent down-Shifting Molecules: Photophysical Studies and Photovoltaic Applications in a CdTe Solar Cell from Small to Large Units. *Phys. Chem. Chem. Phys.* **2014**, *16* (47), 26193–26202.

66. Lippert, E. Dipolmoment Und Elektronenstruktur von Angeregten Molekülen. *Zeitschrift fur Naturforsch. - Sect. A J. Phys. Sci.* **1955**, *10* (7), 541–545.

67. Bonvoisin, J.; Launay, J.-P.; Van Der Auweraer, M.; De Schryver, F. C. Organic Mixed-Valence Systems: Intervalence Transition in Partly Oxidized Aromatic Polyamines. Electrochemical and Optical Studies. *J. Phys. Chem. A* **1994**, *98* (19), 5052–5057.

68. Lor, M.; Jordens, S.; De Belder, G.; Schweitzer, G.; Fron, E.; Viaene, L.; Cotlet, M.; Weil, T.; Mullen, K.; Verhoeven, J. W.; Van der Auweraer, M.; De Schryver, F. C. Direct Proof of Electron Transfer in a Rigid First Generation Triphenyl Amine Core Dendrimer Substituted with a Peryleneimide acceptor Dedicated to the Memory of Nobel Laureate, Lord George Porter FRSC FRS OM. *Photochem. Photobiol. Sci.* **2003**, *2* (5), 501.

69. Lor, M.; Thielemans, J.; Viaene, L.; Cotlet, M.; Hofkens, J.; Weil, T.; Hampel, C.; Müllen, K.; Verhoeven, J. W.; Van der Auweraer, M.; De Schryver, F. C. Photoinduced Electron Transfer in a Rigid First Generation Triphenylamine Core Dendrimer Substituted with a Peryleneimide Acceptor. *J. Am. Chem. Soc.* **2002**, *124* (33), 9918–9925.

70. Thangthong, A.; Prachumrak, N.; Tarsang, R.; Keawin, T.; Jungsuttiwong, S.; Sudyoadsuk, T.; Promarak, V. Blue Light-Emitting and Hole-Transporting Materials Based on 9,9-bis(4-Diphenylaminophenyl)fluorenes for Efficient Electroluminescent Devices. *J. Mater. Chem.* **2012**, *22* (14), 6869.

71. Kim, K.; Jordan, K. D. Comparison of Density Functional and MP2 Calculations on the Water Monomer and Dimer. *J. Phys. Chem.* **1994**, *98* (40), 10089–10094.

72. Becke, A. D. Density-Functional Thermochemistry. III. The Role of Exact Exchange. *J. Chem. Phys.* **1993**, *98* (7), 5648.

73. Miyaura, N.; Suzuki, A. Palladium-Catalyzed Cross-Coupling Reactions of Organoboron Compounds. *Chem. Rev.* **1995**, *95* (7), 2457–2483.

74. Tanley, S. W. M.; Schreurs, A. M. M.; Helliwell, J. R.; Kroon-Batenburg, L. M. J. Experience with Exchange and Archiving of Raw Data: Comparison of Data from Two Diffractometers and Four Software Packages on a Series of Lysozyme Crystals. *J. Appl. Crystallogr.* **2013**, *46* (1), 108–119.

75. Mcardle, A. P.; Crystallogr, J. A. (Referencias Tomadas Do Programa WINGX - Algunhas Non Están Actualizadas-) Referencias a Programas : **2008**.

76. Brouwer, A. M. Standards for Photoluminescence Quantum Yield Measurements in Solution (IUPAC Technical Report). *Pure Appl. Chem.* **2011**, *83* (12), 2213–2228.].

77. Liu, Y.; Liu, M. S.; Jen, A. K.-Y. Synthesis and Characterization of a Novel and Highly Efficient Light-Emitting Polymer. *Acta Polym.* **1999**, *50* (2-3), 105–108.

Design, synthesis, PL and EL studies of a novel carbazole derivative Cz(PhCF₃)₂, as an emitter in OLEDs
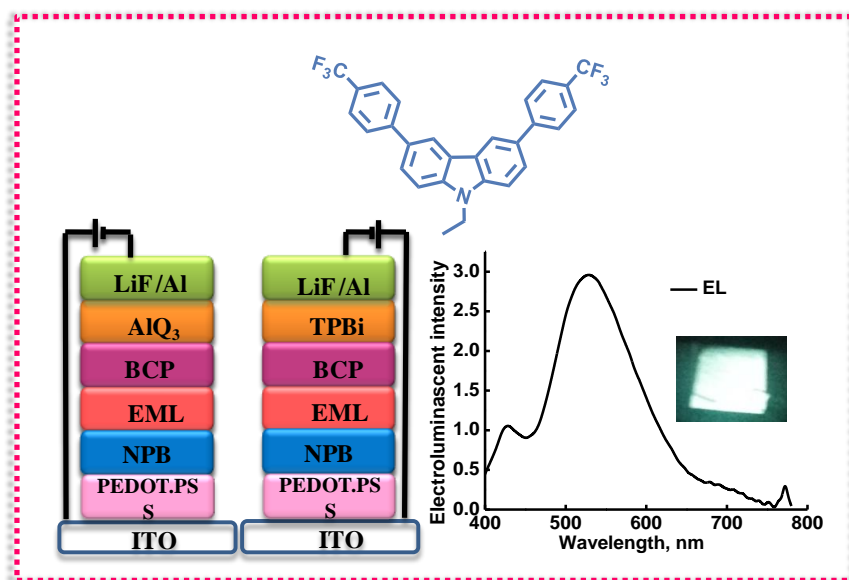
3.1 Abstract

*Achieving white electroluminescence from a single small organic molecule has always been a highly desirable objective in OLED research as this would overcome many serious and multiple problems involved in device fabrication. Herein, we report the design, synthesis, photoluminscence (PL) and electroluminiscence (EL) studies of a carbazole derivative - 9-ethyl-3,6-bis(4-(trifluoromethyl)phenyl)-carbazole (**Cz(PhCF₃)₂**), which exhibited white light emission by way of harvesting both singlet and triplet emissions. The blue emission of the singlet state and the broad emission from the room temperature phosphorescence (RTP) of the molecule resulted in white light electroluminescence with a CIE colour coordinate of (**0.39, 0.39**). A device was successfully fabricated using (**Cz(PhCF₃)₂**) as the emissive layer and characterized. This approach to generate white light from a single small molecule for OLED*

applications is novel and less troublesome from the standpoint of device fabrication. The method offers a promising way to improve the efficiency of future white OLEDs.

3.2 Introduction

Ever since the original work by Tang and VanSlyke[1] in 1987, organic light emitting diodes (OLEDs) attracted massive attention due to their widespread applications. From the ancient days of OLED research, attaining white light emitting diodes remained as the centre of attraction and scientists tried different approaches to accomplish this viz. getting simultaneous emission of light from three primary colours (red, green and blue) or of two complementary colours (e.g. orange and blue),[2-6] combining fluorescent and phosphorescent emitters as host and dopant,[7-10] using molecules showing excited state intra-molecular proton transfer (ESIPT),[11-13] combining monomer-excimer emission[5,6,14] etc. But still, developing pure and efficient white light emitting OLEDs are challenging. In the case of multilayer emitting diodes, the energy transfer between the layers must be controlled by proper designing strategy so that the excitons will funnel from the highest energy to the lowest energy resulting in emission from the lowest energy. In the case of hybrid materials, the compatibility between the organic and inorganic materials may lead to poor working of the diode. Circumventing the multiple problems associated with optimising many parameters, to fabricate an efficient OLED having high efficiency, is a herculean task. In this context, strategies to design and develop a single white light emitting molecule is therefore exciting and challenging. The succeeding sections of this chapter elaborate on our efforts towards achieving this goal.

3.2.1 Carbazoles in OLEDs

Carbazoles are used extensively in the field of organic light emitting diodes, as an emissive layer or as a hole transporting layer. Recently many research groups have shown more interest in this particular class of compounds mainly due to their inherent properties like intrinsic spin-orbit coupling, high thermal stability, small ΔE_{ST}, thermally activated delayed fluorescence (TADF) etc. The first report on a carbazole derivative showing TADF came in 2011 and in fact that was the first report of a purely

organic molecule showing this property. Detailed discussions on this 3rd generation of OLEDs that work on the principle of TADF are presented in Chapter 1. Other than as an emissive layer, carbazole derivatives are widely used as hole transporting materials and as host materials. 4,4′-Bis(*N*-carbazolyl)-1,1′-biphenyl(CBP) is one of the carbazole derivatives used extensively as a hole-transporting material (Figure 3.1).[14]
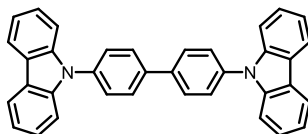
Figure 3.1. *Molecular structure of CBP*

Adachi *et.al*[15] designed and synthesized three carbazole derivatives which exhibited sky-blue, green and orange electroluminescence. The energy diagram of a conventional organic molecule, a TADF emitter and the molecular structures of carbazole derivatives are reproduced as represented in the original paper, in Figure 3.2.
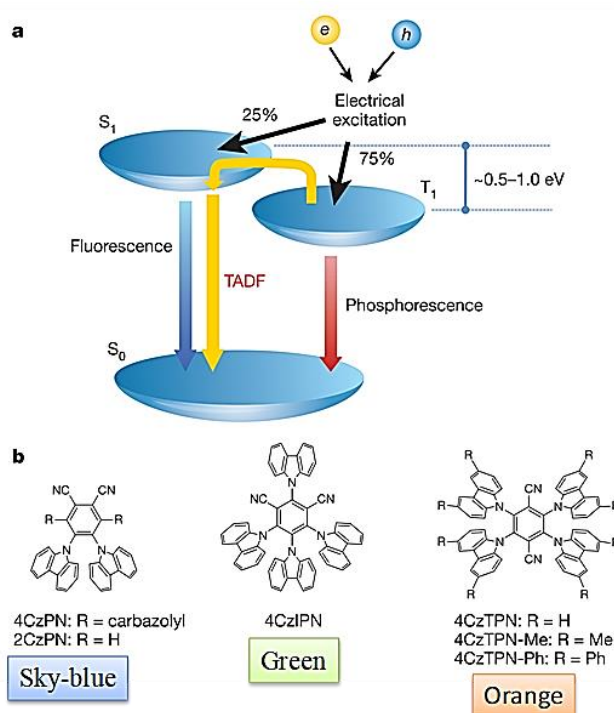
Figure 3.2. *a. Energy diagram of TADF molecules and conventional organic molecule. b Molecular structures of carbazole derivatives.*

The device structure of the green OLED which showed maximum external quantum efficiency (EQE) of 20% was composed of multiple layers of indium tin oxide (ITO) as anode,4,4'-bis[N-(1-naphthyl)-N-phenylamino]-biphenyl (α-NPB, 35 nm) as hole

transporting layer, 5.61 wt% of 4CzTPN-Ph:CBP as emissive layer (15 nm), TPBi (65nm) as the electron transporting layer and LiF (0.8nm) and Al (70 nm) as cathode. The orange and sky-blue OLEDs had EQEs of 11.261% and 8.061% respectively. Kido *et.al*[16] reported two 3,6-di-*tert*-butylcarbazole derivatives namely DTC-mBPSB and DTC-pBPSB which were novel blue TADF emitters due to their low singlet-triplet exchange energies of 0.05 and 0.24 eV. DTC-mBPSB with 1,3-bis(phenylsulfonyl) benzene as the core exhibited a deep blue emission and an EQE of 5.5% while DTC-pBPSB with 1,4-bis(phenylsulfonyl) benzene core exhibited a slightly red-shifted EL spectrum but superior EQE above 10%.

Monkman *et.al*[17] reported that carbazoles substituted at 3, 6 positions, showed better delayed fluorescent properties, phosphorescence and smaller ΔE_{ST}. In that report, they studied a series of molecules and established that the carbazole derivatives with 'linear' substitution exhibited very low ΔE_{ST} and were susceptible to show delayed fluorescence (DF). The characteristics of carbazoles *viz.* small ΔE_{ST}, intrinsic SOC[19] (Figure 3.3) and a triplet excited state which is predominantly having $\pi-\pi^*$ temperament[20] make them prone to show efficient room temperature phosphorescence (RTP).[18]
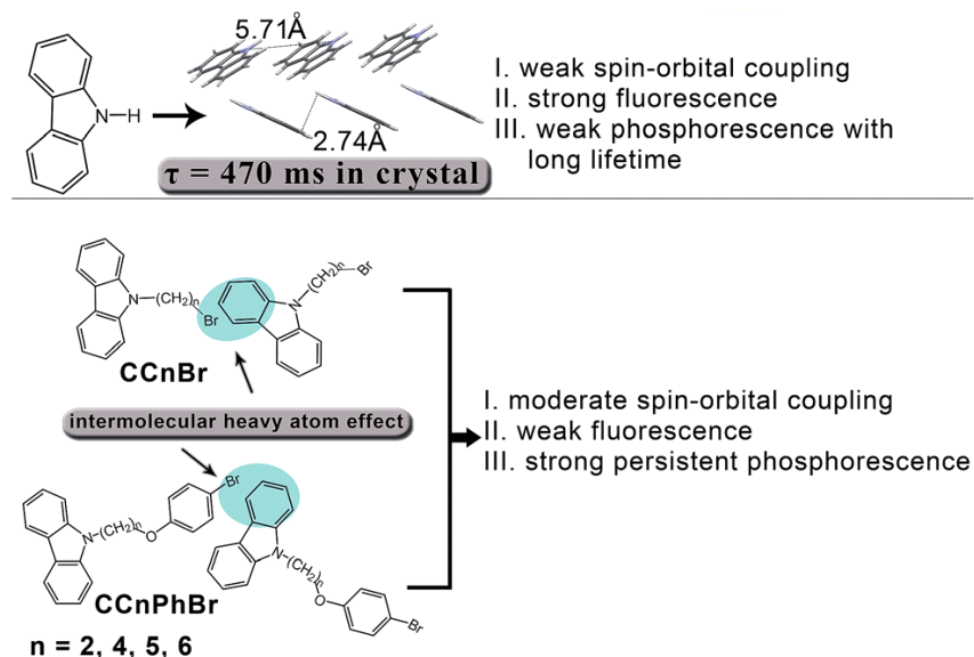
Figure 3.3. Intrinsic SOC of carbazole derivatives

Tang *et.al*[21] reported a persistent RTP from carbazole derivatives in crystal state, where the carbazoles (at the N-atom) were substituted at the *para*-position of the phenyl group

of benzophenone. Later the same group reported a persistent white light emission from a benzophenone derivative with the aid of RTP.[22] From this group itself another report came on the RTP of a different carbazole derivative[23] in the crystal state establishing the importance of carbazoles in designing pure organic RTP molecules. Chemical structures of some carbazole derivatives which showed RTP are presented in Figure 3.4.
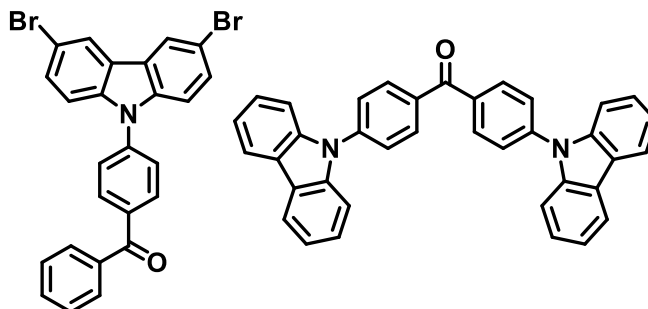
Figure 3.4. Molecular structures of the carbazole derivatives reported to show RTP

3.3 Definition of the problem

To exploit the intrinsic properties of carbazoles *viz.* spin-orbit coupling, low ΔE_{ST}, high thermal stability and hole transporting properties, we decided to select carbazole as the main core which will be structurally modified further, with an ultimate aim of designing an efficient emissive material for OLED applications. Considering the fact that 3,6-substitution on carbazole can reduce the ΔE_{ST} and increase the probability of showing delayed fluorescence of the resultant molecule, we chose to synthesise a carbazole substituted at its 3,6 position with *para*-trifluoromethyl phenyl group [-Ph(CF$_3$)]. The design strategy is pictorially represented in Figure 3.5. We expected that the –CF$_3$ group could act as a good acceptor and the carbazole moiety as a good donor. Accordingly we synthesised 9-ethyl-3,6-bis(4-(trifluoromethyl)phenyl)-carbazole which is abbreviated as **Cz(PhCF$_3$)$_2$**. Synthesis, spectral characterization, PL, thermal, electrochemical, DFT and EL studies of this molecule are the subject matter of this chapter.
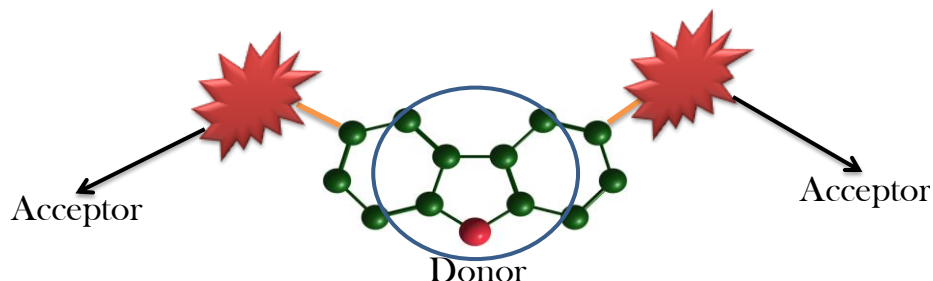
3.4 Results and discussion

3.4.1 Synthesis and characterization

The molecule **Cz(PhCF₃)₂** was synthesized using Suzuki-Miyaura coupling[28] (Scheme 3.1). The starting material carbazole was N- ethylated using ethyl iodide in presence of NaH as a base to get **Cz-Et**. The resultant molecule **Cz-Et** was then subjected to a mild bromination using re-crystallized NBS to yield **Cz(Br)₂** which on Suzuki-Miayura coupling with trifluromethylphenylboronic acid gave the desired molecule, **Cz(PhCF₃)₂.** The synthetic procedure is efficient, less time consuming and the carbazole derivatized at 3,6 position with the *para*-orienting trifluoromethyl substituted phenyl group was obtained in 38% overall yield.
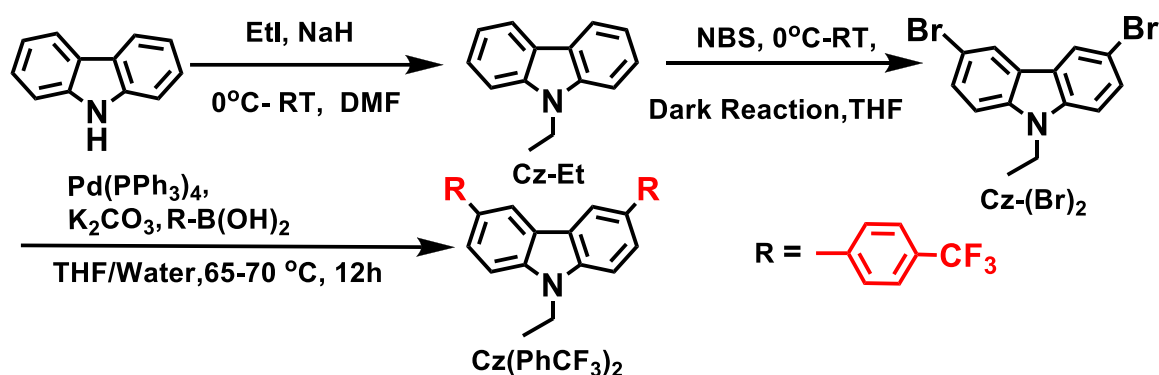
Scheme 3.1. *Synthetic procedure towards* **Cz(PhCF₃)₂**

The structure of **Cz(PhCF₃)₂** was confirmed by IR, NMR spectroscopy and HRMS. IR spectrum of the molecule was consists of aromatic stretching vibrations in the range from 3000 to 2900 cm^{-1} as dominant peaks since the molecule contains no functional groups in it. In the ^{1}H NMR spectrum (Figure 3.6), the aromatic protons appeared in the region δ 8.38 to δ 7.51. The CH₂ protons of the N-ethyl group resonated in the range δ 4.46 - δ 4.42 ppm as a quartet and the CH₃ protons resonated between δ 1.51-1.40 ppm as a triplet. The ^{13}C NMR spectrum contained peaks corresponding to the aromatic carbon atoms ranging from δ 145 to δ 109 ppm. The ethyl carbons resonated at δ 37.92 and δ 13.90 ppm. The Mass spectrum (Figure 3.7) showed the M^{+} peak at m/z 483.1425.
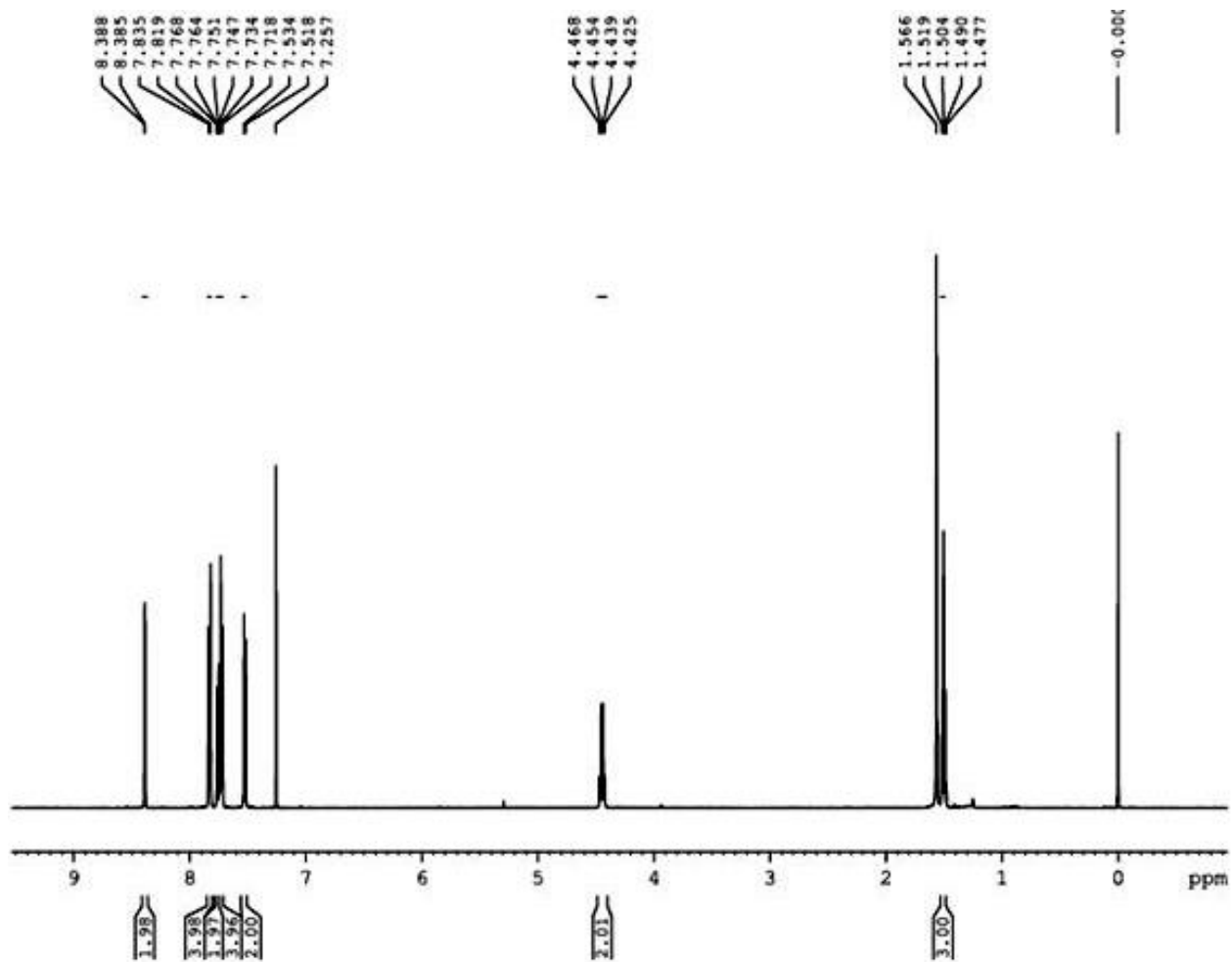
Figure 3.6. ¹H NMR spectrum of **Cz(PhCF₃)₂**
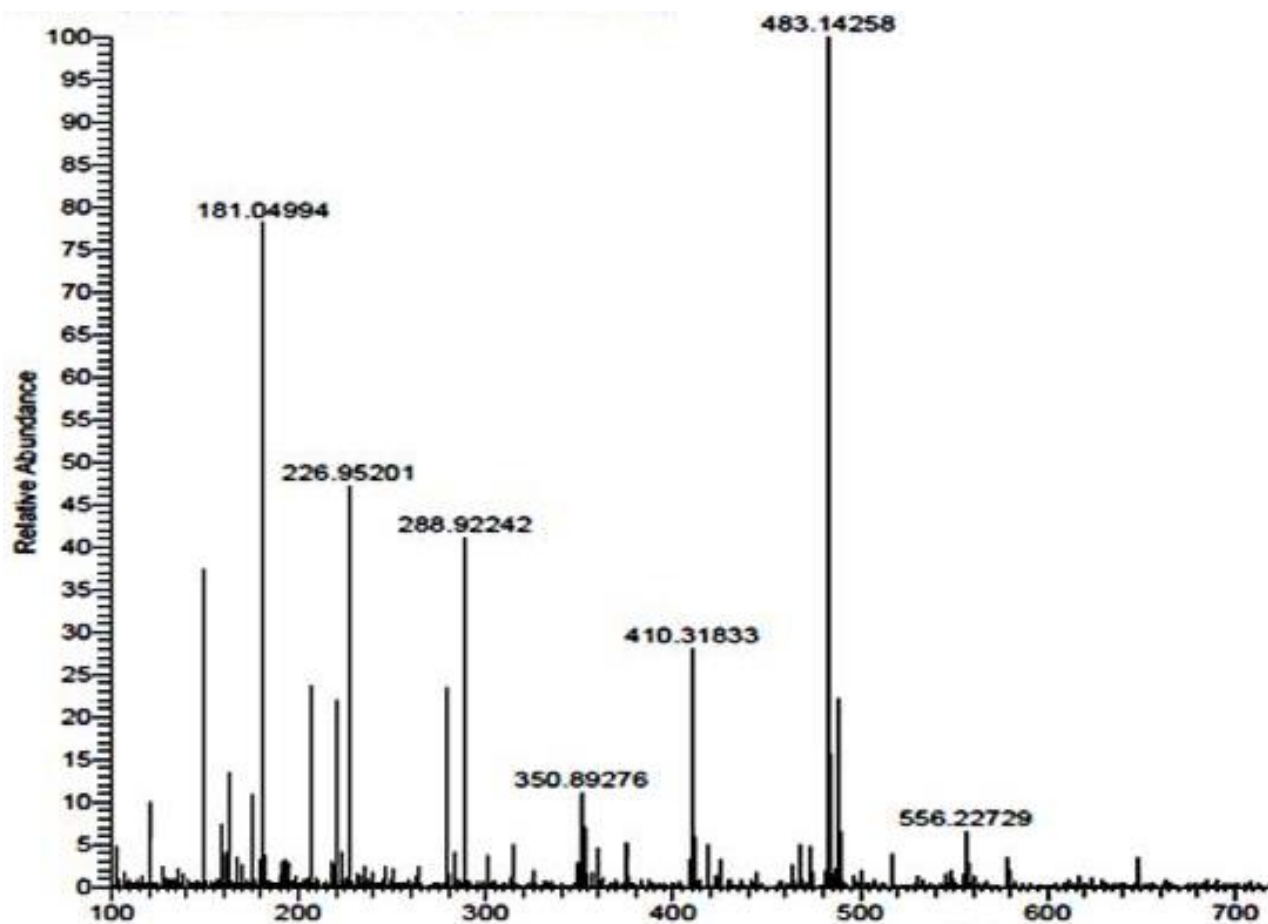
Figure 3.7. Mass spectrum of Cz(PhCF₃)₂

3.4.2 Photoluminescence studies

3.4.2.1 Room temperature absorption and emission studies in solution state

The steady state absorption spectra of **Cz(PhCF₃)₂** were recorded in different solvents at room temperature and the results are presented in Figure 3.8. The absorption profile consisted of two peaks, one at 300 nm (λ_{max}) and the other as a shoulder peak at 340 nm. On closer evaluation of the absorption spectrum, we could infer that the spectrum was more or less similar to that of of N-ethyl carbazole.[24] The absorption spectrum of **Cz(PhCF₃)₂** also remained unchanged irrespective of the solvent polarity.
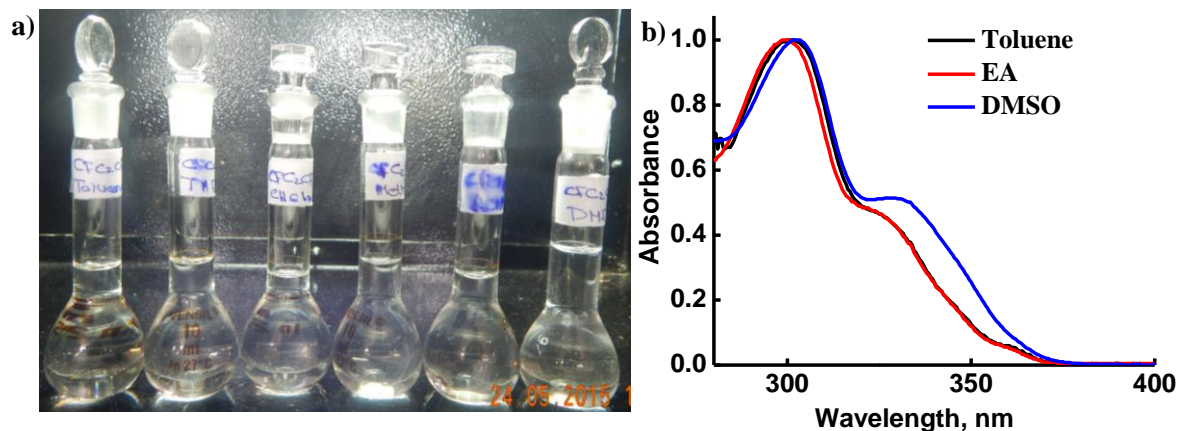
Figure 3.8. *a) Absorption of* **Cz(PhCF₃)₂** *in different solvents b) Absorption profile of* **Cz(PhCF₃)₂** *in toluene (Black), Ethylacetate (EA) and Dimethylsulphoxide (DMSO)*

The steady state fluorescence spectrum for the molecule was recorded initially in THF solution. It showed a structured emission profile similar to that of N-ethyl carbazole[24] with no profound contributions from the CF₃ groups. The emission profile of the molecule exhibited a peak maximum at 389 nm with two shoulder peaks at 369 nm and 407 nm. It showed a Stokes shift value of 7626 cm⁻¹. The fluorescence quantum yield for the molecule was calculated as 35 ±5%, with respect to quinine sulphate as reference. Figure 3.9a shows the photograph displaying the solution state emission of the molecule in different solvents and Figure 3.9b the emission spectra in toluene, ethylacetate and DMSO. The polarity of the solvent did not show any influence on the emission maxima of **Cz(PhCF₃)₂**. This observation infers that there is no charge transfer state associated with the molecule at the excited state.

It was also observed that the structured emission of the molecule got broadened as the polarity of the solvent increased. In DMSO, the two shoulder peaks almost disappeared to give a broad emission (Figure 3.9). The colour coordinates for the emission were found to be (0.09, 0.17), which is very close to that of the pure blue emission whose CIE colour coordinate (0.08, 0.14). The more or less pure blue emission from **Cz(PhCF₃)₂** prompted us to move further with the studies.
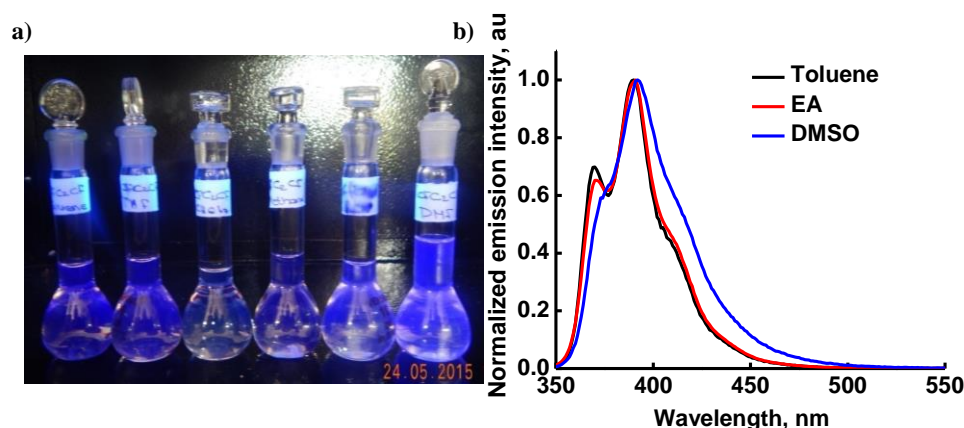
Figure 3.9. *a) Emission of **Cz(PhCF₃)₂** in different solvents b) Emission spectrum for **Cz(PhCF₃)₂** in Toluene (Black), Ethylacetate (Red), DMSO (Blue)*

3.4.2.2 Room temperature absorption and emission studies in solid state

The solid state absorption spectrum (Figure 3.10a) for the molecule was a broad structure-less one ranging from 220 nm to 370 nm. It exhibited two peaks, one at (λ_{max}) 306 nm and the other at 360 nm. Solid state emission of the molecule was recorded by exciting **Cz(PhCF₃)₂** at 306 nm. Similar to the solution state emission spectrum (Figure 3.9), the solid state emission spectrum (Figure 3.10b) also exhibited a structured emission. The emission profile showed two emission maxima, one at (λ_{max}) 356 nm and the other at (λ_{max}) 376 nm with a small shoulder peak at 400 nm (Figure 3.10). The slight deviation observed in the solid state emission profile for **Cz(PhCF₃)₂** from its solution state spectrum could be due to the molecular aggregation present in the solid state. The emission of the molecule was recorded in film state also. This film state emission (Figure 3.10b) however resembled the solution state emission of the molecule (Figure 3.9)
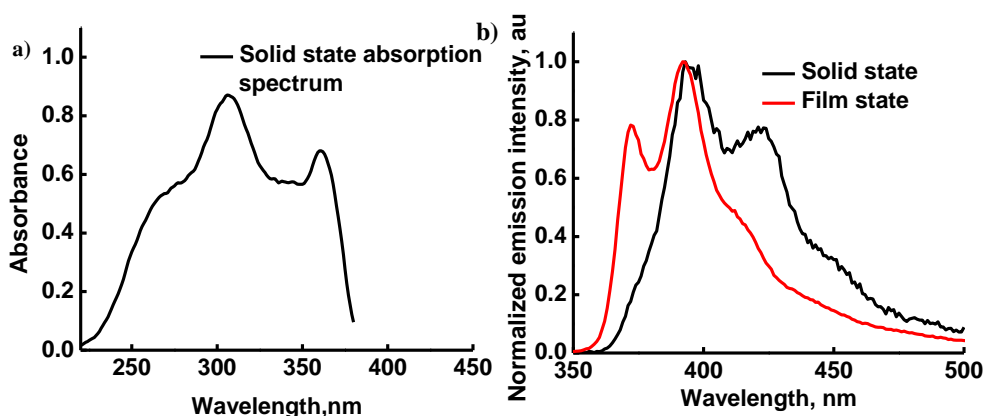
Figure 3.10. *a) solid state absorption spectrum for **Cz(PhCF₃)₂** b) Solid state as well as film state emission spectrum for **Cz(PhCF₃)₂***

3.4.2.3 Emission studies at 77 K (Liquid nitrogen)

To calculate the ΔE_{ST} for **Cz(PhCF$_3$)$_2$**, low temperature emission for the molecule was recorded in frozen THF at 77 K (Figure 3.11). The low temperature emission for the molecule showed two emissions corresponding to the fluorescence and phosphorescence. The value for ΔE_{ST} was calculated as 0.61 eV. (Table 3.1) from the offset of fluorescence and phosphorescence.
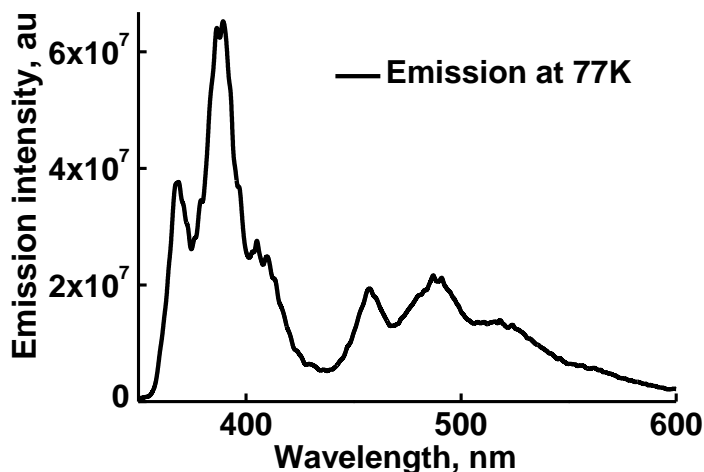
Figure 3.11. *Low-temperature emission spectrum for* **Cz(PhCF$_3$)$_2$**

Table 3.1. Values for ΔE_S, ΔE_T and ΔE_{ST}

Compound	ΔE_S (eV)	ΔE_T (eV)	ΔE_{ST} (eV)
Cz(PhCF$_3$)$_2$	3.36	2.75	0.61

3.4.2.4 Phosphorescence studies at 77 K and at room temperature

Figure 3.12 shows the phosphorescence spectrum of Cz(PhCF$_3$)$_2$, taken in frozen THF at 77 K with a flash delay of 0.5 ms.. The excitation wavelength used for phosphorescence measurements was 300 nm. The structured phosphorescence emission spectrum consisted of three peaks at (λ_{max}) 457 nm, 489 nm and 520 nm. The emission profile was similar to that of N-ethyl carbazole. [24]
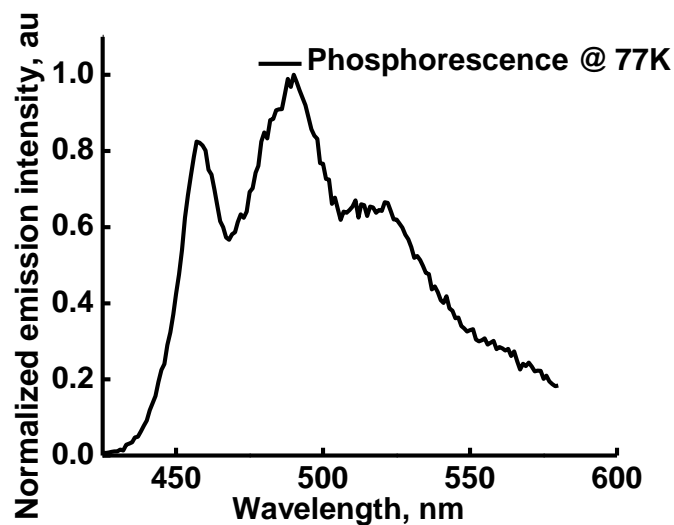
Figure 3.12. *Phosphorescence emission spectrum for **Cz(PhCF₃)₂***

The room temperature phosphorescence spectrum for **Cz(PhCF$_3$)$_2$** was recorded in solid state since in solution state the dissolved oxygen can interfere with the triplet state. The normal phosphorimeter setup was used for taking room temperature phosphorescence. The experimental conditions used for RTP measurement is as follows "**S1(R928) (Phosphorimeter):** Sample window: 0.10**,** Time per Flash: 61.00 **,** Flash Count: 60". The flash delay for the experiment was changed for each measurements. The excitation wavelength was kept constant at 300 nm. The first spectrum was recorded using a flash delay of 0.05 ms, it contained two emission peaks one in the range of fluorescence and the other in the range of phosphorescence as shown in Figure 3.13a. As the flash time increased from 0.05 ms to 0.1 ms the first peak vanished completely and the second peak, which resembled phosphorescence, remained.

A comparison between the RTP emission profile with solid state emission and the phosphorescence of the molecule is presented in Figure 3.13b. These results indicated that our molecule has a room temperature phosphorescence resulting from the intrinsic spin-orbit coupling of carbazole which was further boosted by the molecular structure of **Cz(PhCF$_3$)$_2$**.
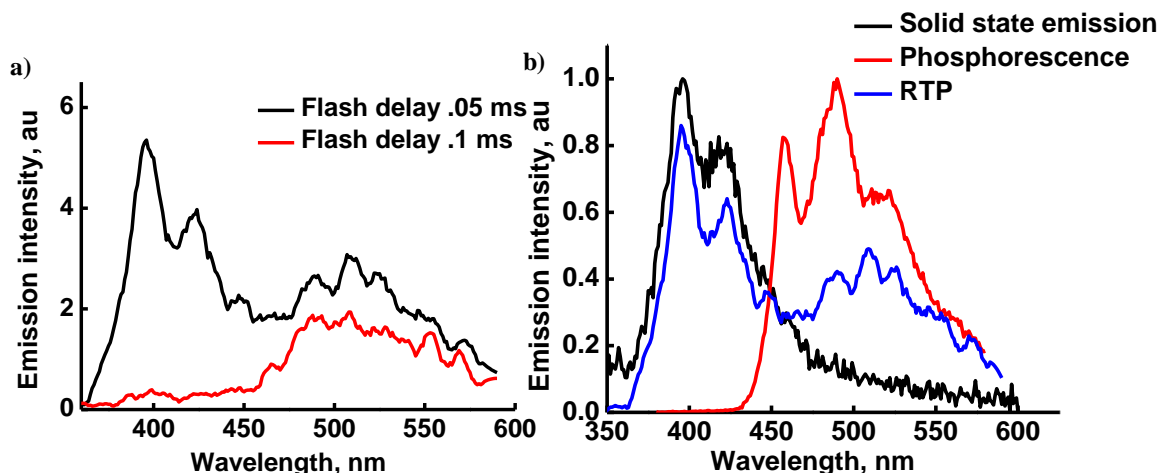
Figure 3.13. *a) The room temperature emission spectrum for the molecule with different flash delay excited at 300 nm b) A comparison between RTP, solid state fluorescence and phosphorescence*

3.4.3 Electrochemical analysis and HOMO/LUMO calculations

The CV profile of the molecule (Figure 3.14a) was recorded to have an idea about its electrochemical behaviour. It showed a reversible oxidation potential equal to 1.20 eV. The values for highest occupied molecular orbital and lowest unoccupied molecular orbital were calculated from the solid state absorption, emission and CV profiles as shown below.
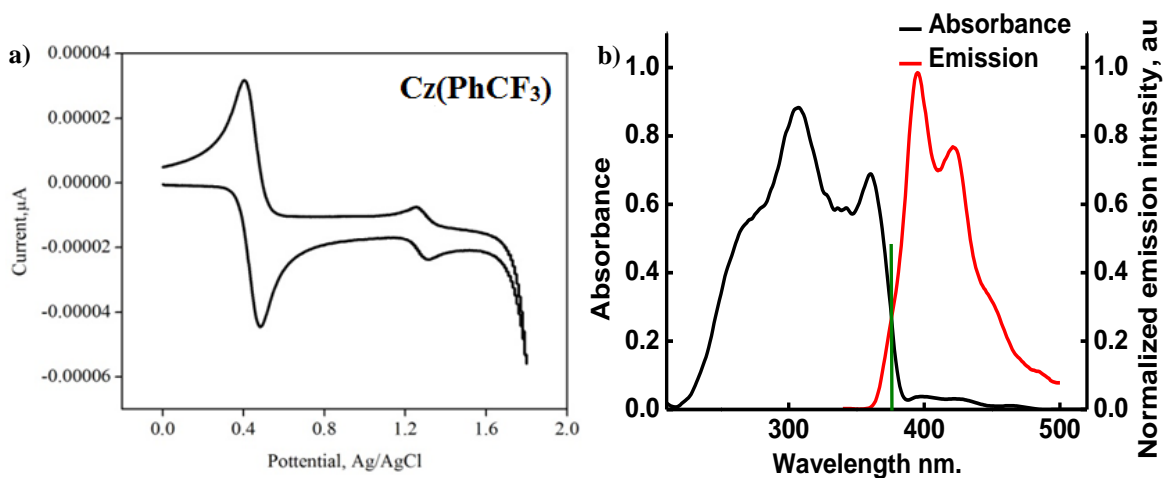
Figure 3.14. *a) CV profile of **Cz(PhCF₃)₂** b) Calculation of band gap from solid state emission and absorption*

Calculations

E_{Fc} (Vs Ag/AgCl) = 0.41V

E_{ox} (Vs Ag/AgCl) =1.20 V

E_{ox} (Vs Fc)   = 1.20-0.41= 0.79V

HOMO   = {-E_{ox} (Vs Fc) - 4.8 eV}

                  = {-0.79-4.8eV} = **-5.59eV.**

LUMO= HOMO- Band gap

= -5.59- 3.22

= **- 2.37 eV**

Band gap was calculated from the intercept of solid state absorption and emission (Figure 3.14b). Results for electrochemical analysis and HOMO/LUMO calculations are presented in Table 3.2.

Table 3.2. Results for HOMO/LUMO calculation.

Compound	Band Gap (eV)	HOMO (eV)	LUMO (eV)
$Cz(PhCF_3)_2$	3.22	- 5.59	- 2.4

3.4.4 Thermal analysis

For considering one molecule towards OLED application, it should be thermally stable. To get an idea about the thermal stability of $Cz(PhCF_3)_2$, differencial scanning calorimetry analysis (DSC) was carried out. The molecule showed thermal stability up to 200 °C, which could be due to the presence of six fluorine atoms in it.
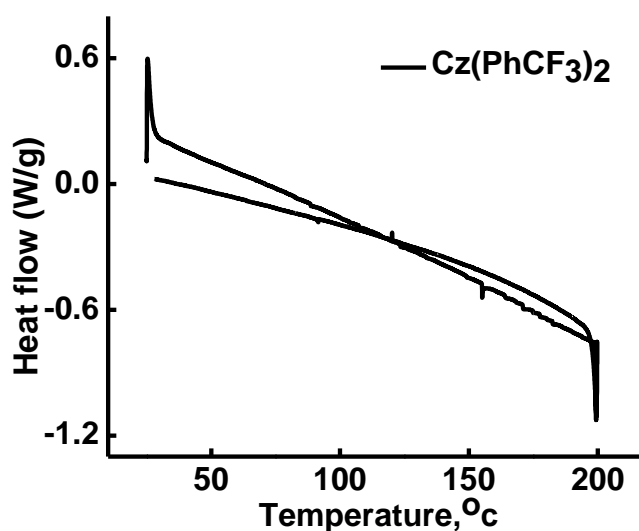
Figure 3.15. TGA diagram for $Cz(PhCF_3)_2$

3.4.5 Density functional theory (DFT) calculations

Computational studies on the molecule in the ground state were carried out using the polarizable continuum model (PCM)[25] implicit solvation effect (solvent = THF) incorporated B3LYP/6-31G$^{*[26]}$ level of density functional theory as implemented in Gaussian09.[27a] The excited singlet (S^1) and triplet (T^1) states were also optimized with TD-DFT method in the solvent phase. All the structures were verified as energy minima by frequency calculation. The optimized geomatry of **Cz(PhCF₃)₂** in the S^0 state showed a torsional twist (θ) 36° between the trifluoromethylphenyl moiety and the carbazole moiety (Figure 3.16). In S^1 state, θ was 18°. In T^1 state, one of the θs was close to zero (0.5°) and the other was 36°. Spin densty distribution of T^1 showed the delocalization of the unpaired electrons over the carbazole unit and the trifluoromethylphenyl unit. The presence of stable triplet excited state in **Cz(PhCF₃)₂** can be attributed to this observation in theory. Overall the geometry change from S^0 to S^1 transtion is very small and accounts for the negligible Stocks shift exhibited by the molecule.
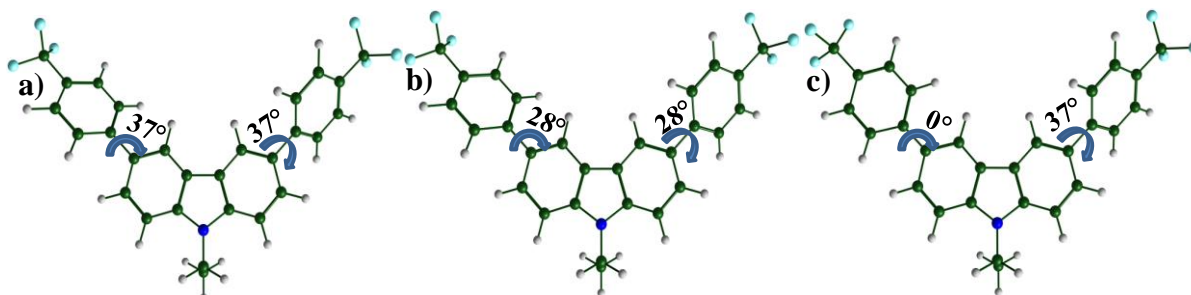
***Figure 3.16**. Optimized geometries of Cz(PhCF₃)₂ a) S⁰ b) S¹ c) T¹*

Figure 3.17 shows the spatial distribution of HOMOand LUMO of **Cz(PhCF₃)₂**. HOMO is distributed on the carbazole moiety while the LUMO shows strong delocalization over the whole π-region. Regardless of the presence of the strong donor carbazole moiety and the strong acceptor trifluoromethyl moiety, **Cz(PhCF₃)₂** showed no intramolecular charge transfer (ICT) state in the experiment which can be attributed to the presence of the highly delocalized LUMO of the molecule. The calculated λ_{max} (282 nm) and the shoulder peak (320 nm) agreed well with the experimental value. The 320 nm corresponds to HOMO-1 to LUMO+1 transition which occurs within the carbazole unit while the λ_{max} corresponds

to HOMO to LUMO transition. The spatial arrangement for frontier orbital of **Cz(PhCF₃)₂** is given in table 3.3.
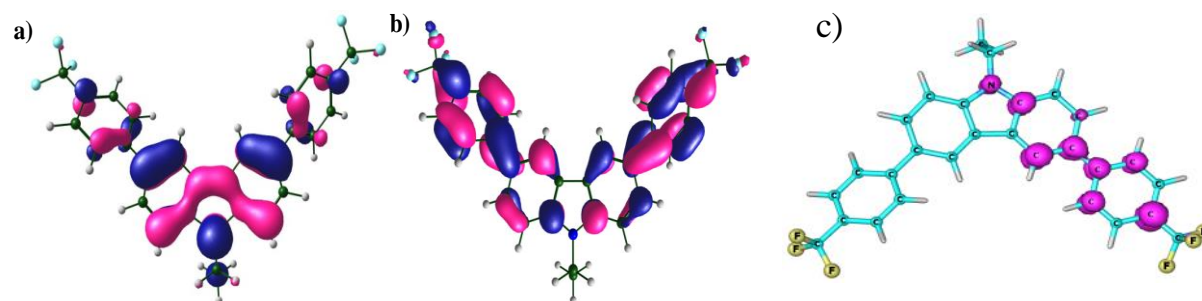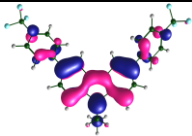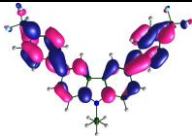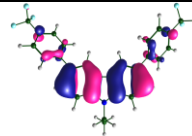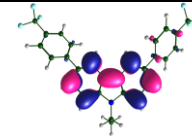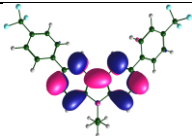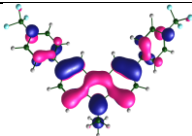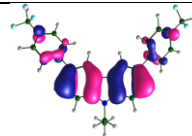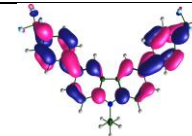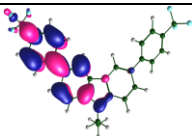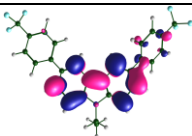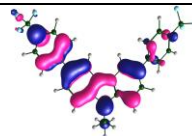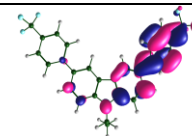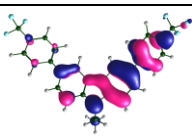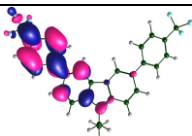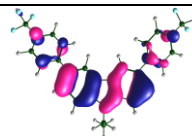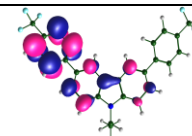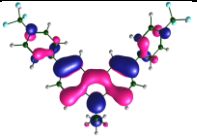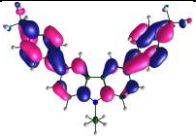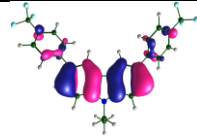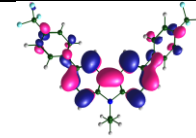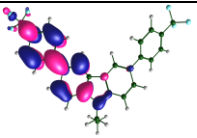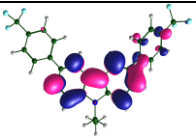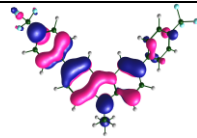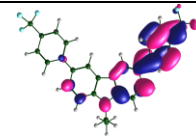
Figure 3.17. *a) HOMO b) LUMO. Computed HOMO = 5.55 eV LUMO = 1.76 eV c) Spin density distribution in T₁ state*

Table 3.3. Frontier molecular orbitals of **Cz(PhCF₃)**

State	HOMO/L UMO experiment al(eV)	Spatial arrangement HOMO (eV)	Spatial arrangement LUMO (eV)	Spatial arrangement HOMO-1 (eV)	Spatial arrangement LUMO+1 (eV)
GS (g)		124- 5.55	125-1.18	123-6.02	126-1.12
SS (g)		124-5.49	125-1.33	123-6.01	126-1.27
TS (g)		125-2.96	126-1.32	124-5.75	1.17
GS (s)	5.59/3.01	124-5.45	125-1.18	123- 5.95	126-1.05

SS (s)					
		124-5.11	**125-1.92**	**123- 5.86**	**126-1.14**
TS (S)					
		125-2.9	**126-1.33**	**124-5.76**	**127-120**

3.5 Electroluminescence (EL) studies

3.5.1 Cz(PhCF$_3$)$_2$ as emitter

To examine the electroluminescent properties of Cz(PhCF$_3$)$_2$, we initially fabricated a device with the following configuration. (ITO (Indium tin oxide)/ PEDOT:PSS [Poly(3,4- ethylene dioxythiophene)-poly(styrene sulfonate)] / NPB [(N,N′-Di(1-naphthyl)-N,N′-diphenyl-(1,1′biphenyl)-4,4′-diamine] / **Cz(PhCF$_3$)$_2$** [(9-ethyl-3,6 bis(4(trifluoromethyl)- phenyl)-9H carbazole)] / BCP [(2,9-dimethyl-4,7diphenyl-1,10-phenanthroline)] / Alq$_3$ (tris-(8-hydroxyquinoline)–aluminium / LiF: [Lithium Fluoride]) (Device 1). The device stacking for the fabricated device is given in Figure 3.18a. The device gave a broad electroluminescent emission with two peak maxima (λ_{max} at 426 nm and 540 nm (Figure 3.18b). The white light emission from the device with CIE coordinates at (0.31, 0.44), started from about 5V and was stable up to 16V. The energy level diagram for the device 1 is given in figure 3.19a. The peak at 426 nm can be attributed to the normal singlet emission of the molecule red shifted due to the difference between optical and electrical band gap. But the origin of the second broad emission peak ranging from 480 nm to 700 nm was questionable. One major concern about the origin of this peak was the electron transporting layer used in the device that is, Alq$_3$. Alq$_3$ also emits in the same green region similar to the second peak in the EL spectrum for **Cz(PhCF$_3$)$_2$**. This possibility directed us to the fabrication of a second device with the same device structure without **Cz(PhCF$_3$)$_2$**. This device furnished a feeble green emission at voltages higher than 12V. So to prove that the origin of the

low energy band is indeed from our molecule, a third device was built with the device configuration as follows: (ITO (150nm) / PEDOT:PSS (30nm) / Poly (4-butylphenyl-diphenyl-amine) (polyTPD) (30nm) / **Cz(PhCF₃)₂** (30nm) / 2,2′,2″- (1,3,5-Benzinetriyl)-tris (1-phenyl-1-H benzimidazole) (TPBi) (40nm) / LiF(1nm) /Al (100 nm). In this case we got an EL spectrum with two peaks one at 426 nm and a second broad emission from 480 nm to 750 nm. This EL spectrum resembled the EL spectrum for device 1. Since the EL profiles obtained for device 3 and device 1 are comparable with each other, we assume that the emission is due to the EL from **Cz(PhCF₃)₂**.
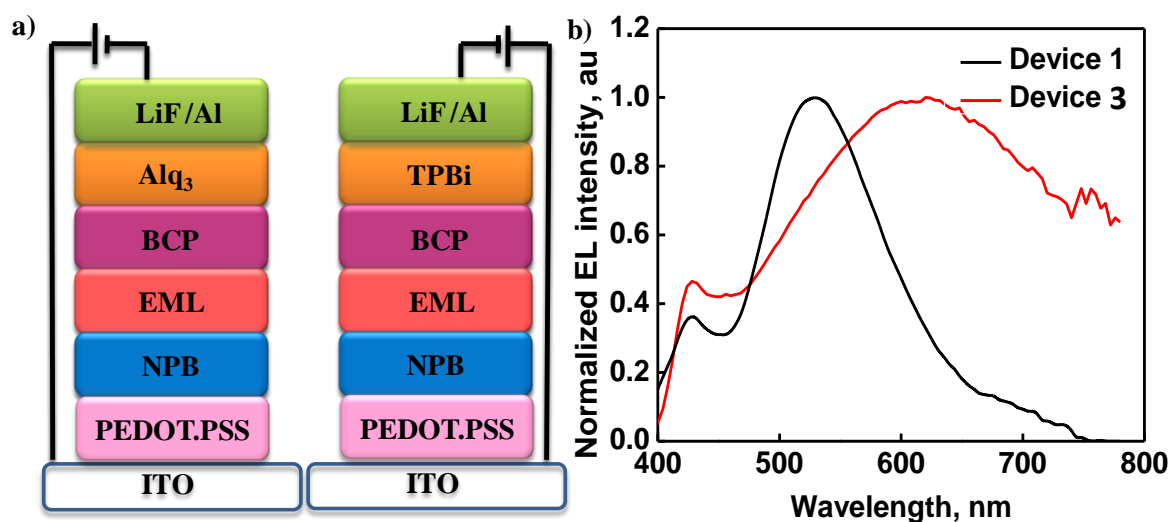
Figure 3.18. *a) Device configuration for device 1 and device 3 b) Electroluminescence spectra for the white OLED based on* **Cz(PhCF₃)₂**

A second plausible explanation for the low energy band can be the formation of an electroplex. There are many reports quoting the presence of electroplex in the carbzole based OLEDs. Tian *et al*, in 2010 reported a white organic light emitting diode using the electroplex emission to generate the white light in a device based on polyvinyl carbazole and carbazole oligomer blends.[27b] Since our molecule has a very similar emission and phosphorescence of N-ethylcarbazole, that possibility should also be considered. Electroplex, $(M^+M^-)^*$ is formed by cross recombination of electrons and holes in acceptor (N) and donor (M) molecules, respectively,[27c] under a high-electric field inside a LED, but not under photoexcitation. The emission of an electroplex must be equal to the energy difference between the LUMO of electron transporting layer and the HOMO of emissive layer (Figure 3.19c). In the case of device 1 as shown in figure

3.19d the energy difference between the HTL (NPB) and EML (**Cz(PhCF₃)₂**) was calculated as 2.5 eV that is equivalent to about 496 nm. In the case of **Cz(PhCF₃)₂**, the second broad emission peak has a λ_{max} at 540 nm, which shows that the low energy emission from **Cz(PhCF₃)₂** in EL is not due to the presence of an electroplex. Furthermore, if the second band in figure 3.18b arises from an electroplex, on increasing the voltage the emission from electroplex must also increase.[27d] So in order to verify this, we recorded the EL emission of our device at voltages 6 V and 10 V. Since the second emission peak in the electroluminescence profile of **Cz(PhCF₃)₂**, showed no profound increase with respect to the voltage, we assumed that the emission was not coming out of an electroplex (Figure 3.19d).
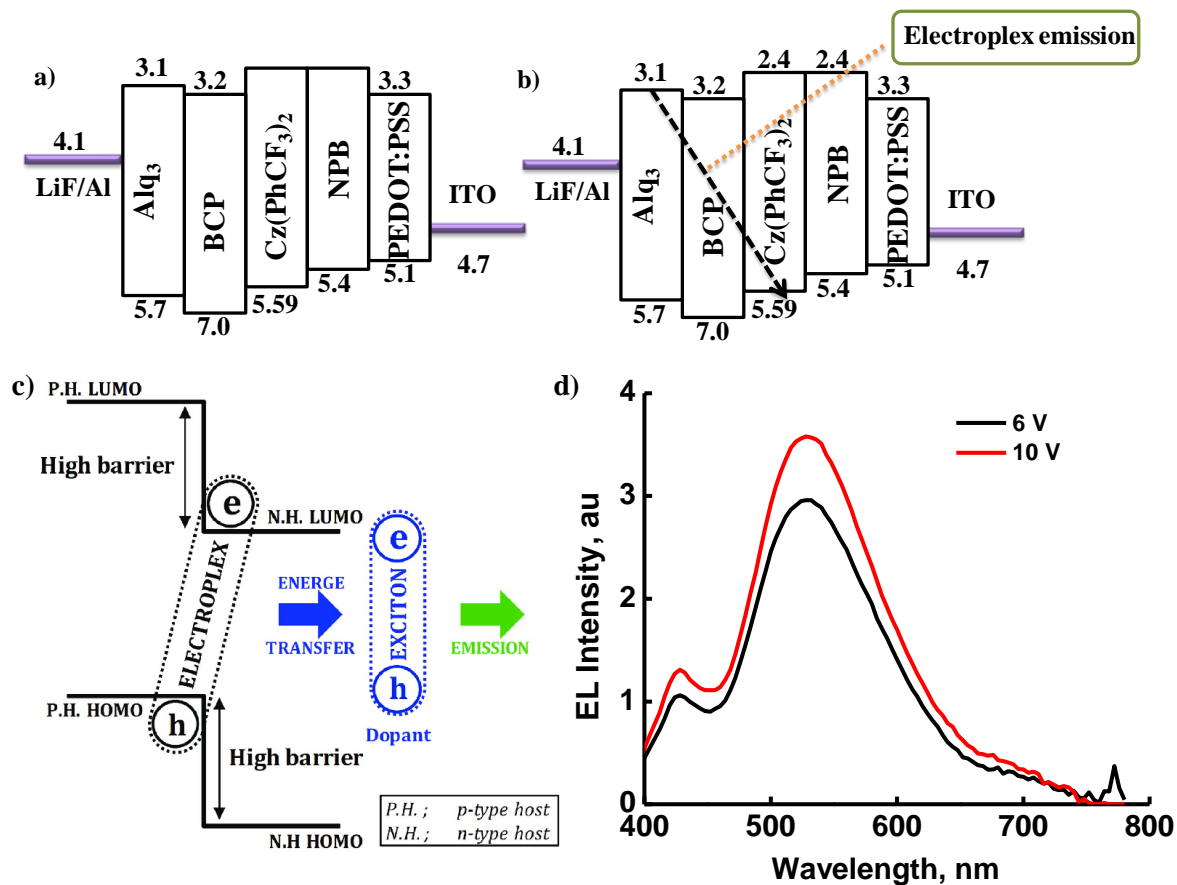
Figure 3.19. *a) Energy level diagram for device 1 b) Showing the plausible emission from an electroplex if it were present in the system c) Calculating the electroplex emission (Taken as such from the reference)[r] d) Electroluminescence emission from the molecule at 6 V and 10 V*

In these devices based on **Cz(PhCF₃)₂**, we successfully harvested both the singlet and the triplet emissions coming out from our molecule with the help of RTP. The properties

of device 1 are presented in Table 3.4 and the device characterization curves are presented in Figure 3.20. Though the efficiency for the device fabricated with **Cz(PhCF₃)₂** was not appreciable, but developing a single small molecule showing white electroluminescence was exciting and stimulating to go further. Also we expected that since the device fabricated with **Cz(PhCF₃)₂** harvested white EL with the aid of singlet and triplet excitons, a better design in the molecular level may enhance the efficiency of white EL. The next chapter discusses our efforts towards that direction.

Table 3.4. Device properties for the fabricated white device

Voltage (V)	Current (I) mA	Luminance (lv)	Current Density $(J, mA/cm^2)$	Current Efficiency (cd/A)	Power efficiency (lm/W)
4	1.42	0.18	1.02	0.02	0.01
8	1.17	3.19	8.38	0.04	0.01
9.5	4.77	18.60	34.09	0.05	0.02
10	6.39	20.77	45.63	0.05	0.01
12	1.34	18.08	95.34	0.02	0.01
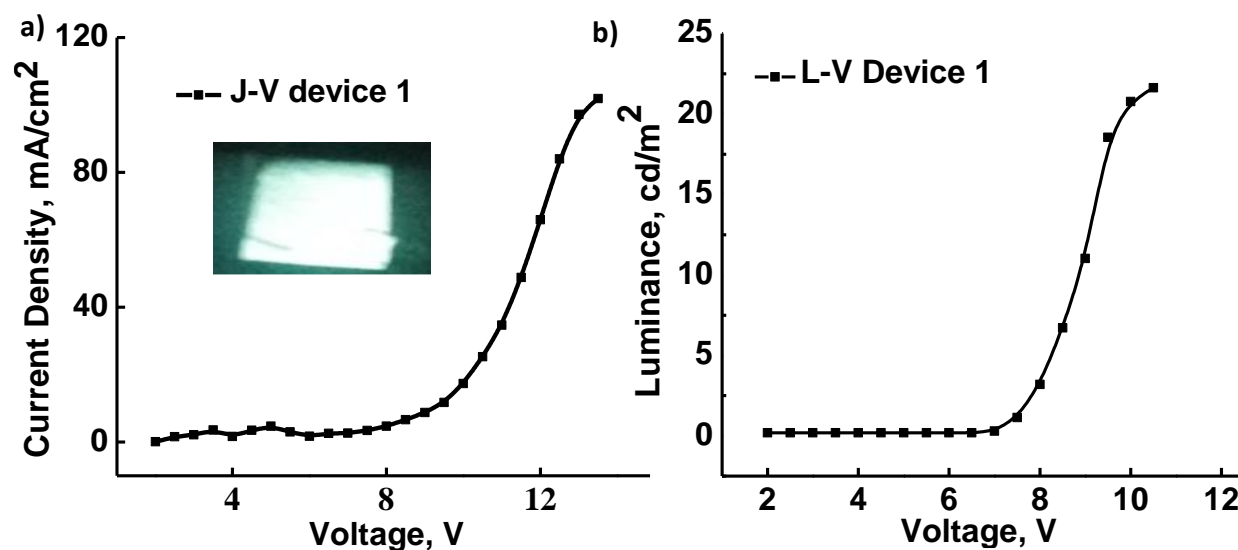
Figure 3.20. *a) J-V curve for device 1 (inset shows the white OLED fabricated) b) L-V curve for the devices*

3.5.2 Cz(PhCF₃)₂ as host for yellow and red fluorescent emitters

The high triplet energy of 2.8 eV calculated from low temperature emission profile for the molecule, **Cz(PhCF₃)₂**, prompted us for examining its host properties. As a primary analysis PL emissions of **Cz(PhCF₃)₂** along with three emitters (blue, yellow, red) were examined. We selected rubrene, as yellow, DPV as the blue and DCJTB as the red emitter. We observed that in all the cases there was energy transfer between the host and the emitter except for the mixture containing the blue emitter. With the yellow emitter **Cz(PhCF₃)₂** was used as the sole host, while in the case of red emitter a mixture of **Cz(PhCF₃)₂** and rubrene was used as host, the energy level diagram for the fabricated devices are given in Figure 3.22. The chemical structures for the molecules used for this study are given in Figure 3.22
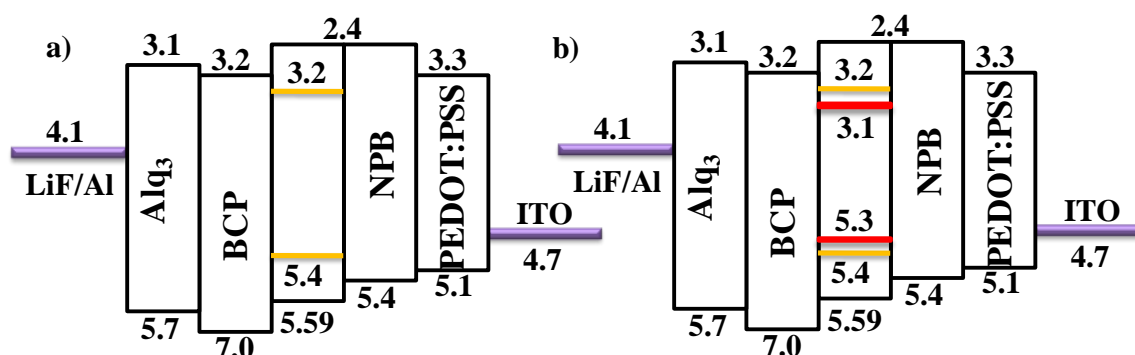
Figure 3.21 . *Energy level diagrams for the devices fabricated with a) Rubrene, where the yellow line represents the energy levels of rubrene b) DCJTB, where the yellow line represents the energy levels of rubrene and red line represents the energy levels for DCJTB*
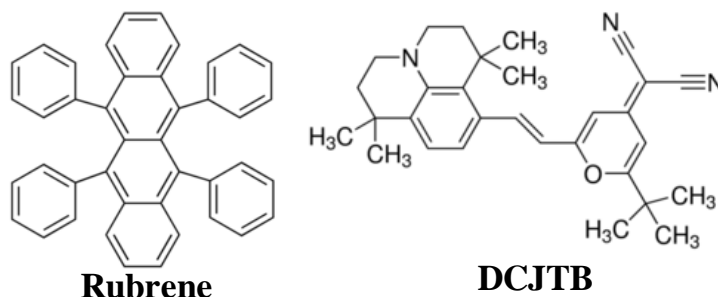
Rubrene **DCJTB**

Figure 3.22. *molecular structures for the blue, yellow and red emitters*

The PL emission spectra for rubrene and the rubrene+DCJTB mixture are presented in Figure 3.23, from the spectra it is very clear that there is efficient energy transfer between the molecules. The emission was recorded in different doping concentrations. In the case of

rubrene 20% doping is found to be efficient while in the case of DCJTB 5% doping is found to be efficient.
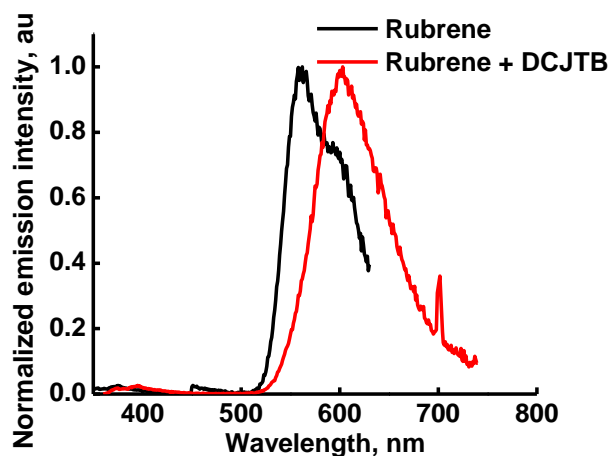
Figure 3.23*. PL emission spectra for the mixture of host and dopants.*

Figure 3.24 shows the EL emission spectra for the host + dopant systems. Device characterization curves for the yellow device is given in Figure 3.25 and the corresponding device performance data are presented in Table 3.5. The device characterization curves for the red device is presented in Figure 3.26 and the corresponding device performance data are given in Table 3.6 From the device performance data the fabricated devices were not efficient enough for further studies.
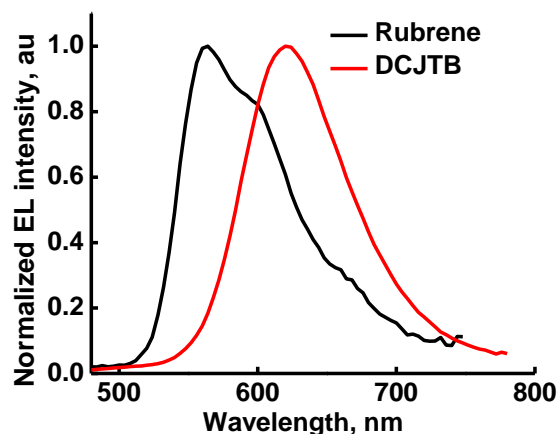
Figure 3.24. *EL emission spectra for the fabricated yellow and red devices*
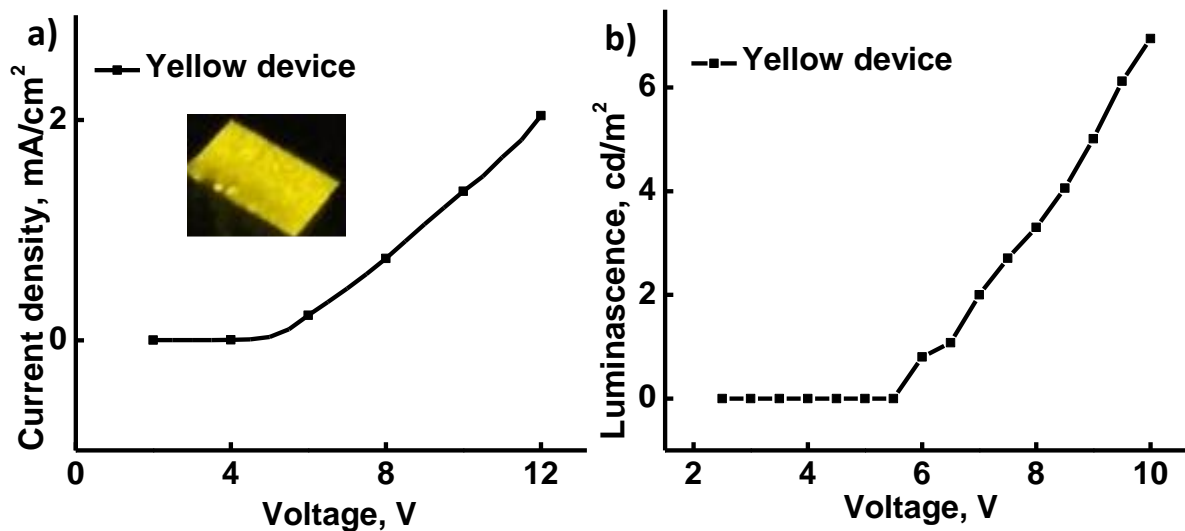
Figure 3.25.*a) J-V curve for device 1 (inset shows the yellow OLED fabricated) b) L-V curve for the devices*

Table 3.5. Device characterization of yellow device

Voltage (V)	Current (mA)	Luminance (lv)	Current Density (J, mA/cm^2)	Current Efficiency (cd/A)	Power efficiency (lm/W)
4.00	1.17	1.74	11.18	0.02	0.01
8.00	3.12	1.70	297.98	5.72×10^{-4}	2.24×10^{-4}
9.50	3.80	3.83	362.27	0.01	3.50×10^{-4}
1.00	3.91	2.42	373.05	6.50×10^{-4}	2.04×10^{-4}
12.00	4.63	0.18	441.79	4.14×10^{-4}	1.08×10^{-4}
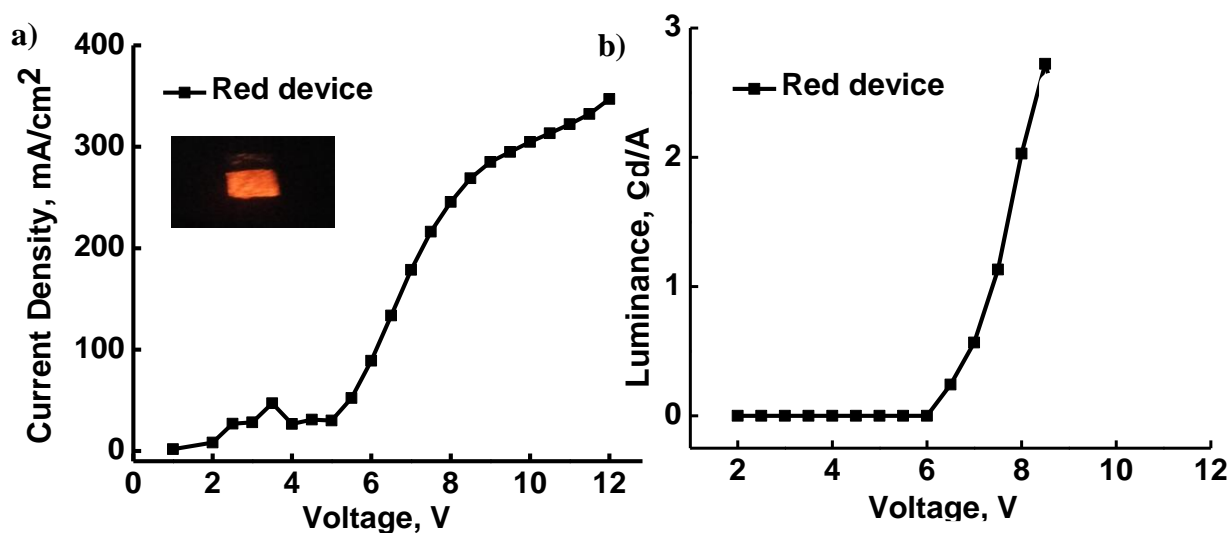
Figure 3.26. a) J-V curve for device 1 (inset shows the red OLED fabricated) b) L-V curve for the devices

Table 3.6. Device characterization of red device

Voltage (V)	Current (I) mA	Luminance (lv)	Current Density (J, mA/cm^2)	Current Efficiency (cd/A)	Power efficiency (lm/W)
4	1.17	1.75	11.18	0.02	0.01
8	3.13	1.70	297.98	5.70×10^{-4}	2.24×10^{-4}
9.5	3.80	3.84	362.28	0.01×10^{-4}	3.50×10^{-4}
12	4.64	0.18	441.79	4.14×10^{-4}	1.08×10^{-4}

3.6. Conclusions

In summary, we have developed a new straightforward method for achieving white light emission from a single molecule by appropriately manipulating the structure of carbazole. The device performance of the white light emitting diodes can be improved with the current route by harvesting both singlet and triplet energy thereby overcoming the spin statistical limit of

25%. **Cz(PhCF₃)₂** showed a very prominent room temperature phosphorescence achieved through molecular design using the intrinsic SOC of carbazole and the 3, 6 substitutions on the carbazole. The small ΔE_{ST} of the molecule helped to tune the phosphorescence near to fluorescence and thereby covering the entire visible range. Further tuning of the ΔE_{ST} and the efficiency of the SOC can certainly increase the device performance and also the purity of white light emission.

3.7. Experimental Section

3.7.1. General information and materials

The solvents were purchased from Merck Millipore. Boronic acids and carbazole were purchased from Sigma Aldrich and used without further purification. NBS was purchased from Spectrochem and used after re-crystallizing from water. Na_2CO_3, Na_2SO_3 and activated aluminium oxide for column chromatography were also purchased from Spectrochem. The catalyst Pd(PPh₃)₄ and silica gel for column chromatography were purchased from Alfa Aesar. Reactions were carried out under an inert atmosphere of argon in oven-dried glassware. The progress of the reaction was monitored by TLC using commercial Silica Gel TLC plates (Merck-Millipore, 60 F254) and UV detection (254 nm and 365 nm). Column chromatography was done using activated aluminium oxide and silica gel. The ^{1}H and ^{13}C NMR spectra were recorded using Bruker NMR spectrometer (AV500) with working frequency of 500 MHz for ^{1}H NMR and 125 MHz for ^{13}C NMR. The chemical shifts are reported in δ (ppm) relative to TMS as an internal standard. The signal splitting is abbreviated as follows: s = singlet; d = doublet; t = triplet; q = quartet; and m = multiplet. All coupling constants (*J*) are given in Hertz (Hz). Mass spectra were recorded using ESI/ HRMS at 60000 resolutions (Thermo Scientific Exactive)

3.7.2 Synthesis of the molecules

3.7.2.1. General Procedure for the Suzuki-MiyauraCoupling[28]

The boronic acid (1 equivalent.) and bromo compound (1 equivalent) were taken in a reaction vessel along with Pd(PPh₃)₄ (catalyst). To this, THF was added with 2N Na_2CO_3 dissolved in

water in the ratio 2:1. The reaction mixture was degassed with argon and allowed to stir at 65-70 °C for 12 h.

3.7.2.2. Synthesis of 9-ethyl-9,9a-dihydro-4a*H*-carbazole (Cz-Et)

To a solution of carbazole (5g, 0.029 mol) in THF (50 mL) at 0 °C, NaH (1.43 g, 0.0598 mol) was added. The heterogeneous mixture was stirred for 15 min. at 0 °C, and for 1 h at room temperature. The mixture was then cooled to 0 °C and treated with ethyl iodide (5 mL, 0.0598 mol) and the mixture was allowed to warm to room temperature. After 30 min., the reaction mixture was cooled to 0 °C and quenched with NH$_4$Cl. It was then extracted with 25 mL ether (3 times) and the combined ether extracts were washed with brine and dried over anhydrous sodium sulpahte. The crude product obtained after the removal of ether was used as such for further reaction.

Spectral characterization of Cz-Et
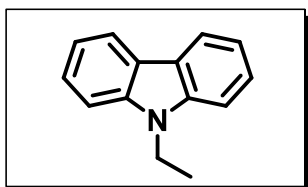
Yield: 75% as a creamy white solid.

^{1}H NMR (500 MHz, CDCl$_3$): δ 8.16-8.14 (d, *J* = 3 Hz, 2H), 7.52-7.49 (t, *J* = 7.5 Hz, 2H), 7.46-7.44 (d, *J* = 8 Hz, 2H), 7.29-7.26 (t, *J* = 7.25 Hz, 2 H)4.32 (q, 2H), 1.415 (t, *J* = 7.25 Hz, 3H). ppm

^{13}C NMR (125 MHz, CDCl$_3$): δ 140.0, 130.0, 125.6, 120.4, 118.7, 108.4, 37.5, 13.8. ppm

HRMS (ESI) for C$_{14}$H$_{13}$N, Calcd 196.1166`, Found: 196.1117.(M+H)$^+$.

3.7.2.3.Synthesis of 3,6-dibromo-9-ethyl-8a,9-dihydro-4bH-carbazole (Cz(Br)$_2$)

Cz-Et (1 g, 0.005 mol) dissolved in toluene (35 mL) was taken in a two–necked round bottom flask equipped with a magnetic stirrer bar, a nitrogen gas inlet and a 250 mL addition funnel. The system was then cooled in an ice bath. A solution of N-bromosuccinimide (NBS) (1.986 g, 0.0112 mol) in DMF (100 mL) was added to the flask through the funnel. After 30 min., the mixture was poured into cold water to precipitate out the product which was filtered and washed with cold methanol. The product was crystallized from MeOH / hexane (5: 1).

Spectral characterization of Cz(Br)$_2$
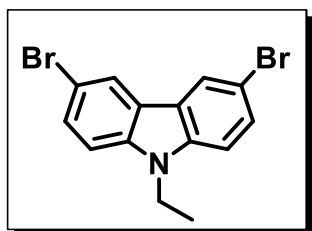
Yield: 80% as a brownish white solid

^{1}H NMR [500 MHz, CDCl$_3$]: δ, 8.16- 8.18 (d, *J* = 2Hz, 2H), 7.58-7.55 (dd, *J* = 2 Hz, *J* = 9 Hz, 2H), 7.28-7.27 (d, *J* = 10 Hz, 2H), 4.34- 4.30 (q, 2H), 1.43- 1.40 (t, *J* = 7.25 Hz, 3H). ppm

^{13}C NMR [125 MHz, CDCl$_3$]: δ: 129.4, 126.9, 123.15, 120.6, 110.1, 108.4. ppm

HRMS (ESI) for C$_{14}$H$_{11}$NBr$_2$, Calcd 352.92, Found: 353.9220 (M+1).

3.7.2.4.Synthesis of 9-ethyl-3,6-bis(4-(trifluoromethyl)phenyl)-9H-carbazole (Cz(PhCF$_3$)$_2$)

3,6-Dibromo-9-ethyl-8a,9-dihydro-4bH-carbazole (0.2 g, 0.000586 mol) and 4-trifluoromethyl- phenylboronic acid (0.220 g, 0.00011 mol) were added to the Schlenk tube along with Pd(PPh$_3$)$_4$ as the catalyst. THF (6 mL) along with 2N Na$_2$CO$_3$ solution (3 mL) was added to the reaction mixture. The reaction mixture was degassed with argon and allowed to stir at 65-70 °C for 12 h. The reaction mixture was monitored by TLC and on completion, it was worked up by extracting with 10 mL DCM twice. The organic layers were combined, washed with brine and evaporated to get the crude product which was subjected to column chromatography on activated aluminium oxide using 5% ethyl acetate / hexane mixture as elutent to afford the product in good yield (63%).

Spectral characterization of Cz(PhCF$_3$)$_2$
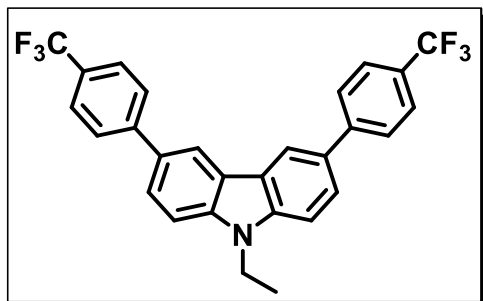
Yield: 64% as a white solid

^{1}H NMR [500 MHz, CDCl$_3$]: δ 8.39-8.38 (d,*J*=5Hz, 2H), 7.83-7.81(d, *J* = 10 Hz,4H), 7.77-7.75 (dd, 2H), 7.73-7.72 (d, *J* = 5 Hz, 4H), 7.53-7.52 (d, *J* = 5 Hz, 2H) 4.34- 4.30 (q, 2H), 1.43-1.40 (t, *J* = 7.25 Hz, 3H). ppm

^{13}C NMR [125 MHz, CDCl$_3$]: δ (ppm) 145.4, 140.38, 131.1, 128.6, 128.41, 127.3, 125.8, 125.7, 125.5, 123.5, 123.3, 119.2, 109.2, 99.9, 37.9, 13.9.

HRMS (ESI) for $C_{28}H_{19}F_6N$, Calcd: 483.14217, Found: 483.1425 (M+)

3.7.3. Instrumentation

3.7.3.1 Photophysical studies

Absorption spectra were recorded using a Shimadzu UV-2600UV-Visible spectrophotometer. The optical diffuse reflectance spectra were measured for solid samples using the aforementioned spectrometer equipped with an integrating sphere. $BaSO_4$ was used as the reference material, and the solid samples were ground well before the measurement. The absorption (α/S) data were calculated from the reflectance spectra using the Kubelka–Munk function: $\alpha/S = (1 - R)2/2R$, in which R is the reflectance at a given wavelength, α is the absorption coefficient, and S is the scattering coefficient (practically wavelength independent when the particle size is larger than 5 mm). Steady-state fluorescence experiments were performed using FluoroLog-322(Horiba) which was equipped with a 450 W Xe arc lamp by using optically dilute solutions. The fluorescence quantum yields in various solvents were determined by the relative method employing an optically matched solution of quinine sulphate in 0.1N sulphuric acid as the reference ($\Phi_R = 0.54$). The following equation (1) was used for calculating the quantum yield,[29]

$$\Phi_S = \frac{Abs_R}{Abs_s} \times \frac{Area_S}{Area_R} \times \frac{nS^2}{nR^2} \times \Phi_R \underline{\hspace{6cm}}(1)$$

where the subscript R and S refer to the reference and samples respectively. Abs, Area, and n are the absorbance at the excitation wavelength, the area under the fluorescence spectrum and refractive index of the solvent respectively. Solid state photoluminescence spectra were also recorded using the front face mode with the same Fluorologspectro - fluorimeter. Time-resolved fluorescence spectra and lifetime experiments were performed by using an IBH pico second single photon counting system employing the 375 nm nano LED as excitation sources and a Hamamatsu C4878-02 micro channel plate (MCP) detector. Decay in the

fluorescence intensity (I) with time (t) was fitted either by a double/triple-exponential function:

$$I = A_1 e^{-t/\tau_1} + A_2 e^{-t/\tau_2} \underline{\hspace{7cm}} \quad (2)$$

$$I = A_1 e^{-t/\tau_1} + A_2 e^{-t/\tau_2} + A_3 e^{-t/\tau_3} \quad \underline{\hspace{5cm}}$$
(3)

where τ_1, τ_2, and τ_3 are the lifetimes of different species, and A_1, A_2, and A_3 are their respective amplitudes. The weighted mean lifetime ($\langle \tau \rangle$) was calculated according to equation (4):

$$\langle \tau \rangle = \Sigma \tau_i A_i \quad \underline{\hspace{6cm}} \quad (4)$$

The quality of the fits was checked by examining the residual distribution and the χ^2 value. The solid state samples were recorded with the front face mode. All the experiments were conducted at room temperature.

3.7.3.2 Cyclic voltammetry

Cyclic voltammetry experiments were carried out using a BAS 50 W voltammetric analyzer using three electrode cell assemblies. Platinum wires were used as counter electrodes, a silver wire was used as an Ag/Ag$^+$ quasi-reference electrode, and a platinum electrode was used as a working electrode. Measurements were carried out in acetonitrile solution with tetrabutylammoniumhexafluorophosphate as the supporting electrolyte at a scan rate of 100 mV s^{-1}. Concentrations of the molecules and the supporting electrolyte were 5×10^{-3} and 0.1 M, respectively. The ferrocenium/ferrocene couple (FeCp2$^+$/FeCp2^0) was used as an internal reference. The energy level of FeCp2$^+$/FeCp2^0 was assumed at -4.8 eV to vacuum.[30] All solutions for the electrochemical studies were deaerated with pre-purified argon gas before the measurements.

3.7.3.3 Computational methods

The ground (S^0) geometries of model systems **Cz(PhCF3)2** was optimized by using density functional theory (DFT) based method with Becke's three-parameter functional and the Lee-

Yang-Parr functional (B3LYP) with 6-31G* basis set. Based on the gas phase optimized geometry of **Cz(PhBz)₂** spectral properties in chloroform were calculated by time dependent density functional theory (TD-DFT) method with Polarizable Continuum Model (PCM) at PBE0/6-31G* level. All the calculations were carried out using Gaussian 09 program package.

3.7.3.4 Thermal analysis

Differential scanning calorimetry was performed using a TA Q20 general-purpose DSC instrument in sealed aluminum pans under nitrogen flow at a heating/cooling rate of 5 °C min^{-1}.

3.7.3.5 Device fabrication

Patterned ITO coated substrates (sheet resistance 10 Ω/m^2), brushed with soap solution, and cleaned in an ultrasonic bath with 2-propanol and de-ionized water were used as substrates. Devices were fabricated by spin coating of different organic layers expect Alq₃ under nitrogen atmosphere including emissive layer. The cathode aluminum and Alq₃ were thermally evaporated at high vacuum condition (~10-8 Torr). Devices were encapsulated with a cover glass and UV- curable epoxy resin in nitrogen atmosphere before evaluation. The measured device area is 9 mm^2 for **Cz(PhCF₃)₂**.

3.8 Reference

1. Tang, C. W.; Vanslyke, S. A. Organic Electroluminescent Diodes. *Appl. Phys. Lett.***1987**, *51* (12), 913–915.

2. D'Andrade, B. W.; Holmes, R. J.; Forrest, S. R. Efficient Organic Electrophosphorescent White-Light-Emitting Device with a Triple Doped Emissive Layer. *Adv. Mater.***2004**, *16* (7), 624–628.

3. Tanaka, H.; Shizu, K.; Nakanotani, H.; Adachi, C. Twisted Intramolecular Charge Transfer State for Long-Wavelength Thermally Activated Delayed Fluorescence. *Chem. Mater.***2013**, *25* (18), 3766–3771.

4. Reineke, S.; Thomschke, M.; Lussem, B.; Leo, K. White Organic Light-Emitting Diodes: Status and Perspective. *Rev. Mod. Phys.* **2013**, *85* (3), 1245–1293.

5. D'Andrade, B. W.; Forrest, S. R. White Organic Light-Emitting Devices for Solid-State Lighting. *Adv. Mater.* **2004**, *16* (18), 1585–1595.

6. Farinola, G. M.; Ragni, R. Electroluminescent Materials for White Organic Light Emitting Diodes. *Chem. Soc. Rev.* **2011**, *40* (7), 3467–3482.

7. Sun, N.; Wang, Q.; Zhao, Y.; Chen, Y.; Yang, D.; Zhao, F.; Chen, J.; Ma, D. High-Performance Hybrid White Organic Light-Emitting Devices without Interlayer between Fluorescent and Phosphorescent Emissive Regions. *Adv. Mater.* **2014**, *26* (10), 1617–1621.

8. Zhang, B.; Tan, G.; Lam, C. S.; Yao, B.; Ho, C. L.; Liu, L.; Xie, Z.; Wong, W. Y.; Ding, J.; Wang, L. High-Efficiency Single Emissive Layer White Organic Light-Emitting Diodes Based on Solution-Processed Dendritic Host and New Orange-Emitting Iridium Complex. *Adv. Mater.* **2012**, *24* (14), 1873–1877.

9. Cherpak, V.; Stakhira, P.; Minaev, B.; Baryshnikov, G.; Stromylo, E.; Helzhynskyy, I.; Chapran, M.; Volyniuk, D.; Tomkuté-Lukšiené, D.; Malinauskas, T.; Getautis, V.; Tomkeviciene, A.; Simokaitiene, J.; Grazulevicius, J. V. Efficient "warm-white" OLEDs Based on the Phosphorescent Bis-Cyclometalated iridium(III) Complex. *J. Phys. Chem. C.* **2014**, *118* (21), 11271–11278.

10. Liu, Y.; Cui, L.; Xu, M.; Shi, X.; Zhou, D.; Wang, Z.; Jiang, Z.; Liao, L. Highly Efficient Single-Layer Organic Light-Emitting Devices Based on a Bipolar Pyrazine/carbazole Hybrid Host Material. *J. Mater. Chem. C* **2014**, *2* (4), 2488–2495.

11. Kim, S. H.; Park, S.; Kwon, J. E.; Park, S. Y. Organic Light-Emitting Diodes with a White-Emitting Molecule: Emission Mechanism and Device Characteristics. *Adv. Funct. Mater.* **2011**, *21* (4), 644–651.

12. Zhao, J.; Ji, S.; Chen, Y.; Guo, H.; Yang, P. Excited State Intramolecular Proton Transfer (ESIPT): From Principal Photophysics to the Development of New Chromophores and Applications in Fluorescent Molecular Probes and Luminescent Materials. *Phys. Chem. Chem. Phys.***2012**, *14* (25), 8803–8817.

13. Tang, K.-C.; Chang, M.-J.; Lin, T.-Y.; Pan, H.-A.; Fang, T.-C.; Chen, K.-Y.; Hung, W.-Y.; Hsu, Y.-H.; Chou, P.-T. Fine Tuning the Energetics of Excited-State Intramolecular Proton Transfer (ESIPT): White Light Generation in A Single ESIPT System. *J. Am. Chem. Soc.***2011**, *133* (44), 17738–17745.

14. Zhu, M.; Yang, C. Blue Fluorescent Emitters: Design Tactics and Applications in Organic Light-Emitting Diodes. *Chem. Soc. Rev.* **2013**, *42* (12), 4963–4976.

15. Uoyama, H.; Goushi, K.; Shizu, K.; Nomura, H.; Adachi, C. Highly Efficient Organic Light-Emitting Diodes from Delayed Fluorescence. *Nature.***2012**, *492* (7428), 234–238.

16. M. Liu, Y. Seino, D. Chen, S. Inomata, S. J. Su, H. Sasabe, J. Kido, Chem. Commun. **2015**, 51 (15), 16353.

17. Dias, F. B.; Bourdakos, K. N.; Jankus, V.; Moss, K. C.; Kamtekar, K. T.; Bhalla, V.; Santos, J.; Bryce, M. R.; Monkman, A. P. Triplet Harvesting with 100% Efficiency by Way of Thermally Activated Delayed Fluorescence in Charge Transfer OLED Emitters. *Adv. Mater.***2013**, *25* (27), 3707–3714.

18. Wang, S.; Yuan, W. Z.; Zhang, Y.; Gong, Y.; Chen, G.; Peng, Q.; Yuan, W. Z.; Xie, Y.; Li, S. Achieving Persistent Room Temperature Phosphorescence and Remarkable Mechanochromism from Pure Organic Luminogens. *Adv. Mater.***2015**, *2 (9)*, 6195–6201.

19. Xue, P.; Wang, P.; Chen, P.; Yao, B.; Gong, P.; Sun, J.; Zhang, Z.; Lu, R. Bright Persistent Luminescence from Pure Organic Molecules through a Moderate Intermolecular Heavy Atom Effect. *Chem. Sci., 2017,8 (9), 6060-6065*

20. Haggquist, G. W.; Burkhart, R. D. Photophysics of N-Ethylcarbazole in Fluid Solution: Evidence for Solvent Dependence and Triplet Excimer Formation. *J. Phys. Chem.* **1993**, *97* (11), 2576–2584.

21. Wang, S.; Yuan, W. Z.; Zhang, Y.; Gong, Y.; Chen, G.; Peng, Q.; Yuan, W. Z.; Xie, Y.; Li, S. Achieving Persistent Room Temperature Phosphorescence and Remarkable Mechanochromism from Pure Organic Luminogens. *Adv. Mater.* **2015**, 27(*2)*, 6195–6201.

22. He, Z.; Zhao, W.; Lam, J. W. Y.; Peng, Q.; Ma, H.; Liang, G.; Shuai, Z.; Tang, B. Z. White Light Emission from a Single Organic Molecule with Dual Phosphorescence at Room Temperature. *Nat. Commun.* **2017**, *8* (1), 416.

23. Li, C.; Tang, X.; Zhang, L.; Li, C.; Liu, Z.; Bo, Z.; Dong, Y. Q.; Tian, Y. H.; Dong, Y.; Tang, B. Z. Reversible Luminescence Switching of an Organic Solid: Controllable On-Off Persistent Room Temperature Phosphorescence and Stimulated Multiple Fluorescence Conversion. *Adv. Opt. Mater.* **2015**, *3* (9), 1184–1190.

24. Keita Tani, a YasuoTohda, a Hiroyuki Takemura, b Hideo Ohkita, c S. I. and M.; Yamamotoc. Synthesis and Photophysical Properties of [3.3] carbazolophens. *Chem. Commun.* **2001**, *296* (34), 1914–1915.

25. Miertuš, S.; Scrocco, E.; Tomasi, J. Electrostatic Interaction of a Solute with a Continuum. A Direct Utilizaion of AB Initio Molecular Potentials for the Prevision of Solvent Effects. *Chem. Phys.* **1981**, *55* (1), 117–129.

26. Kim, K.; Jordan, K. D. Comparison of Density Functional and MP2 Calculations on the Water Monomer and Dimer. *J. Phys. Chem.* **1994**, *98* (40), 10089–10094.

27. a) Becke, A. D. Density-Functional Thermochemistry. III. The Role of Exact Exchange. *J. Chem. Phys.* **1993**, *98* (7), 5648. b) Chen, F. P.; Xu, B.; Zhao, Z. J.; Tian, W. J.; Lü, P.; Im, C. White Organic Light-Emitting Diodes Based on

Electroplex from Polyvinyl Carbazole and Carbazole Oligomers Blends. *Chinese Phys. B* **2010**, *19* (3). c) Cocchi, M.; Virgili, D.; Giro, G.; Fattori, V.; Di Marco, P.; Kalinowski, J.; Shirota, Y. Efficient Exciplex Emitting Organic Electroluminescent Devices. *Appl. Phys. Lett.* **2002**, *80* (13), 2401–2403. d) Zhen, H.; Xu, W.; Yang, W.; Chen, Q.; Xu, Y.; Jiang, J.; Peng, J.; Cao, Y. White-Light Emission from a Single Polymer with Singlet and Triplet Chromophores on the Backbone. *Macromol. Rapid Commun.* **2006**, 27(24), 2095–2100

28. Miyaura, N.; Suzuki, A. Palladium-Catalyzed Cross-Coupling Reactions of Organoboron Compounds. *Chem. Rev.***1995**, *95* (7), 2457–2483.

29. Brouwer, A. M. Standards for Photoluminescence Quantum Yield Measurements in Solution (IUPAC Technical Report). *Pure Appl. Chem.***2011**, *83* (12), 2213–2228.

30. Liu, Y.; Liu, M. S.; Jen, A. K.-Y. Synthesis and Characterization of a Novel and Highly Efficient Light-Emitting Polymer. *ActaPolym.***1999**, *50* (2), 105–108.

Chapter 4

Design, synthesis, PL and EL studies of a carbazole - benzophenone derivative Cz(PhBz)$_2$ as a white light emitter in organic light emitting diodes
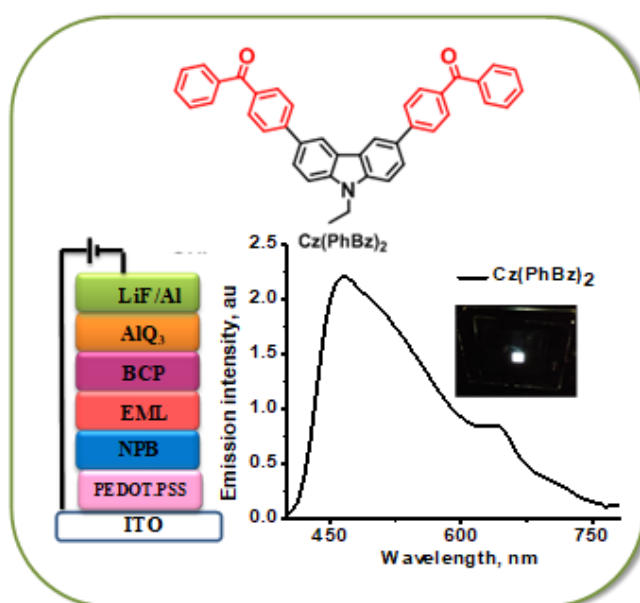
4.1 Abstract

*Based on the encouraging results that we obtained in producing white electroluminescence from the carbazole derivative Cz(PhCF$_{3)2}$, a new carbazole derivative **Cz(PhBz)$_2$** having a stronger electronegative group (Benzophenyl group) at 3,6 positions was successfully synthesised. **Cz(PhBz)$_2$** also gave a white electroluminescence emission with better efficiency (110 cd/m^2) than Cz(PhCF$_3$)$_2$ (20 cd/m^2). The device fabricated with **Cz(PhBz)$_2$** as the emissive layer showed better colour purity and device efficiency. A detailed discussion on the design, synthesis, charecterization and EL properties of the molecule **Cz(PhBz)$_2$** is the subject matter of chapter 4.*

4.2 Introduction

In the previous chapter we reported relatively an unexplored path for the generation of white light using a single small molecule $Cz(PhCF_3)_2$ where the blue emission from the singlet state along with the greenish yellow emission from the triplet state resulted in white light emission. In an effort to improve the efficiency and colour purity of the white organic light emitting diode, we decided to substitute the 3,6-positions of carbazole with a stronger electronegative acceptor containing a carbonyl group.

The carbonyl group present will reduce the ΔE_{ST} value due to its small overlap integral *J*. According to theory

$$\Delta E_{ST} = E_S - E_T \quad = E_0\,(n,\,\pi^*) + K\,(n,\,\pi^*) + J\,(n,\,\pi^*) - [E_0\,(n,\,\pi^*) + K\,(n,\,\pi^*) - J\,(n,\,\pi^*)]$$

$$\Delta E_{ST} \qquad\qquad = E_S - E_T = 2J\,(n,\,\pi^*) > 0$$

where *J* is the overlap integral between the two orbitals involved. From the above equation it is clear that the ΔE_{ST} is directly proportional to the *J* value. In the case of (π, π^*) the overlap is maximum and in (n, π^*) it is minimum due to the orientation of the orbitals as shown in Figure 4.1. So the $n-\pi^*$ transition involved with the ketone group will reduce the ΔE_{ST}..
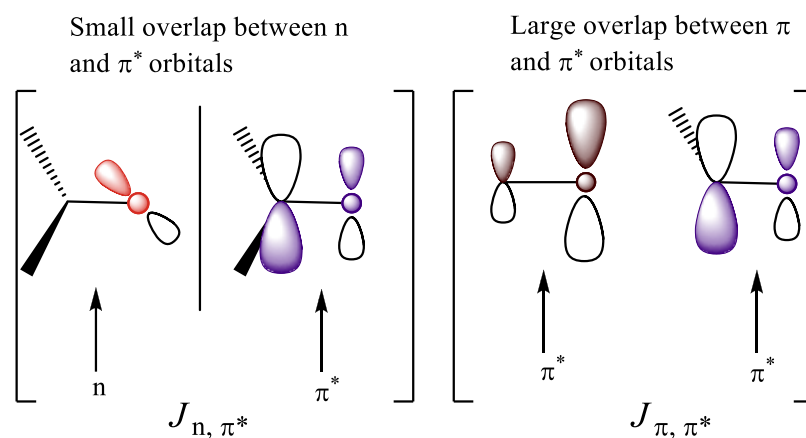
Figure 4.1. *The orbital diagram showing the orbital overlap of n, π and π^* orbitals*

Obtaining RTP from a pure organic molecule is a difficult task due to weak intersystem crossing because of low spin-orbit coupling. Many groups reported RTP induced by crystallization,[1] halogen bonding,[2] aggregation,[3] self-assembly[4] etc. Recently there was a report on the structural requirements that need to be adopted in designing molecules for the occurrence of RTP.[5] Due to intrinsic spin-orbit coupling, carbazoles are already reported to exhibit RTP[6-10] giving a strong blue fluorescence and weak yellow room temperature phosphorescence.[11]

Very recently Tang *et.al* reported the occurrence of room temperature phosphorescence from the crystals of a carbazole-benzophenone derivative (1CA).[12] Figure 4.2 shows the chemical structure and room temperature phosphorescence emission of 1CA.
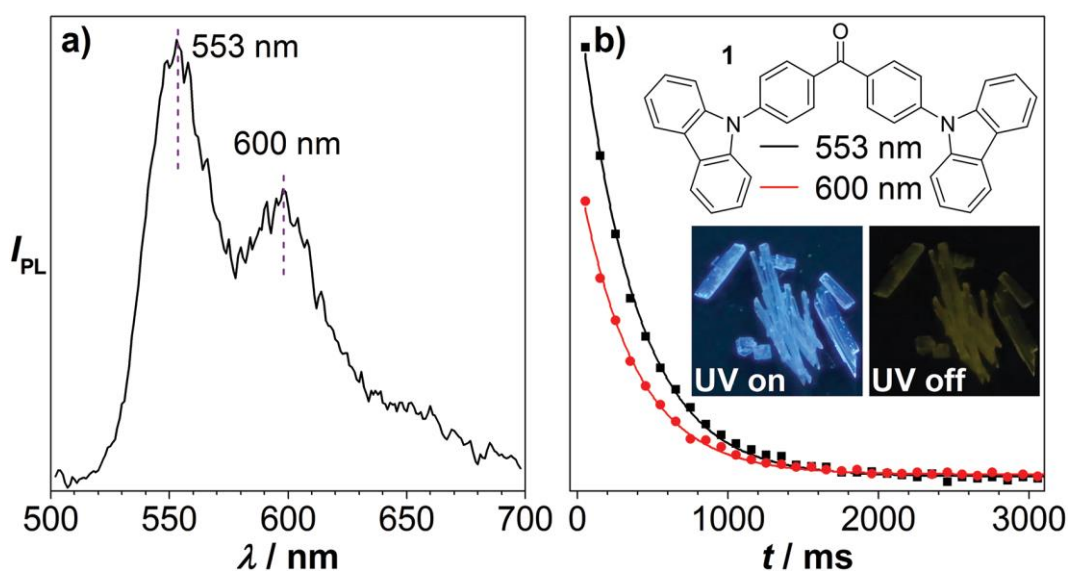
Figure 4.2. *a) RTP spectrum of the crystal 1CA obtained through re-crystallization from chloroform solution; excitation wavelength: 350 nm; b) RTP decay curve of 1CA at 553 nm and 600 nm; inset: snapshot image before and immediately after turning UV lamp off. The Figure has been reproduced as such from the reference[12]*

In 2017, the same group reported white colour emission from another benzophenone derivative in its powder state.[13] In that report published in *Nature*, they design and synthesis a single pure organic phosphor, namely 4-chlorobenzoyldibenzothiophene (ClBDBT), emitting white room temperature phosphorescence with Commission *Internationale de l'Éclair-age* coordinates of (0.33, 0.35). Experimental and theoretical investigations revealed that the source of white light emission was from dual phosphorescence emissions from the first and second excited triplet states. So they thus

successfully demonstrated the the validity of this strategy to achieve metal-free pure phosphorescent single molecule white light emitters by intra-system mixing dual room temperature phosphorescence arising from the low- and high-lying triplet states. (Figure 4.3)
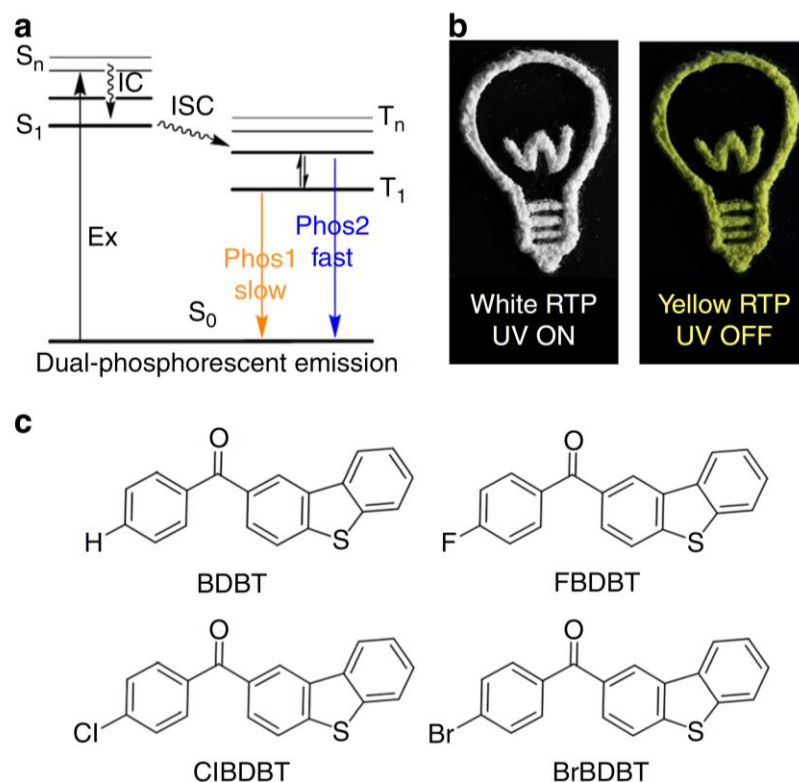
Figure 4.3. *a) Jablonski diagram for dual phosphorescent emission. b) Photo-pattern of ClBDBT. c) Molecular structures of room temperature phosphors studied in this paper. Reproduced as such from the reference.* [13]

The same group investigated on the basic designing criteria for getting RTP from pure organic molecules, and they reported that, aromatic carbonyls are the best candidates for getting the same.[14] This is due to the fact that, according to the El-Sayed rule,[15] effective spin-orbit coupling (SOC) occurs during the transition from the singlet state with an electronic configuration such as $^1(n, \pi^*)$ or $^1(\pi, \pi^*)$ to a triplet state with configuration $^3(\pi, \pi^*)$ or $^3(n, \pi^*)$, respectively. This is because these orbitals can effectively overlap under the operation of the orbital angular momentum operator (Figure 4.4). In contrast, the intersystem crossing (ISC) from $^1(\pi, \pi^*)$ to $^3(\pi, \pi^*)$ and $^1(n,\pi^*)$ to $^3(n,\pi^*)$ are not favored because, the SOC is insignificant as a result of the in-

efficient orbital overlapping prohibited by the angular momentum operator. Thus, the existence of n orbitals that are perpendicular to the π orbitals becomes crucial.
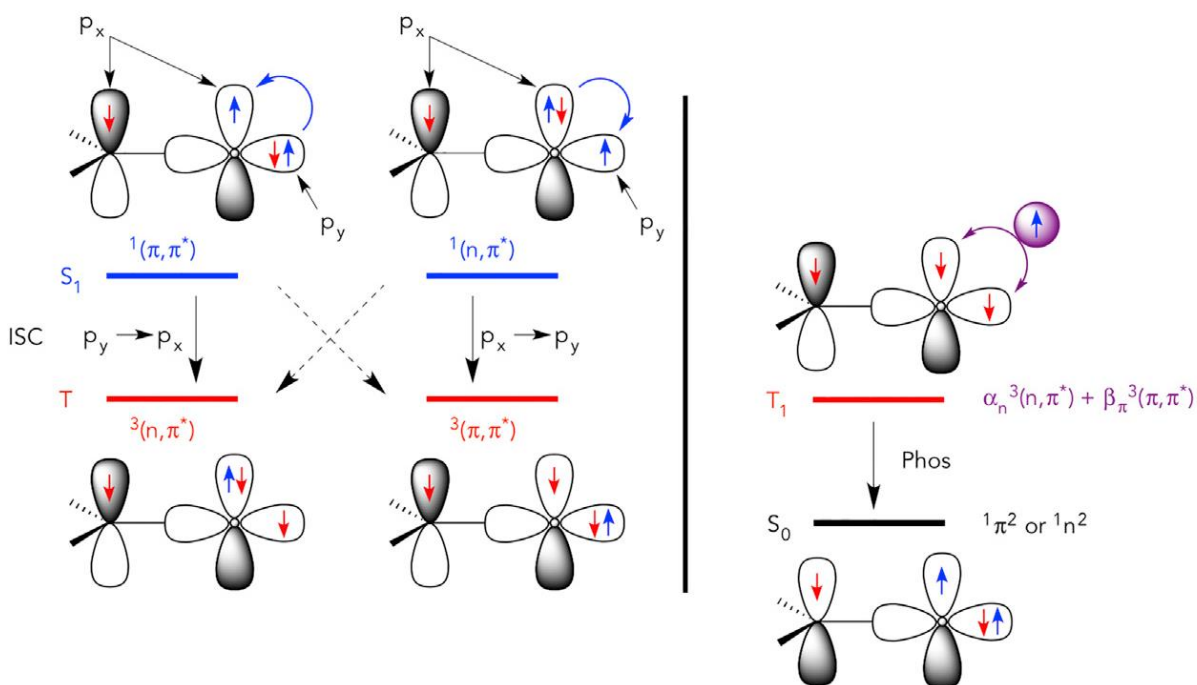
Figure 4.4*. (Reproduced as such from reference). Schematic representation of the El-Sayed rule for ISC and molecular-orbital hybridization of the lowest triplet states for tuning the rate of phosphorescence decay. Generally, persistent organic phosphorescence results from an extremely slow radiative decay rate of T1 with a pure $^3(\pi,\pi^*)$ configuration[15]*

4.3 Definition of the problem

From the above discussion, it can be envisaged that, (1) the existence of n orbitals and (2) the T1 state with an early pure $^3(\pi,\pi^*)$ configuration are the general structural requirements for developing a pure organic persistent and efficient RTP phosphor without the presence of heavy atoms. For such a molecular design, carbonyl groups especially aromatic carbonyls are the best candidates. Accordingly, we designed and synthesized a novel carbazole-benzophenone derivative, **Cz(PhBz)₂**. The results of our investigations on the PL and EL studies of **Cz(PhBz)₂** are the subject matter of this chapter.

4.4 Results and discussions

4.4.1 Synthesis and characterization of Cz(PhBz)₂
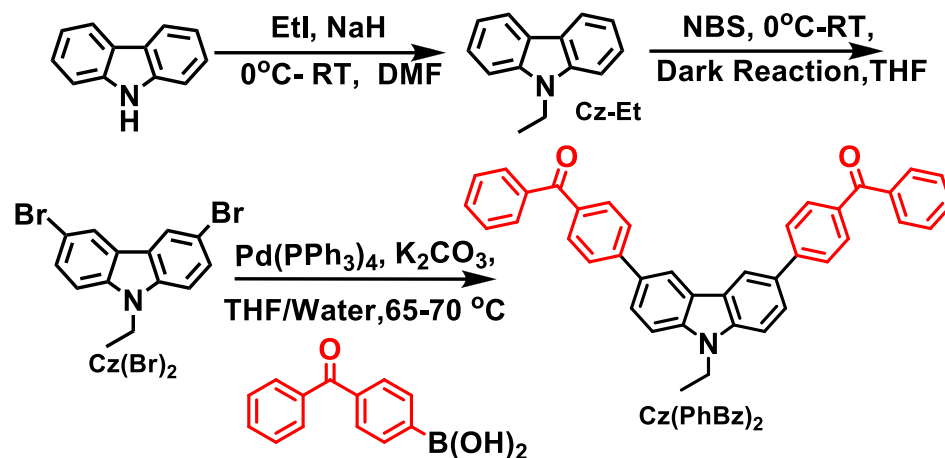
Scheme 4.1**. Synthetic route towards the molecule, **Cz(PhBz)₂

Cz(PhBz)₂ was synthesized using Suzuki-Miyaura coupling. The starting material, **Cz(Br)₂** was prepared by the controlled bromination of **Cz-Et. Cz-Et** was in turn prepared from carbazole and ethyl iodide by N-alkylation as described in the experimental section. The resultant molecule named as **Cz-Et** was then subjected to a mild bromination using re-crystallized NBS, to get **Cz(Br)₂. Cz(Br)₂** on Suzuki-Miayura coupling with benzophenylboronic acid gave the desired molecule, **Cz(PhBz)₂.** (Scheme 1) The synthetic procedure is efficient, less time consuming and the product was obtained in 64% yield.

The structure of **Cz(PhBz)₂** was confirmed by IR, ^{1}H, ^{13}C NMR spectral techniques and HRMS and all the spectra are reproduced in Figure 4.5. The IR spectrum of the molecule showed the vibrations corresponding to C-H stretching at 3000-3100 cm^{-1} and the ketone group vibration frequency at around 1717 cm^{-1}. The ^{1}H NMR spectrum showed aromatic protons in the region δ 8.46 to δ 7.48 ppm. The ethyl -CH₂ resonated in the range 4.46- 4.42 ppm as a quartet and the -CH₃ protons resonated between 1.51-1.40 as triplet. The ^{13}C NMR spectrum contained peaks corresponding to the aromatic carbon atoms from δ 160 to δ 109 ppm. The carbonyl carbon resonated at 196 ppm and

the ethyl carbons at 37.95 and 13.93 ppm. Mass spectrum showed $(M+H)^+$ peak at m/z 556.2283.
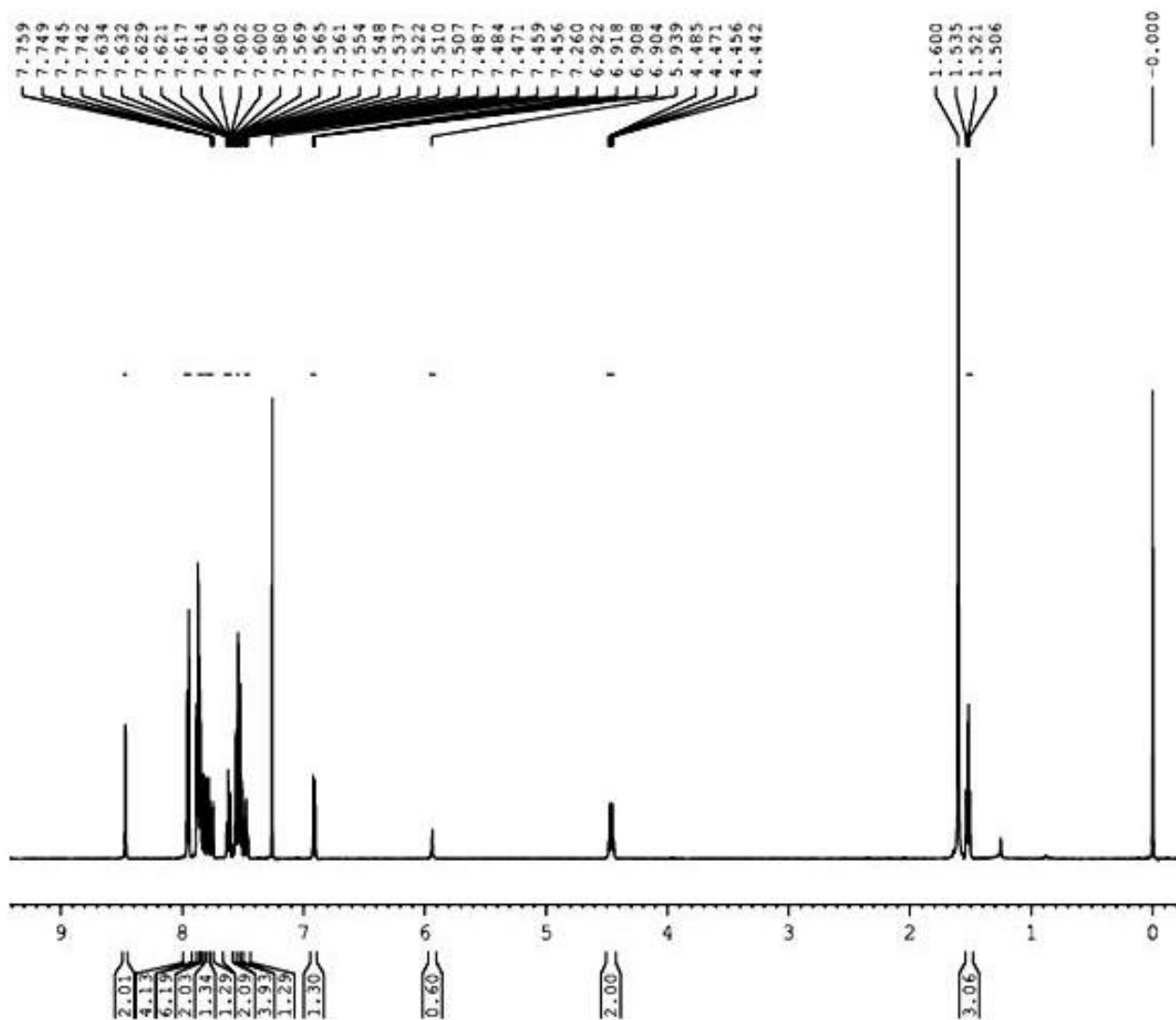
Figure 4.5. *^1H NMR spectrum for* **Cz(PhBz)$_2$**
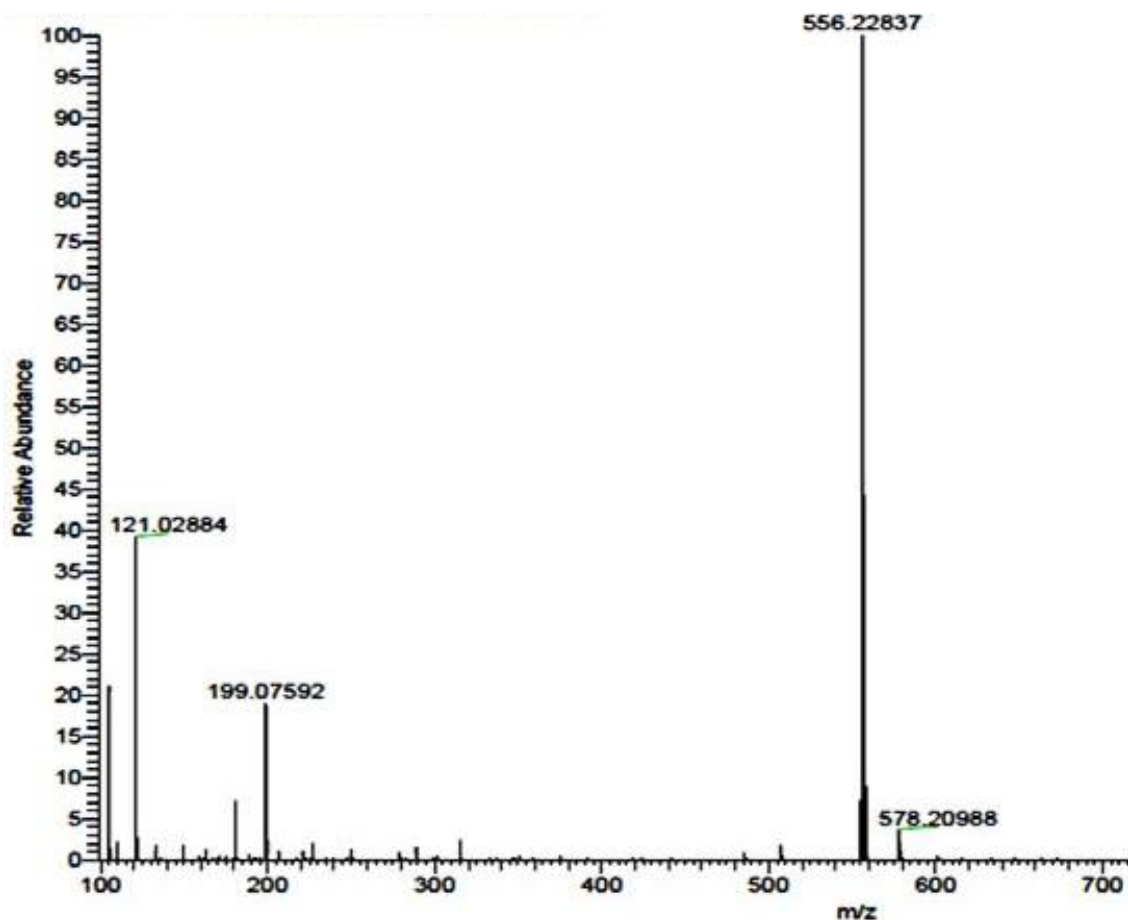
Figure 4.6. *Mass spectrum of **Cz(PhBz)₂***

4.4.2 Photoluminescence studies

4.4.2.1 Room temperature absorption and emission studies in solution state

The steady state aborption spectra of **Cz(PhBz)₂** were recorded in toluene, ethyl acetate, acetonitrile and dimethylformamide, which consisted of two major peaks. (Figure 4.7) Among the two peaks the high energy peak remained unchanged in all the polarities. The second peak around 350 nm showed a slight red shift of about 10 nm when the spectrum was recorded in DMF.
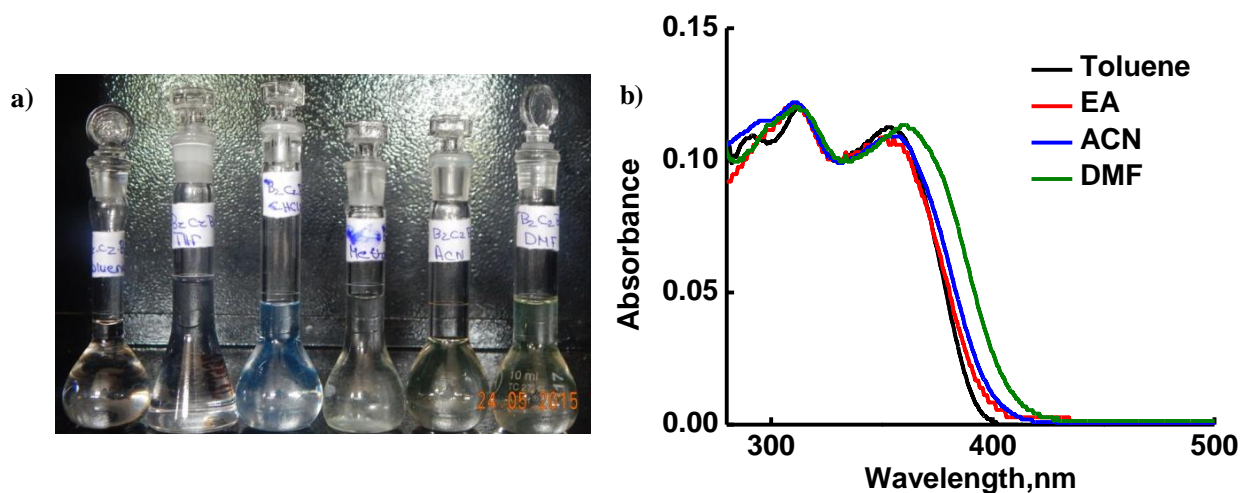
Figure 4.7. *a) Absorption of **Cz(PhBz)₂** in different solvents b) Absorption profile of **Cz(PhBz)₂** in toluene (Black), Ethylacetate (EA,red), Acetonitril (ACN, blue) and dimethylformamide (DMF, green)*

The steady state fluorescence spectra **Cz(PhBz)₂** was also recorded in toluene, ethyl acetate, acetonitrile and dimethylformamide (Figure 4.7). It showed a non-structured emission profile, unlike its –CF$_3$ counterpart. Upon excitation of a solution in toluene at λ_{exc} 310 nm, the emission maximum was observed at 428 nm. The experiment was repeated by exciting the solution at λ_{exc} 350 nm, which also resulted in an almost similar emission profile. The emission spectrum showed a Stocks shift value of 10,100 cm^{-1} in toluene and 13,210 cm^{-1} in DMF. This indicated the presence of a charge transfer state in the molecule as we expected unlike in the case of Cz(PhCF$_3$)$_2$ where the CT state was absent. The fluorescence quantum yield for the molecule was found to be 43 ± 5%, in THF with respect to coumarine as reference. Figure 4.8 shows the solution state emission and the corresponding spectra.

From this emission profile of **Cz(PhBz)₂** recorded in solvents of increasing polarity (toluene < ethyl acetate < acetonitrile < DMF). It is evident that the molecule exhibited profound solvatochromism (Figure 4.8). The emission spectra showed a Stockes shift value of 10,100 cm^{-1} in toluene and 13, 210 cm^{-1} in DMF. Another observation made after emission studies was that the molecule showed high emission intensities in high polar solvents.
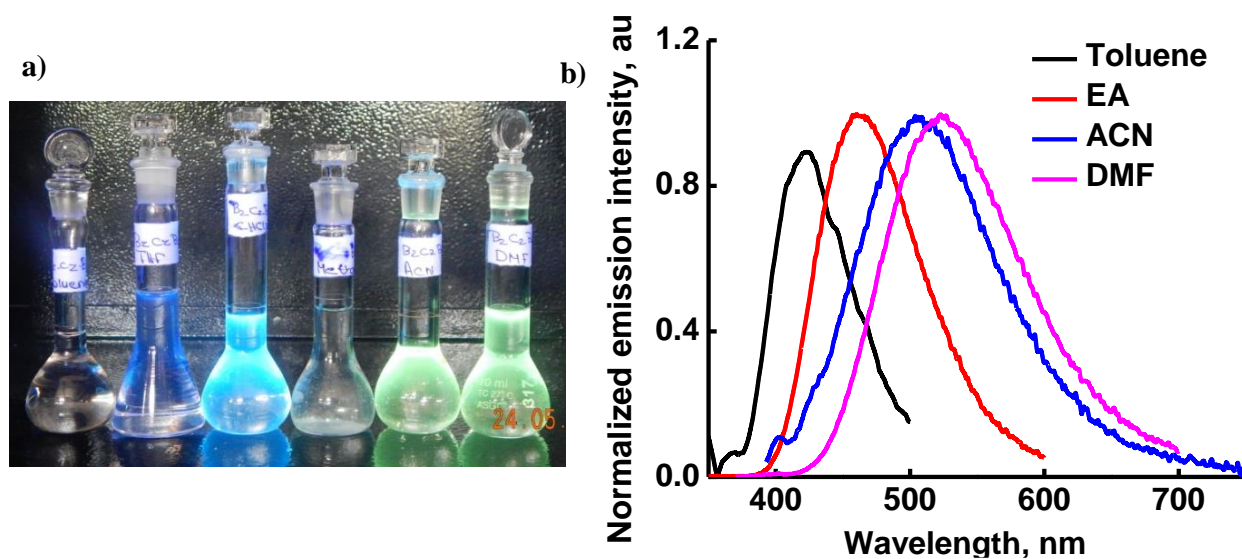
Figure 4.8. *a) Emission of **Cz(PhBz)₂** in different solvents b) Emission spectrum for **Cz(PhBz)₂** in toluene, ethyl acetate, acetonitrile and dimethylformamide*

4.4.2.2 Room temperature steady state PL studies in solid state

The absorption and emission spectrum of **Cz(PhBz)₂** were recorded in solid state also (Figure 4.9). The solid state absorption spectrum of **Cz(PhBz)₂** recorded at room temperature was a broad one ranging from 300 nm to 500 nm. Solid state emission of the molecule was recorded by exciting **Cz(PhBz)₂** at 330 nm and also at 370 nm. In both the cases molecule showed similar emission profile (Figure 4.9). The emission profile was also a broad one ranging from 436 nm to 600 nm, with an emission maximum at 490 nm.

The solid state fluorescence quantum yield of the molecule was calculated using absolute method and a value of 1.9% was obtained, which was surprisingly lower than that of solution state quantum yield. This observed low quantum yield value in solid state is interesting, because in most of the thermally activated delayed fluorescent materials the solid state quantum yields are reported to be very low [16-20]
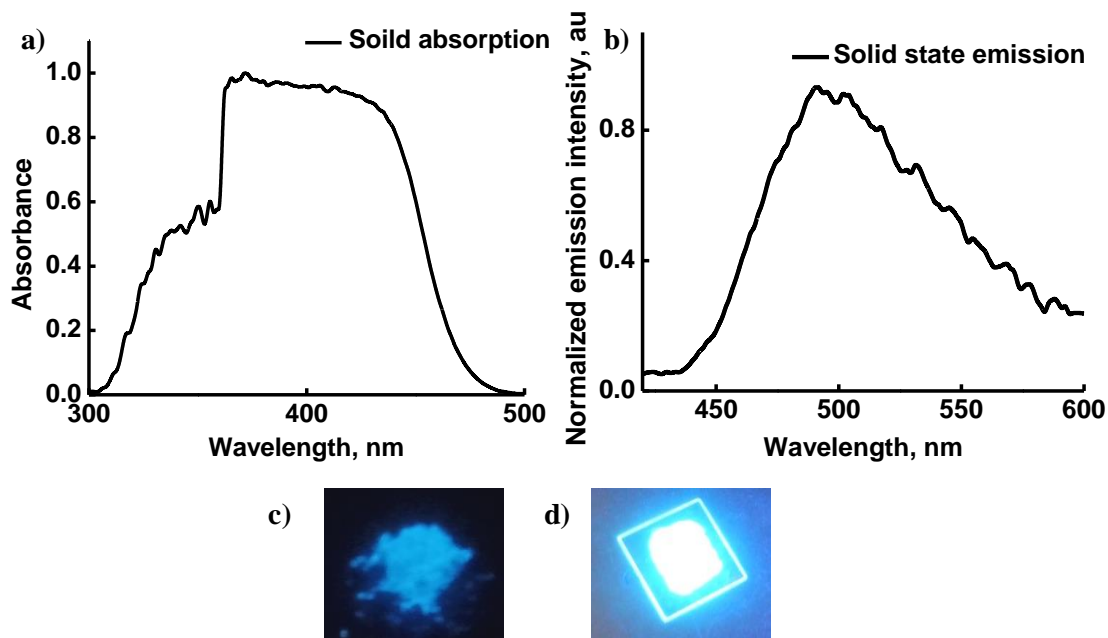
*Figure 4.9. a) Solid state absorption spectrum of **Cz(PhBz)₂** b) Solid state emission spectrum of **Cz(PhBz)₂** c) Powder emission and d) film state emission*

4.4.2.3 Emission studies at 77 K (Liquid nitrogen)

To calculate the ΔE_{ST} for the molecule, **Cz(PhBz)₂**, low temperature emission was recorded in frozen THF at 77 K (Figure 4.10). The low temperature emission profile showed two emissions corresponding to the fluorescence and phosphorescence. The ΔE_{ST} for **Cz(PhBz)₂** was calculated from the offset of fluorescence and phosphorescence emission as 0.3 eV. Results are summarized in table 3.1
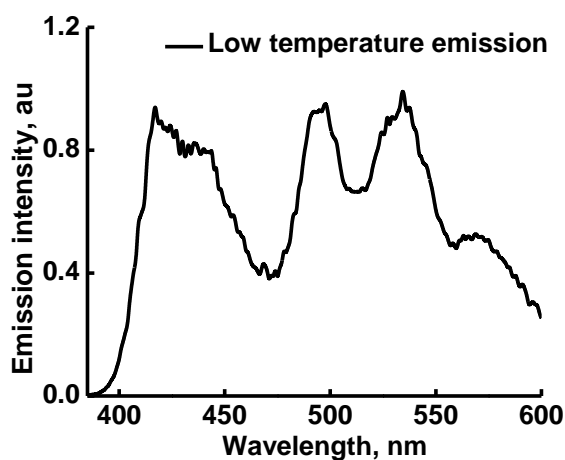
*Figure 4.10. Low-temperature emission spectrum for **Cz(PhBz)₂***

Table 4.1. Values for ΔE_S, ΔE_T energies and ΔE_{ST}

Compound	ΔE_s (eV)	ΔE_t (eV)	ΔE_{st} (eV)
Cz(PhBz)₂	3.11	2.81	**0.30**

4.4.2.4 Phosphorescence studies at 77 K and at room temperature

Figure 4.11 shows the phosphorescence spectrum of **Cz(PhBz)₂**, taken in frozen THF at 77 K with a flash delay of 0.5 ms. The excitation wavelength used for phosphorescence measurements was 350 nm. The phosphorescence spectrum showed a structured emission indicating the $\pi-\pi^*$ nature of the triplet state. The structured phosphorescence emission spectrum consisted of three peaks at 500 nm, 536 nm and 578 nm.
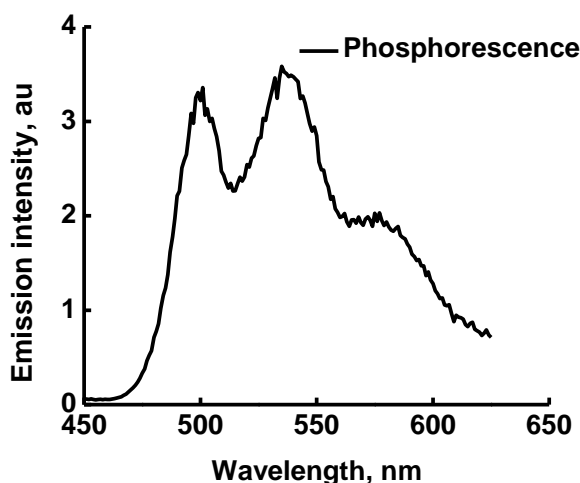
*Figure 4.11. Phosphorescence emission spectrum for **Cz(PhBz)₂***

The room temperature phosphorescence spectrum of **Cz(PhBz)₂** was recorded in solid state since in solution state the dissolved oxygen can interfere with the triplet state. The normal phosphorimeter setup was used for taking room temperature phosphorescence. The experimental conditions used for RTP measurement is as follows "S1(R928) (Phosphorimeter): Sample window: 0.10, Time per Flash: 61.00, Flash Count: 60". The flash delay for the experiment was changed for each measurements. The excitation wavelength was kept constant at 350 nm.

The first spectrum was recorded using a flash delay of 50 μs. In contrast to the RTP spectrum for Cz(PhCF₃)₂ the RTP spectrum of **Cz(PhBz)₂** gave only a single broad peak (Figure 4.12).

This was infact a little confusing to us initially but on a closer evaluation we concluded that this emission could be an additive of both solid state and phosphophorescence emission. A small ΔE_{ST} of the molecule might have resulted in this observation of a single broad peak. Also at 100 µs the broad spectrum changed to a structured one similar to the phosphorescence profile of the molecule, further supporting our assumption. After 100 µs, there was no emission observed.
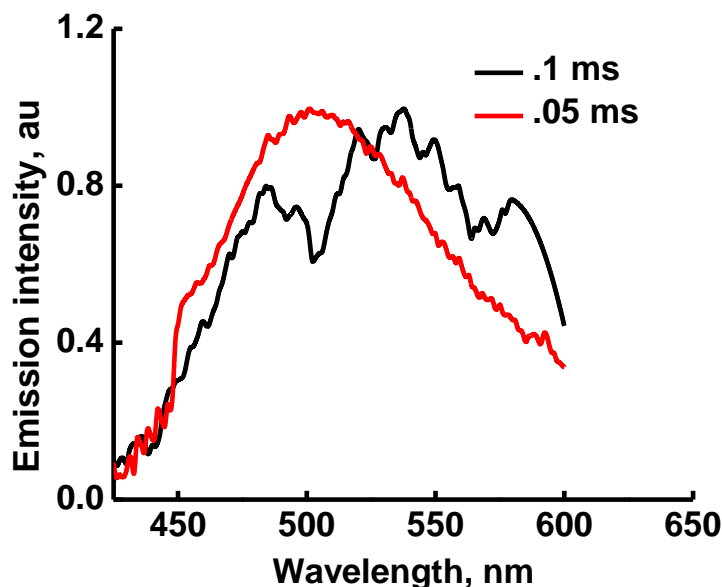
Figure 4.12*.The room temperature emission spectrum for the molecule with different flash delay excited at 350 nm*

4.4.3 Electrochemical analysis and HOMO/LUMO calculations

The CV profile for the molecule was recorded, to have an idea about the electrochemical behaviour of the molecule, (Figure 4.13a). It showed a reversible oxidation potential equal to 1.27 eV. The values for highest occupied molecular orbital and lowest unoccupied molecular orbital were calculated from solid state absorption, emission and CV profile (Figure 4.13). The calculated HOMO value for the molecule, **Cz(PhBz)$_2$** was found to be 5.66 eV and the LUMO value as 2.96 eV. The value obtained for band gap for the molecule was experimentally determined as 2.7 eV from the intercept of solid state absorption and emission.
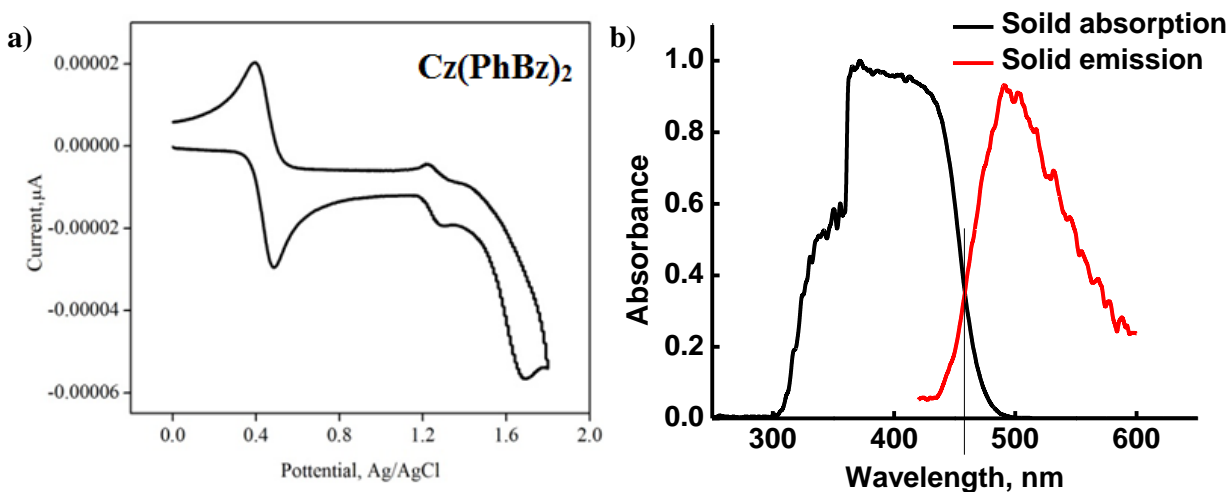
***Figure 4.13**. a) CV profile for **Cz(PhBz)₂** b) Calculation of band gap from solid state emission and absorption*

Calculations

E_{Fc} (Vs Ag/AgCl) = 0.41V

E_{ox} (Vs Ag/AgCl) = 1.27 V

E_{ox} (Vs Fc)   = 1.27-0.41= 0.86V

HOMO   = {-E_{ox} (Vs Fc) - 4.8 eV}

          = {-0.86-4.8eV} = **-5.66eV.**

LUMO= HOMO- Band gap

          = -5.66- 2.7

          = **- 2.96 eV**

Band gap was calculated from the intercept of solid state absorption and emission (Figure 4.13b). Results for electrochemical analysis and HOMO/LUMO calculations are presented in table 4.2.

Table 4.2. Results for HOMO/LUMO calculation.

Compound	Band Gap (eV)	HOMO (eV)	LUMO (eV)
Cz(PhBz)₂	2.7	- 5.66	- 2.96

4.4.4 Thermal analysis

A differential scanning calorimetry (DSC) was applied for determining information of glass transition (Tg) and melting (Tm) temperatures. Figure 4.13 shows the DSC curve of **Cz(PhBz)₂** sample in the range of temperature from 25 °C up to approximately 200 °C. The plot shows the heat flow as a function of sample temperature and an endothermic response is oriented downwards. In the DSC measurements a melting temperature of 125 ºC and a second exothermic peak at 181 ºC was observed. In the second cycle, the molecule showed a glass transition at 53 ºC.

Compound	Glass transition (Tg, ºC)	Melting temperature (ºC)	Second exothermic peak
Cz(PhBz)₂	53	125	181

Table 4.3. Summary of thermal studies
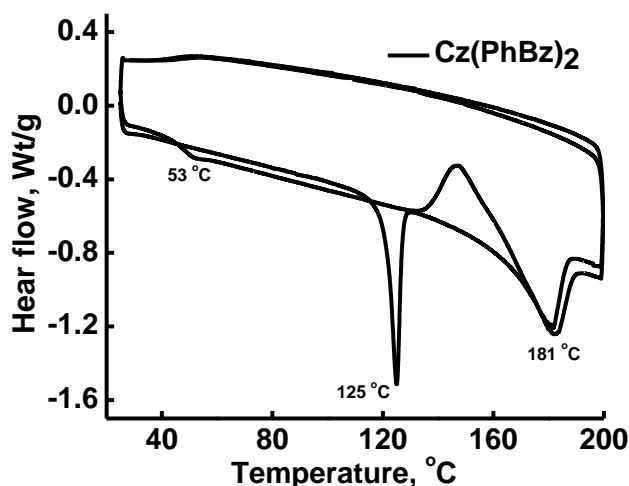
*Figure 4.14.DSC diagram for **Cz(PhCF₃)₂***

4.4.5 Density functional theory (DFT) calculations

Computational studies on the molecule in the ground state were carried out using the polarizable continuum model (PCM)[21] implicit solvation effect (solvent = THF) incorporated B3LYP/6-31G*[22] level of density functional theory as implemented in Gaussian 09.[23a] The excited singlet (S^1) and triplet (T^1) states were also optimized with TD-DFT method in the solvent phase. All the structures were verified as energy minima by frequency calculation. The optimized geomatry in the case of **Cz(PhBz)₂**, also showed an increase in the planarity from S^0 to S^1 to T^1 states, similar to **Cz(PhCF₃)₂**. The benzoylphenyl substituent was twisted at 36° with respect to the carbazole moiety (Figure 4.15) in S^0 while this twist angle in S^1 and T^1 states was 28° and 17°, respectively. More planarization of the molecule in T^1 state suggests increased delocalization of their π-electrons compared to S^0 and S^1 states. The planar nature of T^1 state may improve the RTP lifetime of the molecules. While evaluating the spatial arrangement of frontier orbitals in **Cz(PhBz)₂** we could see that, HOMO is mainly localized on the carbazole moiety and LUMO is mainly localized on the acceptor moiety, *ie* benzophenyl. This observation was indeed contradictory to the observation in Cz(PhCF₃)₂, where the LUMO was delocalized over the donor and acceptor fragments. Figure 4.15 shows the optimized geometries for the molecule. Figure 4.16 presents the special arrangements for HOMO/LUMO. Table 4.4 depicts the arrangement for frontier orbitals and their corresponding energy.
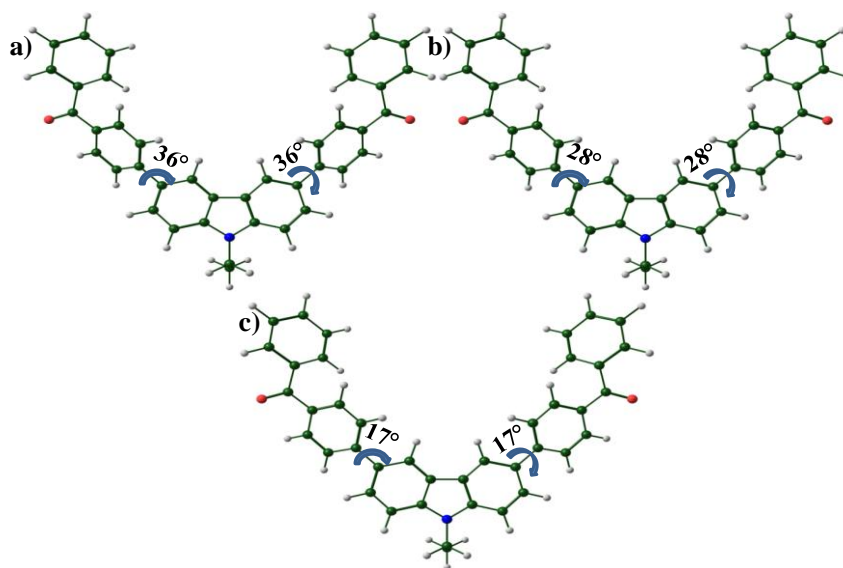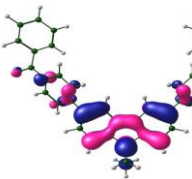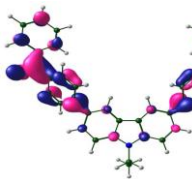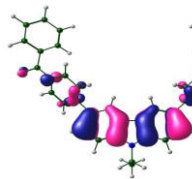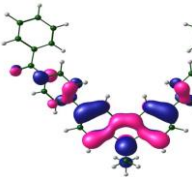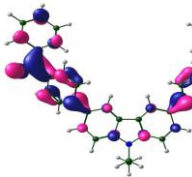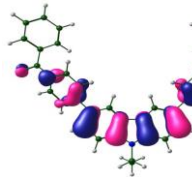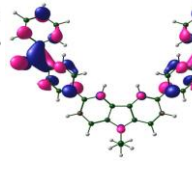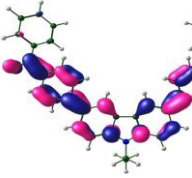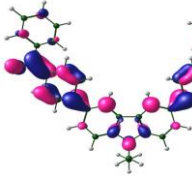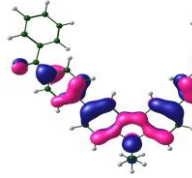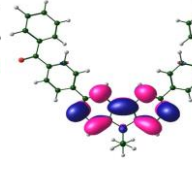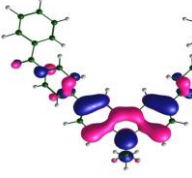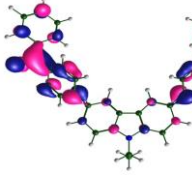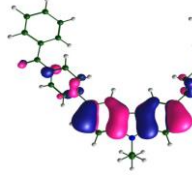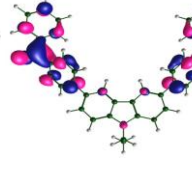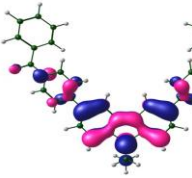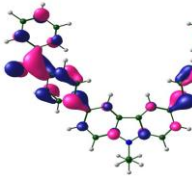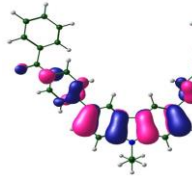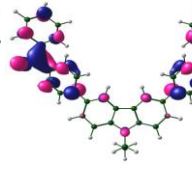
Figure 4.15. *Optimized geometries of **Cz(PhBz)₂** a) S^0 b) S^1 c) T^1*

State	HOMO/LUMO (eV)	Spatial arrangement HOMO (eV)	Spatial arrangement LUMO (eV)	Spatial arrangement HOMO-1 (eV)	Spatial arrangement LUMO+1 (eV)
GS (g)	-	146-5.45	147- 1.76	145- 5.93	148- 1.69
SS (g)	-	146-5.35	147- 1.91	145- 5.91	148- 1.81
TS (g)	-	147- 2.73	148- 2.13	146- 5.87	149- 1.53
GS (s)	-5.66/-2.96	146-5.43	147- 1.92	145- 5.93	148- 1.85
SS (s)	-	146-5.34	147- 2.09	145- 5.94	148-1.98
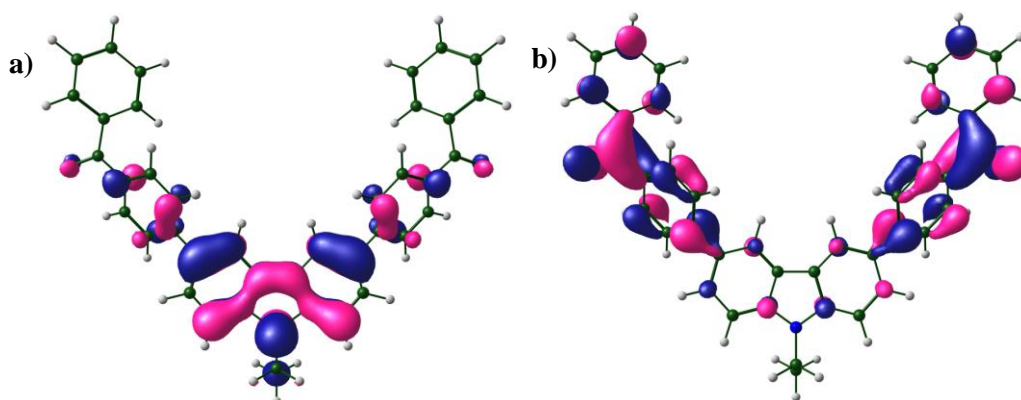
Figure 4.16. *a) HOMO b) LUMO. Computed HOMO = **5.45** eV LUMO = **2.0** eV*

4.5 Electroluminescence studies

To examine the electroluminescent properties of **Cz(PhBz)₂**, we fabricated a device with the following device configuration: (ITO: Indium tin oxide PEDOT:PSS: Poly(3,4-ethylene dioxythiophene)-poly(styrene sulfonate). NPB: N,N′-Di(1-naphthyl)-N,N′-diphenyl-(1,1′biphenyl)-4,4′-diamine.   **Cz(PhBz)₂**(9-ethyl-9H-carbazole-3,6-diyl)bis(4,1-phenylene))   diethanone).   BCP: 2,9-dimethyl-4,7diphenyl-1,10-phenanthroline Alq₃: tris-(8-hydroxyquinoline)–aluminum. LiF: Lithium Fluoride).

The device stacking for the fabricated devices are given in Figure 4.17a. The device gave a broad electroluminescent emission starting from around 400 nm to 750 nm, thereby covering the entire visible range (Figure 4.17b). The white light emission from the device started from about 5V and was stable up to 20V with CIE coordinates at (0.30, 0.35). The luminance value of the device was found to be 110 cd/m^2. This device fabricated with **Cz(PhBz)₂**as an emissive layer showed an improved efficiency (four-fold) than that of the device fabricated with **Cz(PhCF₃)₂**.
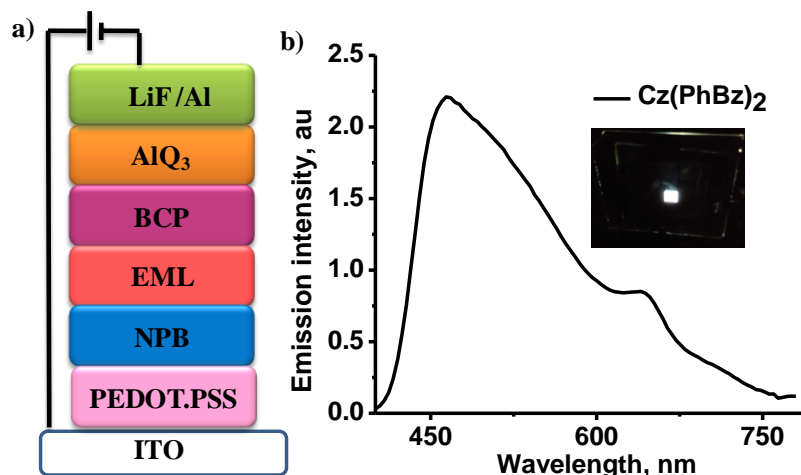
Figure 4.17. a) Device configuration for device b) Electroluminescence spectra for the white OLED based on *Cz(PhBz)₂* (inset shows the white OLED fabricated)

Similar to $Cz(PhCF_3)_2$, **Cz(PhBz)₂** also showed a white light emission arising from two peaks one at 480 nm and the other at 640 nm. The first emission can be assigned to the singlet emission of the molecule under study and the second emission at 640 nm can be assigned to either electroplex or electrophosphorescence. The possibility of emission from any other layer can be here, because no other layer in the device is having an emission in 640 nm range. Figure 4.18a shows the energy level diagram for the device fabricated with **Cz(PhBz)₂** and Figure 4.18b shows the plausible emission for an electroplex if it were present in the system. From that the emission range for the electroplexcan be calculated as 477 nm. Furthermore, if the second band in figure 4.17b arises from an electroplex, on increasing the voltage the emission from electroplex must also increase.[23b] That means the overall EL should show a non linear increase with respect to the voltage. So in order to verify this, we recorded the EL emission of our device at different voltages. Since the second emission peak in the electroluminescence profile of **Cz(PhCF₃)₂**, showed only a linear increase with respect to the voltage, we assumed that the emission was not coming out of an electroplex (Figure 18c). The remaining possibility for the presence of a second emission based on previous literature reports is electrophosphorescence.[23c,23d] So we assumed that the second emission peak in the EL of our molecule can be its phosphorescence component.
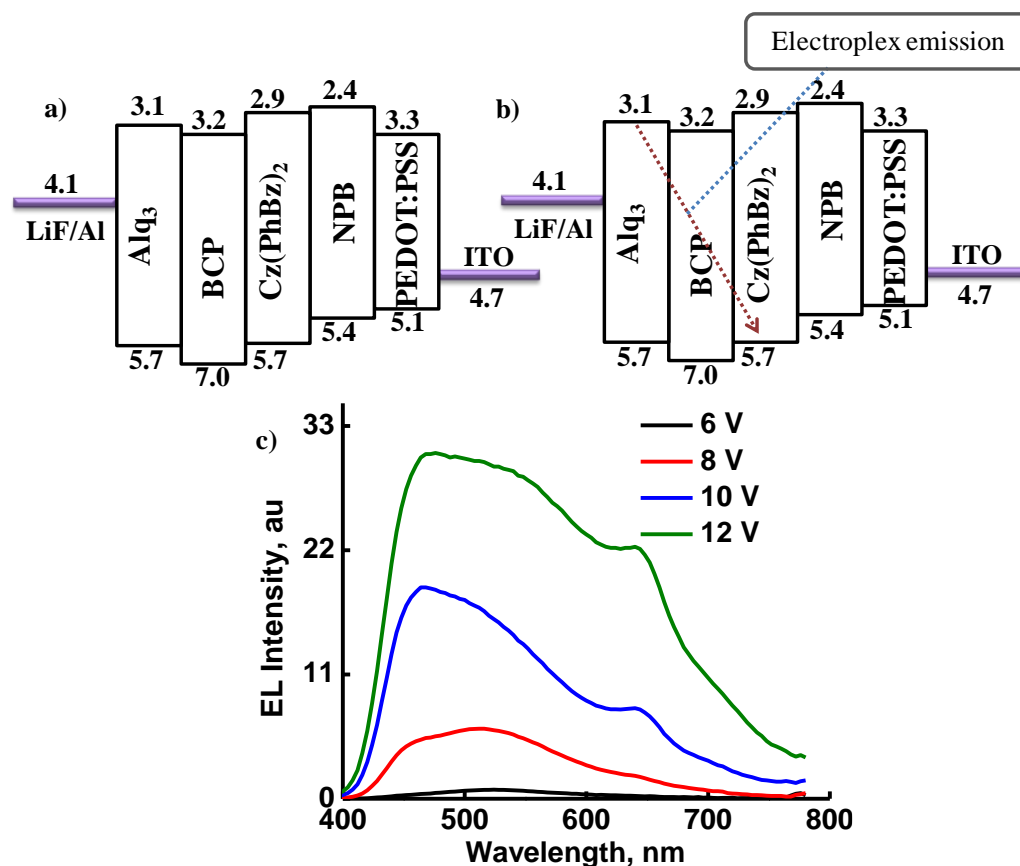
Figure 4.18. *a) Energy level diagram for device 1 b) Showing the plausible emission from an electroplex if it were present in the system*

In this device based on **Cz(PhBz)₂**, we successfully harvested both the singlet and the triplet excitons coming out from the molecule with the help of RTP. The device's properties are presented in table 4.5 and the device characterization curves are presented in Figure 4.18. So we hereby proved that the method we developed for achieving white light emitting OLEDs can be extended and also with adequate molecular and device designing we could achieve better efficiencies.
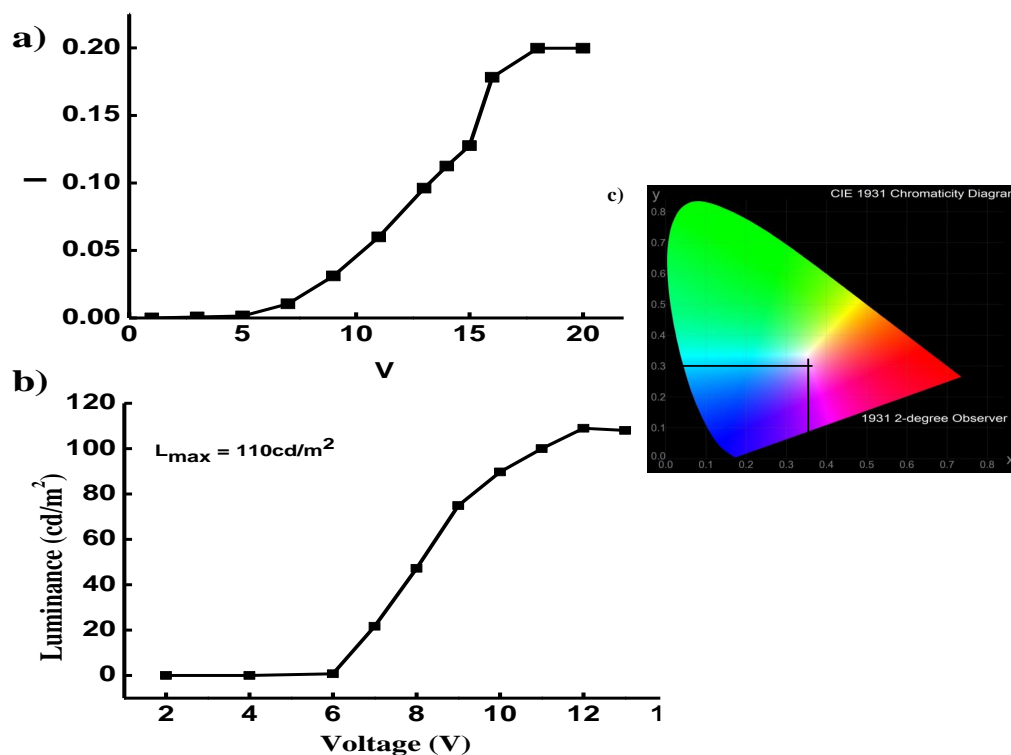
Figure 4.19. *a) J-V curve for device 1 b) L-V curve for the devices c) CIE-Colour coordinator for the white light emission*

Table 4.5. Device performance for **Cz(PhBz)₂**

Voltage (V)	Current (I) mA	Luminance (cd/M²)	Current density (A/m²)	Current efficiency (cd/A)	Power efficiency (lm/W)	Luminance efficiency (Cd/A)
5	1.11	105.20	69.19	1.52	1.17×10^{-6}	1.52
9	3.89	79.93	2430.62	0.03	1.73×10^{-5}	0.03
13	8.51	90.35	5317.50	0.02	2.97×10^{-5}	0.02
17	8.31	44.71	5195.00	0.01	1.09×10^{-5}	0.01

4.6 Conclusion

In summary, we have successfully designed and synthesised another single molecule white organic light emitting diode, as a continuation of our work described in the previous chapter. By using **Cz(PhBz)₂** as the emissive layer we could improve the device performance by four fold. The device also gave better colour purity for white light. The device performance of the

white light emitting diodes can be improved with the current route by harvesting both singlet and triplet excitons thereby overcoming the spin statistical limit of 25%. Through proper molecular design strategy using the intrinsic SOC of carbazole and the 3, 6 substitutions with benzophenone moiety on the carbazole we could successfully synthesize **Cz(PhBz)₂** which exhibited a very prominent room temperature phosphorescence. The small ΔE_{ST} of the molecule helped to tune the phosphorescence near to fluorescence and thereby covering the entire visible range. We strongly believe that, this relatively new approach of molecular design can indeed lead to efficient organic white light emitting diodes.

4.7. Experimental Section

4.7.1. General Information and Materials

The solvents were purchased from Merck Millipore. Boronic acids and carbazole were purchased from Sigma Aldrich and used without further purification. NBS was purchased from Spectrohem and used after re-crystallizing from the water. Na_2CO_3, Na_2SO_3 and activated aluminium oxide for column chromatography were also purchased from Spectrochem. The catalyst $Pd(PPh_3)_4$ and silica gel for column chromatography were purchased from Alfa Aesar. Reactions were carried out under an inert atmosphere of argon in oven-dried glassware. The progress of the reaction was monitored using commercial Silica Gel TLC plates (Merck-Millipore, 60 F254) and UV detection (254 nm and 365 nm). Column chromatography was done using activated aluminium oxide and silica gel. The ^1H and ^{13}C NMR spectra were recorded using Bruker NMR spectrometer (AV500) with working frequency of 500 MHz for ^1H NMR and 125 MHz for ^{13}C NMR. The chemical shifts are reported in δ (ppm) relative to TMS as an internal standard. The signal splitting is abbreviated as follows: s = singlet; d = doublet; t = triplet; q = quartet; and m = multiplet. All coupling constants (*J*) given are in Hertz (Hz) Mass spectra were recorded using ESI/ HRMS at 60000 resolutions (Thermo Scientific Exactive)

4.7.2. Synthesis of the materials

4.7.2.1 General procedure for the Suzuki-Miyaura coupling[24]

The boronic acid (1 equivalent) and the bromo compound (1equivalent) were taken in a Schlenk tube along with 5 mol% Pd(PPh₃)₄.THF along with 2N Na₂CO₃ dissolved in water (2:1) was added to the reaction mixture. The reaction mixture was degassed with argon and allowed to stir at 65‑70 °C for 12 h.

4.7.2.2 Synthesis of 9-ethyl-9,9a-dihydro-4aH-carbazole (Cz-Et)

To a solution of Carbazole (5 g, 0.029 mol) in THF (50 mL) at 0 °C, NaH (1.43 g, 0.0598 mol) was added. The heterogeneous mixture was stirred for 15 min at 0 °C, and for 1 h at room temperature. The mixture as then cooled to 0 °C and treated with ethyl iodide (5 mL, 0.0598 mol) and allowed to warm to room temperature. After 30 min, the reaction mixture was cooled to 0 °C and quenched with NH₄Cl. It was then extracted with ether and washed in brine. The crude product obtained after the removal of ether was used as such for further reaction.

4.7.2.3 Synthesis of 3,6-dibromo-9-ethyl-8a,9-dihydro-4bH-carbazole (CzBr₂)

Cz-Et (1 g, 0.005 mol) dissolved in toluene (35 mL) was taken in a two‑necked round bottom flask equipped with a magnetic stirrer bar, a nitrogen gas inlet and a 250 mL addition funnel. The system was then cooled in an ice bath. A solution of N-bromosuccinimide (NBS) (1.986 g, 0.0112 mol) in DMF (100 mL) was added to the flask through the funnel. After 30 min, the mixture was poured into cold water to precipitate out the product which was filtered and washed with cold methanol. The product was crystallized from MeOH/hexane (5:1).

4.7.2.4 Synthesis of 1,1′ -(4,4′ -(9-ethyl-9H-carbazole-3,6-diyl)bis(4,1 phenylene)) diethanone (Cz(PhBz)₂

3,6-Dibromo-9-ethyl-8a,9-dihydro-4bH-carbazole (CzBr₂, 0.2 g, 0.00058 mol) and 4-benzoyl phenyl boronic acid (0.265 g, 0.13108 mol) were added to the Schlenk tube along with Pd(PPh₃)₄ as the catalyst. THF (6 mL) along with 2N Na₂CO₃ solution (3 mL) was added to the reaction mixture. There action mixture was then degassed with argon and allowed to stir at 65‑70 °C for 12 h. The reaction mixture was monitored by

TLC and on completion, it was worked up by extracting with 10 mL DCM twice. The organic layers were combined, washed with brine and evaporated to get the crude product which was subjected to column chromatography on activated aluminium oxide using 25% ethyl acetate/hexane mixture as elutent to afford the product in good yield (50%).

Spectral characterization of Cz(Bz)₂

Yield: 50% as a lemon yellow solid

¹H NMR [500 MHz, CDCl₃]: δ, 8.46 (S, 2H), 7.94 (d, *J* = 5 Hz, 4H), 7.85 (t, *J* = 5 Hz, 8H), 7.85 (d, J = 5 Hz, 2H), 7.74 (d, *J* = 5 Hz, 1H), 7.62 (q, *J* = 7.25 Hz 7H),7.46 (t, *J* = 7.25 Hz, 1H), 4.34- 4.30 (m, 2H), 1.42 (t, *J* = 7.25 Hz, 3H) ppm.
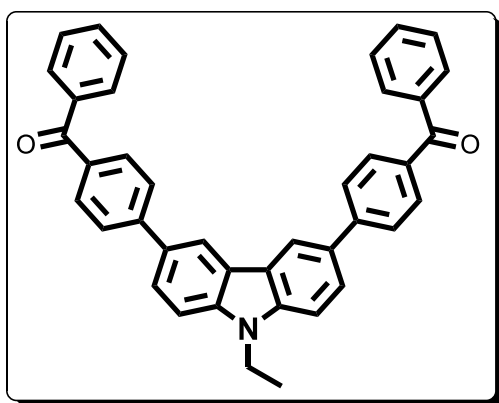
¹³C NMR [125 MHz, CDCl₃]: δ: 196.6, 160.1, 146.1, 140.4, 137.9, 135.3, 132.9, 132.3, 131.9, 131.2, 130.9, 129.7, 128.3, 128.2, 126.9, 125.6, 123.6, 119.3,115.2, 109.2, 37.9, 13.9 ppm.

HRMS (ESI) for C₄₀H₂₉NO₂, (M+H)+: 556.2276 Found: 556.2270

4.7.3. Instrumentation

4.7.3.1 Photophysical studies

Absorption spectra were recorded using a Shimadzu UV-2600 UV-Visible spectrophotometer. The optical diffuse reflectance spectra were measured for solid samples using the aforementioned spectrometer equipped with an integrating sphere. BaSO₄ was used as the reference material, and the solid samples were ground well before the measurement. The absorption (α/S) data were calculated from the reflectance spectra using the Kubelka–Munk function: $\alpha/S = (1 - R)^2/2R$, in which R is the reflectance at a given wavelength, α is the absorption coefficient, and S is the scattering coefficient (practically wavelength independent

when the particle size is larger than 5 mm). Steady-state fluorescence experiments were performed using FluoroLog-322 (Horiba) which was equipped with a 450 W Xe arc lamp by using optically dilute solutions. The fluorescence quantum yields in various solvents were determined by the relative method employing an optically matched solution of quinine sulphate in 0.1N sulphuric acid as the reference ($\Phi_R = 0.54$). The following equation (1) was used for calculating the quantum yield,[25]

$$\Phi_S = \frac{Abs_R}{Abs_S} \times \frac{Area_S}{Area_R} \times \frac{n_S}{n_R} \times \Phi_R \tag{1}$$

where the subscript R and S refer to the reference and samples respectively. Abs, Area, and n are the absorbance at the excitation wavelength, the area under the fluorescence spectrum and refractive index of the solvent respectively. Solid state photoluminescence spectra were also recorded using the front face mode with the same Fluorolog spectrofluorimeter. Time-resolved fluorescence spectra and lifetime experiments were performed by using an IBH picosecond single photon counting system employing the 375 nm nano LED as excitation sources and a Hamamatsu C4878-02 microchannel plate (MCP) detector. Decay in the fluorescence intensity (I) with time (t) was fitted either by a double/triple-exponential function:

$$I = A_1 e^{-t/\tau_1} + A_2 e^{-t/\tau_2} \tag{2}$$

$$I = A_1 e^{-t/\tau_1} + A_2 e^{-t/\tau_2} + A_3 e^{-t/\tau_3} \tag{3}$$

where τ_1, τ_2, and τ_3 are the lifetimes of different species, and A_1, A_2, and A_3 are their respective amplitudes. The weighted mean lifetime ($\langle\tau\rangle$) was calculated according to equation (4):

$$\langle\tau\rangle = \Sigma\tau_i A_i \tag{4}$$

The quality of the fits was checked by examining the residual distribution and the χ^2 value. The solid state samples were recorded with the front face mode. All the experiments were conducted at room temperature.

4.7.3.2 Cyclic voltammetry

Cyclic voltammetry experiments were carried out using a BAS 50 W voltammetric analyzer using three electrode cell assemblies. Platinum wires were used as counter electrodes, a silver wire was used as an Ag/Ag^+ quasi-reference electrode, and a platinum electrode was used as a working electrode. Measurements were carried out in acetonitrile solution with tetrabutylammoniumhexafluorophosphate as the supporting electrolyte at a scan rate of 100 mV s^{-1}. Concentrations of the molecules and the supporting electrolyte were 5×10^{-3} and 0.1 M, respectively. The ferrocenium/ferrocene couple ($FeCp^{2+}/FeCp^{20}$) was used as an internal reference. The energy level of $FeCp^{2+}/FeCp^{20}$ was assumed at -4.8 eV to vacuum.[26] All solutions for the electrochemical studies were deaerated with pre-purified argon gas before the measurements.

4.7.3.3 Computational methods

The ground (S^0) geometries of model systems **Cz(PhBz)₂** was optimized by using density functional theory (DFT) based method with Becke's three-parameter functional and the Lee-Yang-Parr functional (B3LYP) with 6-31G* basis set. Based on the gas phase optimized geometry of **Cz(PhBz)₂** spectral properties in chloroform were calculated by time dependent density functional theory (TD-DFT) method with Polarizable Continuum Model (PCM) at PBE0/6-31G* level. All the calculations were carried out using Gaussian 09 program package.

4.7.3.4 Thermal analysis

Differential scanning calorimetry was performed using a TA Q20 general-purpose DSC instrument in sealed aluminum pans under nitrogen flow at a heating/cooling rate of 5 °C min^{-1}.

4.7.3.5 Device fabrication

Patterned ITO coated substrates (sheet resistance 10 Ω/m^2), brushed with soap solution, and cleaned in an ultrasonic bath with 2-propanol and de-ionized water were used as substrates. Devices were fabricated by spin coating of different organic layers expect Alq₃ under nitrogen atmosphere including emissive layer. The cathode aluminum and Alq₃ were thermally evaporated at high vacuum condition (~10-8 Torr). Devices were encapsulated with a cover glass and UV- curable epoxy resin in nitrogen atmosphere before evaluation. The measured device area is 16 mm^2 for **Cz(PhBz)₂**.

4.8 Reference

1. Gong, Y.; Tan, Y.; Mei, J.; Zhang, Y.; Yuan, W.; Zhang, Y.; Sun, J.; Tang, B. Z. Room Temperature Phosphorescence from Natural Products: Crystallization Matters. *Sci. China Chem.***2013**, *56* (9), 1178–1182.

2. Bolton, O.; Lee, K.; Kim, H. J.; Lin, K. Y.; Kim, J. Activating Efficient Phosphorescence from Purely Organic Materials by Crystal Design. *Nat. Chem.***2011**, *3* (3), 205–210.

3. An, Z.; Zheng, C.; Tao, Y.; Chen, R.; Shi, H.; Chen, T.; Wang, Z.; Li, H.; Deng, R.; Liu, X.; Huang, W. Stabilizing Triplet Excited States for Ultralong Organic Phosphorescence. *Nat. Mater.***2015**, *14* (7), 685–690.

4. Fermi, A.; Bergamini, G.; Roy, M.; Gingras, M.; Ceroni, P. Turn-on Phosphorescence by Metal Coordination to a Multivalent Terpyridine Ligand: A New Paradigm for Luminescent Sensors. *J. Am. Chem. Soc.***2014**, *136* (17), 6395–6400.

5. Zhao, W.; He, Z.; Lam, J. W. Y.; Peng, Q.; Ma, H.; Shuai, Z.; Bai, G.; Hao, J.; Tang, B. Z. Rational Molecular Design for Achieving Persistent and Efficient Pure Organic Room Temperature Phosphorescence. *Chem.***2016**, *1* (4), 592–602..

6. Li, C.; Tang, X.; Zhang, L.; Li, C.; Liu, Z.; Bo, Z.; Dong, Y. Q.; Tian, Y. H.; Dong, Y.; Tang, B. Z. Reversible Luminescence Switching of an Organic Solid: Controllable On Off Persistent Room Temperature Phosphorescence and Stimulated Multiple Fluorescence Conversion. *Adv. Opt. Mater.***2015**, *3* (9), 1184–1190.

7. Chen, Z.; Liu, G.; Wang, R.; Pu, S. Highly Emissive Carbazole-Based Gold (I) Complex with a Long Room-Temperature Phosphorescence Lifetime and Self-Reversible Mechanochromism Characteristics. *RSC Adv.***2017**, *7* (25), 15112–15115.

8. Castex, M. C.; Olivero, C.; Pichler, G.; Adès, D.; Siove, A. Fluorescence, Room Temperature Phosphorescence and Photodegradation of Carbazole Compounds in Irradiated Poly(methyl Methacrylate) Matrices. *Synth. Met.***2006**, *156* (9–10), 699–704.

9. Gong, Y.; Chen, G.; Peng, Q.; Yuan, W. Z.; Xie, Y.; Li, S. Achieving Persistent Room Temperature Phosphorescence and Remarkable Mechanochromism from Pure Organic Luminogens. *Adv. Mater.***2015**, *27*, 6195–6201.

10. Yang, Z.; Mao, Z.; Zhang, X.; Ou, D.; Mu, Y.; Zhang, Y.; Zhao, C.; Liu, S.; Chi, Z.; Xu, J.; Wu, Y. C.; Lu, P. Y.; Lien, A.; Bryce, M. R. Intermolecular Electronic Coupling of Organic Units for Efficient Persistent Room-Temperature Phosphorescence. *Angew. Chemie - Int. Ed.***2016**, *55* (6), 2181–2185.

11. Xue, P.; Wang, P.; Chen, P.; Yao, B.; Gong, P.; Sun, J.; Zhang, Z.; Lu, R. Bright Persistent Luminescence from Pure Organic Molecules through a Moderate Intermolecular Heavy Atom Effect. *Chem. Sci.***2016**, 1–6.

12. Li, C.; Tang, X.; Zhang, L.; Li, C.; Liu, Z.; Bo, Z.; Dong, Y. Q.; Tian, Y. H.; Dong, Y.; Tang, B. Z. Reversible Luminescence Switching of an Organic Solid: Controllable On-Off Persistent Room Temperature Phosphorescence and Stimulated Multiple Fluorescence Conversion. *Adv. Opt. Mater.* **2015**, *3* (9), 1184–1190.

13. He, Z.; Zhao, W.; Lam, J. W. Y.; Peng, Q.; Ma, H.; Liang, G.; Shuai, Z.; Tang, B. Z. White Light Emission from a Single Organic Molecule with Dual Phosphorescence at Room Temperature. *Nat. Commun.* **2017**, *8* (1), 416.

14. Zhao, W.; He, Z.; Lam, J. W. Y.; Peng, Q.; Ma, H.; Shuai, Z.; Bai, G.; Hao, J.; Tang, B. Z. Rational Molecular Design for Achieving Persistent and Efficient Pure Organic Room-Temperature Phosphorescence. *Chem* **2016**, *1* (4), 592–602.

15. Shimakura, N.; Fujimura, Y.; Nakajima, T. Theory of Intersystem Crossing in Aromatic Compounds: Extension of the El-Sayed Rule. *Chem. Phys.* **1977**, *19* (2), 155–163.

16. Méhes, G.; Nomura, H.; Zhang, Q.; Nakagawa, T.; Adachi, C. Enhanced Electroluminescence Efficiency in a Spiro-Acridine Derivative through Thermally Activated Delayed Fluorescence. *Angew. Chemie - Int. Ed.* **2012**, *51* (45), 11311–11315.

17. Ryoichi Ishimatsu, Shigeyuki Matsunami, Katsuyuki Shizu, Chihaya Adachi, Koji Nakano, T. I. Solvent E Ff Ect on Thermally Activated Delayed Fluorescence by. *J. Phys. Chem. A* **2013**, *117*, 5607–5612.

18. Uoyama, H.; Goushi, K.; Shizu, K.; Nomura, H.; Adachi, C. Highly Efficient Organic Light-Emitting Diodes from Delayed Fluorescence. *Nature* **2012**, *492* (7428), 234–238.

19. Zhang, Q.; Li, B.; Huang, S.; Nomura, H.; Tanaka, H.; Adachi, C. Efficient Blue Organic Light-Emitting Diodes Employing Thermally Activated Delayed Fluorescence. *Nat. Photonics* **2014**, *8* (4), 326–332.

20. Youn Lee, S.; Yasuda, T.; Nomura, H.; Adachi, C. High-Efficiency Organic Light-Emitting Diodes Utilizing Thermally Activated Delayed Fluorescence from Triazine-Based Donor–acceptor Hybrid Molecules. *Appl. Phys. Lett.* **2012**, *101* (9), 093306.

21. Miertuš, S.; Scrocco, E.; Tomasi, J. Electrostatic Interaction of a Solute with a Continuum. A Direct Utilizaion of AB Initio Molecular Potentials for the Prevision of Solvent Effects. *Chem. Phys.***1981**, *55* (1), 117–129.

22. Kim, K.; Jordan, K. D. Comparison of Density Functional and MP2 Calculations on the Water Monomer and Dimer. *J. Phys. Chem.***1994**, *98* (40), 10089–10094.

23. a) Becke, A. D. Density-Functional Thermochemistry. III. The Role of Exact Exchange. *J. Chem. Phys.***1993**, *98* (7), 5648.
    b) Chen, F. P.; Xu, B.; Zhao, Z. J.; Tian, W. J.; Lü, P.; Im, C. b) Chen, F. P.; Xu, B.; Zhao, Z. J.; Tian, W. J.; Lü, P.; Im, C. White Organic Light-Emitting Diodes Based on Electroplex from Polyvinyl Carbazole and Carbazole Oligomers Blends. *Chinese Phys. B* **2010**, *19* (3).
    c) Cocchi, M.; Virgili, D.; Giro, G.; Fattori, V.; Di Marco, P.; Kalinowski, J.; Shirota, Y. Efficient Exciplex Emitting Organic Electroluminescent Devices. *Appl. Phys. Lett.* **2002**, *80* (13), 2401–2403.
    d) Zhen, H.; Xu, W.; Yang, W.; Chen, Q.; Xu, Y.; Jiang, J.; Peng, J.; Cao, Y. White-Light Emission from a Single Polymer with Singlet and Triplet Chromophores on the Backbone. *Macromol. Rapid Commun.* **2006**, 27(24), 2095–2100

24. Miyaura, N.; Suzuki, A. Palladium-Catalyzed Cross-Coupling Reactions of Organoboron Compounds. *Chem. Rev.* **1995**, *95* (7), 2457–2483.

25. Brouwer, A. M. Standards for Photoluminescence Quantum Yield Measurements in Solution (IUPAC Technical Report). *Pure Appl. Chem.***2011**, *83* (12), 2213–2228.

26. Liu, Y.; Liu, M. S.; Jen, A. K.-Y. Synthesis and Characterization of a Novel and Highly Efficient Light-Emitting Polymer. *Acta Polym.* **1999**, *50* (2-3), 105–108.

Summary

The thesis entitled "**Design, synthesis, photophysical and electroluminescence studies of triphenylamine and carbazole derivatives"** embodies the results of our investigations carried out in the research area of organic light emitting diodes. The thesis is divided into four chapters.

Chapter 1 provides a brief introduction to the conjugated small organic molecules based on triphenylamines and carbazoles followed by a description about their applications in the area of organic light emitting diodes. The chapter also highlights recent developments in this field and major objectives of the present thesis. The next three chapters describe the work carried out in detail on the subject matter of the thesis.

Chapter 2 deals with the design, synthesis and photophysical studies of a set of three triphenylamine-thiophene donor-acceptor molecules **TPT, TPT-Ben**, and **TPT-Ac,** followed by the demonstration of their use as RGB emitters in white light generation. Electroluminescent studies on these molecules are also discussed in this chapter.
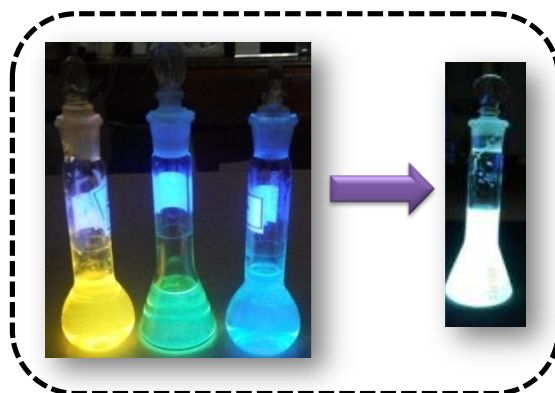
Figure 1. *Pictorial representation of the generation of white light using a 3: 2: 1 combination ofthe synthesized triphenylaminederivativesTPT, TPT- Ben and TPT- Ac.*

The device with **TPT-Ben** gave a green electroluminescence while the one with **TPT-Ac** showed broad electroluminescence with a yellowish-white emission. The luminance value for **TPT-Ben** was found to be 332 cd/m^2, and for TPT-Ac it was found to be 22 cd/m^2. Thus we demonstrated the use of our molecules as OLED emitters.

Chapter 3 describes our work on the design, synthesis and photophysical and electroluminescence study of a carbazole derivative substituted namely **Cz(PhCF₃)₂.** It exhibited a blue emission in solution state in DMSO (QY 35%) and in solid state (QY13.9%). The ΔE_{ST} value for the molecule was found to be 0.36 eV. However the molecule showed no ICT character regardless of the presence of an active donor (carbazole) and an active acceptor (trifluoromethyl) group. DFT calculations on the molecules explained this observation as due to the delocalization of the LUMO over the whole π-region. To examine the electroluminescence properties of **Cz(PhCF₃)₂**, we fabricated an unoptimized solution processable device which gave a broad electroluminescent emission with two peak maxima at 426 nm and 528 nm. The white light emission from the device started from ~ 7V and was stable up to ~ 16V with CIE coordinates at (0.31, 0.44). The second band at 528 nm in the EL can be attributed to the phosphorescent emission of the molecule. Harvesting both singlet and triplet excitons in the device resulted in white light emission.

Next section of this chapter deals with the utilization of **Cz(PhCF₃)₂** as a host for commercially available organic electroluminescent materials. The high triplet energy, comparable to many of the commercially available host materials, prompted us to examine the host properties of the
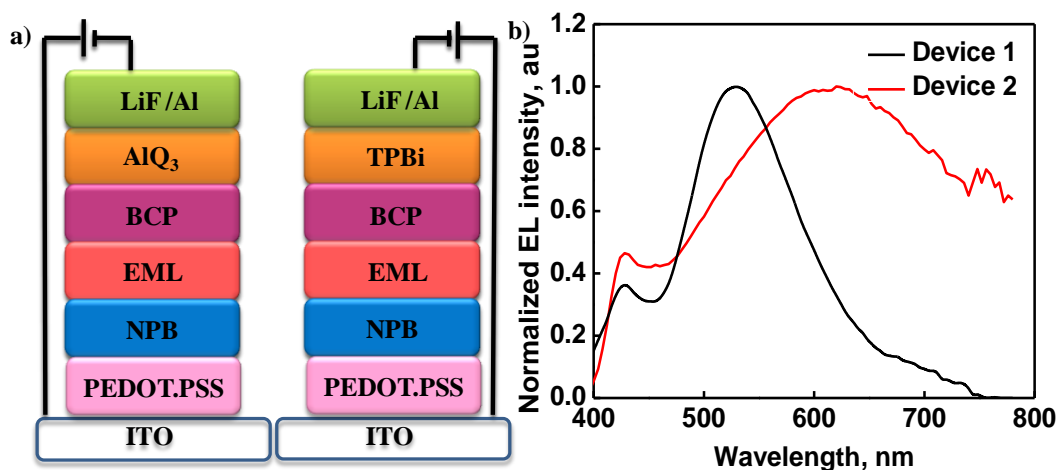

Figure 2. *a) Device configuration for device 1 and device 3 b) Electroluminescence spectra for the white OLED based on **Cz(PhCF₃)₂***

molecule. Rubrene (yellow) and DCJTB (red) were chosen as EL materials. Two devices fabricated with **Cz(PhCF₃)₂** as the host material showed device properties at very low turn-on

voltages and gave emissions akin to the electroluminescent materials used, confirming the utility of our molecule, **Cz(PhCF₃)₂** as a host for yellow and red devices.

Chapter 4 details our work on the synthesis, photophysical and electroluminescence studies of **Cz(PhBz)₂**which contains a stronger electron acceptor viz, -benzoylphenyl (-Ph-CO-Ph) group at the 3,6-position of the carbazole. As expected, the benzoylphenyl substitution resulted in better RTP due to the presence of non-bonding orbitals in the CO group which had the capability to boost room temperature phosphorescence. The **Cz(PhBz)₂**exhibited a better EL (4-fold increase) compared to that of **Cz(PhCF₃)₂**. **Cz(PhBz)₂** showed two absorption peaks, one at 312 nm and the other at 353 nm. The relative quantum yield for the molecule was found to be 43% in a solution of DMSO. The ΔE_{ST} value of **Cz(PhBz)₂** was found to be 0.10 eV which was much lower than that of **Cz(PhCF₃)₂**. To examine the electroluminescence properties of **Cz(PhBz)₂**, we fabricated a device (structures unoptimized) by solution processing. This device also showed white electroluminescence with a colour coordinate of (0.29, 0.35) and a luminance value of 120 cd/m^2.
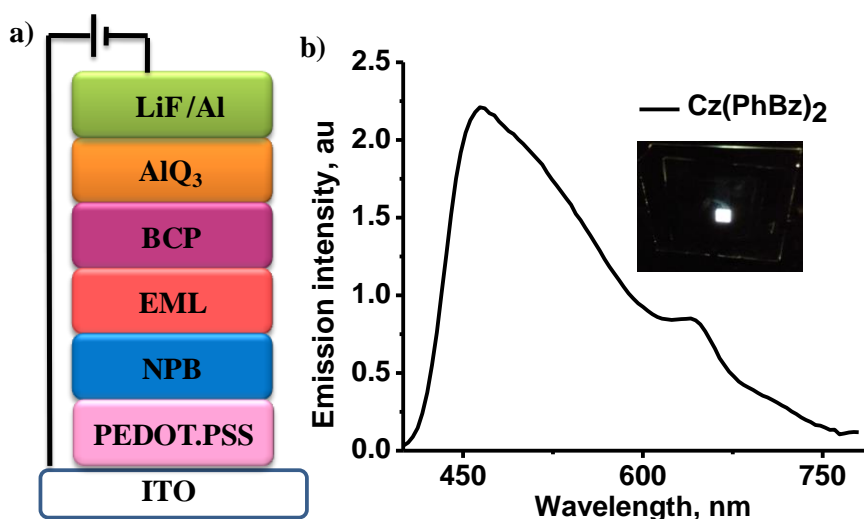

Figure 4.. *a) Device configuration for device b) Electroluminescence spectra for the white OLED based on* **Cz(PhBz)₂***(inset shows the white OLED fabricated)*

The relevance of our work lies in the fact that the current strategy of harvesting both singlet and triplet emissions in electroluminescence with appropriate molecule design, gives an easy and straightforward method for achieving single molecule solution processable white electroluminescent materials.

List of publications

[1] Maya, R. J.; **Krishna, A**.; Sirajunnisa, P.; Suresh, C. H.; Varma, R. L. Lower Rim-Modified Calix[4]arene-Bentonite Hybrid System as a Green, Reversible, and Selective Colorimetric Sensor for Hg2+Recognition. ACS Sustain. Chem. Eng. 2017, 5 (8), 6969–6977.

[2] **Krishna, A**.; Darshan, V.; Suresh, C. H.; Unni, K. N. N.; Varma, R. L. Journal of Photochemistry & Photobiology A : Chemistry Solution Processable Carbazole Derivatives for Dopant Free Single Molecule White Electroluminescence by Room Temperature Phosphorescence. J. Photochem. Photobiol. A Chem. 2018, 360 (April), 249–254.

[3] Krishna, A.; Varathan, E.; Sreedevi, P.; Subramanian, V.; Karunakaran, V.; Varma, R. L. Design, Synthesis and Photophysical Investigation of Triphenylamine-Bithiophene Dyes as RGB Emitters for White Light Applications. Dye. Pigment. 2018, 159 (May), 77–84

List of papers/posters presented in conference proceedings

[1] **Krishna, A**.; Subramanian, V.; Reddy, M. L. P.; Varma, R. L. Thiophene based blue emitters: promising candidates for organic light emitting diodes. TAPSUN, CSIR – Central Leather Research Institute (CSIR-CLRI), Adyar, Chennai 600 020 (September 13-14, 2013).

[2] **Krishna, A**.; Jisha, B.; Varma, R. L. Quinaldic acid Functionalized Gold nanoparticles: A Nanomolar Level Detector for Zn Ions in Aqueous Solutions, TFoC, National Institute for Interdisciplinary Science and Technology (CSIR), Trivandrum- 695 019 (October 9-11, 2014).

[3] **Krishna, A**.; Varma, R. L. Design, synthesis and photophysical studies of carbazole based small organic molecule for OLED application, Nascent Developments in Chemical Sciences: Opportunities for Academia-Industry Collaboration (NDCS), Bits Pilani, VidyaVihar Campus, Pilani, Rajasthan 333031, (October 16-18, 2015).

[4] **Krishna, A**.; Varma, R. L. Carbazole derivatives as thermally activated delayed fluorescent (TADF) molecules towards the next-generation organic light emitting diodes, CRSI-2016 at NBU, Darjeeling, West Bengal (July 14-16, 2016).

[5] **Krishna, A**.; Darshan, V.; Suresh, C. H.; Unni, K. N. N.; Varma, R. L. Carbazole Derived TADF Molecules: Next Generation OLED EAS8, National Institute for Interdisciplinary Science and Technology (CSIR), Trivandrum- 695 019 (September 20-22, 2017).

[6] **Krishna, A**.; Darshan, V.; Suresh, C. H.; Unni, K. N. N.; Varma, R. L. Non -doped single small organic molecule based white light emitting diode -exploiting both singlet and triplet emissions, 30th Kerala Science Congress (30th KSC), Govt. Brennen College, Thalassery, Kerala- 670106 (January 28-30, 2018). (**Oral Presentation**)